UC Santa Barbara
UC Santa Barbara Electronic Theses and Dissertations

Title

Renewable Uses of Lignocellulosic Biomass and Produced Water: For Biomaterial and a Lithium Source

Permalink

https://escholarship.org/uc/item/4wx780wp

Author

Hanson, Kalin

Publication Date

2021

Peer reviewed|Thesis/dissertation

UNIVERSITY OF CALIFORNIA

Santa Barbara

Renewable Uses of Lignocellulosic Biomass and Produced Water: For Biomaterial and a

Lithium Source

A dissertation submitted in partial satisfaction of the requirements for the degree Doctor of

Philosophy in Chemistry

by

Kalin G. Hanson

Committee in Charge:

Professor Mahdi. M. Abu-Omar, Chair

Professor Trevor Hayton

Professor Christopher M. Bates

Professor Lior Sepunaru

September 2021

The dissertation of Kalin G. Hanson is approved.

_____

Trevor Hayton

_____

Christopher M. Bates

_____

Lior Sepunaru

_____

Mahdi M. Abu-Omar, Committee Chair

September 2021

Renewable Uses of Lignocellulosic Biomass and Produced Water: For Biomaterial and a

Lithium Source

by

Kalin G. Hanson

ACKNOWLEDGEMENTS

VITA OF KALIN G. HANSON

September 2021

EDUCATION

B.A. Chemistry, Mount Holyoke College, May 2016

Ph.D. Chemistry, University of California, Santa Barbara, September 2021

PROFESSIONAL EMPLOYMENT

2016-2021: Graduate Student Researcher, University of California, Santa Barbara

2016-2019: Teaching Assistant, General and Organic Chemistry Lab, University of California, Santa Barbara

2015: Teaching Assistant, Organic Chemistry Lab, Mount Holyoke College

2015: Research Intern, University of Massachusetts, Amherst CURE REU

2014: Research Intern, Naval Air Warfare Center- Aircraft Division

AWARDS

Mellichamp Academic Initiative in Sustainability Summer Fellowship, University of California, Santa Barbara (2017-2019)

Chemistry and Biochemistry Departmental Service Award, University of California, Santa Barbara (2018, 2019)

21st Century Scholar Award, Mount Holyoke College (2012-2016)

PUBLICATIONS

1. Warnock, S. J.; Sujanani, R.; Zofchak, E. S.; Zhao, S.; Dilenschneider, T. J.; Hanson, K. G.; Mukherjee, S.; Ganesan, V.; Freeman, B. D.; Abu-Omar, M. M.; Bates, C. M. "Engineering Li/Na Selectivity in 12-Crown-4 Functionalized Polymer Membranes: The Impact of Specific Interactions on Ion Transport"

2. Hanson, K. G.; Lin, C. H.; Abu-Omar, M. M. "Preparation and Proerties of Renewable Pollyesters Based on Lignin-derived Bisphenol"

3. Hanson, K. G.; Lin, C. H.; Abu-Omar, M. M. "Crosslinking of Renewable Polyesters with Epoxides to form Bio-based Epoxy Thermosets"

4. Zofchack, E. S.; Zhang, Z.; Wheatle, B. K.; Sujanani, R.; Warnock, S. J.; Dilenschneider, T. J.; Hanson, K. G.; Zhao, S.; Mukherjee, S.; Abu-Omar, M. M.; Bate, C. M.; Freeman, B. D.; Ganesan, V. "Origins of Lithium/Sodium Reverse Permeability Selectivity in 12-Crow-4 Ether Functionalized Polymer Membranes"

ABSTRACT

Renewable Uses of Lignocellulosic Biomass and Produced Water: For Biomaterial and a

Lithium Source

by

Kalin G. Hanson

Herein, I present two main ideas that aim to utilize two different waste feedstocks,

lignocellulosic biomass and produced water. While they are fundamentally different, they

both offer an opportunity to take advantage of a waste product for environmentally relevant

study.

Aromatic molecules are essential to many mass-produced polymers, like polystyrene,

epoxy resins, and poly(ethyleneterephthalate) (PET). The monomer precursors for these

polymers are largely sourced from petroleum. Chemicals like benzene, toluene, and xylene

are common products of refineries and critical to polymer synthesis. Herein, I present lignin,

a component of lignocellulosic biomass, and a naturally occurring aromatic macromolecule

as a viable feedstock for aromatic monomers. I will introduce novel renewable polyesters and

bio-derived thermosets from the lignin-derived molecule isoeugenol. Thermal properties of

these renewable polyesters are tunable to those of industrially relevant polyesters like PET.

Further, a bio-derived epoxide was synthesized, and the polyester active esters were utilized

to create crosslinked thermoset networks that give predictable thermal and mechanical

properties.

I will also discuss the potential use of produced water, a waste stream from the oil

and gas industry, as a lithium source. With the need for energy storage rising, lithium is a

resource that will continue to be in high demand. I will introduce two different membrane

systems, and the synthesis of several ion selective ligands for each system. The incorporation of 12-crown-4 ether into the membrane framework was thought to selectively bind lithium, yet we saw reverse LiCl/NaCl permeability selectivity from the expected results. This gave insights into the fundamental relationship between Li^+ and 12-crown-4 ether in aqueous environments. Building on that result, more ligands were synthesized to investigate both crown ether size and linker length on the ion transport properties of the membranes.

Table of Contents

Chapter 1

Introduction: Lignin as a Feedstock for Polymer Building Blocks

1.1 Motivation

A multitude of polymers that we encounter every day includes aromatic backbones. This includes poly(ethyleneterephthalate) (PET), polystyrene, and many epoxy resins. The petroleum industry has been the main feedstock of aromatic molecules, providing molecules like phenol and *p*-xylene as polymer building blocks.[1] As the need to lessen our reliance on fossil fuels has increased exponentially over recent years, so too has the need to find a suitable replacement feedstock for these aromatic molecules. One of the most promising sustainable feedstocks is non-food lignocellulosic biomass.

Lignocellulosic biomass is a waste product of many industries, such as agriculture, forestry, and paper.[2] It can also be obtained from fast-growing woody plants like poplar, willow, elephant grass, and bamboo.[3] These woody plants require fewer resources and less desirable land to grow compared to most vegetable crops, which indicates the cultivation of these plants would have little impact on the food industry.[3] In addition to extracting lignin for phenolic monomers from these plants, the cellulosic components can be broken down into sugars. These sugars can be fermented into fuels like ethanol or further reacted to obtain value-added chemicals. Lignocellulosic biomass in its entirety can also be used as an energy source via combustion, gasification, or pyrolysis.[4-8] Therefore, lignocellulosic biomass is readily available in large quantities as waste, supply can be sustainably maintained via fast-growing plants, and has a variety of uses that could supplement or replace petroleum feedstocks. This chapter will introduce lignin as a feedstock, discuss the process of isolating

and breaking it down into usable monomers, and report on some previous studies using lignin-derived monomers for polymer synthesis.

1.2 Lignin: Nature's Phenolic Macromolecule

In the cell wall, the three main components are lignin, hemicellulose, and cellulose. Representative structures of these components can be seen in Figure 1.1. It should be noted that for any specific biomass, the composition of lignin, cellulose, and hemicellulose will vary. Lignin generally ranges from 10-40%, cellulose 35-50%, and hemicellulose 15-35%.[9,11]
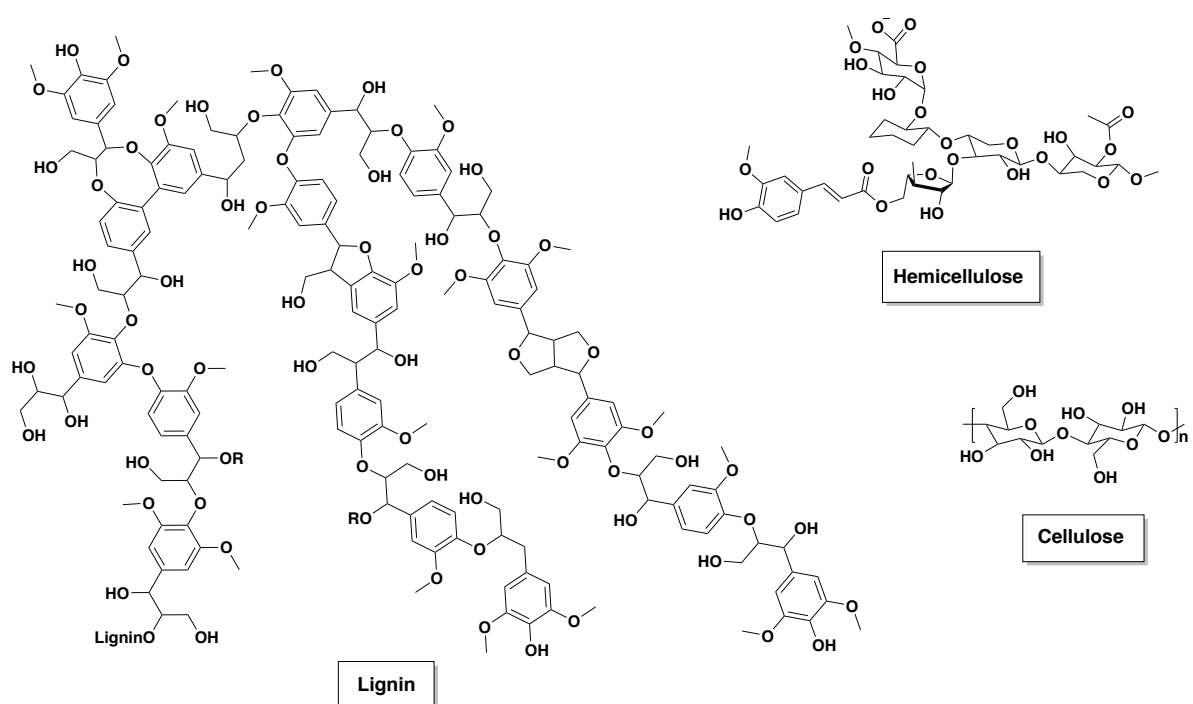
Figure 1.1. Representative structures of lignin, hemicellulose, and cellulose.

Both cellulose and hemicellulose are sugar-based macromolecules, with cellulose being a β(1,4)-linked glucose chain, and hemicellulose being composed of a variety of sugars (arabinose, galactose, glucose, mannose, and xylose). These cellulosic components of biomass have been studied and used for the production of a number of compounds including furans, polyols, carboxylic acids, ethanol, and lactones.[12-14] One of the most notable

2

compounds obtained from cellulose is hydroxymethyl furfural (HMF), which has been used to synthesize poly(ethylenefuranoate) as a bio-derived plastic material.[15-17]

Lignin, however, has been shown to give phenolic monomers that are very similar or the same as monomers currently obtained from petroleum.[18-23] The successful extraction of these monomers from lignin could mean that lignin could directly replace or supplement petroleum as a feedstock for such monomers. This will not be possible until an economically feasible technique is developed, which is one reason why there has been an outpouring of work done investigating various techniques and the results.

1.3 Lignin Isolation and Depolymerization into Small Molecules

To obtain the variety of aromatic monomers available from lignin, lignin has to be isolated from the other components of biomass, and then further depolymerized into usable monomeric units. There have been various techniques used for both the isolation and depolymerization of lignin that will be discussed in this chapter.

1.3.1   Lignin Isolation Techniques

Lignin isolation starts from the raw biomass, which is commonly either wood chips or grasses. Currently, there are four main techniques for lignin isolation, Kraft, Sulfite, Soda, and organosolv.

The Kraft process is the main form of chemical pulping, and the most dominant process to obtain lignin. It involves using an aqueous sodium hydroxide (NaOH) and sodium sulfide (Na_2S) solution, called white liquor, to treat the lignocellulosic biomass. This is done at temperatures that range from 423-253 K for 1-2 hr. After this reaction, cellulose is separated from the liquid portion, the black liquor. This black liquor contains hemicellulose and lignin. The lignin is soluble because of the ionization of the phenolic groups present.

3

This lignin-rich portion is obtained by either evaporation or acidification of the black liquor.[24-28]

Sulfite lignin is generated by using sulfur dioxide and/or bisulfate ions to react with the lignin, forming sulfonated lignin. The sulfonate groups attached to the lignin make it water soluble. This process, compared to the Kraft Process, is done at a lower temperature and for longer times. Though it can yield lignin with high molecular weight, the resultant lignin is often impure.[27-30]

The soda process, like the Kraft process, uses NaOH as the main cooking reagent. However, unlike the Kraft process, soda puling does not use sulfur containing compounds. It is also mainly used for non-wood biomass. The basic aqueous liquid promotes hydrolytic cleavage of the lignin linkages and deprotonates the phenols found in lignin. This results in smaller, soluble lignin fragments. These fragments can then be precipitated out of solution by the addition of acid to obtain a mixture of lignin fragments.[28, 31, 32]

The organosolv process for lignin extraction uses organic solvents to treat the biomass. This liquid can be acetic acid, formic acid, ethanol, peroxide, etc. This process avoids the use and generation of sulfur containing products, gives low molecular weight lignin, and can produce high purity cellulose, hemicellulose, and lignin. The main restraint on this process is its economic feasibility due to the use of organic solvents and multiple separation steps.[26, 33] Example structures of lignin obtained from each technique can be seen

in Figure 1.2.
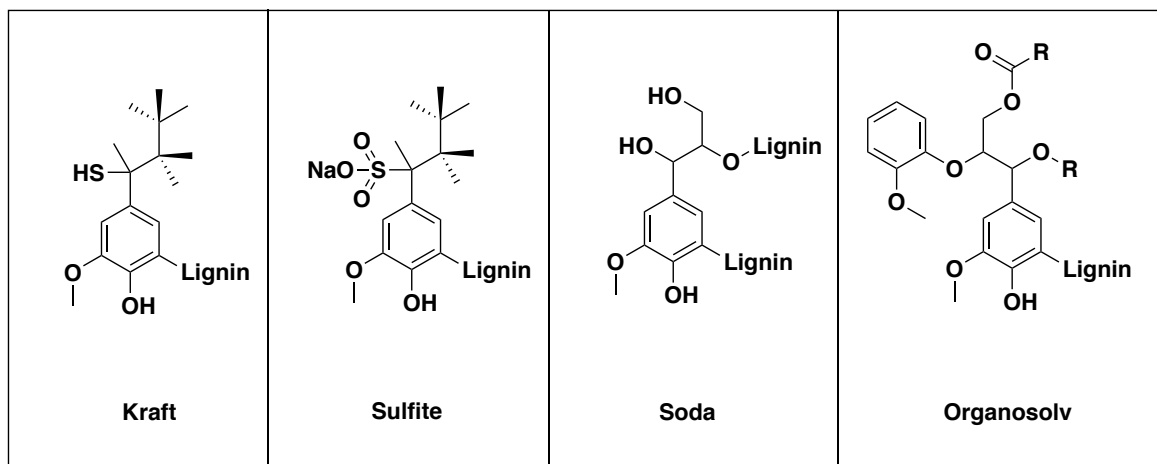
Figure 1.2. Representative structures of the lignin obtained from the four isolation techniques (Kraft, Sulfite, Soda, and Organosolv). Figure adapted from Kai et al.[33]

1.3.2   Lignin Depolymerization Techniques

Once lignin is isolated from cellulose and hemicellulose it must still be depolymerized into usable oligomers and monomers. Smaller fragments mean better solubility, lower viscosity, and increased similarity to common polymer precursors and fuels. The depolymerization of lignin has been a major field of study in recent years. To depolymerize lignin, the ether linkages are targeted because they are easier to break compared to C-C bonds. Common linkage structures found in lignin are shown in Figure 1.3. The most common linkage is the β-O-4 linkage. In order to target these linkages, a variety of techniques have been developed including catalytic, thermal, and hydrothermal processes.
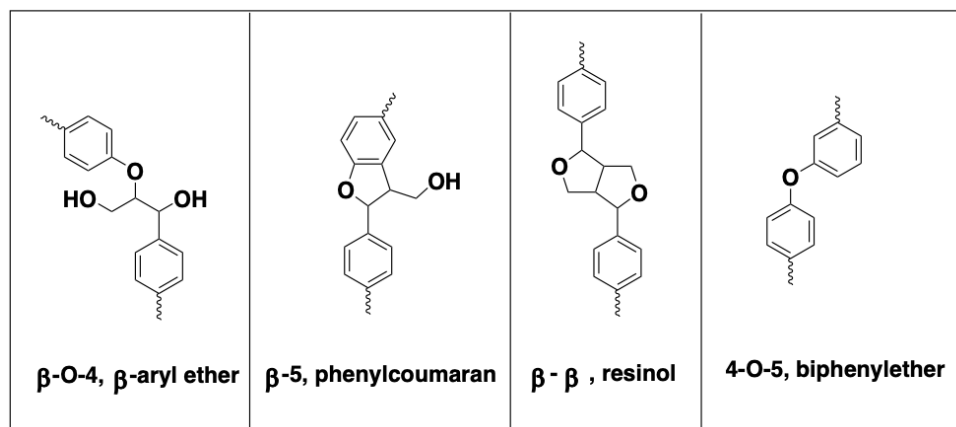
Figure 1.3. Representative structures of the major linkages present in lignin.

Lignin depolymerization is often a thermochemical process and can occur via a variety of mechanisms including pyrolysis, oxidation, and combustion.[34] The majority of the processes discussed also utilize a catalyst to improve yield and selectivity, whether it be metallic, acidic, or basic.

The most studied cleaving mechanism is pyrolysis, which can take many forms. "Neat" pyrolysis (thermolysis) simply relies on the thermal decomposition of lignin at high temperatures (250 °C -1000 °C) in the absence of oxygen.[34] Given the different linkages present in lignin, which will decompose at different temperatures there is some selectivity that is possible using pyrolysis depending on the temperature. Additionally, introducing a catalyst will affect both overall yield and selectivity. However, pyrolysis creates undesirable byproducts like char, which can inhibit further processing of the lignin monomers particularly when catalysts are added.[35-37]

Hydrogenolysis shares many similarities with neat pyrolysis, the difference being the addition of a hydrogen source. This mechanism involves either hydrogen gas or a hydrogen-donating solvent to be the hydrogen source. Methanol and isopropanol are hydrogen-donating solvents that are often used. Hydrogenolysis reactions commonly also utilize a

6

heterogeneous catalyst.[19, 34, 38-44] Hydrogenolysis is often preferred to neat pyrolysis due to higher conversion, higher yield, and lower char formation.[34]

Another cleaving mechanism is oxidation, which takes advantage of the hydroxyl groups present in the structure of lignin. The target of the majority of oxidative cleavage of lignin studies is obtaining aldehyde-containing molecules, like vanillin. Though hydrogen peroxide can be used as the main reagent or combined with ferrous sulfate to create Fenton's reagent, the targeted aldehyde molecules are intermediate species that are quickly degraded further into carboxylic acid species like oxalic, formic, and acetic acid.[45,46] To target aldehyde products mild oxidants like nitrobenzene, metal oxides, and oxygen are used.[47-50]

Supercritical liquids have also been used for the depolymerization of lignin, with water commonly being used as the solvent. A supercritical fluid is a liquid that is above the critical point for temperature or pressure. The depolymerization of lignin under supercritical liquids has been shown to be a viable process, though often requires the addition of an organic co-solvent and/or a catalyst to achieve high conversion.[51-57] The formation of char when using a supercritical fluid is another aspect of this method for consideration.

1.3.3   Monomers Obtained from Lignin

Lignin can provide a wide variety of aromatic and phenolic monomers once depolymerized. Changing the isolation technique, depolymerization technique, reaction conditions, or starting biomass will change the type of monomers obtained and/or the ratios of the monomers obtained. Figure 1.4 shows the general structures of some monomers that are obtained from lignin.[19, 58-60] These monomers include alkyl aromatics as well as aromatic alcohols, carboxylic acids, and aldehydes. Many of these monomers are oxygen-containing,

which is beneficial for many polymer studies but would have to be deoxygenated in order to be used for hydrocarbon applications like fuels.
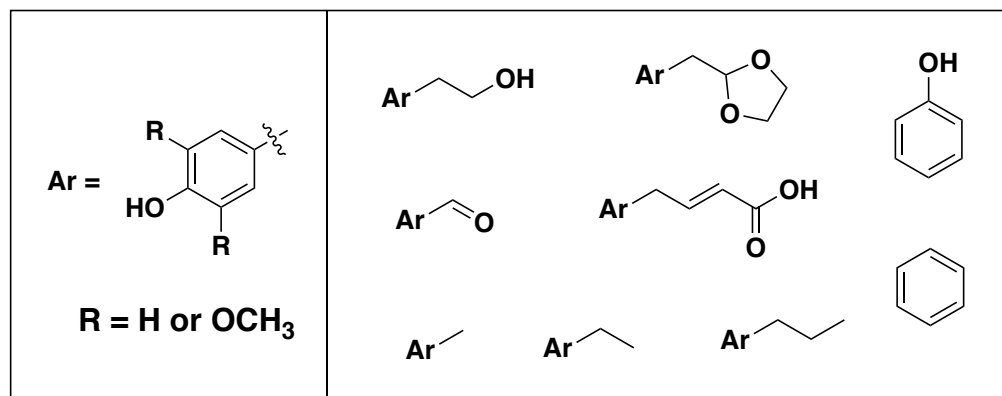
Figure 1.4. General structures of common monomers obtained from lignin.

While Figure 1.4 gives general structures for lignin-derived monomers, the full scope of monomers is immense. Notable in regard to this thesis is the phenol-like monomers. This includes molecules such as phenol, isoeugenol, eugenol, and propyl syringol. Phenol itself is largely being sourced from petroleum and is used as a precursor to molecules such as cyclohexanone and bisphenol A (BPA). While it has been shown that phenol can be derived from lignin, yield, purity, and financial viability are all obstacles that need to be addressed before lignin can supplement petroleum as a phenol source.

1.4 Lignin-Derived Molecules Used in Polymer Studies

Being a readily available, sustainable feedstock for phenolic monomers, lignin has been a topic of great interest in the field of bio-based polymers. The abundance of phenols leads to easy polymerization as well as functionalization. Other functional groups like carboxylic acids, hydroxyl groups, and aldehydes are also viable options for polymerization and

functionalization. Additionally, the methoxy groups present in many of the monomers can be

easily demethylated to yield catechol moieties or even triphenols.

1.4.1 Polyesters

When you think of polyesters, a variety of objects come to mind, such as plastic

bottles, disposable food containers, fabric, rugs, etc. While there are many different

polyesters, poly(ethyleneterephthalate) (PET) is often used synonymously with the word

polyester. PET consists of two monomers, terephthalic acid and ethylene glycol. Terephthalic

acid is an aromatic molecule that is synthesized from *p*-xylene, which is sourced from

petroleum. Due to the aromatic structure of lignin, there has been a multitude of work

utilizing lignin-based molecules as polyester building blocks to produce PET-like polyesters.

Lignin-derived polyesters are often extremely brittle because of the rigid aromatic

structure, so the addition of a less rigid component is often attractive. Poly(caprolactone)

(PCL) has been used in multiple instances as an additive to lignin to address the brittleness.

In addition to adding a less rigid chain, PCL also extends the hydroxyl functionality away

from the complex lignin structure, allowing it to be more easily accessed and reacted with.

Poly(lacticacid) (PLA) is another polymer that has been used with lignin as a copolymer.[61-66]

There has also been work done by Nguyen et al. that used lignin-derived phenols during PCL

and PLA polymerization to increase the glass transition temperature, T_g.[67] Other studies that

modify and crosslink lignin utilize polybutadiene (PBD) to synthesize lignin-derived

polyesters.[68,69] Succinic anhydride has also been used to functionalize lignin, and the

succinylated lignin underwent self-crosslinking creating a thermosetting polyester coating.[70]

Lignin-derived compounds such as vanillin, syringaldehyde, and ferulic acid have

also been used extensively to create PET-like polyesters. Some examples include Mialon et

al. who used vanillin and acetic anhydride to create a polyester that had similar thermal properties to PET.[71] They also published a study that used benzoic acid derivatives of lignin-derived compounds to synthesize polymers with alternating aromatic and aliphatic segments, which allows thermal tunability based on the aliphatic chain length.[72] Gioia et al. synthesized a similar series of poly(ethylenevanillate) derivatives using caprolactone and ethylene carbonate. They were still able to tune thermal properties by varying the feed ratios of caprolactone and ethylene carbonate.[73] Kreye et al. employed ferulic acid monomers and fatty acid derivatives to synthesize a renewable polyester.[74] Figure 1.5 shows an example of a synthetic route from ferulic acid and vanillin to lignin-derived polyesters.[74,75]
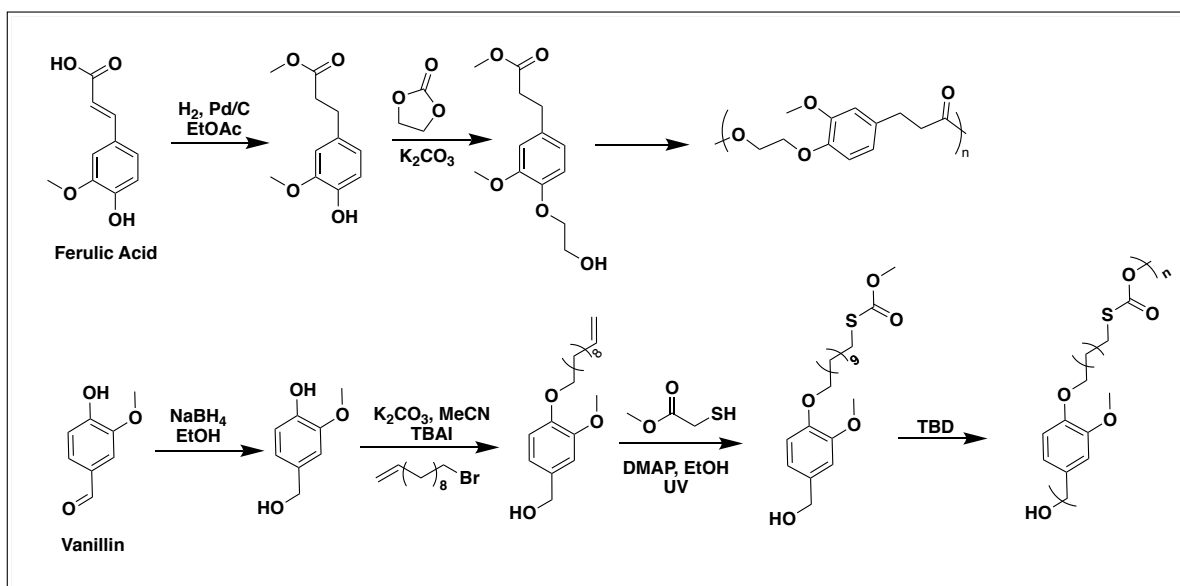
Figure 1.5. Synthetic route from ferulic acid (top) and vanillin (bottom) to lignin-derived polyesters. TBD = 1,5,7-triazabicyclo[4.4.0]dec-5-ene, a catalyst. Adapted from Llevot et al.[76]

In addition to being synthesized into nonsymmetrical monomers, many lignin-derived molecules can be coupled into difunctional, symmetrical monomers. When coupled, the resulting product is often a bisphenol, having a phenol group on either side of the molecule. These bisphenols work well for polyester synthesis due to their reactivity and tunability.

10

Figure 1.6 shows some possible routes to bisphenol from vanillin and a ferulic acid derivate with a variety of linking moieties.[77,78] The ability to introduce these linkers between the phenols allows for polymer property tunability and optimization. Bisphenols can easily undergo polycondensation reactions to synthesize polyesters with difunctional carboxylic monomers,[79-83] and can even be further modified for use in other polymer systems, like epoxy thermosets.
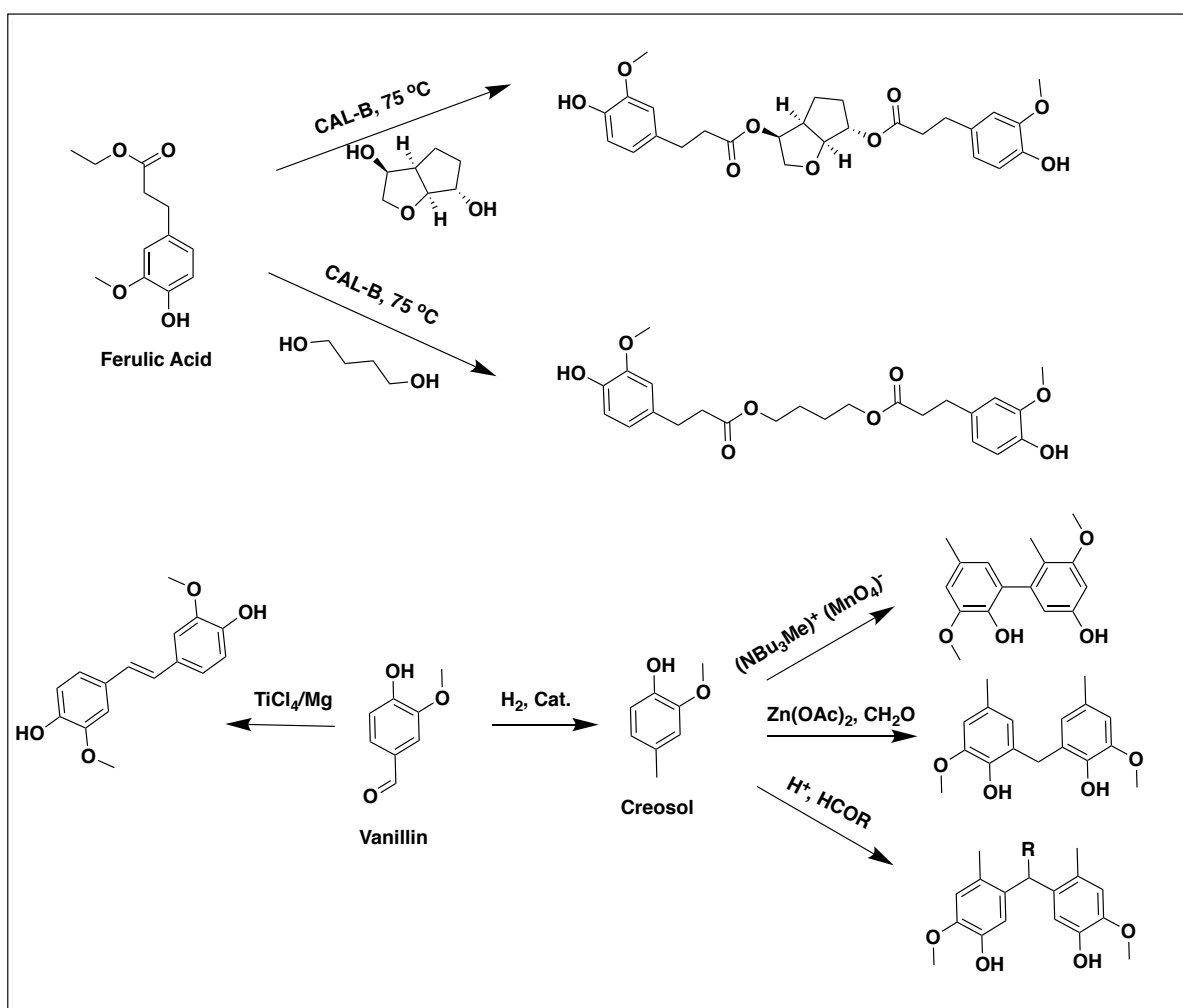
Figure 1.6. Synthetic route from ferulic acid (top) and vanillin (bottom) to lignin-derived bisphenols. Adapted from Llevot et al.[76]

1.4.2 Epoxy Thermosets

Epoxy thermosets are desirable for their characteristics, which include high strength as well as chemical, corrosion, and electrical resistance. They have a wide variety of applications including electronics, floorings, coatings, adhesives, and wind turbines.[84] Bisphenol A (BPA), and the corresponding glycidyl ether (DGEBA) is used for the majority of epoxy resin production. In addition to being sourced from petroleum-based phenol, there have been reproductive health risks associated with BPA, an endocrine disruptor.[85] This has driven many to look for a biobased, sustainable source of similar aromatic molecules. There is extensive work in the field of lignin-based epoxy thermosets, due to the aromatic structure of lignin. An epoxide group can be easily attached to a molecule that contains either a hydroxyl group or a double bond. Both these general reactions are shown in Figure 1.7. In the case of lignin and lignin-derived monomers, these groups are in abundance. Also, as discussed previously, many lignin-derived monomers can be coupled into bisphenols, or demethylated to allow for di- or tri-functional epoxides.
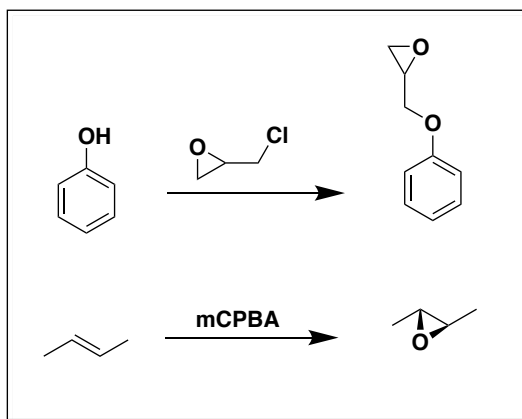
Figure 1.7. General epoxidation reactions utilizing epichlorohydrin (top) or mCPBA (bottom) as the epoxide source.

Various lignin-derived phenols such as eugenol,[86-89] dihydroeugenol,[90,91] isoeugenol,[92,93] n-propylsyringol,[94] guaiacol,[95] and vanillin[96-102] have been used to create epoxides. Depolymerized lignin oligomers[103-107] and technical lignin[108-113] have also been used. Some example structures of epoxidized lignin monomers are shown in Figure 1.8.
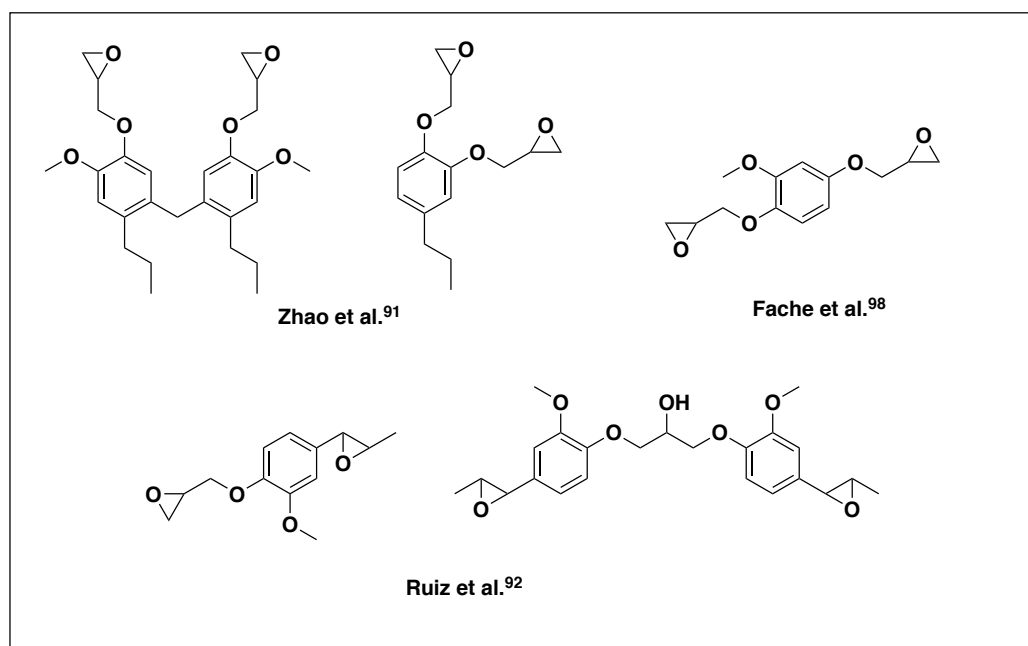
Figure 1.8. Some examples of lignin-derived epoxides.

The structure of lignin-derived monomers lends itself well to the synthesis of lignin-derived epoxides due to the abundance of moieties that allow for facile functionalization, including phenol, aldehyde, allyl, and carboxylic acid groups. The lignin-based epoxide monomers can then be crosslinked utilizing multifunctional amines or anhydrides to form the thermoset networks. Properties of these thermosets can be tuned by varying the amine:epoxy ratio, crosslinker used, and the addition of fillers.

1.4.3 Carbon Fibers

Carbon fibers are known for their strength-to-weight ratio. They are able to maintain high stiffness, strength, temperature tolerance, and chemical resistance while maintaining a relatively light weight compared to other materials. Approximately 90% of carbon fibers are produced from the precursor polyacrylonitrile (PAN).[114] While this gives high performance, both PAN and the production are expensive. Introducing more high-performance carbon fibers into the market as well as increasing production volume can help lower the cost. Lignin represents a feedstock with high potential to supplement the carbon fiber market.[115] While lignin has not been able to produce carbon fibers suitable for aerospace applications, there is a large automotive market for low-cost carbon fibers.[116] There are many advantages to replacing PAN with a lignin precursor – independence from fossil fuels, minimal toxicity, reduced CO_2/kg fiber, and high carbon yield.[115] In order to synthesize a carbon fiber, lignin must go through multiple processing steps; extrusion, oxidation, and carbonization.

The most common method of extrusion for lignin is melt-spinning. Melt spinning is a process in which the lignin, or polymer, is melted and extruded through a spinneret that has holes in the bottom. After the fibers of lignin flow through the holes, they are immediately exposed to cold air to solidify the strands.[117] These strands are referred to as the lignin green fiber. Melt-spinning is a preferred extrusion process because it does not require other components such as solvents or additives. Some carbon fiber precursors, like PAN, are unable to be melt spun.

Once the lignin green fiber is obtained, it undergoes oxidation, also called thermostabilization. This is to increase the glass transition temperature (T_g) of the fiber to avoid softening before the higher temperatures of the carbonization step. To increase the T_g, oxidized groups are introduced to crosslink the lignin, removing thermoplastic behavior.[118]

This process must be done at slow heating rates so that the oxidation and subsequent crosslinking can occur to increase the T_g faster than the temperature increases.[118] The optimal temperature range for the thermostabilization of lignin green fiber is 260 °C – 290 °C.[119] Compared to PAN, lignin green fibers require lower temperature and less time to stabilize.

Once stabilized, the lignin fibers undergo carbonization under an inert atmosphere at temperatures up to 1000 °C. The carbonation step consists of a significant loss in mass due to the loss of functional groups. The total carbon yield from lignin green fibers has been reported to be 30-50%.[116, 120, 121] Lignin-based carbon fibers have been produced from neat lignin,[120, 122, 123] lignin-polymer blends,[120, 124-128] mixtures of hardwood and softwood lignins,[129,130] functionalized lignin,[131-136] and lignin with added fillers.[137]

1.4.4 Polyurethanes

Polyurethanes are synthesized via the reaction between a polyol and diisocyanate. This process usually also includes a catalyst and other additives. The wide range of polyols and diisocyanates available mean that polyurethane properties can be tailored to a broad spectrum of applications. These applications include coating, adhesives, sealants, elastomers, foams, and textiles.[138]

Despite having an abundance of hydroxyl groups, due to the complex structure of lignin many of these hydroxyl groups are hindered from participating in polymerization. Lignin also produces polyurethanes that do not have well defined hard and soft segments, due to dispersity, solubility, and impurities.[139-143] Studies that have used lignin directly as a polyol source we able to produce polyurethanes, but they were generally rigid and brittle because of the stiffness of lignin as well as commonly used diisocyanates.[144,145]

15

To better use lignin for polyurethane synthesis, it can be used as a co-polyol with long chain polyols. Some lignin-derived polyurethanes utilize vegetable-oil based polyols to incorporate "softer" segments into the rigid, aromatic lignin structure.[146,147] Others utilize industrially used polyols like poly(ethyleneglycol) or poly(propyleneglycol).[148-151]

Other ways to combat the brittleness of lignin-based polyurethanes include fractionating lignin into lower dispersity fractions, depolymerizing lignin into oligomers, and chemically modifying lignin. Utilizing fractionated lignin, both soft and hard polyurethanes have been produced.[152-159] Depolymerized lignin gives the advantage of lower molecular weight, and more functionality.[160,161] The lignin oligomers have been used to synthesize polyurethane foams,[162-164] and in some cases elastomers.[165] Further, chemical modification of lignin enables a more effective way to incorporate lignin into polyurethanes by increasing solubility, improving reactivity, and decreasing brittleness.[147] The main modification of lignin for polyurethane production is hydroxyalkylation to transform the phenolic hydroxyl groups to aliphatic hydroxyl groups, which are more reactive with isocyanate groups for polyurethane synthesis.[166] Hydropropyl lignin has been used for synthesizing rigid polyurethane foams.[167-170] Other modifications such as dealkylation,[171,172] esterification,[173,174] nitration,[175,176] and amination[177,178] have also been employed to obtain lignin-derived polyurethanes.

1.5 Conclusion

Lignin is a renewable feedstock that can be sustainably sourced from industry waste and fast-growing plants that shows great promise as an alternate aromatic monomer source. The studies of isolation, depolymerization, and utilization of lignin and lignin-derived monomers continue to be research topics of great interest. Though many approaches have been

developed for the depolymerization of lignin, but there is still a considerable economic burden to overcome in order for lignin to realistically supplement petroleum as an aromatic monomer feedstock. This being said, there is still a vast area of potential in exploring novel lignin-based monomers and polymers. Numerous studies have been done on a broad spectrum of lignin-based polymers, and there are still many areas in that field that have yet to be fully explored. The focus of chapter 2 and chapter 3 of this dissertation is the modification, utilization and polymerization of lignin-derived phenol, isoeugenol.

1.6 References

1.   Hopewell, J.; Dvorak, R.; Kosioer, E., Plastics recycling: challenges and opportunities. *Phil. Trans. R. Soc. B,* **2009**, *364*, 2115-2126.

2.   Biomass--Renewable Energy from Plants and Animals, 2018. Available at: https://www.eia.gov/energyexplained/?page=biomass_home. Accessed on June 2021.

3.   Potters, G.; Van Goethem, D.; Schutte, F., Promising Biofuel Resources: Lignocellulose and Algae. *Nature Education*, **2010**, *3(9)*, 14.

4.   Oak Ridge National Laboratory. "Bioenergy conversion factors." Oak Ridge, TN. **2006**

5.   Mabee, W. E.; Gregg, D. J.; Arato, C.; Berlin, A.; Bura, R.; Gilkes, N.; Mirochnik, O.; Pan, X.; Pye, E. K.; Saddler, J. N., Update on softwood-to-ethanol process development. *Applied Biochem. and Biotech,* **2006**, *29*, 55-70.

6.   Sims, R. E. H.; Mabee, W.; Saddler, J. N.; Taylor, M., An overview of second generation biofuel technologies. *Bioresource Tech,* **2010**, *101*, 1570-1580.

7.   Bridgwater, A. V.; Meier, D.; Radlein, D., An overview of fast pyrolysis of biomass. *Organic Geochemistry*, **1999**, *30*, 1479-1493.

8.   Lu, Q.; Li, W. J.; Zhu, X. F., Overview of fuel properties of biomass fast pyrolysis oils. *Energy Conservation and Management*, **2009**, *50*, 1376-1383.

9.   Wei, H.; Yan, Y. T.; Yi, W. S.; Tang, J. H., Lignocellulosic Biomass Valorization: Production of Ethanol. In *Encylopedia of Sustainable Technologies*; edited by Martin A. Abraham; Hangzhou Dianzi University, China, 2017; Vol. 3, pp 601-604.

10.   Peng, F.; Ren, J. L.; Xu, F.; Bian, J.; Peng, P.; Sun, R. C., Fractional Study of Alkali-Soluble Hemicelluloses Obtained by Graded Ethanol Precipitation from Sugar Cane Bagasse. *J. Agric. Food Chem.*, **2010**, *58(3)*, 1768-1776.

11.   Naseem, A.; Tabasum, S.; Zia, K. M.; Zuber, M.; Ali, M.; Noreen, A., Lignin-derivatives based polymers, blends and composites: A review. *International Journal of Biological Macromolecules*, **2016**, *93*, 296-313.

12.   Jing, Y.; Guo, Y.; Xian, Q.; Liu, X.; Wang, Y., Catalytic Production of Value-Added Chemicals and Liquid Fuels from Lignocellulosic Biomass. *Chem*, **2019**, *5*, 2520-2546.

13.   Song, J.; Fan, H.; Ma, J.; Han, B., Conversion of glucose and cellulose into value-added products in water and ionic liquids. *Green Chemistry*, **2013**, *15*, 2619-2635.

14.   Wu, Z.; Ge, S.; Ren, C.; Zhang, M.; Yip, A.; Xu, C., Selective conversion of cellulose into bulk chemicals over Brønsted acid-promoted ruthenium catalyst: one-pot vs. sequential process. *Green Chemistry*, **2012**, *14*, 3336-3343.

15. Rosenboom, J. G.; Hohl, D. K.; Fleckenstein, P.; Storti, G.; Morbidelli, M., Bottle-grade polyethylene furanoate from ring-opening polymerization of cyclic oligomers. *Nature Communications*, **2018**, *9*, 2701-2707.

16. Burgess, S. K.; Leison, J. E.; Kraftschik, B. E.; Mubarak, C. R.; Kriegel R. M.; Koros, W. J., Chain Mobility, Thermal, and Mechanical Properties of Poly(ethylene furanoate) Compared to Poly(ethylene terephthalate). *Macromolecules,* **2014**, *47*, 1383-1391.

17. EUR 25 Million Subsidy Granted: Industry Consortium Receives Funds for Polyethylene Furanoate (PEF), 2017. Available at: https://www.synvina.com/news/eur-25-million-subsidy-granted-industry-consortium-recei ves-funds-polyethylenfuranoate-pef/. Accessed June 2021.

18. Zhu, H.; Chen, Y.; Qin, T.; Wang, L.; Tang, Y.; Sun, Y.; Wan, P., Lignin depolymerization via an integrated approach of anode oxidation and electro-generated H2O2 oxidation. *RSC Advances*, **2014**, *4*, 6232-6238.

19. Luo, H.; Klein, I. M.; Jiang, Y.; Zhu, H.; Liu, B.; Kenttamaa, H. I.; and Abu-Omar, M. Total Utilization of Miscanthus Biomass, Lignin and Carbohydrates, Using Earth Abundant Nickel Catalyst. *ACS Sustainable Chem. Eng.,* **2016**, *4*, 2316-2322.

20. Galkin, M. G. and Samec, J. S. M., Selective Rouse to 2-Propenyl Aryls Directly from Wood by a Tandem Organosolv and Palladium-Catalyzed Transfer Hydrogenolysis. *ChemSusChem*, **2014**, *7*, 2154-2158.

21. Galkin, M. G.; Smit, A. T.; Subbotina, E.; Artemenko, K. A.; Bergquist, J.; Huijgen, W. J. J.; Samec, J. S. M., Hydrogen-free catalytic fractionation of woody biomass. *ChemSusChem,* **2016**, *9*, 3280-3287.

22.   Jastrzebski, R.; Constant, S; Lancefield, C. S.; Westwood, N. J.; Weckhuysen, B. M.; Bruijnincx, P. C. A., Tandem Catalytic Depolymerization of Lignin by Water-Tolerant Lewis Acids and Rhodium Complexes. *ChemSusChem*, **2016**, *9*, 2074-2079.

23.   Xiao, L. P.; Wang, S.; Li, H.; Li, Z.; Shi, Z. J.; Xiao, L.; Sun, R. C.; Fang, Y.; Song, G., Catalytic Hydrogenolysis of Lignins into Phenolic Compounds over Carbon Nanotube Supported Molybdenum Oxide. *ACS Catal.*, **2017**, *7*, 7535-7542.

24.   Cheremisinoff, N. P.; Rosenfeld, P. E., Chapter 6: Sources of air emission from pulp and paper mills. In *Handbook of Pollution Prevention and Cleaner Production*, **2010**, pp 179-259.

25.   Ahmad, E.; Pant, K. K., Chapter 14: Lignin Conversion: A Key to the Concept of Lignocellulosic Biomass-Based Integrated Biorefinery. In *Waste Biorefinery*, **2018**, pp 409-444.

26.   Luo, H.; Abu-Omar, M. M., Sustainable Energy Technologies and Sustainable Chemical Processes. In *Encyclopedia of Sustainable Technologies,* edited by Martin A. Abraham; Hangzhou Dianzi University, China, 2017; Vol. 3, pp 573-585.

27.   Froass, P. M.; Ragauskas, A. J.; Jiang, J., Chemical structure of residual lignin from kraft pulp. *Journal of Wood Chemistry and Technology*, **1996**, *16(4)*, 347-365.

28.   Windeisen, E.; Wegener, G., Polymers for a Sustainable Environment and Green Energy. In *Polymer Science: A Comprehensive Reference*, edited by Krzysztof Matyjaszewski and Martin Möller; **2012**, pp 255-265.

29.   Hintz, H. L., Paper: Pulping and Bleaching. In *Encylopedia of Materials: Science and Technology*, edited by K. H. Jürgen Buschow, Merton C. Flemings, Edward J.

Kramer, Patrick Veyssière, Robert W. Cahn, Bernhard, Ilschner, and Subhash Mahajan; **2001**, pp 6707-6711.

30.   Glasser, W. G., Lignin-based Polymers. In *Encyclopedia of Materials: Science and Technology*, edited by K. H. Jürgen Buschow, Merton C. Flemings, Edward J. Kramer, Patrick Veyssière, Robert W. Cahn, Bernhard, Ilschner, and Subhash Mahajan; **2001**, pp 1-4.

31.   Bajpai, P., Chapter 12: Pulping Fundamentals. In *Biermann's Handbook of Pulp and Paper (Third Edition)*, pp 295-351.

32.   Vishtal, A.; Kraslawaski, A., Challenges in Industrial Application of Technical Lignins. *Bioresources*, **2011**, *6(3)*, 3547-3568.

33.   Kai, D.; Tan, M. J.; Chee, P. L.; Yap, Y. L.; Loh, X. J., Towards lignin-based functional materials in a sustainable world. *Green Chemistry*, **2016**, *18*, 1175-1200.

34.   Pandey, M. P.; Kim, C. S., Lignin Depolymerization and Conversion: A Review of Thermochemical Methods. *Chem. Eng. Technol.*, **2011**, *34(1)*, 29-41.

35.   Amen-Chen, C.; Pakdel, H.; Roy, C., Production of monomeric phenols by thermochemical conversion of biomass. *Bioresour. Technol.,* **2001**, *277*, 277-299.

36.   Liu, C.; Hu, J.; Zhang, H. Y.; Xiao, R., Thermal conversion of lignin to phenols: relevance between chemical structure and pyrolysis behaviors. *Fuel*, **2016**, *182*, 864-870.

37.   Hu, C. S.; Zhang, H. Y.; Xiao, R., Effects of nascent char on ex-situ catalytic fast pyrolysis of wheat straw. *Energy Convers. Manag.*, **2018**, *117*, 765-772.

38.   Huber, G. W.; Iborra, S.; Corma, A., Synthesis of transportation fuels from biomass: Chemistry, catalysts, and engineering. *Chem. Rev.,* **2006**, *8*, 313.

39. Zhou, C. H.; Xia, X.; Lin, C. X.; Tong, D. S.; Beltramini, J., Catalytic conversion of lignocellulosic biomass to fine chemicals and fuels. *Chem. Soc. Rev.*, **2011**, *40*, 5588-5617.

40. Wang, H.; Tucker, M.; Ji, Y., Recent Development in Chemical Depolymerization of Lignin: A Review. *Journal of Applied Chemistry*, **2013**, *9*

41. Ma, H.; Li, H.; Zhao, W.; Li, L.; Liu, S.; Long, J.; Li, X., Selective depolymerization of lignin catalyzed by nickel supported on zirconium phosphate. *Green Chemistry*, **2019**, *21*, 658-668.

42. Zhai, Y.; Li, C.; Xu, G.; Ma, Y.; Liu, X.; Zhang, Y., Depolymerization of lignin via a non-precious Ni-Fe alloy catalyst supported on activated carbon. *Green Chemistry*, **2017**, *19*, 1895-1903.

43. Jiang, B.; Hu, J.; Qiao, Y.; Jiang, X.; Lu, P., Depolymerization of Lignin over a Ni-Pd Bimetallic Catalyst Using Isopropanol as an in Situ Hydrogen Source. *Energy Fuels*, **2019**, *33(9)*, 8786-8793.

44. Klien, I.; Saha, B.; Abu-Omar, M. M., Lignin depolymerization over Ni/C catalyst in methanol, a continuation: effect of substrate and catalyst loading. *Catal. Sci. Technol.,* **2015**, *5*, 3242-3245.

45. Bentivenga, G.; Bonini, C.; Auria, M. D.; Bona, A. D., Degradation of steam-exploded lignin from beech by using Fenton's reagent. *Biomass Bioenergy*, **2003**, *24*, 233-238.

46. Xiang, Q.; Lee, Y. Y., Oxidative cracking of precipitated hardwood lignin by hydrogen peroxide. *Applied Biochemistry and Biotechnology*, **2000**, *84*, 153-162.

47.   Villar, J. C.; Caperos, A.; Garcia-Ochoa, F., Oxidation of Hardwood Kraft-Lignin to

Phenolic Derivatives. Nitrobenzene and Copper Oxide as Oxidants. *Journal of Wood

Chemistry and Technology*, **1997**, *17(3)*, 259-285.

48.   Villar, J. C.; Caperos, A.; Garcia-Ochoa, F., Oxidation of hardwood kraft-lignin to

phenolic derivatives with oxygen as oxidant. *Wood Science and Technology*, **2001**,

35, 245-255.

49.   Xiang, Q.; Lee, Y. Y., Production of oxychemicals from precipitated hardwood

lignin. *Applied Biochemistry and Biotechnology*, **2001**, *91*, 71-80.

50.   Voitl, T.; von Rohn, P. R., Demonstration of a Process for the Conversion of Kraft

Lignin into Vanillin and Methyl Vanillate by Acidic Oxidation in Aqueous Methanol.

Ind. Eng. Chem. Res., **2010**, *49(2)*, 520-525.

51.   Ehara, K.; Takada, D.; Saka, S., GC-MS and IR spectroscopic analyses of the lignin-

derived products from softwood and hardwood treated in supercritical water. *Journal

of Wood Science*, **2005**, *51*, 256-261.

52.   Yoshida, T.; Matsumura, Y., Gasification of Cellulose, Xylan, and Lignin Mixtures in

Supercritical Water. *Ind. Eng. Chem. Res.*, **2001**, *40(23)*, 5469-5474.

53.   Aida, T. M.; Sato, T.; Sekiguchi, G.; Adschiri, T.; Arai, K., Extraction of Taiheyo

coal with supercritical water-phenol mixtures. *Fuel*, **2002**, *81*, 1453-1461.

54.   Fang, Z.; Sato, T.; Smith, R. L. Jr.; Inomata, H.; Arai, K.; Kozinski, J. A., Reaction

chemistry and phase behavior of lignin in high-temperature and supercritical water.

Bioresource Technology, **2008**, *99*, 3424-3430.

55.   Saisu, M.; Sato, T.; Watanabe, M.; Adschiri, T.; Arai, K., Conversion of Lignin with

Supercritical Water-Phenol Mixtures. *Energy Fuels*, **2003**, *17(4)*, 922-928.

56.   Hidajat, M. J.; Riaz, A.; Park, J.; Insyani, R.; Verma, D.; Kim, J., Depolymerization of concentrated sulfuric acid hydrolysis lignin to high-yield aromatic monomers in basic sub-and supercritical fluids. *Chemical Engineering Journal*, **2017**, *317*, 9-19.

57.   McClelland, D. J.; Galebach, P. H.; Motagamwala, A. H.; Wittrig, A. M.; Karlen, S. D.; Buchanan, J. S.; Dumesic, J. A.; Huber, G. W., Supercritical methanol depolymerization and hydrodeoxygenation of lignin and biomass over reduced porous metal oxides. *Green Chemistry*, **2019**, *21*, 2988-3005.

58.   Huang, X.; Koranyi, T. I.; Boot, M. D.; Hensen, E. J. M., Catalytic Depolymerization of Lignin in Supercritical Ethanol. *ChemSusChem*, **2014**, *7*, 2276-2288.

59.   Deuss, P. J.; Scott, M.; Tran, F.; Westwood, N. J.; de Vries, J. G.; Barta, K., Aromatic Monomers by in Situ Conversion of Reactive Intermediates in the Acid-Catalyzed Depolymeriztion of Lignin. *J. Am. Chem. Soc.*, **2015**, *137*, 7456-7467.

60.   Deepa, A. K.; Dhepe, P. L., Lignin Depolymerization into Aromatic Monomers over Solid Acid Catalysts. *ACS Catalysis*, **2015**, *5(1)*, 365-379.

61.   Glasser, W. G., Multiphase materials with lignin. 11. Starlike copolymers with caprolactone. *Macromolecules*, **1994**, *27*, 5-11.

62.   Laurichesse, S.; Avéros, L., Synthesis, thermal properties, rheological and mechanical behaviors of lignin-grafted-poly(ε-caprolactone). *Polymer*, **2013**, *54*, 3882-3890.

63.   Chung, Y. L.; Olsson, J. V.; Li, R. J.; Frank, C. W.; Waymouth R. M.; Billington S. L.; Sattely, E. S., A Renewable Lignin-Lactide Copolymer and Application in Biobased Composites. *ACS Sustainable Chem. Eng.,* **2013**, *1*, 1231-1238.

64.   Liu, X.; Zong, E.; Jiang, J.; Fu, S.; Wang, J.;Xu, B.; Li, W.; Lin, X.; Xu, Y.; Wang, C.; Chu, F., Preparation and characterization of Lignin-graft-poly(ε-caprolactone)

copolymers based on lignocellulosic butanol residue. *International Journal of Biological Macromolecules*, **2015**, *81*, 521-529.

65.   Matsushita, Y.; Inomata, T.; Takagi, Y.; Hasegawa, T.; Fukushima, K., Conversion of sulfuric acid lignin generated during bioethanol production from lignocellulosic materials into polyesters with ε-caprolactone. *Journal of Wood Science*, **2011**, *57*, 214-218.

66.   Sun, Y.; Yang, L.; Lu, X.; He, C., Biodegradable and renewable poly(lactide)-lignin composites: synthesis, interface and toughening mechanism. *Journal of Materials Chemistry A,* **2015***, 3*, 3699-3709.

67.   Nguyen, H. T. H.; Short, G. N.; Qi, P.; Miller, S. A., Copolymerization of lactones and bioaromatics via concurrent ring-opening polymerization/polycondensation. *Green Chemistry*, **2017**, *19*, 1877-1888.

68.   Saito, T.; Brown, R. H.; Hunt, M. A.; Pickel, D. L.; Pickel, J. M.; Messman, J. M.; Baker, F. S.; Keller, M.; Naskar, A. K., Turning renewable resources into value-added polymer: development of lignin-based thermoplastic. *Green Chemistry*, **2012**, *14*, 3295-3303.

69.   Lee, Y.; Park, C. H.; Lee, E. Y., Chemical modification of methanol-insoluble kraft lignin using oxypropylation under mild conditions for the preparation of bio-Polyester. *J. Wood Chem. Technol.*, **2017**, *37*, 334-342.

70.   Scarica, C.; Suriano, R.; Levi, M.; Turri, S.; Griffini, G., Lignin Functionalized with Succinic Anhydride as Building Block for Biobased Thermosetting Polyester Coatings. *ACS Sustainable Chem. Eng.*, **2018**, *6(3)*, 3392-3401.

71. Mialon, L.; Pemba, A. G.; Miller, S. A., Biorenewable polyethylene terephthalate mimics derived from lignin and acetic acid. *Green Chemistry*, **2010**, *12*, 1704-1706.

72. Mialon, L.; Vanderhenst, R.; Pemba, A. G.; Miller, S. A., Polyalkylenehydroxybenzoates (PAHBs): biorenewable aromatic/aliphatic polyesters from lignin. *Macromol. Rapid Commun.*, **2011**, *32*, 1386-1392.

73. Giola, C.; Banella, M. B.; Marchese, P.; Vannini, M.; Colonna, M.; Celli, A., Advances in the synthesis of bio-based aromatic polyesters: novel copolymers derived from vanillic acid and ε-caprolactone. *Polym. Chem.*, **2016**, *7*, 5396-5406.

74. Kreye, O.; Oelmann, S.; Meier, M. A. R., Renewable aromatic-aliphatic copolyesters derived from rapeseed. *Macromol. Chem. Phys.*, **2013**, *214*, 1452-1464.

75. Firdaus, M.; Meier, M. A. R., Renewable co-polymers derived from vanillin and fatty acid derivatives. *European Polymer Journal*, **2013**, *49(1)*, 156-166.

76. Llevot, A.; Grau, E.; Carlotti, S.; Grelier, S.; Cramail, H., From Lignin-derived Aromatic Compounds to Novel Biobased Polymers. *Macromol. Rapid Commun.*, **2016***, 37*, 9-28.

77. Meylemans, H. A.; Groshens, T. J.; Harvey, B. G., Synthesis of Renewable Bisphenols from Creosol. *ChemSusChem*, **2012**, *5*, 206-210.

78. Pion, F.; Ducrot, P. H.; Allais, F., Renewable Alternating Aliphatic-Aromatic Copolyesters Derived from Ferulic Acid, Diols, and Diacids: Sustainable Polymers with Tunable Thermal Properties. *Macromol. Chem. & Phys.,* **2014**, *215(5)*, 431-439.

79. Nakamura, H.; Imanishi, S.; Sanui, K.; Ogata, N., Synthesis of Aromatic Polyesters by Interfacial Polycondensation Using Immiscible Binary Solvents. *Polymer Journal*, **1979**, *11(8)*, 661-664.

80. Tagle, L. H.; Diaz, F. R.; Roncero, S., Polymerization by phase transfer catalysis. 14. Polyesters from terephthalic acid and related diacids with bisphenol A. *Polymer International*, **1992**, *29*, 265-268.

81. Bucio, E.; Lara-Estévez, J. C. I.; Ruiz-Treviño, F. A.; Acosta-Huerta, A., Synthesis and Characterization of New Polyesters Derived from Diphenols and Aromatic Diacids Chlorides. *Polymer Bulletin*, **2006**, *56*, 163-170.

82. Edlund, U.; Albertsson, A. C., Polyesters based on diacid monomers. *Advanced Drug Delivery Reviews*, **2003**, *55(4)*, 585-609.

83. Sanadhya, S. G.; Oswal, S. L.; Parmar, K. C., Synthesis and characterization of aliphatic-aromatic polyesters using interfacial polycondensation technique. *J. Chem. Pharm. Res.*, **2014**, *6(4)*, 705-714.

84. Bilyeu, B.; Brostow, W.; Menard, K. P., Epoxy thermosets and their applications I: Chemical structures and applications. *Journal of Materials Education*, **1999**, *12(5&6)*, 281-286.

85. Rubin, B. S., Bisphenol A: An endocrine disruptor with widespread exposure and multiple effects. *The Journal of Steroid Biochemistry and Molecular Biology*, **2011**, *127(1&2)*, 27-34.

86. Qin, J.; Liu, H.; Zhang, P.; Wolcott, M.; Zhang, J., Use of eugenol and rosin as feedstocks for biobased epoxy resins and study of curing and performance properties. *Polym. Int.,* **2014**, *63*, 760-765.

87. Faye, I.; Decostanzi, M.; Ecochard, Y.; Caillol, S., Eugenol bio-based epoxy thermosets: from cloves to applied materials. *Green Chemistry*, **2017**, *19*, 5236-5242.

88.   Liu, T.; Hao, C.; Wang, L.; Li, Y.; Liu, W.; Xin, J.;Zhang, J., Eugenol-Derived Biobased Epoxy: Shape Memory, Repairing, and Recyclability. *Macromolecules*, **2017**, *50(21)*, 8588-8597.

89.   Miao, J. T.; Yuan, L.; Guan, Q.; Liang, G.; Gu, A., Biobased epoxy resin derived from eugenol with excellent integrated performance and high renewable carbon content. *Polymer International*, **2018**, *67(9),* 1194-1202.

90.   Zhao, S.; Abu-Omar, M. M., Biobased Epoxy Nanocomposites Derived from Lignin-Based Monomers. *Biomacromolecules*, **2015**, *16*, 2025-2031.

91.   Zhao, S.; Abu-Omar, M. M., Renewable Epoxy Networks Derived from Lignin-Based Monomers: Effect of Cross-Linking Density. *ACS Sustainable Chem. Eng.*, **2016**, *4*, 6082-6089.

92.   Ruiz, Q.; Pourchet, S.; Placet, V.; Plasseraud, L.; Boni, G., New Eco-Friendly Synthesized Thermosets from Isoeugenol-Based Epoxy Resins. *Polymers*, **2020**, *12*, 229-244.

93.   François, C.; Pourchet, S.; Boni, G.; Fontaine, S.; Gaillard, Y.; Placet, V.; Galkin, M. V.; Orebom, A.; Samec, J.; Plasseraud, L., Diglycidylether of iso-eugenol: a suitable lignin-derived synthon for epoxy thermoset applications. *RSC Adv,* **2016**, *6(73),* 68732-68738.

94.   Koelewijm, S. F.; Cooreman, C.; Renders, T.; Andecochea Saiz, C.; Van den Bosch, S.; Schutyser, W.; De Leger, W.; Smel, M.; Van Puyvelde, P.; Witters, H.; Van der Bruggen, B.; Sels, B. F., Promising bulk production of a potentially benign bisphenol A replacement from a hardwood lignin platform. *Green Chem.,* **2018**, *20*, 1050-1058.

95.   Nicastro, K. H.; Kloxin, C. J.; Epps III, T. H., Potential Lignin-Derived Alternatives to Bisphenol A in Diamine-Hardened Epoxy Resins. *ACS Sustainable Chem. Eng.*, **2018**, *6(11),* 14812-14819.

96.   Savonnet, E.; Grau, E.; Grelier, S.; Defport, B.; Carmail, H., Divanillin-Based Epoxy Precursors as DGEBA Substitutes for Biobased Epoxy Thermosets. *ACS Sustainable Chem. Eng.*, **2018**, *6(8),* 11008-11017.

97.   Fache, M.; Auvegne, R.; Boutevin, B.; Caillol, S., New vanillin-derived diepoxy monomers for the synthesis of biobased thermosets. *Eur. Polym. J,* **2015**, *67,* 527-538.

98.   Fache, M.; Viola, A.; Auvergne, R.; Boutevin, B.; Caillol, S., Biobased epoxy thermosets from vanillin-derived oligomers. *Eur.Polym. J.,* **2015**, *68,* 526−535.

99.   Fache, M.; Boutevin, B.; Caillol, S., Epoxy thermosets from model mixtures of the lignin-to-vanillin process. *Green Chem.*, **2016**, *18(3),* 712-725.

100.   Wang, S.; Ma, S.; Xu, C.; Liu, Y.; Dai, J.; Wang, Z.; Liu, X.; Chen, J.; Shen, X.; Wei, J.; Zhu, J., Vanillin-derived high-performance flame retardant epoxy resins: facile synthesis and properties. *Macromolecules*, **2017**, *50(5),* 1892-1901.

101.   Su, X.; Zhou, Z.; Liu, J.; Luo, J.; Liu, R., A recyclable vanillin-based epoxy resin with high-performance that can compete with DGEBA. *European Polymer Journal*, **2020**, *140,* 110053.

102.   Mogheiseh, M.; Karimian, R.; Khoshsefat, M., Vanillin-derived epoxy monomer for synthesis of bio-bsed epoxy thermosets: effect of functionality on thermal, mechanical, chemical and structural properties. *Chemical Papers*, **2020**, *74,* 3347-3358.

103.   van de Pas, D. J.; Torr, K. M., Biobased Epoxy Resins from Deconstructed Native Softwood Lignin. *Biomacromolecules*, **2017**, *18*, 2640-2648.

104.   Xin, J.; Li, M.; Li, R.; Wolcott, M. P.; Zhang, J., Green Epoxy Resin System Based on Lignin and Tung Oil and Its Application in Epoxy Asphalt. *ACS Sustainable Chem. Eng.,* **2016**, *4*, 2754-2761.

105.   Ferdosian, F.; Yuan, Z.; Anderson, M.; Xu, C., Sustainable lignin-based epoxy resins cured with aromatic and aliphatic amine curing agents: Curing kinetics and thermal properties. *Thermochimica Acta*, **2015**, *618*, 48-55.

106.   Ferdosian, F.; Yuan, Z.; Anderson, M.; Xu, C., Chemically Modified Lignin Through Epoxidation and its Thermal Properties. *J. Sci. & Tech. for Forest Product and Processes,* **2012**, *2(4),* 11-15.

107.   Ferdosian, F.; Yuan, Z.; Anderson, M.; Xu, C., Curing Kinetics and mechanical properties of bio-based epoxy composites comprising lignin-based epoxy resins. *European Polymer Journal*, **2016**, *82*, 153-165.

108.   Over, L. C.; Grau, E.; Grelier, S.; Meier, M. A. R.; Cramail, H., Synthesis and Characterization of Epoxy Thermosetting Polymers from Glycidylated Organosolv Ligning and Bisphenol A. *Macromol. Chem. Phys.*, **2017**, *218*, 1600411.

109.   Zhao, S.; Abu-Omar, M. M., Synthesis of Renewable Thermoset Polymers through Successive Lignin Modification Using Lignin-Derived Phenols. *ACS Sustainable Chem. Eng.*, **2017**, *5*, 5059-5066.

110.   Yin, Q.; Yang, W.; Sun, C.; Di, M., Preparation and properties of lignin-epoxy resin composite. *BioResources*, **2012**, *7*, 5737-5748.

111. El Mansouri, N. E.; Yuan, Q.; Huang, F., Synthesis and characterization of Kraft lignin-based epoxy resins. *BioResources*, **2011**, *6*, 2492-2503.

112. Thakur, V. K.; Thakur, M. K.; Raghavan, P.; Kessler, M. R., Progress in green polymer composites from lignin for multifunctional applications: a review. *ACS Sustainable Chem. Eng.*, **2014**, *2*, 1072-1092.

113. Gouveia, J. R.; Garcia, G. E. S.; Antonino, L. D.; Tavares, L. B.; dos Santos, D. J., Epoxidation of Kraft Lignin as a Tool for Improving the Mechanical Properties of Epoxy Adhesive. *Molecules,* **2020**, *25 (11),* 2513.

114. Bhatt, P.; Goe, A., Carbon Fibres: Production, Properties and Potential Use. *Material Science Research India*, **2017**, *14(1)*, 52-57.

115. Souto, F.; Calado, V.; Pereira Jr, N., Lignin-based carbon fiber: a current overview. *Materials Research Express*, **2018**, *5*, 072001.

116. Eberle, C., Oak Ridge National Laboratory. Carbon Fibers from Lignin. Presented at the 10th annual world congress on industrial biotechnology. **2013**. Available from: (https://bio.org/sites/default/files/BIO%20WC%20Eberle%2020130618%20DRAFT_ cliff_eberle_0.pdf) Accessed June 2021.

117. Asmatulu, R.; Khan, W. S., Introduction to electrospun nanofibers. In *Synthesis and Applications of Electrospun Nanofibers,* **2019**, pp 1-15.

118. Braun, J. L.; Holtman, K. M.; Kadla, J. F., Lignin-based carbon fibers: oxidative thermostabilization of kraft lignin. *Carbon*, **2005**, *43*, 385-394.

119. Li, Y.; Cui, D.; Tong, Y.; Xu, L., Study on structure and thermal stability properties of lignin during thermostabilization and carbonization. *International Journal of Biological Macromolecules*, **2013**, *62*, 663-669.

120. Kadla, J. F.; Kubo, S. Venditi, R. A.; Gilbert, R. D.; Compere, A. L.; Grittith, W., Lignin-based carbon fibers for composite fiber applications. *Carbon*, **2002**, *40*, 2913-2920.

121. Mainka, H.; Täger, O.; Körner, E.; Hilfert, L.; Busse, S.; Edelmann, F. T.; Herrmann, A. S., Lignin—an alternative precursor for sustainable and cost-effective automative carbon fiber. *Journal of Materials Research and Technology*, **2015**, *4*, 283-296.

122. Kubo, S.; Uraki, Y.; Sano, Y., Preparation of carbon fibers from softwood lignin by atmospheric acetic acid pulping. *Carbon*, **1998**, *36*, 1119-1124.

123. Baker, D. A.; Gallego, N. C.; Baker, F. S., On the characterization and spinning of an organic-purified lignin toward the manufacture of low-cost carbon fiber. *J. Appl. Polym. Sci.*, **2012**, *124*, 227-234.

124. Kubo, S.; Kadla, J. F., Kraft lignin/poly(ethylene oxide) blends: effect of lignin structure on miscibility and hydrogen bonding. *J. Appl. Polym. Sci.*, **2005**, *98*, 1437-1444.

125. Marandur, S. P.; Kim, C. H.; Kim S. Y.; Kim B. H.; Kim, W. C.; Yang, K., Preparation of carbon fibers from a lignin copolymer with polyacrylonitrile. *Synth. Met.*, **2012**, *162*, 453-459.

126. Chen, K., Bio-renewable fibers extracted from lignin/polylactide (PLA) blend. *Master Dissertation*, **2012**, Iowa State University, Iowa, USA.

127. Wang, S.; Li, Y.;Xiang, H.; Zhou, Z.; Chang, T.; Zhu, M., Low cost carbon fibers from bio-renewable lignin/poly(lactic acid) (PLA) blends. *Compos. Sci. Technol.*, **2015**, *119*, 20-25.

128. Li, Q.; Xie, S.; Serem, W. K.; Naik, M. T.; Liu, L.; Yuan, J. S., Quality carbon fiber from fractionated lignin. *Green Chemistry*, **2017**, *19*, 1628-1634.

129. Nordström, Y.; Norberg, I.; Sjöholm, E.; Drougge, R., A new softening agent for melt spinning of softwood kraft lignin. *J. Appl. Polym. Sci.*, **2012**, *129*, 1274-1279.

130. Hosseinaei, O.; Harper, D. P.; Bozell, J. J.; Rials, T. G., Improving processing and performance of pure lignin carbon fibers through hardwood and herbaceous lignin blend. *International Journal of Molecular Sciences*, **2017**, *18*, 1410.

131. Sudo, K.; Shimizu, K., A new carbon fiber from lignin. *J. Appl. Polym. Sci.*, **1992**, *44*, 127-134.

132. Sudo, K.; Shimizu, K.; Nakashima, N; Yokoyama, A., A new modification method of exploded lignin for the preparation of a carbon fiber precursor. *J. Appl. Polym. Sci.*, **1993**, *48*, 1485-1491.

133. Eckert, R. C.; Abdullah, Z., Carbon Fiber from kraft softwood lignin. *Patent US*7678358, **2007**.

134. Lin, J.; Kubo, S.; Yamada, T.; Koda, K.; Uraki, Y., Thermostabilized carbon fibers from softwood. *Bioresources*, **2012**, *7*, 5634-5646.

135. Chatterjee, S.; Clingenpeel, A.; McKenna, A.; Orlando, R.; Johs, A., Synthesis and characterization of lignin-based carbon materials with tunable microstructure. *RCS Advances*, **2013**, *4*, 4743-4753.

136. Zhang, M.; Ogale, A. A., Carbon fibers from dry-spinning of acetylated softwood kraft lignin. *Carbon. Dezembro*, **2013**, *69*, 626-629.

137. Qin, W.; Kadla, J. F., Effect of organoclay reinforcement on lignin-based carbon fibers. *Ind. Eng. Chem. Res.*, **2011**, *50*, 12548-12555.

138. Das, A.; Mahanwar, P., A brief discussion on advances in polyurethane applications. *Advanced Industrial and Engineering Polymer Research*, **2020**, *3*, 93-101.

139. Upton, B. M.; Kasko, A. M., Strategies for the conversion of lignin to high-value polymeric materials: review and perspective. *Chem. Rev.*, **2016**, *116*, 2275-2306.

140. Duval, A.; Lawoko, M., A review on lignin-based polymeric, micro- and nano-structured materials. *React. Funct. Polym.*, **2014**, *85*, 78-96.

141. Laurichesse, S.; Avérous, L., Chemical modification of lignins: towards biobased poltmers. *Prog. Polym. Sci.*, **2014**, *39*, 1266-1290.

142. Cateto, C. A.; Barreiro, M. F.; Rodrigues, A. E.; Brochier-Salon, M. C.; Thielemans, W.; Belgacem, M. N., Lignins as a macromonomer for polyurethane synthesis: A comparative study on hydroxyl group determination. *J. Appl. Polym. Sci.*, **2008**, *109*, 3008-3017.

143. Alinejad, M.; Henry, C.; Nikafshar, S.; Gondaliya, A.; Bagheri, S.; Chen, N.; Singh, S. K.; Hodge, D. B.; Nejad, M., Lignin-Based Polyurethanes: Opportunities for Bio-Based Foams, Elastomers, Coatings, and Adhesives. *Polymers*, **2019**, *11*, 1202-1223.

144. Duong, L. D.; Nam, G. Y.; Oh, J. S.; Park, I. K.; Luong, N. D.; Yoon, H. K.; Lee, S. H.; Lee, Y.; Yun, J. H.; Lee, C. G.; Hwang, S. H.; Nam, J. D., High molecular-weight thermoplastic polymerization of kraft lignin macromers with diisocyanate. *Bioresources*, **2014**, *9*, 2359-2371.

145. Bonini, C.; D'Auria, M.; Emanuele, L.; Ferri, R.; Pucciariello, R.; Sabia, A. R., Polyurethanes and polyesters from lignin. *J. Appl. Polym. Sci.*, **2005**, *98*, 1451-1456.

146. Desroches, M.; Escouvois, M.; Auvergne, R.; Caillol, S.; Boutevin, B., From vegetable oil to polyurethanes: synthetic routes for polyols and main industrial products. *Polym. Rev.*, **2012**, *52*, 38-79.

147. Li, H.; Liang, Y.; Li, P.; He, C., Conversion of biomass lignin to high-value polyurethane: A review. *Journal of Bioresources and Bioproducts*, **2020**, *5*, 163-179.

148. Hatakeyama, H., Polyurethanes Containing Lignin. In *Chemical Modification, Properties, and Usage of Lignin*. Edited by Hu, T. Q., **2002**, pp 41-56.

149. Wang, Z. M.; Yang, X. H.; Zhou, Y. H.; Liu, C. G., Mechanical and thermal properties of polyurethane films from peroxy-acid wheat straw lignin. *Bioresources*, **2013**, *8*, 3833-3843.

150. Xue, B. L.; Wen, J. L.; Sun, R. C., Lignin-based rigid polyurethane foam reinforced with pulp fiber: synthesis and characterization. *ACS Sustainable Chem. Eng.*, **2014**, *2*, 1474-1480.

151. Jeong, H.; Park, J.; Kim, S.; Lee, J.; Ahn, N., Compressive viscoelastic properties of softwood kraft lignin-based flexible polyurethane foams. *Fibers Polym.*, **2013**, *14*, 1301-1310.

152. Yoshida, H.; Mörck, R.; Kringstad, K. P.; Hatakeyama, H., Kraft lignin in polyurethanes I. Mechanical properties of polyurethanes from kraft lignin-polyether triol-polymeric MDI system. *J. Appl. Polym. Sci.*, **1987**, *34*, 1187-1198.

153. Reimann, A.; Mörck, R.; Yoshida, H.; Hatakeyama, H.; Kringstad, K. P., Kraft lignin in polyurethanes. III. Effects of the molecular weight of PEG on the properties of polyurethanes from a kraft lignin-PEG-MDI system. *J. Appl. Polym. Sci.*, **1990**, *41*, 39-50.

154. Thring, R. W.; Vanderlaan, M. N.; Griffen, S. L., Polyurethanes from alcell ® lignin. **1997**, *13*, 125-132.

155. Arashanitsa, A.; Krumina, L.; Telysheva, G.; Dizhbite, T., Exploring the application potential of incompletely soluble organosolv lignin as a macromonomer for polyurethane synthesis. *Ind. Crop. Prod.*, **2016**, *92*, 1-12.

156. Pan, X. J.; Saddler, J. N., Effect of replacing polyol by organosolv and kraft lignin on the property and structure of rigid polyurethane foam. *Biotechnol. Biofuels*, **2013**, *6*, 12.

157. Wang, Y. Y.; Wyman, C. E.; Cai, C. M.; Ragauskas, A. J., Lignin-based polyurethanes from unmodified kraft lignin fractionated by sequential precipitation. *ACS Appl. Polym. Mater.*, **2019**, *1*, 1672-1679.

158. Griffini, G.; Passoni, V.; Suriano, R.; Levi, M.; Turri, S., Polyurethane coatings based on chemically unmodified fractionated lignin. *ACS Sustainable Chem. Eng.*, **2015**, *3*, 1145-1154.

159. de Haro, J. C.; Allegretti, C.; Smit, A. T.; Surri, S.; D'Arrigo, P.; Griffini, G., Biobased polyurethane coatings with high biomass content: tailored properties by lignin selection. *ACS Sustainable Chem. Eng.*, **2019**, *7*, 11700-11711.

160. Mahmood, N.; Yuan, Z. S.; Schmidt, J.; Xu, C., Production of polyols via direct hydrolysis of kraft lignin: effect of process parameters. *Bioresour. Technol.*, **2013**, *139*, 13-20.

161. Chio, C.; Sain, M.; Qin, W. S., Lignin utilization: a review of lignin depolymerization from various aspects. *Renew. Sustain. Energy Rev.*, **2019**, *107*, 232-249.

162. Mahmood, N.; Yuan, Z. S.; Schmidt, J.; Xu, C., Preparation of bio-based rigid polyurethane foam using hydolytically depolymerized Kraft lignin via direct replacement or oxypropylation. *Eur. Polym. J.*, **2015**, *68*, 1-9.

163. Cinelli, P.; Anguillesi, I.; Lazzeri, A., Green synthesis of flexible polyurethane foams from liquefied lignin. *Eur. Polym. J.*, **2013**, *49*, 1174-1184.

164. Bernardini, J.; Cinelli, P.; Anguillesi, I.; Coltelli, M. B.; Lazzeri, A., Flexible polyurethane foams green production emplying lignin or oxypropylated lignin. *Eur. Polym. J.*, **2015**, *64*, 147-156.

165. Li, H.; Sun, J. T.; Wang, C.; Liu, S. L.; Yuan, D.; Zhou, X.; Tan, J.; Stubbs, L.; He, C. B., High *Modulus*, strength, and toughness polyurethane elastomer based on unmodified lignin. *ACS Sustainable Chem. Eng.*, **2017**, *5*, 7942-7949.

166. Kelley, S. S.; Glasser, W. G.; Ward, T. C., Effect of soft-segment content on the properties of lignin-based polyurethanes. In *ACS Symposium Series, American Chemical Society*, Washington, DC. **1989**, pp 402-413.

167. Wang, S. Y.; Liu, W. F.; Yang, D. J.; Qiu, X. Q., Highly resilient lignin-containing polyurethane foam. *Ind. Eng. Chem. Res.*, **2019**, *58*, 496-504.

168. Saraf, V. P.; Glasser, W. G., Engineering plastics from lignin. III. Structure property relationships in solution cast polyurethane films. *J. Appl. Polym. Sci.*, **1984**, *29*, 1831-1841.

169. Zhang, X. F.; Kim, Y.; Elsayed, I.; Taylor, M.; Eberhardt, T. L.; Hassan, E. B.; Shmulsky, R., Rigid polyurethane foams containing lignin oxylated with ethylene carbonate and polyethylene glycol. *Ind. Crop. Prod.*, **2019**, *141*, 111797.

170.   Li, Y.; Ragauskas, A. J., Kraft lignin-based rigid polyurethane foam. *J. Wood Chem. Technol.*, **2012**, *32*, 210-224.

171.   Chung, H.; Washburn, N. R., Improved lignin polyurethane properties with lewis acid treatment. *ACS Appl. Mater. Interfaces*, **2012**, *4*, 2840-2846.

172.   Chen, Y. C.; Fu, S. Y.; Zhang, H., Signally improvement of polyurethane adhesive with hydroxy-enriched lignin from bagasse. *Colloids Surfaces A: Physicochem. Emg. Aspects*, **2020**, *585*, 124164.

173.   Laurichesse, S.; Huillet, C.; Avérous, L., Original polyols based on organosolv lignin and fatty acids: new bio-based building blocks for segmented polyurethane synthesis. *Green Chemistry*, **2014**, *16*, 3958-3970.

174.   Jeong, H.; Park, J.; Kim, S.; Lee, J.; Ahn, N.; Roh, H. G., Preparation and characterization of thermoplastic polyurethanes using partially acetylated kraft lignin. *Fibers Polym.*, **2013**, *14*, 1082-1093.

175.   Zhang, L. N.; Huang, J., Effects of hard-segment compositions on properties of polyurethane-nitrolignin films. *J. Appl. Polym. Sci.*, **2001**, *81*, 3251-3259.

176.   Zhang, L. N.; Huang, J., Effects of nitrolignin on mechanical properties of polyurethane-nitrolignin films. *J. Appl. Polym. Sci.*, **2001**, *80*, 1213-1219.

177.   Zhou, W. P.; Chen, F. G.; Zhang, H.; Wang, J., Preparation of a polyhydric aminated lignin and its use in the preparation of polyurethane film. *J. Wood Chem. Technol.*, **2017**, *37*, 323-333.

178.   Huo, S. P.; Nie, M. C.; Kong, Z. W.; Wu, G. M.; Chen, J., Crosslinking kinetics of the formation of lignin-aminated polyol-based polyurethane foam. *J. Appl. Polym. Sci.*, **2012**, *125*, 152-157.

Chapter 2

Preparation and Properties of Renewable Polyesters Based on Lignin-derived Bisphenol

2.1 Abstract

The biophenol molecule isoeugenol has been shown to be a major product of lignin-first reductive catalytic fractionation (RCF) of lignocellulosic biomass. Here, we describe the use of isoeugenol as a starting material for bio-based polyesters. A series of novel bio-based polyesters are synthesized from lignin-derived bisphenol and various acyl chlorides via a polycondensation reaction. NMR is used to confirm the structure as well as approximate molecular weight. Thermal properties of the resulting bio-polyesters are directly related to the length of the aliphatic chain of the diacid. Glass transition temperatures were in the range from 19 °C to 108 °C and can be tuned to be more in line with petroleum-based polyesters like PET (T_g = 80 °C) by employing mixtures of lignin-based bisphenols (T_g = 83 °C). In addition to thermal tunability, these renewable polyesters can have up to 100% bio-content by mass.

2.2 Introduction

Many polymers that are industrially produced have aromatic backbones. These includes polyesters like poly(ethyleneterephthalate) (PET) and polystyrene, as well as thermosets that incorporate bisphenol A (BPA). All these aromatic based polymers are currently sourced from petroleum.[1] Two of the main chemicals used to make these materials are bis-phenol A (BPA) and terephthalic acid (TPA). BPA is used in epoxy resins and polycarbonates, and TPA is the building block of an extensively used food packaging plastic, PET. Both

chemicals are sourced from petroleum, with BPA being derived from phenol and TPA from

p-xylene. The need to move away from fossil resources is becoming increasingly important.

One feedstock that has great promise as a potential replacement of petroleum is non-food

lignocellulosic biomass. Biomass is composed of three main polymers, lignin, cellulose, and

hemicellulose. Since biomass is produced as a waste product from many industries such as

agriculture, forestry, and paper,[2] sourcing monomers from biomass is attractive. The

cellulosic components of biomass have been widely used for the production of furanic based

compounds.[3-12] In contrast to sugar-based cellulose and hemicellulose, lignin is unique to

other biomacromolecules because it is composed of phenolic monomers.

Lignin can be isolated from biomass via four main isolation techniques, Kraft, sulfite,

soda, and organosolv.[13-17] The lignin obtained from each technique varies slightly in structure

due to different reagents used during processing,[17] but regardless of the isolation method the

lignin has to then be further upgraded into oligomers and monomers. There have been a

multitude of studies on the depolymerization of lignin, with many targeting the common β-

O-4 linkage. This can be done via a variety of methods including pyrolysis, hydrogenolysis,

oxidation, and catalysis.[18] The number of monomers that can be obtained from lignin is large.

Any variation in biomass source, isolation technique, or depolymerization method will yield

different monomers and monomer ratios from lignin.

This work builds off of the small molecule isoeugenol, which has been shown to be a

major product from reductive catalytic fractionation (RCF) of biomass.[19-23] In addition,

isoeugenol is used in the cosmetic industry, being sourced largely from clove oil,[24] meaning

that the infrastructure to obtain it as a monomer is already in place. It has also been shown

that via metathesis, a bis-isoeugenol (BIE) molecule can be obtained.[25-27] In addition, Hitce et

40

al. were able to hydrogenate the internal double bond in BIE to obtain the hydrogenated variant, HBIE, which is also used in our study.[25] BIE and HBIE have also been sourced from vanillin, another lignin derived molecule.[26] Though many lignin-derived molecules have been used in polyester synthesis,[28-33] the use of BIE and HBIE has been largely unexplored.

We synthesize and characterize a variety of novel renewable polyesters form both BIE and HBIE. We are able to tune the properties of these polyesters by incorporating comonomers of varying alkyl chain length and by incorporating ratios of BIE and HBIE into the polyester structure. By incorporating different carboxylic acid derivatives and BIE:HBIE ratios, the glass transition temperature, T_g, can range from 19 ^{o}C to 108 ^{o}C without losing thermal stability. With the tunability inherent to these polyesters, they can obtain properties like those of PET. In addition to thermal tunability, many of these renewable polyesters have close to 100 % biocontent by mass.

2.3 Synthetic Procedures

2.3.1 Synthesis of the isoeugenol dimer, BIE

Procedure adapted from Hitce et al.[25] Isoeugenol (30.15 g, 184 mmol) and Grubbs II catalyst (77 mg, 0.05 mol%) were added to a 250 mL round bottom flask with a magnetic stir bar. The solution was heated to 90 ^{o}C. After 5-10 minutes, the solution bubbles and releases the 2-butene byproduct and solidifies. After approximately 20 minutes, the flask is removed from the heat and let cool to room temperature. The solid is broken up inside of the flask and then to it is added DCM (1 vol.) and cold MeOH (2 vol.). It is then stirred for 1h at 0 ^{o}C. After 1 h the product is isolated via vacuum filtered and washed with cold MeOH. The isolated light pink solid is then dried in a 120 ^{o}C oven overnight (20.5 g, 82 %). The product was analyzed by ^{1}H NMR and ^{13}C NMR (Figure 2.1). ^{1}H NMR (600 MHz, CDCl$_3$) δ= 7.00

(d, 1H, ArH), 6.98 (dd, 1H, ArH), 6.87 (d, 1H, ArH), 6.86 (s, 1H, C=C-H), 5.60 (s, 1H, -OH), 3.93 (s, 3H, -OCH$_3$); ^{13}C NMR (400 MHz, CDCl$_3$) δ= 146.7, 145.2, 130.2, 126.4 (internal C=C), 120.1, 114.5, 107.9, 55.9 (-OCH$_3$).
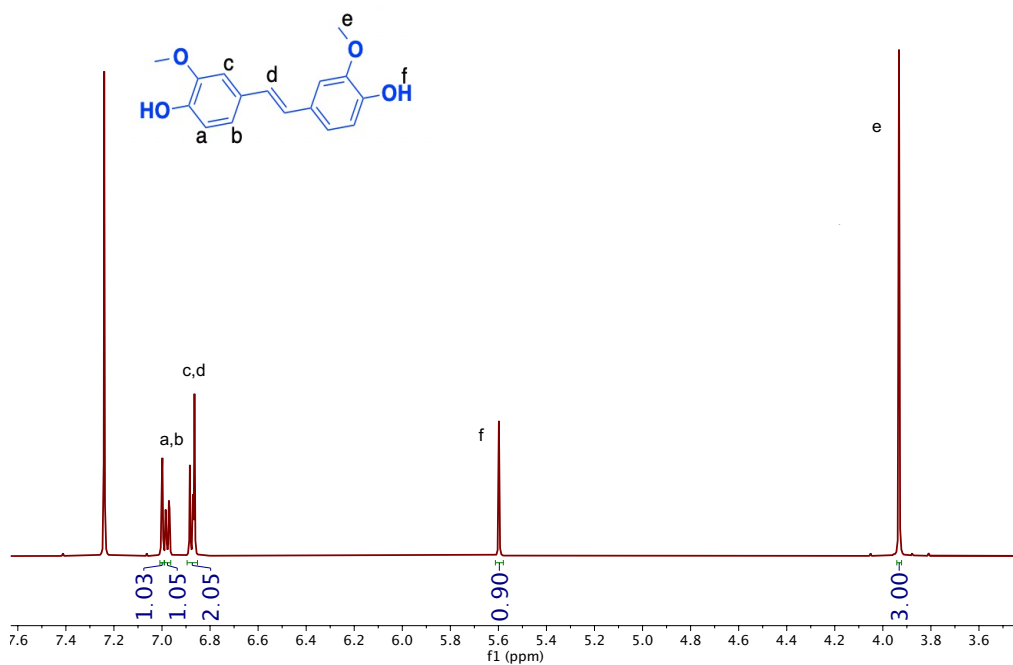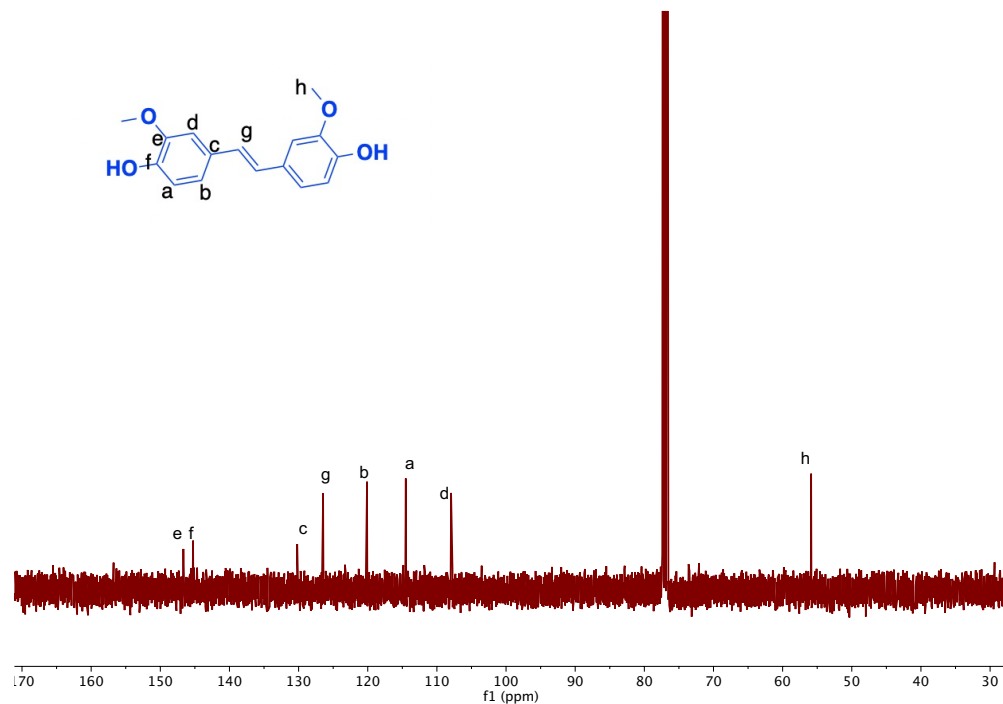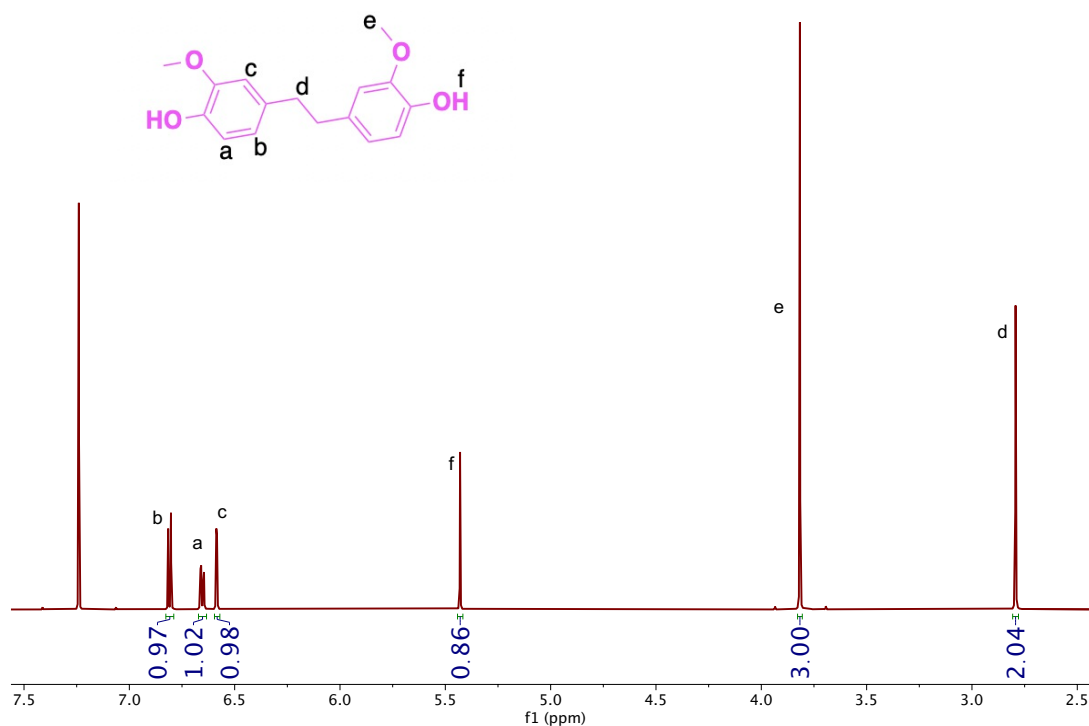

Figure 2.1. ^{13}CNMR (top) and ^{1}HNMR (bottom) spectra of bis-isoeugenol (BIE) in CDCl$_3$.

2.3.2 Hydrogenation of BIE to Synthesize HBIE

Procedure adapted from that of Trita et al.[27] BIE (2.728 g, 10 mmol), Pd/C (15 wt%), and 40 mL of EtOH were added to a stainless-steel Parr reactor with a glass magnetic stir bar. The reactor was then sealed and purged 3 times with H_2 while stirring. The whole system was then pressurized with 10 bar of H_2, heated to 50 °C, and stirred for 5 h. After 5 h, the reactor is brought to room temperature and the solution is filtered and washed with EtOH to give a clear filtrate. The filtrate is then concentrated via rotary evaporation to give a white solid (2.347 g, 85 %). The product was analyzed by ^{1}H NMR and ^{13}C NMR (Figure 2.2). ^{1}H NMR (600 MHz, CDCl$_3$) δ= 6.81 (d, 1H, ArH), 6.65 (dd, 1H, ArH), 6.58 (d, 1H, ArH), 5.43 (s, 1H, -OH), 3.82 (s, 3H, -OCH$_3$), 2.79 (s, 2H, -CH$_2$-); ^{13}C NMR (400 MHz, CDCl$_3$) δ= 146.2, 143.7, 133.7, 121.0, 114.1, 111.1, 55.8 (-OCH$_3$), 37.9 (internal CH$_2$).
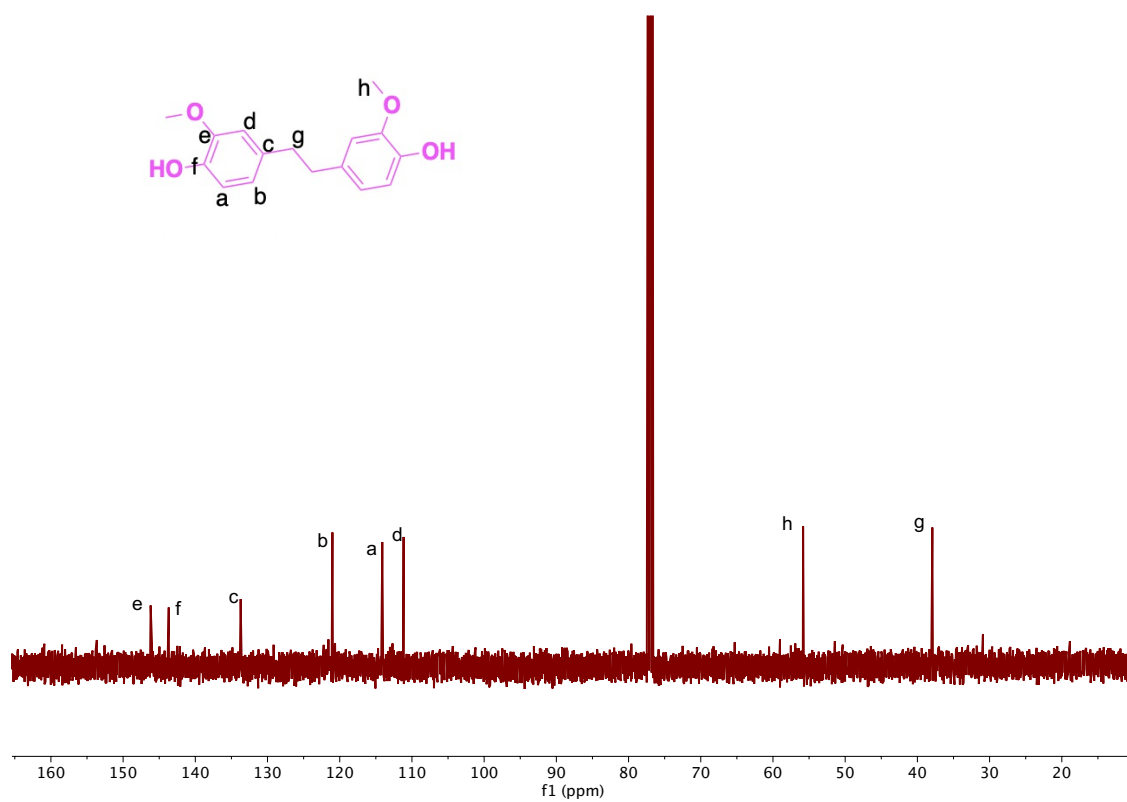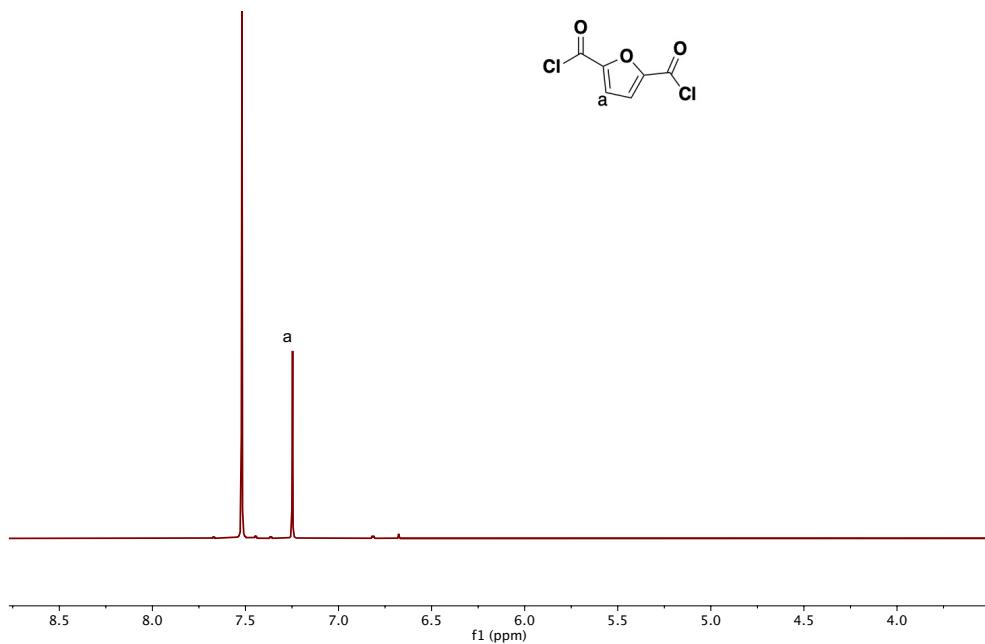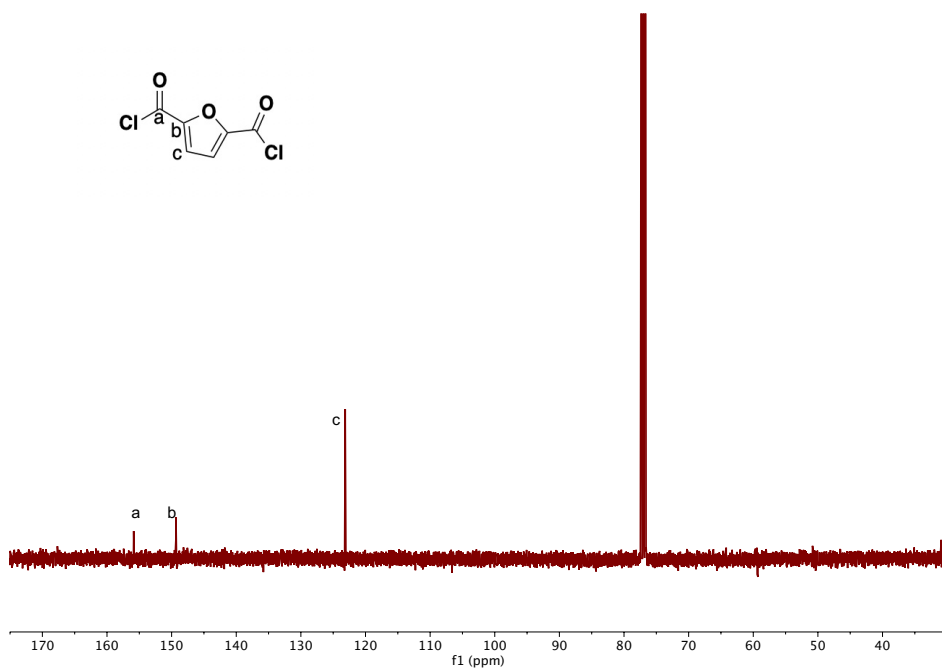
Figure 2.2. ^{13}CNMR (top) and ^{1}HNMR (bottom) spectra of hydrogenated bis-isoeugenol (HBIE) in CDCl$_3$.

2.3.3 Synthesis of Furan dicarbonyl chloride (FDCC)

Procedure adapted from Gomes et al.[8] FDCA (1.0 g, 6.4 mmol) and thionyl chloride (2 mL, 27.6 mmol) and DMF (2 drops) were added to a round bottom flask. The reaction was stirred at reflux for 4 hr. The reaction was then cooled to room temperature and rotary evaporated to give the crude white solid. The crude product was purified via sublimation. The white solid was isolated (1.041 g, 84 %). The product was analyzed by ^{1}H NMR and ^{13}C NMR (Figure 2.3).

Figure 2.3. ^{13}CNMR (top) and ^{1}HNMR (bottom) spectra of furan dicarbonyl chloride (FDCC) in CDCl3.

2.3.4 Interfacial Polymerization Method

Interfacial polymerization method adapted from Gomes et al. and Gharbi et al.[8,9]

Generally, 5 mmol of the bisphenol is dissolved in 30 mL 0.2 M NaOH. 50 mg of

tetrabutylammonium bromide is added to the solution to act as a phase transfer catalyst. Once the bisphenol is dissolved, the acyl chloride (1.1 eq, 5.5 mmol) in 20 mL of DCM is added to the solution dropwise. The biphasic solution is then stirred at room temperature for 24 hr. After 24 hr the solution is acidified with HCl if not already acidic, and then precipitated out in hexanes. This reaction mixture is then vacuum filtered and washed with water, ethanol, and acetone to obtain an off-white to tan colored solid. The solid product is then dried in the oven overnight. Structure characterized by FTIR and NMR spectroscopy. FTIR and NMR spectra of synthesized polyesters can be seen in Appendix A. **PBSU** ^{1}H NMR (600 MHz, $C_2D_2Cl_4$) δ=7.13 (m, 2H, Ar-H), 7.07 (m, 2H, Ar-H), 3.89 (s, 3H, -OCH$_3$), 3.06 (s, 2H, -CH$_2$-).^{13}C NMR (400 MHz, $C_2D_2Cl_4$) δ= 171.7 (C=O), 152.5, 140.5, 137.6, 129.7 (internal C=C), 124.4, 120.5, 111.5, 57.4 (-OCH$_3$), 30.4 (-CH$_2$-). **PBHSU** ^{1}H NMR (600 MHz, $C_2D_2Cl_4$) δ=6.98 (d, 1H, Ar-H), 6.82 (d, 1H, Ar-H), 6.77 (s, 1H, Ar-H), 3.79 (s, 3H, -OCH$_3$), 3.03 (s, 2H, -CH$_2$-), 2.94 (s, 2H, -CH$_2$-).^{13}C NMR (400 MHz, $C_2D_2Cl_4$) δ= 171.9 (C=O), 152.0, 142.1, 138.9, 123.9, 121.8, 114.0, 112.5, 57.3 (-OCH$_3$), 39.1, 30.4. **PBSE** ^{1}H NMR (600 MHz, $C_2D_2Cl_4$) δ=7.11 (m, 2H, Ar-H), 7.03 (m, 2H, Ar-H and C=C-H), 3.88 (s, 3H, -OCH$_3$), 2.59 (m, 2H, -CH$_2$-), 1.77 (m, 2H, -CH$_2$-), 1.40 (m, 2H, -CH$_2$-). ^{13}C NMR (400 MHz, $C_2D_2Cl_4$) δ= 173.3 (C=O), 152.5, 140.7, 137.3, 129.7 (internal C=C), 124.4, 120.5, 111.5, 57.3 (-OCH$_3$), 35.4, 30.5, 30.4, 26.4. **PBHSE** ^{1}H NMR (600 MHz, $C_2D_2Cl_4$) δ=6.94 (d, 1H, Ar-H), 6.81 (dd, 1H, Ar-H), 6.77 (d, 1H, Ar-H), 3.79 (s, 3H, -OCH$_3$), 2.93 (s, 2H, -CH$_2$-), 2.57 (t, 2H, -CH$_2$-), 1.76 (m, 2H, -CH$_2$-), 1.41 (m, 6H, -CH$_2$-). ^{13}C NMR (400 MHz, $C_2D_2Cl_4$) δ= 173.4 (C=O), 152.1, 141.9, 139.2, 124.0, 121.7, 114.1, 57.3 (-OCH$_3$), 39.0, 35.4, 30.5, 30.3, 26.4. **PBA** ^{1}H NMR (600 MHz, $C_2D_2Cl_4$) δ= 7.11 (m, 4H, Ar-H and C=C-H), 3.89 (s, 3H, -OCH$_3$), 2.68 (s-broad, 2H, -CH$_2$-), 1.92 (s-broad, 2H, -CH$_2$-). ^{13}C NMR

(400 MHz, $C_2D_2Cl_4$) δ=172.8 (C=O), 152.4, 140.6, 137.4, 129.6 (internal C=C), 124.3, 120.4, 111.4, 57.2 (-OCH$_3$), 34.9, 25.6. **PBHA** ^{1}H NMR (600 MHz, $C_2D_2Cl_4$) δ=6.96 (d, 1H, Ar-H), 6.81 (dd, 1H, Ar-H), 6.77 (s, 1H, Ar-H), 3.79 (s, 3H, -OCH$_3$), 2.94 (s, 2H, -CH$_2$-), 2.65 (b, 2H, -CH$_2$-). ^{13}C NMR (400 MHz, $C_2D_2Cl_4$) δ=173.0 (C=O), 152.1, 142.0, 139.1, 123.9, 121.7, 114.0, 57.2 (-OCH$_3$), 39.1, 34.9, 25.6.

2.3.5 Solution Polymerization Method

Solution polymerization method adapted from Gomes et al. and Gharbi et al.[8,9] 5mmol of the bisphenol is dissolved in 30 mL of THF. A stoichiometric amount of triethylamine is then added to the solution. Once the bisphenol is completely dissolved, 5 mmol of 2,5-furan dicarbonyl chloride is dissolved in another portion of 20 mL of THF and then added to the bisphenol solution dropwise. The solution is then stirred at room temperature for 24 hr. After 24 hr. the solution is poured into excess hexanes to precipitate out the polymer. The solution is vacuum filtered, rinsed with hexane, water, and acetone. Off white to tan solid obtained and dried in oven overnight. Structure characterized by FTIR and solid-state NMR spectroscopy. FTIR and NMR spectra of synthesized polyesters can be seen in Appendix A.

2.4 Instrumental Analysis Methodology

To obtain the structural characterization of small molecules and polyesters synthesized, both NMR spectroscopy and Attenuated total reflectance Fourier transform infrared (ATR-FTIR) spectrometry were used. Thermogravimetric analysis (TGA) and differential scanning calorimetry (DSC) were used to acquire the thermal properties of polymer networks.

2.4.1 Nuclear Magnetic Resonance Spectroscopy (NMR)

^{1}H NMR spectra were taken on a Varian Unity Inova AS600 600 MHz instrument.^{13}C NMR spectra were taken on a Varian Unity Inova 400 MHz instruments. Deuterated

chloroform or deuterated tetrachloroethane (TCE) were used as the solvent. For **PBF** and

PHBF, solid state NMR spectroscopy was utilized due to solubility constraints. Solid state

NMR spectra were taken on a 500MHz Bruker AVANCE500 WB spectrometer using a 4

mm rotor.

2.4.2 Fourier Transform Infrared Spectroscopy (FTIR)

ATP-FTIR spectra were taken on a Nicolet iS10 FTIR instrument and scanned over a

range of 500-4000 cm^{-1}.

2.4.3 Thermogravimetric Analysis (TGA)

Samples (5-10 mg) were put into a Al_2O_3 crucible, which was then put into a

Discovery Thermo-Gravimetric Analyzer. The sample was then heated from 50 ^{o}C to 600 ^{o}C

at a heating rate of 20 ^{o}C/min under nitrogen flow of 40 mL/min.

2.4.4 Differential Scanning Calorimetry (DSC)

A TA Instruments Q2000 DSC was used. Samples (1-3 mg) were sealed into Tzero

aluminum sample pans with corresponding lids. Once inside the instrument, the samples

were heated and cooled from 0 ^{o}C to 200-325 ^{o}C, depending on their T_{d5} value, at a rate of 10

^{o}C/min under a N_2 gas flow of 50 cm^3/min. Samples went through three cycles of heating and

cooling. T_m was determined by the identification of the temperature at which the endotherm

occurs during the first cycle of heating. All DSC thermograms can be seen in Appendix A.

2.4.5 Matrix-Assisted Laster Desorption Ionization (MALDI)

A Bruker Microflex LRF MALDI TOF mass spectrometer was used for the analysis

of the polyester molecular weight. The MALDI source operates with a 60 Hz nitrogen laser

at 337 nm. The samples were prepared in either DCM or TCE as a solvent, with 2-[3-(4-tert-

Butylphenyl)-2-methyl-2-propenylidene]malononitrile] (DCTB) doped with NaTFA used as

the matrix. If TCE was used as the solvent, samples were heated to ensure complete dissolution. Data was collected from 1-10 kDa. MALDI spectra can be seen in Appendix A.

**2.4.6 Diffusion Ordered Spectroscopy (DOSY)**

A Bruker 300 MHz SWB NMR spectrometer was used to find the diffusion coefficients of the synthesized polyesters. Each NMR tube contained 0.5 mg sample and 1 mL of tetrachloroethane-d_2. Samples were left to equilibrate for at least 10 minutes before running. Experiments were run without spinning. The number of gradient steps was set to 32. Diffusion coefficients were found from the T1/T2 analysis module of Topspin 3.0.

2.5 Results and Discussion

2.5.1 Synthesis and Structural Characterization of Bio-Polyesters

It has been shown that a bis-isoeugenol molecule (BIE) can be synthesized via metathesis of isoeugenol.[25] The hydrogenation of BIE to HBIE is also known.[27] However, the use of these bisphenols in polyesters has not been previously investigated. Polyesters were named based on the use of BIE (**B**) or HBIE (**HB**) with the corresponding acyl chloride used. Polyesters were synthesized with a variety of acyl chlorides (furan dicarbonyl chloride (**F**), succinyl chloride (**SU**), adipoyl chloride (**A**), and sebacoyl chloride (**SE**)) (Figure 2.4). Acyl chlorides were used over the corresponding carboxylic acids because of their higher reactivity to allow for the polymerization reactions to occur at room temperature. For example, the polyester synthesized using BIE (**B**) and succinyl chloride (**SU**) was named **PBSU**, whereas the one using HBIE (**HB**) and succinyl chloride was **PHBSU**. For the furan-based polyesters, furan dicarbonyl chloride (FDCC) was synthesized by reacting 2,5-furan dicarboxylic acid (FDCA) with thionyl chloride with DMF as a catalyst.[8] **PBF** and **PHBF** were synthesized using a solution method in THF with triethylamine as the base.[8,9] This

49

polymerization procedure was not suitable for the aliphatic acyl chloride reagents, therefore a different procedure was used. The polycondensation method, adapted from Gharbi et al., involved a biphasic solution and a phase transfer catalyst (tetrabutylammonium bromide).[8,9]
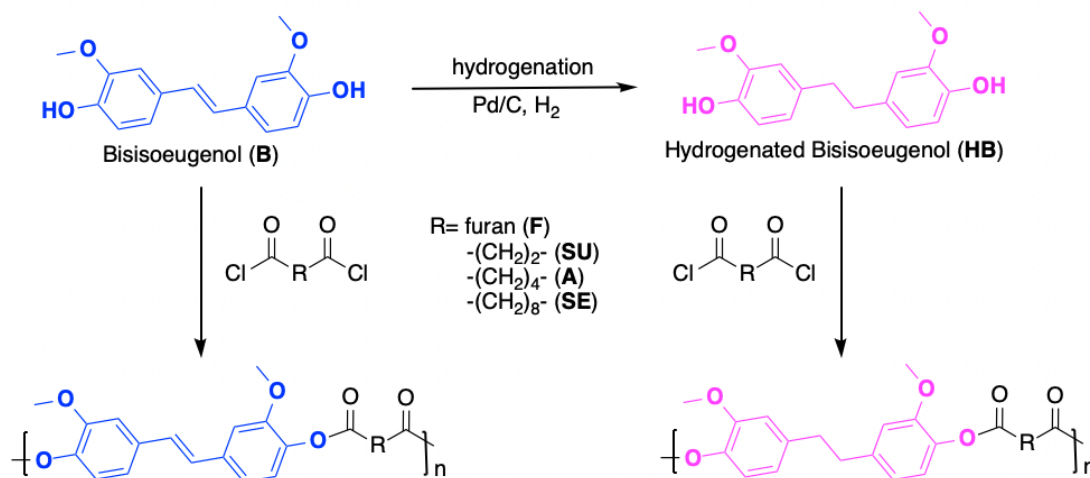
Figure 2.4. General outline of polyester synthesis from lignin-derived bisphenols.

SC and FDCC were chosen as diacids because the corresponding carboxylic acids can be prepared from biomass.[34,35] Further polyesters were synthesized from adipoyl chloride (**AC**), a derivative of adipic acid, which is another monomer that can be derived from biomass. Sebacoyl chloride (**SeC**) was also used to discern the effect of a longer aliphatic chain and to improve solubility and processability of the polyesters. In the case of utilizing SC or AC as the diacid monomer, the resulting polymers would have a high % biocontent because both monomers can be sourced from biomass. In the case of utilizing SU or AC as the diacid monomer, the resulting polymers would have 100% bio-content because both monomers can be sourced from biomass. The use of SEC gives polyesters with approximately 58% bio-content.

FTIR spectra showed strong absorptions corresponding to the carbonyl (C=O) peaks and strong C-O bond signals (Figure 2.5, Appendix A). Also, as expected the sp^3 C-H stretches increased in intensity as the length of the carbon chain of the diacid increased.
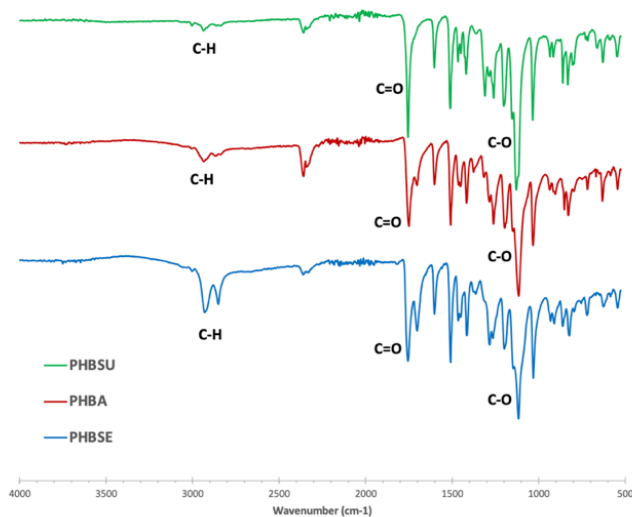

Figure 2.5. FTIR spectra of **PHBSU** (top), **PHBA** (middle), and **PHBSE** (bottom)

The obtained polyesters were not soluble in most organic solvents. However, they are reasonably soluble in 1,1,2,2-tetrachloroethane (TCE), and the use of TCE-d2 enabled us to obtain their ^{1}H and ^{13}C NMR spectra. For insoluble furan-based polymers **PBF**, a solid-state NMR spectrum was acquired to obtain structural information. The solid-state NMR spectrum indicated that there was only one sp^3 carbon with all other signals being in the aromatic and alkene region (Appendix A). NMR spectra further showed that the polyesters had the desired structure. ^{1}H NMR spectra showed peaks corresponding to both the aromatic hydrogens as well as the aliphatic hydrogens for all synthesized polymers, and ^{13}C NMR spectra showed peaks accounting for all carbons that were expected in the polymers (Appendix A). Figure 2.6 shows ^{13}C-NMR spectra for **PBSE** and **PHBSE** as an illustrative example, with the 129.0 ppm, indicative of the internal double bond of the BIE monomer, only present for **PBSE**, and

the 39.0 ppm peak corresponding to the HBIE monomer only present for **PHBSE.**

Additionally**,** both spectra shown in Figure 4 show a carbonyl peak at 173 ppm, peaks

corresponding to the aromatic carbons between 110 - 155 ppm, the peak for the methoxy

carbon at 57 ppm, and sp^3 carbon signals for the aliphatic chain from 25 - 35 ppm.
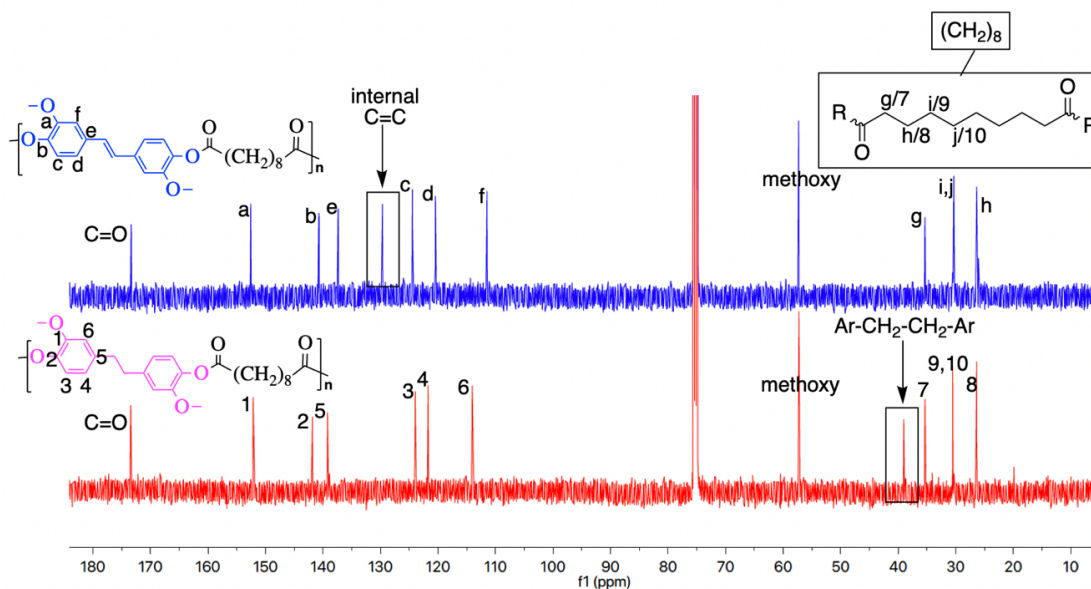
Figure 2.6. ^{13}C NMR spectra of **PBSE** (above) and **PHBSE** (below) highlighting the presence of the internal alkene carbon in **PBSE** versus the alkyl carbon in **PHBSE**. Solvent C$_2$H$_2$Cl$_4$.

Matrix-assisted laser desorption ionization (MALDI) mass spectrometry was used to

obtain insight into the molecular weight of the polyesters. The more commonly used gel

permeation chromatography (GPC) was not used because the polymers were not soluble in

commonly used solvents for ambient temperature GPC up to 50 °C. MALDI spectra showed

that each polyester consisted of molecular weights from oligomeric units to about 20

monomer units, which ranged from approximately 1,000-8,000 Da. Figure 2.7 shows an

example spectrum of **PHBSE**. MALDI spectra of other polyesters can be seen in Appendix

A. Though the MALDI spectra shows oligomeric units, they give limited insight into the true

molecular weights of the polyesters because of the preferential ionization of the shorter

chains and the discrimiation of the longer.
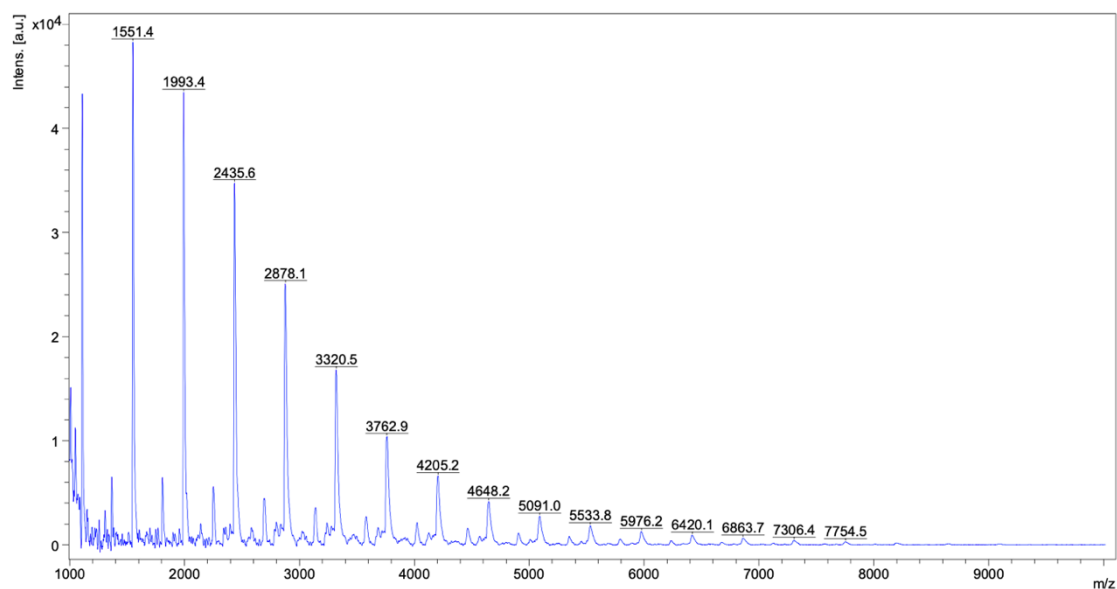
Figure 2.7. MALDI Spectrum of PHBSE.

In addition to the MALDI spectra, diffusion ordered spectroscopy (DOSY) was used to

obtain the molecular weights of the polyesters. Grubbs et al. have shown that the molecular

weights of polymers can be obtained via DOSY in a similar manner to that of GPC.[36]

Essentially, they show how the diffusion coefficent is related to the molecular weight of a

polymer. A calibration curve using polystyrene in TCE-d_2 with a known molecular weight

was obtained and can be seen in Appendix A. The lignin-derived polyesters were then

analyzed, which gave their diffusion coefficients. The diffusion variable gradeient fits were

used to determine diffusion constant, D, of the polyesters. Details are provided in Appendix

A. The peak that gave the best fit was chosen as the most accurate D value. Using the

equation of the calibration curve, approximate moleuclar weights were calculated (Table

2.1).

53

Table 2.1. Diffusion coefficients (D) and extrapolated molecular weights (M_w) for synthesized polyesters

| Polyester	D (10^{-11}) (m^2/s)	Mw (g/mol)[a]
PBSU	4.34	16600
PBA	7.01	7600
PBSE	6.84	7900
PHBSU	3.49	19400
PHBA	4.29	16900
PHBSE	6.02	9800

[a]Values reported are rounded to the nearest hundred.

The results in Table 2.1 confirm that the materials are polymeric and show diffusion coefficients of the same magnitude of the polystyrene standards. For lower molecular weight samples like **PBA** and **PBSE**, this equates to approximately 18 units. The highest molecular weight sample, **PHBSU**, corresponds to approximately 52 repeating units. The M_w of these polyesters have some bearing on their thermal and mechanical properties, which are discussed in the next sections.

2.5.2 Thermal Properties of Bio-Polyesters

Thermogravimetric analysis (TGA) thermograms showed that the synthesized polyesters with aliphatic diacids were all thermally stable up to around 300 °C (Figure 2.9). No specific trend was observed with the 5% degradation temperature (T_{d5}) for the polymers. For the furan containing polyesters, the T_{d5} was significantly lower, being around 200 °C. Since furan rings have shown thermal stability in polyesters such as PEF, the low values for T_{d5} indicated that the furan-based polyesters synthesized in this work probably had low

molecular weight, potentially due to the solution method used for synthesis. This was further supported by the two-step degradation of the furan-based polyesters seen in Figure 2.9, where low weight oligomers degraded in the first step.
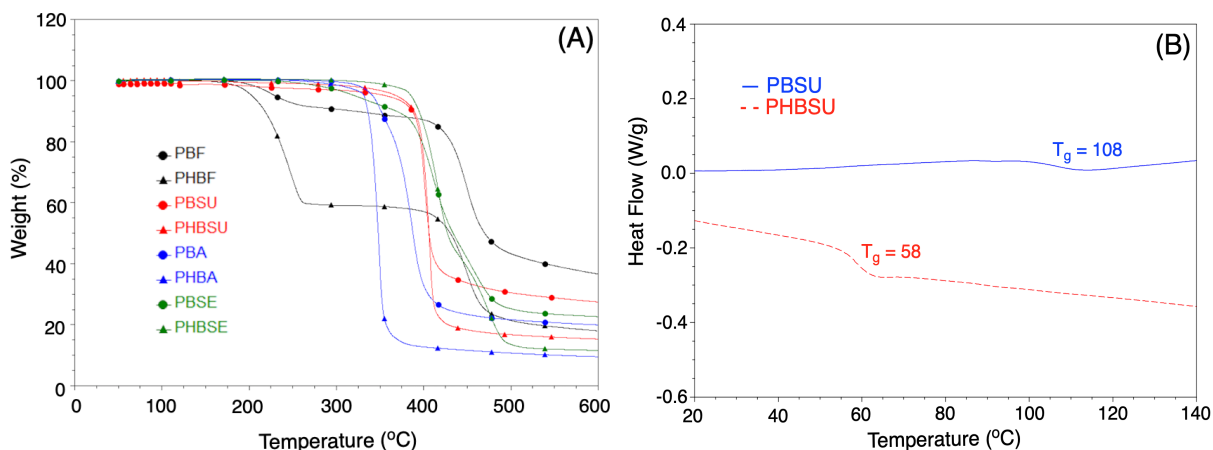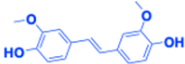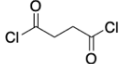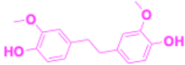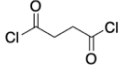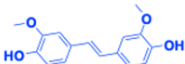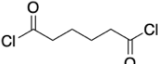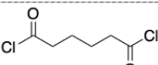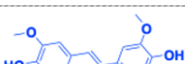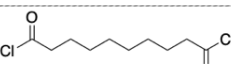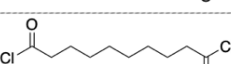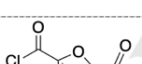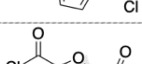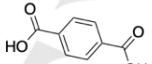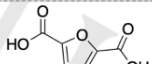

Figure 2.9. (A) TGA thermograms for all polyesters. (B) DSC for **PBSU** (top) and **PHBSU** (bottom) showing T_g

Further study into the glass transition temperature (T_g) and melting temperature (T_m) of the polyesters were evaluated using differential scanning calorimetry (DSC). DSC was not conducted on the furan-based polyesters because they degraded before melting and therefore the heating cycle was not able to reach a high enough temperature. Since the polymers were semi-crystalline powders when isolated, the first heating scan during the DSC resulted in an endotherm corresponding to the T_m of the polyester, but once melted, the polyesters become amorphous and the endotherm was not seen on subsequent heating cycles (Appendix A), which indicated that they are no longer semi-crystalline.

The DSC measurements show that the resulting T_g of the polyesters decreased with an increase in aliphatic chain length of the diacid (Table 1). The same trend can be observed for the T_m of the polyesters, as the increase in chain length allowed for less rigidity in the polymer structure. Polyesters with BIE exhibited higher T_g and T_m than the corresponding

HBIE polyester, also due to the higher rigidity of BIE polyesters (Figure 2.9). This gave the

resulting polyesters predictable thermal properties (Table 2.2). With the exception of **PBSU**,

all the T_g values were significantly lower than both PET and PEF.

Table 2.2. Summary of thermal properties T_{d5}, T_{d50} (Temperature at 5 % and 50 % Weight Loss), T_g (Glass Transition Temperature), and T_m (Melting Temperature) of Polyesters synthesized with bio-based bisphenols BIE and HBIE[a]

Polymer	Bisphenol / Ethylene Glycol	Acid	T_g (°C)[b]	T_m (°C)[b]	T_{d5} (°C)[c]	T_{d50} (°C)[c]
PBSU			108	259	278	373
PHBSU			61	183	348	403
PBA			53	229	306	363
PHBA			43	138	328	346
PBSE			31	146	284	414
PHBSE			19	106	256	395
PBF			nd[d]	nd[d]	217	400
PHBF			nd[d]	nd[d]	207	426
PET[e]			80	251	420	Not Reported[f]
PEF[e]			87	211	389	Not Reported[f]

[a]All reported values for polyesters are the average of three runs. [b]Value obtained from DSC thermograms. [c]Value obtained from TGA thermograms. [d]Degradation temperature below melting point value. [e]Literature values.[4] [f]Not reported in literature[4]

While the different structures have the dominant effect on the thermal properties, the

molecular weights also play a part. Generally, higher molecular weights correspond to more

viscous materials due to the longer chains and higher entanglement. This will impact the T_g

value, with higher molecular weight corresponding to higher T_g. It has been reported that the effect of molecular weight on T_g is insignificant for molecular weights above approximately 5000 g/mol. Since all bio-polyesters reported here are above 5000 g/mol,[37] the difference in molecular weights has little impact on the reported T_g values.

2.5.3 Tunability of Bio-Polyesters

To obtain a T_g more comparable to that of PET and show the tunability of these lignin-derived monomers, BIE and HBIE were used in mixed ratios with succinyl chloride to tune the thermal properties. Integrating the mixture of both the single bonded bisphenol and the double bonded bisphenol created random pockets of a more rigid structure due to the conjugation of the double bond and less rigid pockets where the aromatic rings were broken up with an aliphatic region. This allowed us to tune the thermal properties based on how much of each monomer was incorporated in the polymerization. Thermal properties could even be further adjusted by varying the aliphatic diacid used in synthesis. The tunability results are summarized in Table 2.3.

Table 2.3. Summary of thermal properties T_{d5}, T_{d50} (Temperature at 5 % and 50 % Weight Loss), T_g (Glass Transition Temperature), and T_m (Melting Temperature) of Polyesters made with ratios of BIE: HBIE and succinyl chloride (SU)

Polymer	T_g (°C)[a]	T_m (°C)[a]	T_{d5} (°C)[b]	T_{d50} (°C)[b]
1:1[c]	83	190[d]	334	464
1:2[c]	67	179[d]	206	443
PET[e]	80	251	420	NA[f]
PEF[e]	87	211	389	NA[f]

[a]Value obtained from DSC thermograms. [b]Value obtained from TGA thermograms. [c]Ratios are labeled BIE:HBIE. [d]Melting point exotherms are very broad. [e]Literature values.[4] [f]Not reported in literature

Using a 1:1 ratio of BIE:HBIE, the T_g could be tuned to a comparable value to PET and PEF, though due to the nature of mixtures, the T_m for the mixtures was lowered and broadened. The same trend seen in the pure polyesters was seen in the mixtures. When more HBIE was introduced into the random polymer, the T_g and T_m of the resulting polyester decreased. The decrease in 5% degradation temperature (T_{d5}) for these mixtures was due to a two-step degradation, where the initial degradation was most likely due to lower molecular weight oligomers. The structures were confirmed through ^{1}H and ^{13}C NMR spectroscopy (Figure 2.10, Appendix A). The ^{13}C NMR spectra showed peaks that corresponded to both types of internal carbons as well as all the aromatic carbons corresponding to both monomers. The peak at 129.7 ppm corresponded to the double bond carbons between the aromatic rings in BIE, which is not observed in the ^{13}C NMR spectra of polyesters synthesized with exclusively HBIE. In the ^{1}H NMR spectra, two different shifts for the methoxy groups can be resolved at 3.88ppm (BIE) and 3.80 ppm (HBIE).

Figure 2.10. ^{1}H NMR spectrum (top) and ^{13}C NMR spectrum (bottom) for 1:1 (BIE:HBIE) with succinyl chloride polyester. Solvent $C_2D_2Cl_4$

2.5.4 Mechanical Properties of Bio-Polyesters

Mechanical testing of the renewable polyesters was attempted. Most of the polyesters resulted in material that was extremely brittle. Most of the polyesters resulted in material that was extremely brittle, which did not allow for a dog bone sample to be punched out of a film

of the material in one piece. Only **PBSE** and **PHBSE** gave suitable samples for tensile

testing. Even so, tensile tests only show approximately 3 MPa of stress and 1% strain at

break of pure SE-based polyesters. This indicated that the materials are very brittle and will

break almost immediately if put under any stress. The results of these tensile tests can be

seen in Figure 2.11.
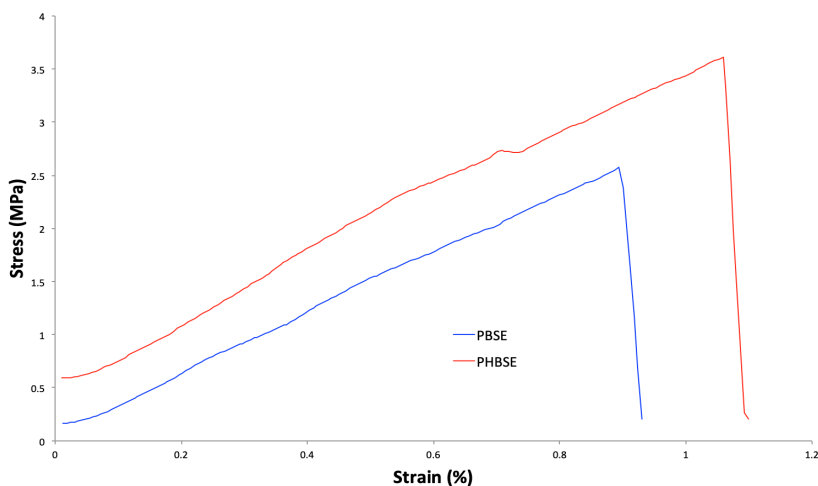
Figure 2.11. Stress-strain curve for PBSE (blue) and PHBSE (red).

This brittleness can be attributed to the rigid aromatic structure present in the bio-derived

bisphenols and lack of crosslinking. The SE-based polyesters have the longest aliphatic,

"flexible," segment incorporated into the structure. Another factor that impacts the

mechanical robustness is the molecular weight. **PBSE** and **PHBSE** have molecular weights

of approximately 7900 g/mol and 9800 g/mol. Like the thermal properties, the structural

difference between the polyesters is the dominant effect on the mechanical properties. One

would still expect that higher molecular weight would correspond to greater stress resistance

and strain at break.[38]

In order to improve the mechanical robustness of these materials, bio-derived epoxides were used to crosslink the polyesters to form thermoset networks. These results are presented and discussed in Chapter 3.

2.6 Conclusion

Isoeugenol, a small molecule that can be obtained from lignin through RCF of lignocellulosic biomass, can be used to synthesize bisphenols and renewable polyesters. DOSY NMR confirmed that all polyesters are polymeric, consisting of 7600 g/mol to 19400 g/mol. The structure of the polyesters had a much more significant effect on the thermal and mechanical properties compared to the molecular weight. All synthesized polymers with aliphatic linkers showed high thermal stability with degradation onset at or above 300 $^{\circ}$C. The effect of aliphatic chain length as well as the effect of the presence or absence of the internal double bond on thermal properties of the resulting polymer networks were delineated, with BIE-based polyesters exhibiting higher T_g values than their HBIE-based counterparts. Further, it was shown that these T_g values could be tuned to be more in line with polyesters like PET ($T_g = 80$ $^{\circ}$C) by incorporating both BIE and HBIE into the polymer. Further work needs to be done to improve the mechanical properties of these bio-derived materials.

2.7 References

1. Hopewell, J.; Dvorak, R.; Kosioer, E., Plastics recycling: challenges and opportunities. *Phil. Trans. R. Soc. B,* **2009**, *364*, 2115-2126.

2. Biomass--Renewable Energy from Plants and Animals, 2018. Available at: https://www.eia.gov/energyexplained/?page=biomass_home. Accessed on June 2018.

3. Sousa, A. F.; Vilela, C.; Fonseca, A. C.; Matos, M.; Freire, C.S.R.; Gruter, G. M.; Coelho, J. F. J.; and A. J. D. Silvestre, Biobased polyesters and other polymers from 2, 5-furandicarboxylic acid: a tribute to furan excellency. *Polym. Chem.,* **2015**, *6*, 5961-5983.

4. Burgess, S. K.; Leison, J. E.; Kraftschik, B. E.; Mubarak, C. R.; Kriegel R. M.; Koros, W. J., Chain Mobility, Thermal, and Mechanical Properties of Poly(ethylene furanoate) Compared to Poly(ethylene terephthalate). *Macromolecules,* **2014**, *47*, 1383-1391.

5. Moore, J. A. and Kelly, J. E., Polymerization of furandicarbonyl chloride with bisphenol A:poly(2,5-furandiylcarbonyloxy-1,4-phenylenedimethylmethylene-1,4-phenyleneoxycarbonyl). *Polymer*, **1979**, *20*, 627-628.

6. Zeng G.; Seino, H.; Ren, J.; Hatanaka, K.; and Yoshie, N., Self-Healing bio-based furan polymers cross-linked with various bis-maleimides. *Polymer*, **2013**, *54*, 5351-5357.

7. Zeng G.; Seino, H.; Ren, J.; Hatanaka, K.; and Yoshie, N., Bio-based Furan Polymers with Self-Healing Ability. *Macromolecules,* **2013**, *46*, 1794-1802.

8. Gomes, M.; Gandini, A.; Silvestre, A. J. D.; Reis, B., Synthesis and Characterization of Poly(2,5-furan dicarboxylate)s Based on a variety of Diols. *J. Poly. Sci. Part A: Polymer Chem.,* **2011,** *49*, 3759-3768.

9. Gharbi, S.; Andreolety, J.; Gandini, A., Polyesters bearing furan moieties IV. Solution and Interfacial polycondensation of 2, 2'-bis(5-chloroformyl-2-furyl)propane with various diols and bisphenols. *European Polymer Journal*, **2000**, *36*, 463-472.

10. van Es, D. S.; van der Klis, F.; Knoop, R. J. I.; Molenveld, K.; Sijtsma, L.; van Haveren, J., (2014). Chapter 9: Other Polyesters from Biomass Derived Monomers, *Bio-Based Plastics* (pp. 241-274). John Wiley & Sons, Ltd.

11. Kainulainen, T. P.; Sirvio, J. A.; Sethi, J.; Hukka, T. I.; Heiskanen, J. P., UV-Blocking Synthetic Biopolymer from Biomass-Based Bifuran Diester and Ethylene Glycol. *Macromolecules,* **2018**, *51*, 1822-1829.

12. EUR 25 Million Subsidy Granted: Industry Consortium Receives Funds for Polyethylene Furanoate (PEF), 2017. Available at: https://www.synvina.com/news/eur-25-million-subsidy-granted-industry-consortium-recei ves-funds-polyethylenfuranoate-pef/. Accessed on July 2018.

13. Froass, P. M.; Ragauskas, A. J.; Jiang, J., Chemical structure of residual lignin from kraft pulp. *Journal of Wood Chemistry and Technology*, **1996**, *16(4)*, 347-365.

14. Bajpai, P., Chapter 12: Pulping Fundamentals. In *Biermann's Handbook of Pulp and Paper (Third Edition)*, pp 295-351.

15. Luo, H.; Abu-Omar, M. M., Sustainable Energy Technologies and Sustainable Chemical Processes. In *Encyclopedia of Sustainable Technologies,* edited by Martin A. Abraham; Hangzhou Dianzi University, China, 2017; Vol. 3, pp 573-585.

16. Cheremisinoff, N. P.; Rosenfeld, P. E., Chapter 6: Sources of air emission from pulp and paper mills. In *Handbook of Pollution Prevention and Cleaner Production*, **2010**, pp 179-259.

17. Kai, D.; Tan, M. J.; Chee, P. L.; Yap, Y. L.; Loh, X. J., Towards lignin-based functional materials in a sustainable world. *Green Chemistry*, **2016**, *18*, 1175-1200.

18. Pandey, M. P.; Kim, C. S., Lignin Depolymerization and Conversion: A Review of Thermochemical Methods. *Chem. Eng. Technol.*, **2011**, *34(1)*, 29-41.

19. Luo, H.; Klein, I. M.; Jiang, Y.; Zhu, H.; Liu, B.; Kenttamaa, H. I.; and Abu-Omar, M. Total Utilization of Miscanthus Biomass, Lignin and Carbohydrates, Using Earth Abundant Nickel Catalyst. *ACS Sustainable Chem. Eng.,* **2016**, *4*, 2316-2322.

20. Galkin, M. G. and Samec, J. S. M., Selective Rouse to 2-Propenyl Aryls Directly from Wood by a Tandem Organosolv and Palladium-Catalysed Transfer Hydrogenolysis. *ChemSusChem*, **2014**, 7, 2154-2158.

21. Galkin, M. G.; Smit, A. T.; Subbotina, E.; Artemenko, K. A.; Bergquist, J.; Huijgen, W. J. J.; Samec, J. S. M., Hydrogen-free catalytic fractionation of woody biomass. *ChemSusChem,* **2016**, 9, 3280-3287.

22. Jastrzebski, R.; Constant, S; Lancefield, C. S.; Westwood, N. J.; Weckhuysen, B. M.; Bruijnincx, P. C. A., Tandem Catalytic Depolymerization of Lignin by Water-Tolerant Lewis Acids and Rhodium Complexes. *ChemSusChem*, **2016**, 9, 2074-2079.

23. Xiao, L. P.; Wang, S.; Li, H.; Li, Z.; Shi, Z. J.; Xiao, L.; Sun, R. C.; Fang, Y.; Song, G., Catalytic Hydrogenolysis of Lignins into Phenolic Compounds over Carbon Nanotube Supported Molybdenum Oxide. *ACS Catal.*, **2017**, 7, 7535-7542.

24. Alma, M. H.; Ertaş, M.; Nitz, S.; Kollmannsberger, H., Chemical Composition and Content of Essential Oil from the Bud of Cultivated Turkish Clove. *BioResources,* **2007**, *2*, 265-269.

25. Hitce, J.; Crutizat, M.; Bourdon, C.; Vives, A.; Marat, X.; and Dalko-Csiba, M., Flash-metathesis for the coupling of sustainable (poly)hydroxyl β-methylstyrenes from essential oils. *Green Chem.*, **2015**, *17*, 3756-3761.

26. Harvey, B.G.; Guenthner, A. J.; Meylemans, H. A.; Haines, S. R.; Lamison, K. R.; Groshens, T. J.; Cambrea, L. R.; Davis, M. C.; Lai, W. W., Renewable thermosetting resins and thermoplastics from vanillin. *Green Chem.*, **2015**, 17, 1249-1258.

27. Trita, A. S.; Over, L. C.; Pollini, J.; Baader, S.; Riegsinger, S.; Meier, M. A. R.; Gooßen, L. J., Synthesis of potential bisphenol A substitute by isomerising metathesis of renewable raw materials. *Green Chem.,* **2017**, *19*, 3051-3060.

28. Liu, X.; Zong, E.; Jiang, J.; Fu, S.; Wang, J.;Xu, B.; Li, W.; Lin, X.; Xu, Y.; Wang, C.; Chu, F., Preparation and characterization of Lignin-graft-poly(ε-caprolactone) copolymers based on lignocellulosic butanol residue. *International Journal of Biological Macromolecules*, **2015**, *81*, 521-529.

29. Laurichesse, S.; Avéros, L., Synthesis, thermal properties, rheological and mechanical behaviors of lignin-grafted-poly(ε-caprolactone). *Polymer*, **2013**, *54*, 3882-3890.

30. Saito, T.; Brown, R. H.; Hunt, M. A.; Pickel, D. L.; Pickel, J. M.; Messman, J. M.; Baker, F. S.; Keller, M.; Naskar, A. K., Turning renewable resources into value-added polymer: development of lignin-based thermoplastic. *Green Chemistry*, **2012**, *14*, 3295-3303.

31. Mialon, L.; Pemba, A. G.; Miller, S. A., Biorenewable polyethylene terephthalate mimics derived from lignin and acetic acid. *Green Chemistry*, **2010**, *12*, 1704-1706.

32. Kreye, O.; Oelmann, S.; Meier, M. A. R., Renewable aromatic-aliphatic copolyesters derived from rapeseed. *Macromol. Chem. Phys.*, **2013**, *214*, 1452-1464.

33. Llevot, A.; Grau, E.; Carlotti, S.; Grelier, S.; Cramail, H., From Lignin-derived Aromatic Compounds to Novel Biobased Polymers. *Macromol. Rapid Commun.*, **2016***, 37*, 9-28.

34. Kawasumi, R.; Narita, S.; Miyamoto, K.; Tominaga, K.; Takita, R.; Uchiyama, M., One-step Conversion of Levulinic Acid to Succinic Acid Using I_2/t-BuOK System: The Iodoform Reaction Revisited. *Scientific Reports,* **2017**, *7*, 1-8.

35. Cok, B.; Tsiropoulos, I.; Roes, A. L.; Patel, M. K., Succinic acid production derived from carbohydrates: An energy and greenhouse gas assessment of a platform chemical toward a bio-based economy. *Biofuel. Bioprod. Bior.*, **2014**, *8*, 16-29.

36. Li, W.; Chung, H.; Daeffler, C.; Johnson, J. A.; Grubbs, R. H., Application of ^{1}H DOSY for Facile Measurement of Polymer Molecular Weights. *Macromolecules*, **2012**, *45*, 9595-9603.

37. Gent, A. N.; Thomas, A. G., Effect of Molecular Weight on the Tensile Strength of Glassy Plastics. *Journal of Polymer Science Part A-2: Polymer Physics*, **1972**, *10*, 571-573.

38. Perkins, W. G.; Capiati, N. J.; Porter, R. S., The effect of molecular weight on the physical and mechanical properties of ultra-drawn high density polyethylene. *Polymer Engineering and Science*, **1976***, 16*, 200-203.

Chapter 3

Utilization of Lignin-Derived Isoeugenol for use in Thermosets

3.1 Abstract

Renewable polyesters reported in chapter 2 were used to synthesize epoxy thermosets by exploiting the active ester groups in the polymer for reaction with epoxide. Chapter 2 outlined the synthesis of renewable polyesters from a hydrogenated bis-isoeugenol (HB) and diacyl chloride monomers such as succinyl chloride (SU), adipoyl chloride (A), and sebecoyl chloride (SE) giving three polyesters PHBSU, PHBA, and PHBSE.A lignin-derived epoxy was synthesized and compared to common industrial epoxies. The result of the cross-linking improves the thermal properties, increasing T_g from 61 °C to 98 °C for PHBSU-based thermosets, 43 °C to 105 °C for PHBA-based thermosets, and 19 °C to 103 °C for PHBSE-based thermosets. The mechanical properties showed storage moduli in the rubber region of 4.7 - 19 MPa and tensile stress of up to 68 MPa. The utilization of a polyester as a crosslinker for epoxy thermosets is a largely untapped mechanism and can expand the library of thermoset materials, especially for bio-based renewable thermoset materials.

3.2 Introduction

Epoxy thermosets are highly desirable materials because of their mechanical strength, chemical resistance, and thermal stability.[1] One of the components in the vast majority of epoxy thermosets is bisphenol A diglycidyl ether (DGEBA), which is the epoxidized from of petroleum-derived bisphenol A (BPA). As a renewable source of aromatics, lignin represents a viable alternative feedstock for DGEBA-like bisphenols for use in epoxy thermosets.[2-7]

There has been extensive work in the area of lignin derived epoxides and thermosets. Work by Zago et al. introduced epoxidized bis-isoeugenol (BIEE).[8] Additionally,

67

epoxy thermosets utilizing lignin-derived phenols have been reported. These bio-phenols include eugenol,[9-12] dihydroeugenol,[13,14] isoeugenol,[15,16] 4-n-propylsyringol,[17] guaiacol,[18] and vanillin[19-25] have all been previously investigated. Technical lignin has also been used directly to create epoxides.[26-30] There are also examples of obtaining epoxy polymers from directly depolymerized lignin.[31-36] The use of bis-isoeugenol (BIE), the hydrogenated variant (HBIE), and epoxide derivatives (BIEE, HBIEE) in thermoset networks represent an area to expand on this field of work.

Additionally, the use of active esters as epoxy curing agents has been shown to be a viable curing mechanism.[37-39] Nakamura and Arima used a trifunctional active ester as an epoxy curing agent,[39] and Nishikubo et al. have shown several examples of using this chemistry for post polymerization modification on polymers with either pendant active esters or pendant epoxides.[40-45] More recently, Lin et al. used this curing mechanism to synthesize low dielectric epoxy thermosets[46], and Chen et al. synthesized self-curing molecules that included both active ester groups and epoxide groups, which yielded high T_g thermosets.[47]

In this chapter, renewable polyesters (Figure 3.1) are cross-linked with epoxides to form thermosets. These polyesters are synthesized from a renewable bisphenolic monomer and various acyl chlorides. The polyesters include active ester linkages that are utilized as an epoxy curing agent to synthesize thermoset networks. In addition to the thermoset synthesis, we describe the effect of the curing mechanism on the thermal and mechanical properties of the resulting material. While there is an expanse of work on bio-based thermosets, there are no other examples of utilization of renewable polyesters as the curing agent.
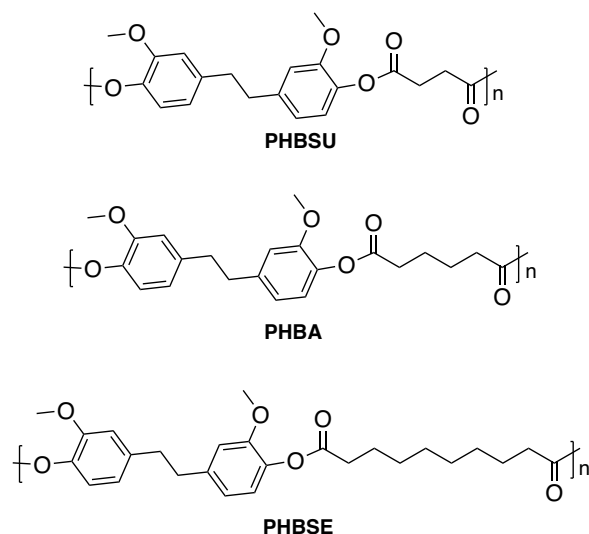
Figure 3.1. Structures of renewable polyesters used in this work to make thermosetting polymers.

3.3 Synthetic Procedures

3.3.1 Synthesis of HBIE epoxide, HBIEE

Epoxidation of bisphenols was done using the method developed by Zhao et al.[13] HBIEE was prepared by reacting HBIE (2.267 g, 8.3 mmol) with epichlorohydrin (15 g, 16.2 mmol) in the presence of tetrabutylammonium bromide (0.115 g, 0.4 mmol) as a phase transfer catalyst. The mixture was heated to 60 °C for 3 h and then 1.3 g of 50% w/w NaOH solution was added to the solution dropwise. The mixture was then stirred at 60 °C for an additional 3 h, after which the mixture was cooled to room temperature, filtered and the solid was washed with water and acetone. White solid was obtained (3.173 g, 99 %) m.p. 115-119 °C. The structure was confirmed via NMR (Figure 3.2). ^{1}H NMR (CDCl$_3$, 600 MHz) δ: 6.83 (d, 1H, ArH), 6.67 (dd, 1H, ArH), 6.65 (d, 1H, ArH), 4.20 (dd, 1H, -OCH$_2$-), 4.01 (dd, 1H, -OCH$_2$-), 3.81 (s, 3H, -OCH$_3$), 3.37 (m, 1H, -CH-), 2.88 (t, 1H, epoxide CH$_2$), 2.83 (s, 2H, -

69

CH$_2$-), 2.72 (q, 1H, epoxide CH). ^{13}C NMR (CDCl$_3$, 400 MHz) δ: 149.3, 146.1, 135.5, 120.4, 114.3, 112.4, 70.4 (epoxide CH$_2$), 55.9 (-OCH$_3$), 50.3 (epoxide ring CH), 45.0 (epoxide ring
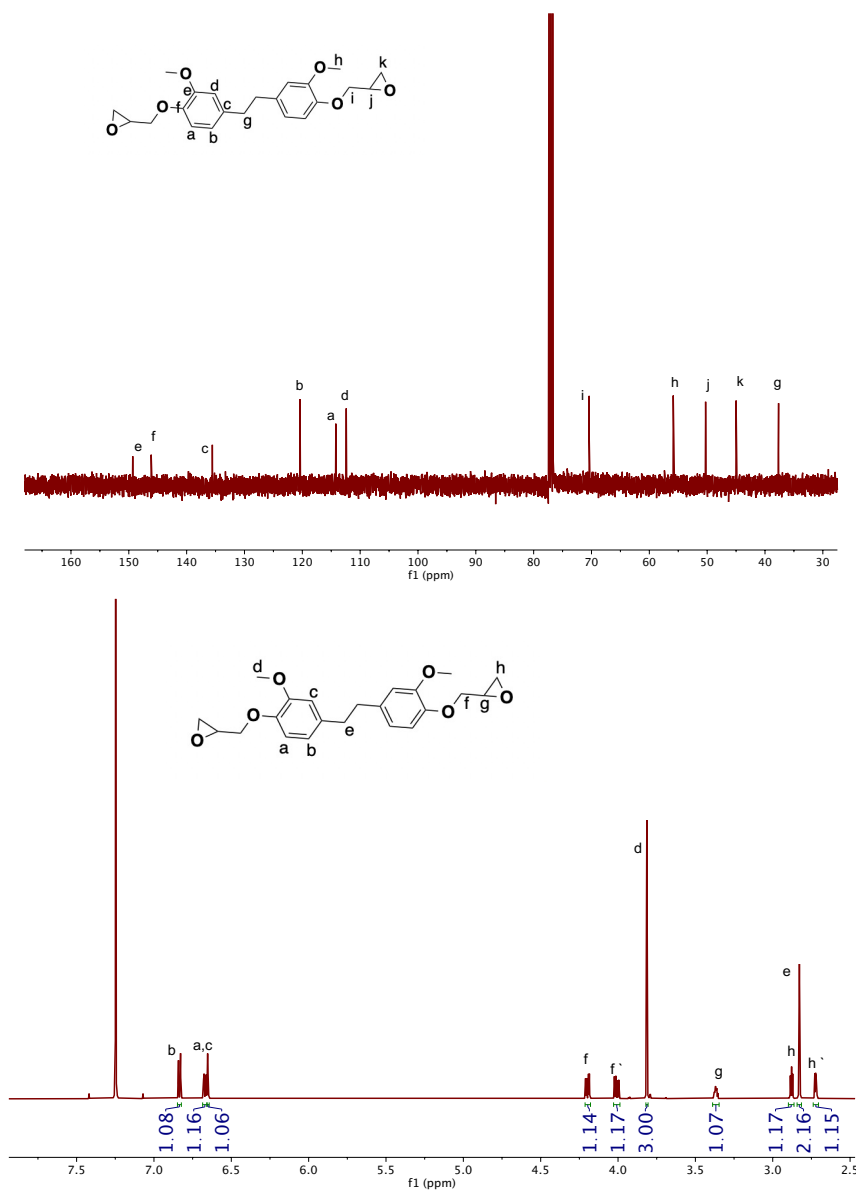
Figure 3.2. ^{13}CNMR (top) and ^{1}HNMR (bottom) spectra of epoxidized hydrogenated bisisoeugenol (HBIEE) in CDCl$_3$.

CH$_2$), 37.7 (internal CH$_2$).

3.3.2 Curing Procedure for Thermosets

Curing procedure adapted from that of Lin et al.[46] Each of the polyesters was dissolved in N-methyl-2-pyrrolidinone (NMP) with the epoxide, and 0.5 wt% of the catalyst 4-(dimethylamino)pyridine (DMAP) to create a 30 wt% solid solution. Epoxide and active ester groups were added in a stoichiometrically 1:1 ratio. This solution was then cast onto an aluminum plate. The resulting film was then cured overnight at 80 °C and then at 140 °C (2 h), 160 °C (2 h), and 180 °C (2 h). Tensile and DMA samples were cut out of the thermoset film into the required shape with a sample punch.

3.4 Instrumental Analysis Methodology

In addition to the methodology described in Chapter 2, section 2.4, the following analysis methods were used to characterize the bio-thermosets.

3.4.1 Tensile Tests

Tensile measurements were taken on a custom high-strain test machine. Samples were cut out with a dog bone shaped punch. Samples were 25 mm in length and 0.1 mm in thickness. Measurements were taken at a data rate of 5 pts/sec and a Crosshead speed (displacement) of 0.5 mm/min. Measurements were taken until the samples broke.

3.4.2 Dynamic Mechanical Analysis (DMA)

Dynamic mechanical properties were characterized using a TA Instruments DMA850. The dimensions of the DMA samples were 20mm x 6 mm x 0.1mm (length, width, thickness), which provided a span-to-thickness ratio of well above 10, as suggested by McAninch et al.[48] Measurements were conducted from 30 °C to 180 °C at a ramp rate of 5 °C/min and a frequency of 1 Hz.

3.5 Results and Discussion

3.5.1 Synthesis and Structural Characterization of Bio-Thermosets

Expanding on the work discussed in Chapter 2, renewable polyesters were crosslinked with lignin-derived bisphenols to enhance the mechanical properties of the resulting material. Due to solubility issues in the curing solvent, polyesters made with BIE were deemed not suitable for making thermoset networks. The epoxidized BIE monomer was synthesized but ran into similar solubility issues when used as a pre-polymer to make thermosets. Therefore, only polyesters incorporating HBIE (**PHBSU**, **PHBA**, and **PHBSE**) were cured with three different epoxide molecules, resulting in nine different thermosets. The epoxides that were used are BPA based DGEBA (EEW = 172-176 g/eq), HBIE based HBIEE, and the industrial epoxide polymer HP7200 (EEW = 260 g/eq) (Figure 3.3). The epoxide equivalent weight (EEW) of the HBIE based epoxide (HBIEE) was calculated via a titration method using hydrochloric acid and sodium hydroxide.[49,50] The EEW was calculated to be 217 g/eq, indicating that most HBIE molecules had two epoxides, like the structure suggests. The
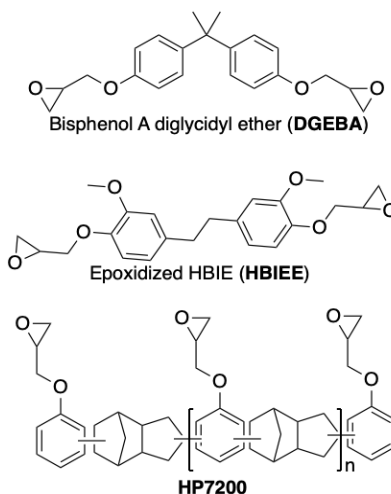
Figure 3.3. Structures of epoxides used for thermoset syntheses

polyester and epoxide were dissolved in N-methyl-2-pyrrolidone (NMP) with 0.5wt% of the catalyst DMAP and then cast on an aluminum plate.

To analyze the structure of the formed thermosets, FTIR was used. When cross-linked, the carbonyl absorption should shift to a lower wavenumber compared to the starting polyester.[46] This is due to the carbonyl transitioning from an Ar-O-C=O to Alkyl-O-C=O based on the mechanism described by Lin et al. between epoxides and polyarylates. In short, the DMAP ring opens the epoxide creating an alkoxy anion. The alkoxy anion attacks the active ester group in the polyesters creating a phenoxy anion. This phenoxy anion can (1) ring open another epoxide moiety, generating another alkoxy anion or (2) substitute onto the

C-N bond releasing the DMAP molecule (Figure 3.4).[46] This reaction sequence (mechanism) can repeat until crosslinking is complete.

Based on the curing mechanism, there are multiple reactions that could occur including the epoxide reacting with carboxylic acid end groups and the epoxide reacting with the internal active esters. Additionally, when reacting with the internal active esters the epoxides cleave the polyester chains. The higher molecular weight polyesters are more likely to be
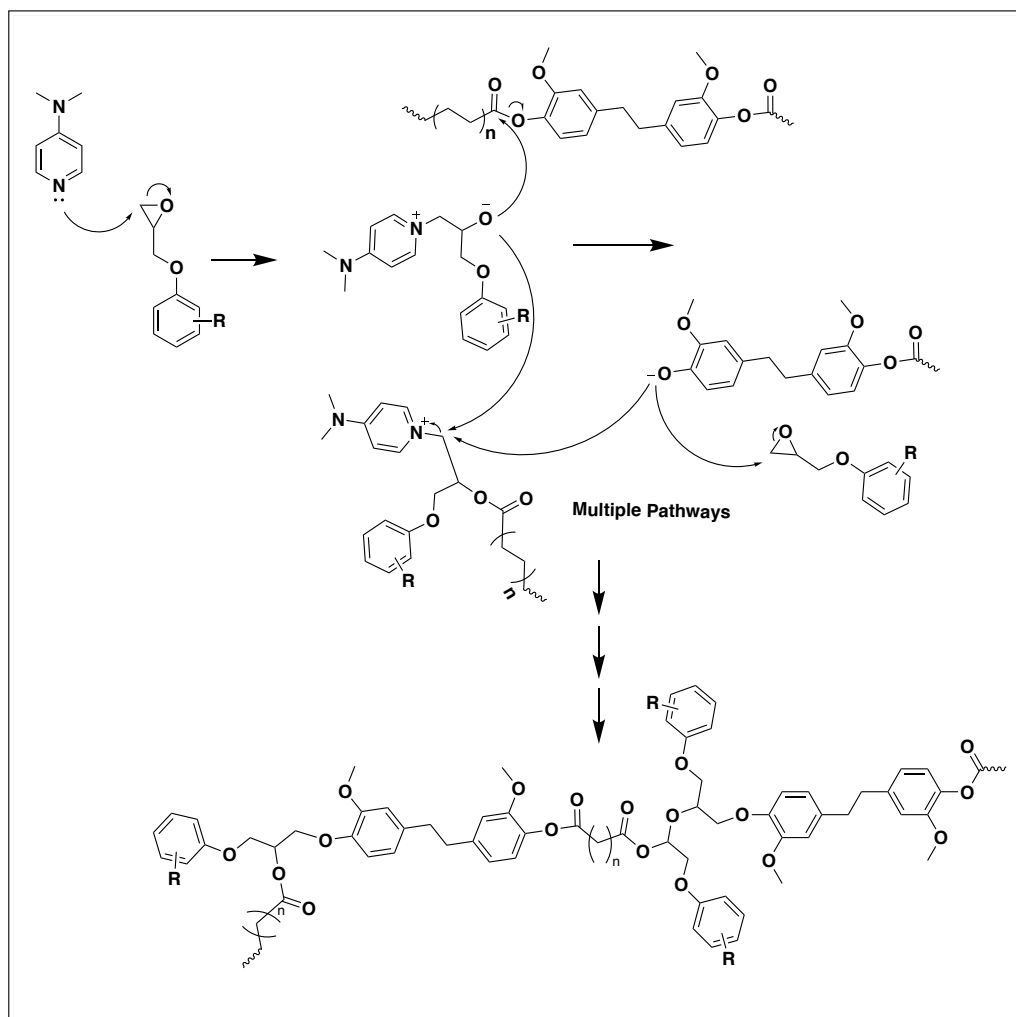
Figure 3.4. Proposed mechanism for crosslinking of polyesters and epoxides catalyzed by DMAP. Reported by Lin et al.[46]

cleaved, creating shorter chains within the thermoset network.

The carbonyl shifts of synthesized thermosets are illustrated in Figure 3.5 and reported in Table 3.1. The carbonyl shifts corresponding to all thermosets occurred at lower wavenumbers than the polyesters, indicating that cross-linking had occurred. For example, the polyester **PHBSE** showed a carbonyl shift at 1756 cm^{-1}, and after curing with DGEBA the carbonyl peak shifted to 1733 cm^{-1}. Further, the emergence of OH bands at ~3400 cm^{-1}, and absence of the epoxy band at ~912 cm^{-1} in the FTIR spectra of cured thermosets indicated that the epoxide moieties had reacted and the corresponding spectra are in Appendix A.
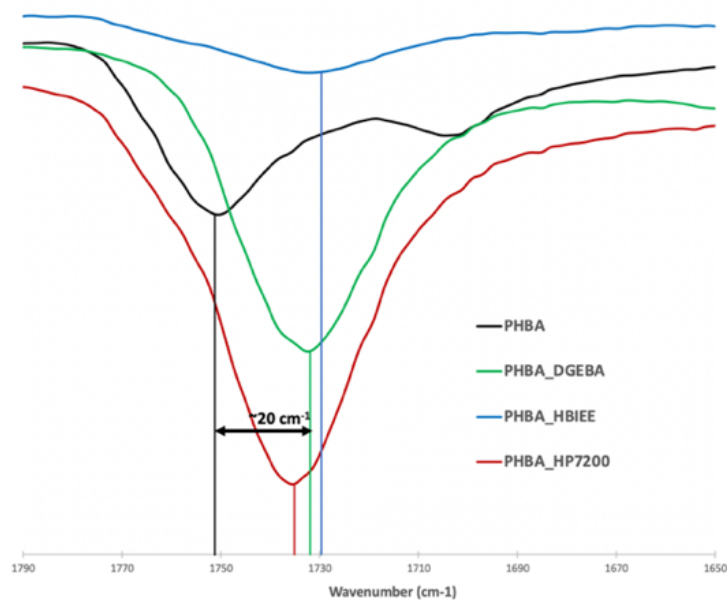
Figure 3.5. FTIR spectra showing the carbonyl region for **PHBA** (black), **PHBA_DGEBA** (blue), **PHBA_HBIEE** (red), and **PHBA_HP7200** (green)

**Table 3.1.** C=O FTIR peaks for all thermosets compared to those of the pure polyesters

Polymer	$\nu_{C=O}$/ cm^{-1}	Epoxide	Corresponding thermoset	$\nu_{C=O}$/ cm^{-1}
PHBSU	1755	DGEBA	PHBSU_DGEBA	1735
		HBIEE	PHBSU_HBIEE	1734
		HP7200	PHBSU_HP7200	1734
PHBA	1751	DGEBA	PHBA_DGEBA	1732
		HBIEE	PHBA_HBIEE	1732
		HP7200	PHBA_HP7200	1735
PHBSE	1756	DGEBA	PHBSE_DGEBA	1733
		HBIEE	PHBSE_HBIEE	1735
		HP7200	PHBSE_HP7200	1735

3.5.2 Thermal Properties of Bio-Thermosets

As one would expect, the same trends seen in the pure polyesters (chapter 2) can be seen

for the thermal properties of the thermosets. With the exception of the PHBSU-series of

thermosets, the T_{d5} of all thermosets increased compared to the polyesters, indicating that the

crosslinking increased the thermal stability of the samples. This trend is even more

pronounced when looking at the T_{d50} values, with all thermoset networks having a T_{d50} over

420 °C (Table 3.2 and Figure 3.6). The thermal properties of the prepared thermosets further

showed that the cross-linking of the active esters with the epoxides occurred because the T_g

of thermoset materials increased in all cases of epoxide curing except PHBSU_HBIEE

(Table 3.2). There were also no indications of endotherms or exotherms on the DSC

measurements indicating that these thermosets are amorphous for all heating cycles, unlike

the polyesters (Appendix A). For samples that underwent mechanical testing, the T_g obtained

via DMA is reported in Table 3.2. These results show slightly higher T_g values, but the trends

remain the same as those of DSC measurements.
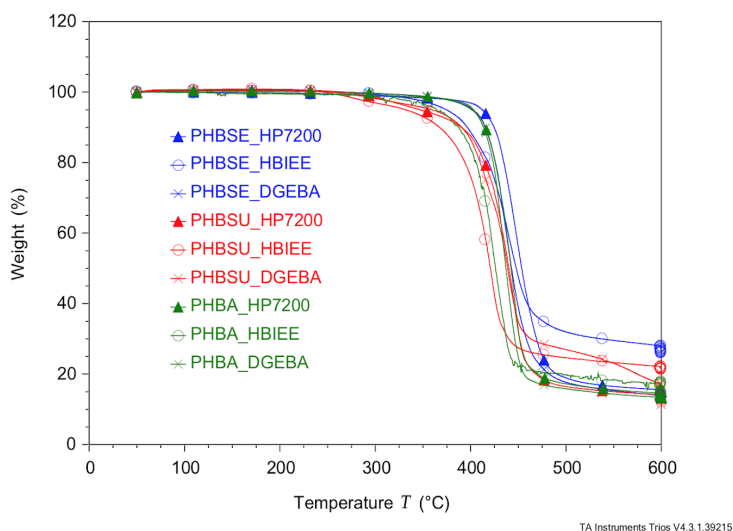
Figure 3.6. TGA thermograms of thermoset networks.

Table 3.2. Thermal Properties T_{d5} (Temperature at 5 % Weight Loss) and T_g (Glass Transition Temperature) of crosslinked thermoset networks[a]

Polymer	T_g (ºC)[b]	T_g (ºC)[c]	T_{d5} (ºC)	T_{d50} (ºC)
PHBSU	61	nd	348	403
PHBSU_DGEBA	96	nd	342	424
PHBSU_HBIEE	50	nd	284	422
PHBSU_HP7200	98	124	332	433
PHBA	43	nd	328	346
PHBA_DGEBA	80	88	364	433
PHBA_HBIEE	54	75	332	422
PHBA_HP7200	105	107	395	440
PHBSE	19	nd	256	395
PHBSE_DGEBA	79	91	401	443
PHBSE_HBIEE	45	55	372	432
PHBSE_HP7200	103	118	401	445

[a]All values are the average of three trials. [b]T_g determined by DSC traces. [c]T_g determined by DMA.

The molecular weights of **PHBSU**, **PHBA**, and **PHBSE** are 19400 g/mol, 16900

g/mol, and 9800 g/mol respectively (see Chapter 2, Table 2.1). The molecular weights of the

polyesters used will have some impact on the thermal properties, though based on the curing

mechanism the impact is insignificant. Due to the inherent cleavage of polyester chains that

takes place during curing, the molecular weights become unreliable because the chains are all

being shortened. The factor that has the most significant impact on thermal properties is the

choice of epoxide. HP7200-based networks resulted in the highest T_g values because of the

polymeric nature and therefore relatively higher molecular weight of HP7200. The curing

mechanism does not cleave the HP7200 chains, so the molecular weight holds significance.

DGEBA and HBIEE are both monomeric so there is no significant impact of molecular

weight on those networks.

3.5.3 Mechanical Properties of Bio-Thermosets

Tensile stress testing was done on the synthesized thermosets. Tensile tests showed some

thermosets were able to ensure stress up to around 70 MPa with a strain percent around 4% at

break (Figure 3.7). This indicated that they are brittle in character, which is expected for

thermosets. The stress values of the **PHBSU_HP7200** and **PHBA_HP7200**, around 65-70

MPa, are comparable to other bio-based thermosets in the literature.[51-53] Compared to the

tensile test run on polyester samples discussed in Chapter 2, which broke at ~1 % strain, the

crosslinked thermoset networks showed an increase in the maximum stress and strain at

break.
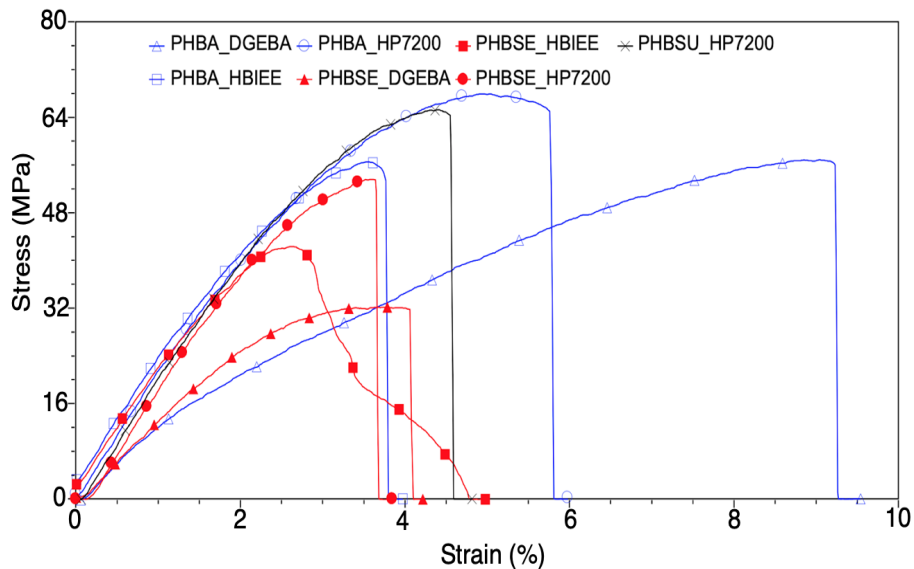
Figure 3.7. Stress-Strain curves for thermoset networks. Vertical line segments indicate the strain % at which the sample broke

The shorter aliphatic chain length in **PHBSU** had an effect both on solubility of the polyesters while curing, making it difficult to obtain a homogenous film, as well as on brittleness of the sample. Therefore, thermoset networks **PHBSU_DGEBA** and **PHBSU_HBIEE** could not be mechanically tested. The thermosets that incorporate **PHBA** showed the highest performance with a maximum stress of 68 MPa and a strain % at break of 5% for **PHBA_HP7200**. Those with **PHBSE** showed both lower stress and lower strain at break compared to PHBA-based thermosets. **PHBSE_HP7200** had maximum values of 54 MPa and 3.7% respectively. Interestingly, the **PHBSU**-based thermoset showed properties between **PHBA**-based and **PHBSE**-based thermosets in regard to both stress and strain with values of 64 MPa at 4.4 %. The **PHBA**-based thermosets showed the most optimal ratios of those two properties. It can be inferred that the aliphatic chain length of the polyester played a significant role in the mechanical properties. PHBSE-based thermosets had a longer aliphatic chain, meaning there was more space between possible crosslink locations and

79

therefore less mechanical toughness. PHBSU-based thermosets were extremely brittle, due to a very short aliphatic chain breaking up the rigid aromatic structure. It seemed that PHBA-based thermosets had optimal spacing between crosslinks, allowing enough crosslinks to occur to give mechanical robustness as well as having enough flexible aliphatic spacers to give usable material.

There was also a trend with the epoxides used. With all polyester components, HP7200 allowed for the most stress to be applied to the sample. This was due to the higher molecular weight of HP7200 compared to the other epoxides. DGEBA cured networks showed the highest strain at break for each respective polyester, which showed that DGEBA gives the resulting thermosets the most elastic properties of the three epoxides used.

One key characteristic of an epoxy network is the cross-link density (ρ). For the cured thermosets ρ was calculated using eq 1:[51-53]

$$\rho = E' / (\Phi RT) \tag{1}$$

where E' is the storage modulus in the rubber region at a temperature above the α-relaxation temperature. $T_\alpha + 30\,^\circ\text{C}$. Φ is the front factor, which is approximated to be 1 in the Flory theory.[54] R is the gas constant, and T is the absolute temperature in Kelvin at $T_\alpha + 30\,^\circ\text{C}$. The results seen in Table 3.3 show that the trend of crosslink density for the thermosets can be summarized as DGEBA-based > HP7200-based > HBIEE-based. Crosslink density of DGEBA-based thermosets are comparable to other DGEBA-based thermosets crosslinked with a more traditional amine curing agent.[52] Further analysis of the data obtained from DMA (Figure 3.8), show that thermosets synthesized with HP7200 gave the highest α

relaxation temperature, T_α. This supports the tensile strength data that showed HP7200-series thermosets, when compared with other epoxides, were able to handle the most stress. Conversely, the HBIEE-series thermosets had the lowest T_α and were shown to have the lowest stress at break. The DGEBA-series thermosets showed T_α values in between HP7200-series and HBIEE-series. This trend is the same as the trend seen in the T_g values for the thermosets. This trend is driven by the molecular weight of the epoxide used, with higher molecular weight corresponding to higher stress as well as higher T_α values. If the curing mechanism did not cleave the polyester chains, the molecular weight of the polyesters would also contribute to this effect.

Table 3.3. Dynamic Mechanical Properties and Cross-link Density (ρ) for bio-based thermosets

Thermoset	Stress (MPa)[a]	Strain (%) [b]	E' (MPa)[c]	T_α + 30 (°C)[d]	E'$_{30}$ (MPa)[e]	ρ (mol/dm^3)
PHBSU_HP7200	65	4.4	350	160	7.8	2.34
PHBA_DGEBA	57	9.0	1100	121	17	5.64
PHBA_HBIEE	54	3.5	320	108	4.7	1.63
PHBA_HP7200	68	5.0	840	139	14	4.42
PHBSE_DGEBA	32	3.7	1100	126	19	6.04
PHBSE_HBIEE	42	2.6	350	88	4.4	1.61
PHBSE_HP7200	54	3.6	660	151	9.2	2.81

[a]Maximum stress value. [b]Strain % at break. [c]Storage modulus at T_α. [d]α-relaxation temperature + 30 °C. [e]Storage modulus at T_α + 30 °C.

In regard to storage modulus, the DGEBA-series of thermosets exhibited the highest value, which shows that this series of thermosets can store the most energy while in the glassy state. The DGEBA-series of thermosets also exhibited the highest strain % at break, indicating that it is the most 'flexible' series, has the highest storage modulus, as well as has

the highest cross-link density. Even though the DGEBA-series thermosets showed

intermediate T_α, the order of magnitude difference in storage modulus was more reflected in
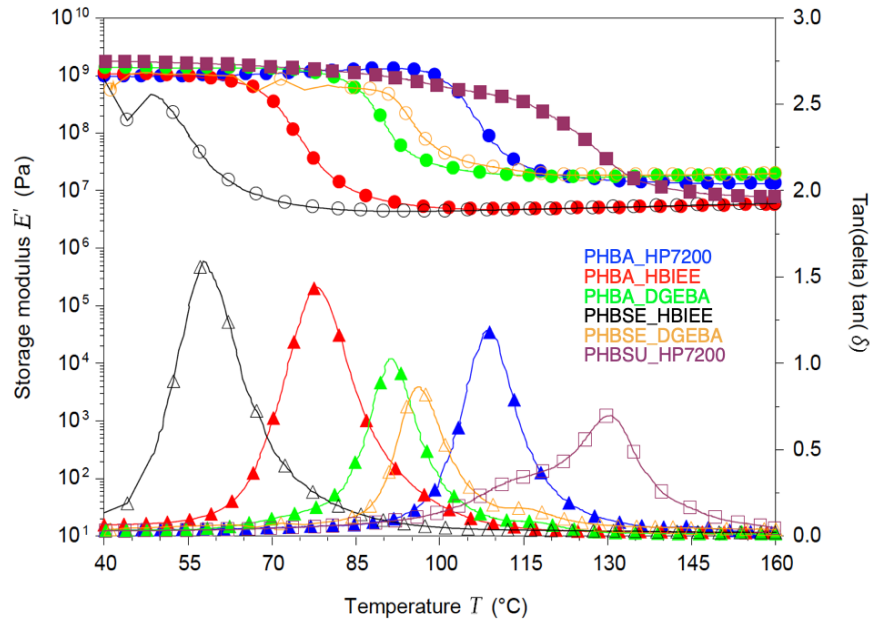
the cross-link density calculations.

Figure 3.8. DMA curves of thermosets showing tan (δ) (bottom) and storage modulus (top)

Molecular weight influences mechanical properties, with higher molecular weights

often corresponding to higher stress, strain, and storage modulus. However, due to the nature

of the curing mechanism, it is difficult to draw conclusions based on molecular weights of

the polyesters because of the chain cleavage. The epoxides will randomly cleave polyester

chains, so the molecular weight of the polyester chains incorporated into the thermoset

network will not correspond to the molecular weights calculated and reported in chapter 2,

Table 2.1.

3.5.4 Comparison of Bio-Thermosets to the Literature

This work introduces novel bio-thermosets based on bio-derived polyesters and bio-derived epoxides based on isoeugenol. There is a multitude of bio-thermosets in the literature to compare to, including recent reviews that do an overview of the expanse of bio-based epoxy thermoset work.[55-60] The thermal and mechanical properties of some of these thermosets are presented and compared to the PHBA-series thermosets in Table 3.4.

One important factor to take into consideration is the % bio-content of the synthesized thermoset networks. To achieve high % bio-content it is critical to use both a renewable epoxy as well as crosslinker. In Table 3.4, the last two entries show that despite having a bio-derived epoxy monomer, the % bio-content can still be 50 % or lower. With the PHBA-series of renewable polyesters presented in this work even the use of petroleum-based DGEBA gives a network with over 70% bio-content. This is a big advantage to utilizing renewable polymers as curing agents. It should be noted that epoxides were not considered to be bio-content because the main source of epichlorohydrin is petroleum. However, Advanced Biochemical Thailand (ABT) produces 120,000 tons per year of bio-based epichlorohydrin under the commercial name epicerol.[61] If using bio-derived epichlorohydrin the % bio-content of all presented works would be even higher.

Regarding thermal properties, the PHBA-series of thermosets presented in this work compare well. The degradation temperature is either higher or comparable to all other works presented in table 3.4. This shows that the PHBA-series of thermosets are temperature resistant and degrade at a temperature that is expected of similar materials. The glass transition temperatures are also within the range of other bio-derived thermosets. It should be noted that the T_g can be adjusted by simply varying the epoxy and/or curing agent, which will also change the % biocontent. A thermoset like the one synthesized by Ecochard et al.[62],

83

which has a $T_g = -26$, would be in the rubbery state at room temperature, whereas the PHBA-series of thermosets would all be in the glassy state at room temperature. Either class of material is useful and can be utilized well depending on the intended application of the material. The cardanol-derived epoxides are also better suited, in general, for rubbery material due to the long alkyl chains inherent to the structure.

In terms of the storage modulus of thermosets, many of those reported in the literature and presented in Table 3.4 show a slightly higher storage modulus than the PHBA-series of thermosets. This indicates that other bio-derived thermosets have a higher crosslink density. This is expected of all thermosets reported in this chapter because the nature of the active ester epoxide chemistry.

In future work, the crosslink density of PHBA-series of thermosets could be increased by using a tri- or tetra-functional epoxide, which would be able to link more polyester chains together. The curing mechanism results in cleavage of the polyester chains where they react with the epoxide. This can result in short chains being linked to other short chains, particularly when a difunctional epoxide is used. Another idea would be to incorporate a "pendant" active ester into the polyester that epoxide could react with, so the backbone stays more intact.

3.6 Conclusion

DGEBA, HP7200, and bio-derived HBIEE were used to create novel, and in some cases fully bio-derived, thermosets in conjunction with isoeugenol-derived polyesters. Utilization of active ester and epoxide chemistry to synthesize thermosets has not been widely used. While there are still many facets to be better developed and understood, this work shows that it is a viable curing mechanism and can produce thermally stable thermosets

with a range of T_g values (43 °C – 105 °C), high tensile strength (68 MPa), and bio content of up to 91%. The utilization of renewable polyesters as the curing agent for epoxy thermosets is crucial to high % bio-content of the resulting networks.

Table 3.4. Thermal and Mechanical Properties of PHBA-series thermosets compared to some other bio-derived thermosets

Epoxy	Curing Agent	T_g (°C)	T_{d5} (°C)	E (MPa)	References
DGEBA	PHBA	88	364	1100	This Work
HBIEE	PHBA	75	332	320	This Work
HP7200	PHBA	107	395	840	This Work
Cardanol-derived					
C-1	MXDA	-26	311	1500	Ecochard et al.[62]
C-2	Cardanol-derived benzoxazine	Not Reported	329.8	1490	Rao and Palanisamy[63]
C-3	IPDA	41	350[a]	Not Reported	Darroman et al.[64]
	IPDA		352[a]	Not Reported	Darroman et al.[64]
Eugenol-derived					
E-1	DETA	40	220	~170	Zhao and Abu-Omar[13]
E-2	DPA	123	332	Not Reported	François et al.[65]
E-3	Eugenol-derived titithiol	70	320	1526	Guzmán et al.[66]
E-4	33DDS	168	338	3470	Wan et al.[67]
Vanillin-derived					
V-1	IPDA	97	361[a]	1500	Fache et al.[20]
V-2	IPDA	176	340[a]	2400	Fache et al.[68]
V-3	IPDA	169	278	3100	Ma et al.[69]
V-4	GCN	100	387	2930	Shibata and Ohkita[70]
Other					
O-1	IPDA	158	292	3600	Tarzia et al.[71]
O-2	IPDA	~60	326, 392[a][b]	3200	Maiorana et al.[72]
O-3	DICY	105	305	2150	Fourcade et al.[73]

[a]Temperatures reported were taken at the point of the maximum rate of decomposition, not 5%. [b]A two-step degradation was reported.
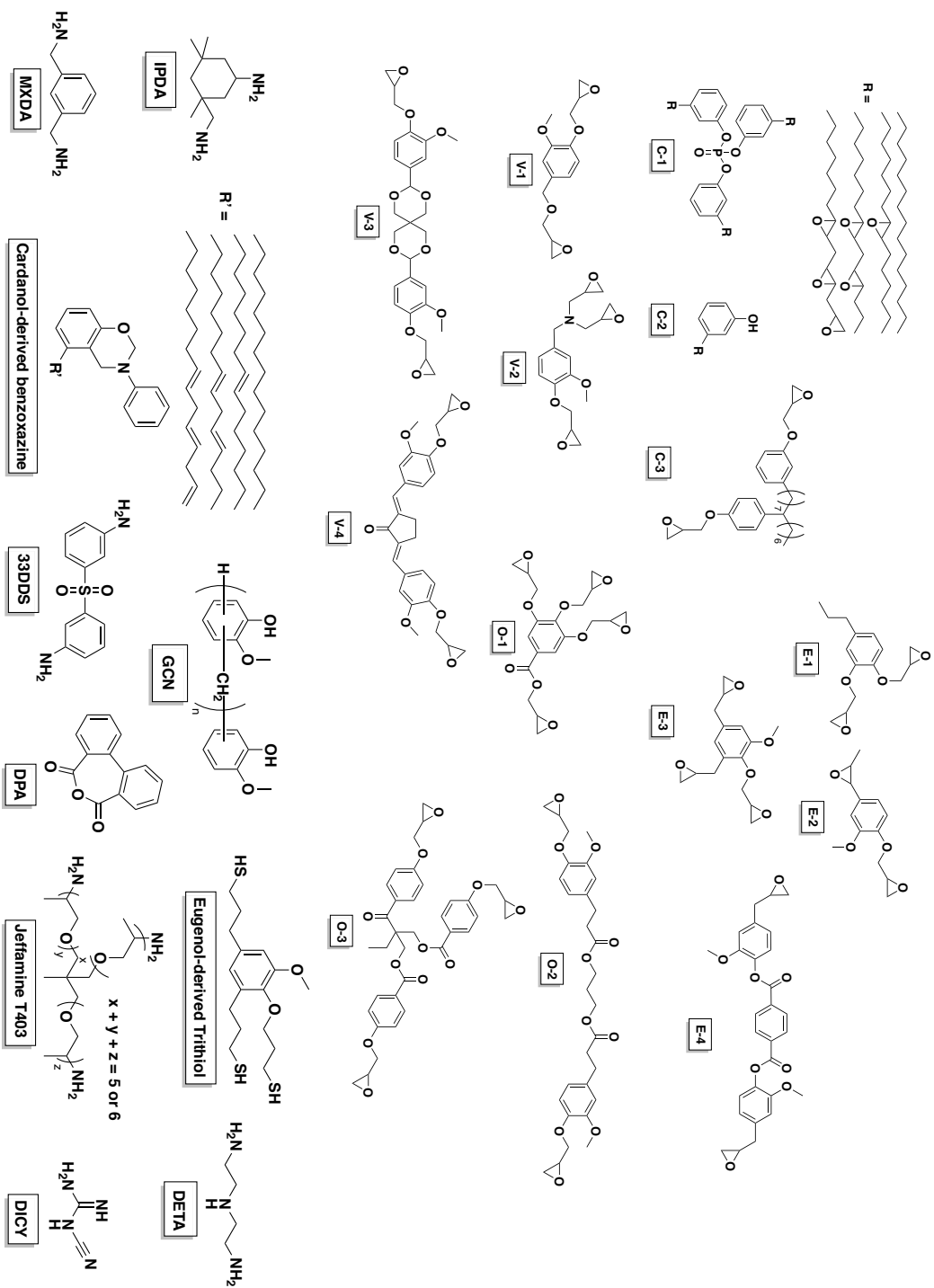
Figure 3.9. Structures of bio-derived epoxides and curing agents used in the works referenced in Table 3.4.

3.7 References

1.   Bilyeu, B.; Brostow, W.; Menard, K. P., Epoxy thermosets and their applications I: Chemical structures and applications. *Journal of Materials Education*, **1999**, *12(5&6)*, 281-286.

2.   Zhu, H.; Chen, Y.; Qin, T.; Wang, L.; Tang, Y.; Sun, Y.; Wan, P., Lignin depolymerization via an integrated approach of anode oxidation and electro-generated H2O2 oxidation. *RSC Advances*, **2014**, *4*, 6232-6238.

3.   Luo, H.; Klein, I. M.; Jiang, Y.; Zhu, H.; Liu, B.; Kenttamaa, H. I.; and Abu-Omar, M. Total Utilization of Miscanthus Biomass, Lignin and Carbohydrates, Using Earth Abundant Nickel Catalyst. *ACS Sustainable Chem. Eng.,* **2016**, *4*, 2316-2322.

4.   Galkin, M. G. and Samec, J. S. M., Selective Rouse to 2-Propenyl Aryls Directly from Wood by a Tandem Organosolv and Palladium-Catalyzed Transfer Hydrogenolysis. *ChemSusChem*, **2014**, *7*, 2154-2158.

5.   Galkin, M. G.; Smit, A. T.; Subbotina, E.; Artemenko, K. A.; Bergquist, J.; Huijgen, W. J. J.; Samec, J. S. M., Hydrogen-free catalytic fractionation of woody biomass. *ChemSusChem,* **2016**, *9*, 3280-3287.

6.   Jastrzebski, R.; Constant, S; Lancefield, C. S.; Westwood, N. J.; Weckhuysen, B. M.; Bruijnincx, P. C. A., Tandem Catalytic Depolymerization of Lignin by Water-Tolerant Lewis Acids and Rhodium Complexes. *ChemSusChem*, **2016**, *9*, 2074-2079.

7.   Xiao, L. P.; Wang, S.; Li, H.; Li, Z.; Shi, Z. J.; Xiao, L.; Sun, R. C.; Fang, Y.; Song, G., Catalytic Hydrogenolysis of Lignins into Phenolic Compounds over Carbon Nanotube Supported Molybdenum Oxide. *ACS Catal.*, **2017**, *7*, 7535-7542.

8.   Zago, E.; Dubreucq, E.; Lecomte, J.; Villeneuve, P.; Fine, F.; Fulcrand, H.; Aouf, C., Sythesis of bio-based epoxy monomers from natural allyl- and vinyl phenols and the estimation of their affinity to the estrogen receptor α by molecular docking. *New J. Chem.*, **2016**, 40, 7701-7710.

9.   Qin, J.; Liu, H.; Zhang, P.; Wolcott, M.; Zhang, J., Use of eugenol and rosin as feedstocks for biobased epoxy resins and study of curing and performance properties. *Polym. Int.,* **2014**, *63*, 760-765.

10.   Faye, I.; Decostanzi, M.; Ecochard, Y.; Caillol, S., Eugenol bio-based epoxy thermosets: from cloves to applied materials. *Green Chemistry*, **2017**, *19*, 5236-5242.

11.   Liu, T.; Hao, C.; Wang, L.; Li, Y.; Liu, W.; Xin, J.;Zhang, J., Eugenol-Derived Biobased Epoxy: Shape Memory, Repairing, and Recyclability. *Macromolecules*, **2017**, *50(21)*, 8588-8597.

12.   Miao, J. T.; Yuan, L.; Guan, Q.; Liang, G.; Gu, A., Biobased epoxy resin derived from eugenol with excellent integrated performance and high renewable carbon content. *Polymer International*, **2018**, *67(9),* 1194-1202.

13.   Zhao, S.; Abu-Omar, M. M., Biobased Epoxy Nanocomposites Derived from Lignin-Based Monomers. *Biomacromolecules*, **2015**, *16*, 2025-2031.

14.   Zhao, S.; Abu-Omar, M. M., Renewable Epoxy Networks Derived from Lignin-Based Monomers: Effect of Cross-Linking Density. *ACS Sustainable Chem. Eng.*, **2016**, *4*, 6082-6089.

15.   Ruiz, Q.; Pourchet, S.; Placet, V.; Plasseraud, L.; Boni, G., New Eco-Friendly Synthesized Thermosets from Isoeugenol-Based Epoxy Resins. *Polymers*, **2020**, *12*, 229-244.

16.   François, C.; Pourchet, S.; Boni, G.; Fontaine, S.; Gaillard, Y.; Placet, V.; Galkin, M. V.; Orebom, A.; Samec, J.; Plasseraud, L., Diglycidylether of iso-eugenol: a suitable lignin-derived synthon for epoxy thermoset applications. *RSC Adv,* **2016**, *6(73),* 68732-68738.

17.   Koelewijm, S. F.; Cooreman, C.; Renders, T.; Andecochea Saiz, C.; Van den Bosch, S.; Schutyser, W.; De Leger, W.; Smel, M.; Van Puyvelde, P.; Witters, H.; Van der Bruggen, B.; Sels, B. F., Promising bulk production of a potentially benign bisphenol A replacement from a hardwood lignin platform. *Green Chem.,* **2018**, *20*, 1050-1058.

18.   Nicastro, K. H.; Kloxin, C. J.; Epps III, T. H., Potential Lignin-Derived Alternatives to Bisphenol A in Diamine-Hardened Epoxy Resins. *ACS Sustainable Chem. Eng.*, **2018**, *6(11),* 14812-14819.

19.   Savonnet, E.; Grau, E.; Grelier, S.; Defport, B.; Carmail, H., Divanillin-Based Epoxy Precursors as DGEBA Substitutes for Biobased Epoxy Thermosets. *ACS Sustainable Chem. Eng.*, **2018**, *6(8),* 11008-11017.

20.   Fache, M.; Auvegne, R.; Boutevin, B.; Caillol, S., New vanillin-derived diepoxy monomers for the synthesis of biobased thermosets. *Eur. Polym. J,* **2015**, *67*, 527-538.

21.   Fache, M.; Viola, A.; Auvergne, R.; Boutevin, B.; Caillol, S., Biobased epoxy thermosets from vanillin-derived oligomers. *Eur.Polym. J.,* **2015**, *68*, 526−535.

22.   Fache, M.; Boutevin, B.; Caillol, S., Epoxy thermosets from model mixtures of the lignin-to-vanillin process. *Green Chem.*, **2016**, *18(3),* 712-725.

23.	Wang, S.; Ma, S.; Xu, C.; Liu, Y.; Dai, J.; Wang, Z.; Liu, X.; Chen, J.; Shen, X.; Wei, J.; Zhu, J., Vanillin-derived high-performance flame retardant epoxy resins: facile synthesis and properties. *Macromolecules*, **2017**, *50(5),* 1892-1901.

24.	Su, X.; Zhou, Z.; Liu, J.; Luo, J.; Liu, R., A recyclable vanillin-based epoxy resin with high-performance that can compete with DGEBA. *European Polymer Journal*, **2020**, *140*, 110053.

25.	Mogheiseh, M.; Karimian, R.; Khoshsefat, M., Vanillin-derived epoxy monomer for synthesis of bio-bsed epoxy thermosets: effect of functionality on thermal, mechanical, chemical and structural properties. *Chemical Papers*, **2020**, *74*, 3347-3358.

26.	van de Pas, D. J.; Torr, K. M., Biobased Epoxy Resins from Deconstructed Native Softwood Lignin. *Biomacromolecules*, **2017**, *18*, 2640-2648.

27.	Xin, J.; Li, M.; Li, R.; Wolcott, M. P.; Zhang, J., Green Epoxy Resin System Based on Lignin and Tung Oil and Its Application in Epoxy Asphalt. *ACS Sustainable Chem. Eng.,* **2016**, *4*, 2754-2761.

28.	Ferdosian, F.; Yuan, Z.; Anderson, M.; Xu, C., Sustainable lignin-based epoxy resins cured with aromatic and aliphatic amine curing agents: Curing kinetics and thermal properties. *Thermochimica Acta*, **2015**, *618*, 48-55.

29.	Ferdosian, F.; Yuan, Z.; Anderson, M.; Xu, C., Chemically Modified Lignin Through Epoxidation and its Thermal Properties. *J. Sci. & Tech. for Forest Product and Processes,* **2012**, *2(4),* 11-15.

30.   Ferdosian, F.; Yuan, Z.; Anderson, M.; Xu, C., Curing Kinetics and mechanical properties of bio-based epoxy composites comprising lignin-based epoxy resins. *European Polymer Journal*, **2016**, *82*, 153-165.

31.   Over, L. C.; Grau, E.; Grelier, S.; Meier, M. A. R.; Cramail, H., Synthesis and Characterization of Epoxy Thermosetting Polymers from Glycidylated Organosolv Ligning and Bisphenol A. *Macromol. Chem. Phys.*, **2017**, *218*, 1600411.

32.   Zhao, S.; Abu-Omar, M. M., Synthesis of Renewable Thermoset Polymers through Successive Lignin Modification Using Lignin-Derived Phenols. *ACS Sustainable Chem. Eng.*, **2017**, *5*, 5059-5066.

33.   Yin, Q.; Yang, W.; Sun, C.; Di, M., Preparation and properties of lignin-epoxy resin composite. *BioResources*, **2012**, *7*, 5737-5748.

34.   El Mansouri, N. E.; Yuan, Q.; Huang, F., Synthesis and characterization of Kraft lignin-based epoxy resins. *BioResources*, **2011**, *6*, 2492-2503.

35.   Thakur, V. K.; Thakur, M. K.; Raghavan, P.; Kessler, M. R., Progress in green polymer composites from lignin for multifunctional applications: a review. *ACS Sustainable Chem. Eng.*, **2014**, *2*, 1072-1092.

36.   Gouveia, J. R.; Garcia, G. E. S.; Antonino, L. D.; Tavares, L. B.; dos Santos, D. J., Epoxidation of Kraft Lignin as a Tool for Improving the Mechanical Properties of Epoxy Adhesive. *Molecules,* **2020**, *25 (11),* 2513.

37.   Nishikubo, T.; Kameyama, A., Addition reactions of cyclic ethers with various carbonyl compounds and their application for polymer synthesis. *Prog. Polym. Sci.*, **1993**, 18, 963-995.

38. Nakamura, S.; Saegusa, Y.; Yanagisawa, H.; Touse, M.; Shirai, T.; Nishikubo, T., Thermal analysis of epoxy curing using polyfunctional active esters as curing agents. *Thermochimica Acta*, **1991**, 183, 269-277.

39. Nakamura, S.; Arima, M.; Characterization of the Network Structure of Epoxy Resins Cured with Active Esters. *Int. J. Polym. Anal. Charact.*, **1995**, 1, 75-86.

40. Nishikubo, T.; Saita, S., New thermo-crosslinking reaction of copolymers of phenyl methacrylates by use of polyfunctional epoxy compounds. *Macromol. Chem. Phys.*, **1987**, 188, 799-809.

41. Nishikubo, T.; Tanaka, K.; A novel reaction of epoxy resins with polyfunctional active esters. *J. Appl. Polym. Sci.*, **1987**, 33, 2821−2831.

42. Nishikubo, T.; Shimokawa, T.; A novel insertion reaction of epoxy compounds into the pendant ester linkage of poly [4-(4- nitrobenzoyloxy) styrene]. *Macromol. Rapid Commun.,* **1986**, 7, 179− 181.

43. Nishikubo, T.; Saita, S.; Fujii, T.; New thermo-crosslinking reactions of polymers containing pendant epoxide groups with various polyfunctional active esters. *J. Polym. Sci., Part A: Polym. Chem.,* **1987**, 25, 1339−1351.

44. Nishikubo, T.; Shimokawa, T.; Hirano, T.; Shiina, A., Novel Insertion reaction of epoxy compounds into phenyl ester linkages in polymer chains. *J. Polym. Sci., Part A: Polym. Chem*, **1989**, 27 (8), 2519-2530.

45. Nishikubo, T.; Iizawa, T.; Saita, S.; Addition reactions of pendant epoxide group in poly (glycidyl methacrylate) with various active esters. J. *Polym. Sci., Part A: Polym. Chem.*, **1986**, 24, 1685−1695.

46. Lin, C. M.; Chen, C. H.; Lin, C. H.; Su, W. C.; Juang, T. Y., Using Dicyclopentadiene-Derived Polyarylates as Epoxy Curing Agents to Achieve High T_g and Low Dielectric Epoxy Thermosets. *ACS Omega*, **2018**, *3*, 4295-4305.

47. Chen, C. H.; Lin, C. M.; Juang, T. Y.; Abu-Omar, M. M.; Lin, C. H., The reaction of activated esters with epoxides for self-curable, highly flexible, A_2B_2- and A_3B_3-type epoxy compounds. *Polym. Chem.*, **2019**, *10*, 3983-3995.

48. McAninch, I. M.; Palmese, G. R.; Lenhart, J. L.; La Scala, J. J., DMA Testing of Epoxy Resins: The Importance of Dimensions. *Poly. Eng. & Sci.* 2015, 55 (12), 2761-2774.

49. Long, H.; Le, W. Method for detecting epoxy equivalent weight. Patent CN102507574B, October 30, 2013.

50. Li, S. R.; Guan, W. C.; W, Z. G.; Lu, J. C.; Gua, J. An Improved Method to Determine Epoxide Index of Epoxy Resins, *Polymer-Plastics Tech. and Eng.*, **2007**, 46 (9), 901-903).

51. Zhao, S.; Huang, X.; Whelton, A. J.; Abu-Omar, M. M., Renewable Epoxy Thermosets from Fully Lignin -Derived Triphenols. *ACS Sustainable Chem. Eng.* **2018**, *6*, 7600-7608.

52. Nouailhas, H.; Aouf, C.; Le Guerneve, C.; Caillol, S.; Boutevin, B.; Fulcrand, H., Synthesis and Properties of Biobased Epoxy Resins. Part 1.Glycidylation of Flavonoids by Epichlorohydrin. *J. Polym. Sci.*, **2011**, *49* (10), 2261-2270.

53. Iijima, T.; Yoshioka, N.; Tomoi, M., Effect of cross-link density on modification of epoxy resins with reactive acrylic elastomers. *Eur. Polym. J.*, **1992**, *28* (6), 573-581.

54. Flory, P. J., Molecular theory of rubber elasticity. *Polymer,* **1979**, *20* (11), 1317-1320.

55.   Wan, J.; Zhao, J.; Zhang, X.; Fan, H.; Zhang, J.; Hu, D.; Jin, P.; Wang, D. Y., Epoxy thermosets and materials derived from bio-based monomeric phenols: Transformations and performances. *Progress in Polymer Science*, **2020**, *108*, 101287.

56.   Kumar, S.; Krishnan, S.; Mohanry, S.; Nayak, S. K., Synthesis and characterization of petroleum and biobased epoxy resins: a review. *Polym. Int.*, **2018**, *67*, 815-839.

57.   Kumar, S.; Samal, S. K.; Mohanty, S.; Nayak, S. K., Recent Development of Biobased Epoxy Resins: A Review. *Polymer Plastics Technology and Engineering*, **2018**, *57*, 133-155.

58.   Auvergne, R.; Caillol, S.; David, G.; Boutevin, B.; Pascault, J. P., Biobased Thermosetting Epoxy: Present and Future. *Chem. Rev.*, **2014**, *114*, 1082-1115.

59.   Bobade, S. K.; Paluvai, N. R.; Mohanty, S.; Nayak, S. K., Bio-based Thermosetting Resins for Future Generation: A Review. *Polymer Plastics Technology and Engineering*, **2016**, *55*, 1863-1896.

60.   Ng, F.; Couture, G.; Philippe, C.; Boutevin, B.; Caillol, S., Bio-Based Aromatic Epoxy Monomers for Thermoset Materials. *Molecules*, **2017**, *22*, 149-197.

61.   Bioenergy International. https://bioenergyinternational.com/biochemicals-materials/abt-increases-bio-based-epichlorohydrin-ech-capacity-to-120-000-tpa (Accessed August 9, 2021).

62.   Ecochard, Y.; Decostanzi, M.; Negrell, C.; Sonnier, R.; Caillol, S., Cardanol and eugenol based flame retardant epoxy monomers for thermostable networks. *Molecules*, **2019**, *24*, 1818-1839.

63. Rao, B. S.; Palanisamy, A., Synthesis of bio based low temperature curable liquid epoxy, benzoxazine monomer system from cardanol: thermal and viscoelastic properties. *Eur. Polym. J.*, **2013**, *49*, 2365-2376.

64. Darroman, E.; Durand, N.; Boutevin, B.; Caillol, S., Improved cardanol derived epoxy coatings. *Prog. Org. Coat.*, **2016**, *91*, 9-16.

65. François, C.; Pourchet, S.; Boni, G.; Rautiainen, S.; Samec, J.; Fournier, L.; Robert, C.; Thomas, C. M.; Fontaine, S.; Gaillard, Y.; Placet, V.; Plasseraud, L., Design and synthesis of biobased epoxy thermosets from biorenewable resources. *Comptes Rendus Chimie*, **2017**, *29*, 1006-1016.

66. Guzmán, D.; Ramis, X.; Fernández-Francos, X.; De la Flor, S.; Serra, A., Preparation of new biobased coating from a triglycidyl eugenol derivative through thiol-epoxy click reaction. *Prog. Org. Coat.*, **2018**, *114*, 259-267.

67. Wan, J.; Gan, B.; Li, C.; Molina-Aldareguia, J.; Li, Z.; Wang, X.; Wang, D. Y., A novel biobased epoxy resin with high mechanical stiffness and low flammability: synthesis, characterization, and properties. *J. Mater. Chem. A*, **2015**, *3*, 21907-21921.

68. Fache, M.; Monteremal, C.; Boutevin, B.; Caillol, S., Amine hardeners and epoxy cross-linker from aromatic renewable resources. *Eur. Polym. J.*, **2015**, *73*, 344-362.

69. Ma, S.; Wei, J.; Jia, Z.; Yu, T.; Yuan, W.; Wang, S.; You, S.; Liu, R.; Zhu, J., Readily recyclable, high-performance thermosetting materials based on a lignin-derived spiro diacetal trigger. *J. Mater. Chem. A*, **2019**, *7*, 1233-1243.

70. Shibata, M.; Ohkita, T., Fully biobased epoxy resin systems composed of a vanillin-derived epoxy resin and renewable phenolic hardeners. *Eur. Polym. J.*, **2017**, *92*, 165-173.

71.   Tarzia, A.; Montanaro, J.; Casiello, M.; Annese, C.; Nacci, A.; Maffezzoli, A.,
        Synthesis, curing, and properties of an epoxy resin derived from gallic acid.
        Bioresources, **2018**, *13,* 632-645.

72.   Maiorana, A.; Reano, A. F.; Centore, R.; Grimaldi, M.; Balaguer, P.; Allais, F.;
        Gross, R. A., Structure property relationships of biobased *n*-alkyl bisferulate epoxy
        resins. *Green Chem.*, **2016**, *18*, 4961-4973.

73.   Fourcade, D.; Ritter, B. S.; Walter, P.; Schönfeld, R.; Mülhaupt, R., Renewable
        resource-based epoxy resins derived from multifunctional poly(4-hydroxybenzoates).
        Green Chem., **2013**, *15*, 910-918.

Chapter 4

Introduction: Ion-Specific Ligands and the Produced Water Problem

4.1 Motivation

Water is an essential compound for sustaining many important industries, including agriculture, energy, and city infrastructure. In addition to being integral to the success of major industries, water is also just simply required for life itself. While there is an abundance of water on earth, the vast majority of it requires purification before it can be used for agriculture or consumed by the population. Membrane technology can be easily incorporated into flow systems, and requires low energy input, and while there are membranes already incorporated into water purification infrastructure, they are largely used for desalination on relatively clean water.[1] Current membrane technology struggles to differentiate between similar ions and compounds and are often subject to fouling, and thus must be constantly monitored and replaced.[2]

With water scarcity an issue in the world, the ability to utilize membrane technology to maximize the use of water resources is paramount.[3] Produced water is not only a large source of water, it also contains various compounds of interest, such as lithium, that would be extremely useful if isolated and collected.[4]

4.2 Produced Water: Contents and Compounds of Interest

In 2017, The United States oil and gas industry produced approximately 10.6 liters/day of produced water.[5] When extracting oil and natural gas from the ground, water is used to essentially push the oil or gas up. Simply, water is injected into the well, it then pushes the

oil or gas out, and then is collected. This water is known as produced water. Produced water is highly contaminated with oil, solids, organics, heavy metals, and naturally occurring radioactive material (NORM), and it is considered to be a waste stream.[6] The most common method of disposal is reinjection into the earth. The composition of produced water depends on the well location, soil composition, and oil/gas composition. There are many components, though, that are commonly found in produced water streams. Table 4.1 shows the inorganic components of a sample produced water source.[7]

Table. 4.1. Inorganic Produced Water Constituents[7]

Constituent List	Units	Conventional	Unconventional
Antimony	mg/L	n/a	ND – 0.005 [e]
Aluminum	mg/L	< 0.50 – 410 [b,d]	0.005 – 1.52 [f,g]
Arsenic	mg/L	0.004 – 151 [a,b,d]	ND – 0.158 [e]
Barium	mg/L	ND – 1740 [a,b,d]	0.445 – 125 [e,g]
Beryllium	mg/L	< 0.001 – 0.004 [d]	n/a
Bicarbonate	mg/L	ND – 14,750 [h]	4.53 – 49,031 [g]
Boron	mg/L	ND – 95 [a,d]	0.05 – 30.6 [e]
Bromide	mg/L	150 – 1,149 [a,b]	ND – 41.1 [e]
Cadmium	mg/L	< 0.005 – 1.21 [a,b,d]	ND – 0.076 [e]
Calcium	mg/L	ND – 74,185 [h]	ND – 5,530 [e,g]
Chloride	mg/L	2 – 254,923 [h]	ND – 52,364 [e,g]
Chromium	mg/L	ND – 1.1 [a,d]	ND – 3.71 [e,g]
Cobalt	mg/L	n/a	ND – 0.010 [e]
Copper	mg/L	< 0.002 – 5 [b,d]	0.001 – 1.448 [e]
Fluoride	mg/L	n/a	0.57 – 20 [f,g]
Iron	mg/L	ND – 1,100 [a]	0.001 – 258 [e,g]
Lead	mg/L	0.002 – 10.2 [b,d]	ND – 0.098 [e]
Lithium	mg/L	3 – 235 [b,d]	ND – 1.50 [g]
Magnesium	mg/L	ND – 46,656 [h]	1.2 – 918.9 [e]
Manganese	mg/L	< 0.004 – 175 [d]	ND – 3.11 [e,g]
Mercury	mg/L	< 0.001 – 0.002 [d]	ND – 0.014 [e]
Molybdenum	mg/L	n/a	ND – 0.448 [e]
Nickel	mg/L	< 0.08 – 9.2 [b]	ND – 0.082 [e]
Nitrogen, ammoniacal (N-NH$_3$)	mg/L	10 – 300 [d]	n/a
Nitrate (N-N0$_3$)	mg/L	n/a	ND – 26.1 [g]
Potassium	mg/L	0 – 14,840 [h]	ND – 1,100 [g]
Selenium	mg/L	n/a	ND – 1.27 [e]
Silver	mg/L	< 0.001 – 7 [b,d]	ND – 0.14 [g]
Sodium	mg/L	1 – 149,836 [h]	97.3 – 32,013 [e]
Strontium	mg/L	0.02 – 6,200 [a,d]	ND – 47.9 [g]
Sulfate	mg/L	ND – 14,900 [h]	ND – 2,200 [e,g]
Tin	mg/L	ND – 1.1 [a]	n/a
Titanium	mg/L	< 0.01 – 0.7 [d]	n/a
Uranium	mg/L	n/a	ND – 2.5 [g]
Vanadium	mg/L	n/a	ND – 0.290 [e]
Zinc	mg/L	0.01 – 35 [d]	0.005 – 5.639 [e]

[1] ND = nondetect; n/a = data not available; a = Fillo and Evans 1990; b = USEPA 2000; c = Shepard, Shore et al. 1992; d = Tibbetts, Buchanan et al. 1992; e = Cheung, Sanei et al. 2009; f = McBeth, Reddy et al. 2003; g = Colorado Oil and Gas Conservation Commission 2010; h = USGS 2002.

There are many advantages to looking at produced water as a system. First, the water is not otherwise used, second, it contains some ions and compounds that are in high demand (e.g., Li^+), and third, it is a huge potential source of water for various industries and human consumption.

4.2.1 Lithium

Lithium is used for various applications, but most prominently energy storage. In the coming years, the demand for batteries will increase with the continuing increase in electric vehicles. The concentration of lithium in produced water is comparable to current lithium sources, such as salt lake brines (100-1000 mg//L), making it a promising potential source of lithium.[4,8] In order to selectively obtain lithium from among the many other components in produced water, it must be differentiated from other cationic species like Na^+, K^+, Mg^{2+}, and Ca^{2+}. The separation of monovalent cations like lithium from divalent magnesium has shown to be successful in utilizing ion-exchange or charged membranes.[9,10] The separation of different monovalent species, like Li^+ and Na^+, has presented a larger challenge to membrane technology.[11] In order to utilize membranes and to source lithium from produced water, this challenge would have to be overcome.

4.2.2 Boron

There are various neutral species present in produced water, notably boron. The challenge with neutral species, compared to charged species, is that they are less likely to complex with the surrounding membrane environment, and are therefore difficult to remove from water streams. Boron, while necessary for many plants in low concentrations, is toxic at just slightly higher concentrations, and there is no current way to effectively remove boron from

water.[12] If produced water is to be used for further applications like agriculture and drinking water, boron concentration would need to be decreased to acceptable levels.

4.3 Current Water Purification Membrane Technology

Membrane technology is generally categorized into reverse osmosis (RO), nanofiltration (NF), ultrafiltration (UF), microfiltration (MF) and conventional filtration (CF). The main distinguishing characteristic between these different membranes is pore size. The smaller the pore size, the more contaminants will be prevented from passing through the membrane, due to sterics. In addition, these membranes all usually rely on transmembrane pressure for filtration. A general comparison figure of these common membrane types, and the size of common water contaminants is shown in Figure 4.1.[13]

Process	RO	NF	UF	MF	CF	
Examples of Common Constituents In Water	Metal Ions	Sugar	Virus / Pyrogen / Colloidal Silica	Carbon Fines	Bacteria	
Approx. Molecular Weight Cut-Off*	100	200	20,000	100,000	500,000	
Microns	0.0001	0.001	0.01	0.1	1.0	10.0

Figure. 4.1. Comparison of membrane processes related to pore size.[13]

4.3.1 Reverse Osmosis

Reverse osmosis (RO) is one of the main technologies used for water desalination, with over 50 % of desalination plants in the world utilizing it. RO membranes are semi-permeable and filter out salts from water by applying an external pressure to overcome the

osmotic pressure of the saltwater. When the external pressure (ΔP) is higher than the osmotic pressure ($\Delta\pi$), the water will flow from high salt concentration to low salt concentration (Figure 4.2).[1,14]
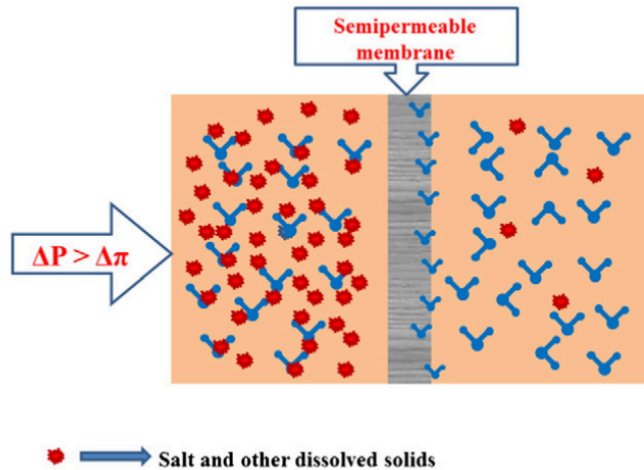
Figure. 4.2. Diagram of Reverse Osmosis Process.[1]

An RO plant usually consists of four steps; pretreatment, high pressure pumping, salt separation, and post treatment. Pretreatment involves filtering out solids from the water source, as well as utilized chemicals, such as sodium hypochlorite, sulfuric acid, sodium bisulfate, and ferric chloride.[15] If solid particles get to the RO membranes, it will cause fouling, and the membrane will have to be replaced.[16-18] High pressure pumping essentially pushes the water feed through the RO membrane, meaning that RO membranes need to have the strength to be able to withstand high pressures. The separation happens at the membrane, with the allowance of water to permeate through and the salts to not. Posttreatment then usually involves the neutralization of the filtered water, degasification, disinfection, and remineralization, so that the water meets the standards of potable water.[19-21]

The first RO membranes were synthesized in the late 1950s by Reid et al. utilizing cellulose acetate as the base material.[22] This initial membrane showed salt rejection of 96%, but water permeability was also low. Further research made use of cellulose diacetate (CDA)

and cellulose triacetate (CTA), which yielded the first usable RO membranes.[23] Advances in cellulosic RO membranes have been largely focused on blending the cellulosic base with some other polymer or monomer to improve flux and salt rejection.[24-29]

Even with some advancements in cellulosic RO membranes, recently, polyamide membranes have taken over the RO market with specifically heavy interest in thin film composite (TFC) polyamide membranes. TFC RO membranes are generally made of multiple layers, including a polyester base, a porous support (often polysulfone), and the active thin film (crosslinked polyamide).[1,30,31] Areas that have garnered a lot of interest are substrate choice and modification[32-39] and thin film monomer choice and modification.[40-50] The main goal of these works is to increase salt rejection, chloride resistance, and fouling resistance of TFC RO membranes.

4.3.2   Microfiltration, Ultrafiltration and Nanofiltration

Microfiltration (MF) membranes are able to filter out contaminants larger than 1 micrometer in size, which means that they can remove species such as suspended particles, pathogens, large bacteria, and proteins.[51] Ultrafiltration (UF) membranes have slightly smaller pores, and in addition to contaminants that can be removed by MF, can remove sugars, macromolecules, colloids, and silica. Nanofiltration (NF) membranes have even smaller pores, of 1 nanometer, and thus can further filter out multivalent salts and small molecules. Because of this, NF membranes are widely used, and the only one of the three that would be able to filter a water stream like produced water with any success. This is why they are not used extensively for water desalination.

NF membranes were developed in the 1980s with pore size of 1nm, being able to reject species larger than 300 to 500 Da.[52] Species can move through membranes via

diffusion (concentration gradient), convection (solvent flow), or electromigration (potential gradient). Nanofiltration membranes can filter out both neutral and charged species. The pore size of the membrane excludes solutes that are larger than the pore opening, and in some cases, this relies on the ability of an ion to give up its hydration shell. Charged particles can also be removed, depending on the charge effects between membrane and solution.[53]

Like RO membranes, polymeric NF membranes are the most prominent in the market, with polyamine TFC membranes leading the way.[54] Nanofiltration membranes are also subject to fouling when the pores get blocked or a layer of solutes that are larger than the pore size forms on the surface. Fouling can be controlled by decreasing the concentration of the water source, module design, and membrane regeneration.[55]

Even with good size exclusion and the ability to remove neutral and charged species, nanofiltration membranes are mainly used for surface water treatment, or pre-treatment for RO. The use of nanofiltration membranes on produced water and other more contaminated sources is not as prevalent, because of fouling potential. Produced water contains a large variety of species that would cause fouling to happen often, but specifically, total organic carbon (TOC) is problematic. TOC concentration in surface water is usually <10 mg/L, whereas in produced water, it can be up to 540 mg/L.[56] Some studies that have investigation nanofiltration membranes on produced water show a reduction of TOC up to approximately 50 % and fouled membrane recovery of up to 31 %.[57,58]

4.3.3   Other types of RO and NF Membranes

Other types of membranes include Inorganic/ceramic, Biomimetic, and mixed-matrix membranes (MMM). Inorganic membranes are often made of zeolites on a porous support, with pore size determining the separation efficiency.[59,60] Biomimetic membranes often

include or are based off of aquaporins, which are proteins that allow water to flow through them.[61,62] MMMs use host-guest interactions to enhance the membrane properties, where inorganic fillers are added to a host polymer matrix to enhance permeability, selectivity, and stability.[1] Common fillers are zeolites, carbon nanotubes, and nanoparticles.[63] The inclusion of these inorganics, biomimics, and fillers both can improve the salt rejection as well as fouling resistance. However, these membranes are limited by cost, which would need to be remedied before large scale incorporation is possible.

To take advantage of the useful components in produced water like lithium, or to remove small neutral species like boron, even further measures need to be taken. Incorporation of specific moieties into membrane frameworks could allow for specific selectivity for lithium or boron, and therefore selective removal from the produced water stream.

4.4 Ion-Specific Moieties

The ability to specifically capture or let permeate a species of interest has a multitude of applications. For an in-demand material like lithium, this would result in capture of lithium in a membrane or a lithium-enriched solution. Both outcomes are favorable. In the case of boron, since it is difficult to remove by conventional membranes, a moiety that binds boron and therefore decreases the concentration of boron in the water stream would be invaluable. The removal of boron from wastewater sources could allow it to be used for agricultural applications, or potentially decrease boron concentrations to acceptable levels for potable water. In order to successfully incorporate a selective moiety into a membrane framework suitable for produced water use, it would have to be tethered to the polymer backbone so as to not leach into the solution and require constant maintenance.

4.4.1 Crown Ether

Crown ethers have been shown to complex with metal cations, depending on the size of the crown ether cavity and the cation radius. There have also been a number of studies of crown ether in ion imprinted polymers,[64-66] porous microspheres,[67] and small molecules[68,69] for cation capture. Specifically, 12-crown-4 has been shown to complex both Li^+ and Na^+ depending on the surrounding chemical environment.[70-73] Incorporation of crown ether into membranes for lithium selectivity has also been done.[74-77] These studies, however, have crown ether free in a liquid membrane, which means they can leach into the solution.

4.4.2 Catechol

In order to capture boron, the moiety that has been investigated the most is catechol. Boron is able to bind with one or two catechol moieties[78,79] meaning that incorporation into membrane frameworks will trap boron within the membrane. Catechol has been used in several studies for boron adsorption.[80-85] While the studies show high adsorption of boron, it is mostly through adding adsorbents to the water, rather than through usage of a membranes for water to flow through. Water purification relies heavily on membrane technology. It should be noted as well, that produced water and other wastewater streams contain other species that complex with catechol, such as iron and copper. These competing interactions will have to be better understood and remedied for large scale use.

4.5 Conclusion

There has been a wealth of research into membranes for water purification and solute capture. Produced water is a potential feedstock that is generated in large quantity and full of useful material (i.e., Li^+), and focus is turning towards produced water as both a water source

and a lithium source. 12-crown-4 ether has been shown to complex with lithium ions and shows promise as a selective moiety to incorporate into membranes for lithium selectivity. Current selective membrane studies using 12-crown-4 show lithium selectivity but are not suitable for continuous filtration and therefore industrial application. Catechol groups have shown affinity for boron binding, and incorporation into membranes show feasible boron capture which is promising for future water purification membrane technology.

4.6 References

1. Shenvi, S. S.; Isloor, A. M.; Ismail, A. F., A review on RO membrane technology: Developments and challenges. *Desalination*, **2015**, *368*, 10-26.

2. Goh, P. S.; Lau, W. J.; Othman, M. H. D.; Ismail, A. F., Membrane fouling in desalination and its mitigation strategies. *Desalination*, **2018**, *425*, 130-155.

3. Bremere, I.; Kennedy, M.; Stikker, A.; Schipper, J., How water scarcity will affect the growth in the desalination market in the coming 25 years. *Desalination*, **2001**, *138*, 7-15.

4. Kumar, A.; Fukuda, H.; Hatton, T. A.; Lienhard V, J. H., Lithium Recovery from Oil and Gas Produced Water: A Need for a Growing Energy Industry. *ACS Energy Lett.*, **2019**, *4*, 1471-1474.

5. Viel, J., U.S. produced water volumes and management practices in 2017. Veil Environmental LLC, **2020**, www.veilenvironmental.com/publications/pw/pw_report_2017_final.pdf. Accessed August 2021.

6. Neff, J.; Lee, K.; DeBlois, E. M., Produced Water: Overview of Composition, Fates, and Effects. In *Produced Water*; Lee, K.; Neff, J.; Springer, New York, NY; **2011**, pp 3-54.

7. Science and Technology Program Report No. 157; **2011**, US Dept. of the Interior.

8. Flexer, V.; Baspineiro, C. F.; Galli, C. I., Lithium recovery from brines: A vital raw material for green energies with a potential environmental impact in its mining and processing. *Sci. Total Environ.*, **2018**, *639*, 1188-1204.

9. Yang, G.; Shi, H.; Liu, W.; Xing, W.; Xu, N., Investigation of Mg^{2+}/Li^+ separation by nanofiltration. *Chin. J. Chem. Eng.*, **2011**, *19*, 586-591.

10. Wu, H.; Lin, Y.; Feng, W.; Liu, T.; Wang, L.; Yao, H.; Wang, X., A novel nanofiltration membrane with [MimAP][Tf$_2$N] ionic liquid for utilization of lithium from brines with high Mg^{2+}/Li^+ ratio. *J. Membr. Sci.*, **2020**, *60*, 117997.

11. Sujanani, R.; Landsman, M. R.; Jiao, S.; Moon, J. D.; Shell, M. S.; Lawler, D. F.; Katz, L. E.; Freeman, B. D., Designing Solute-Tailored Selectivity in Membranes: Perspectives for Water Reuse and Resource Recovery. *ACS Macro Letters*, **2020**, *9*, 1709-1717.

12. Hilal, N.; Kim, G. J.; Somerfield, C., Boron removal from saline water: a comprehensive review. *Desalination*, **2011**, *273*, 23-35.

13. Comparison of Membrane Processes, Applied Membranes, Inc. https://appliedmembranes.com/media/wysiwyg/pdf/membranes/comparison_of_membrane_processes_mf_nf_uf_ro.pdf. Accessed August 2021.

14. Hailemariam, R. H.; Woo, Y. C.; Damtie, M. M.; Kim, B. C.; Park, K. D.; Choi, J. S., Reverse osmosis membrane fabrication and modification technologies and future trends: A review. *Advances in Colloid and Interface Science*, **2020**, *272*, 102100.

15. Rautenbach, R.; Linn, T.; Al-Gobaisi, D. M. K., Present and future pretreatment concepts—strategies for reliable and low-maintenance reverse osmosis seawater desalination. *Desalination*, **1997**, *110*, 97-106.

16. Jiang, S.; Li, Y.; Ladewig, B. P., A review of reverse osmosis membrane fouling and control strategies. *Science of the Total Environment*, **2017**, *595*, 567-583.

17. Bou-Hamad, S.; Abdel-Jawad, M.; Ebrahim, S.; Al-Mansour, M.; Al-Hijji, A., Performance evaluation of three different pretreatment systems for seawater reverse osmosis technique. *Desalination*, **1997**, *110*, 85-92.

18. Johir, A. H.; Khorshed, C.; Vigneswaran, S.; Shon, H. K., In-line flocculation-filtration as a pre-treatment to reverse osmosis desalination.

19. Withers, A., Options for recarbonation, remineralization and disinfection for desalination plants. *Desalination*, **2005**, *179*, 11-24.

20. Delion, N.; Mauguin, G.; Corsin, P., Importance and impact of post treatments on design and operation of SWRO plants. *Desalination*, **2004**, *165*, 323-334.

21. Birnhack, L.; Penn, R.; Lahav, O., Quality criteria for desalinated water and introduction of a novel, cost effective and advantageous post treatment process. *Desalination*, **2008**, *221*, 70-83.

22. Reid, C. E.; Breton, E. J., Water and ion flow across cellulosic membranes. *J. Appl. Polym. Sci.*, **1959**, *1*, 133-143.

23. Sidney, L.; Srinivasa, S., High flow porous membranes for separating water from saline solutions. U.S. Patent US3133137A, 1962.

24. Baker, R. W., Reverse Osmosis. In *Membrane and Technology Applications*; John Wiley & Sons, Ltd, England, **2004**, pp 191-235.

25. Bentvelzen, J. M.; Kimura-Yeh, F.; Hopfenberg, H. B.; Stannett, V., Modification of cellulose acetate reverse osmosis membranes by radiation grafting. *J. Appl. Polym. Sci.*, **1973**, *17*, 809-820.

26. Ferjani, E.; Lajimi, R. H.; Deratani, A.; Roudesli, M. S., Bulk and surface modification of cellulose diacetate-based RO/NF membranes by polymethylhydrosiloxane preparation and characterization. *Desalination*, **2002**, *146*, 325-330.

27. Ferjani, E.; Roudesli, M. S., Modification by polymethylhydrosiloxane and characterization of reverse osmosis cellulose acetate membranes. *Eur. Polym. J.*, **2000**, *36*, 35-49.

28. El-Saied, H.; Basta, A. H.; Barsoum, B. N.; Elberry, M. M., Cellulose membranes for reverse osmosis Part I. RO cellulose acetate membranes including a composite with polypropylene. *Desalination*, **2003**, *159*, 171-181.

29. Perera, D. H. N.; Nataraj, S. K.; Thomson, N. M.; Sepe, A.; Hüttner, S.; Steiner, U.; Qiblawey, H.; Sivaniah, E., Room-temperature development of thin film composite reverse osmosis membranes from cellulose acetate with antibacterial properties. *J. Membr. Sci.*, **2014**, *453*, 212-220.

30. Lee, K. P.; Arnot, T. C.; Mattia, D., A review of reverse osmosis membrane materials for desalination—development to date and future potential. *J. Membr. Sci.*, **2011**, 370, 1-22.

31. Lau, W. J.; Ismail, A. F.; Misdan, N.; Kassim, M. A., A recent progress in thin film composite membrane: a review. *Desalination*, **2012**, *287*, 190-199.

32. Mollahosseini, A.; Rahimpour, A., Interfacially polymerized thin film nanofiltration membranes on TiO_2 coated polysulfone substrate. *J. Ind. Eng. Chem.*, **2014**, *20*, 1261-1268.

33. Zhao, Y.; Dai, L.; Zhang, Q.; Zhou, S.; Zhang, S., Chlorine-resistant sulfochlorinated and sulfonated polysulfone for reverse osmosis membranes by coating method. *J. Colloid Interface Sci.*, **2019**, *541*, 434-443.

34. Pendergast, M. T. M.; Nygaard, J. M.; Ghosh, A. K.; Hoek, E. M. V., Using nanocomposite materials technology to understand and control reverse osmosis membrane compaction. *Desalination*, **2010**, *261*, 255-263.

35. Korikov, A. P.; Kosaraju, P. B.; Sirkar, K. K., Interfacially polymerized hydrophilic microporous thin film composite membranes on porous polypropylene hollow fibers and flat films. *J. Membr. Sci.*, **2006**, *279*, 588-600.

36. Kim, E. S.; Kim, Y. J.; Yu, Q.; Deng, B., Preparation and characterization of polyamide thin-film composite (TFC) membranes on plasma-modified polyvinylidene fluoride (PVDF). *J. Membr. Sci.*, **2009**, *344*, 71-81.

37. Widjojo, N.; Chung, T. S.; Weber, M.; Maletzko, C.; Warzelhan, V., A sulfonated polyphenylenesulfone (sPPSU) as the supporting substate in thin film composite (TFC) membranes with enhanced performance for forward osmosis (FO). *Chem. Eng. J.*, **2013**, *220*, 15-23.

38. Mocanu, A.; Rusen, E.; Diacon, A.; Isopencu, G.; Mustatea, G.; Somoghi, R.; Dinescu, A., Antimicrobial propertied of polysulfone membranes modified with carbon nanofibers and silver nanoparticles. *Materials Chemistry and Physics*, **2019**, *223*, 39-45.

39. Cho, Y. H.; Han, J.; Han, S.; Guiver, M. D.; Park, H. B., Polyamide thin-film composite membranes based on carboxylated polysulfone microporous support membranes for forward osmosis. *J. Membr. Sci.*, **2013**, *445*, 220-227.

40. Kulkarni, A.; Mukherjee, D.; Gill, W. N., Flux enhancement by hydrophilization of thin film composite reverse osmosis membranes. *J. Membr. Sci.*, **1996**, *114*, 39-50.

41. Ghosh, A. K.; Jeong, B. H.; Huang, X.; Hoek, E. M. V., Impacts of reaction and curing conditions on polyamide composite reverse osmosis membrane properties. *J. Membr. Sci.*, **2008**, *311*, 34-45.

42. Liu, M.; Chen, Z.; Yu, S.; Wu, D.; Gao, C., Thin-film composite polyamide reverse osmosis membranes with improved acid stability and chlorine resistance by coating N-isopropylacrylamide-co-acrylamide copolymers. *Desalination*, **2011**, *270*, 248-257.

43. Wang, T.; Dai, L.; Zhang, Q.; Li, A.; Zhang, S., Effects of acyl chloride monomer functionality on the properties of polyamide reverse osmosis (RO) membrane. *J. Membr. Sci.*, **2013**, *440*, 48-57.

44. Wu, H.; Thang, B.; Wu, P., Preparation and characterization of anti-fouling β-cyclodextrin/polyester thin film nanofiltration composite membrane. *J. Membr. Sci.*, **2013**, *428*, 301-308.

45. Zhou, Y.; Yu, S.; Gao, C.; Feng, X., Surface modification of thin film composite membranes by electrostatic self-deposition of polycations for improved fouling resistance. *Sep. Purif. Technol.*, **2009**, *66*, 287-294.

46. Sun, J.; Zhu, L. P.; Wang, Z. H.; Hu, F.; Zhang, P. B.; Zhu, B. K., Improved chlorine resistance of polyamide thin-film composite membranes with a terpolymer coating. *Sep. Purif. Technol.*, **2016**, *157*, 112-119.

47. Kwon, Y.; Hong, S.; Choi, H.; Jung, J.; Moon, J.; Tak, T., Development of fouling-resistant RO membranes using PEGA macromer. *Desalination Water Treat.*, **2010**, *15*, 54-61.

48. Lin, S.; Huang, H.; Zeng, Y.; Zhang, L.; Hou, L., Facile surface modification by aldehydes to enhance chlorine resistance of polyamide thin film composite membranes. *J. Membr. Sci.*, **2016**, *518*, 40-49.

49. Ankoliya, D.; Mahta, B.; Raval, H., Advances in surface modification techniques of reverse osmosis membrane over the years. *Sep. Sci. Technol.*, **2018**, *0*, 1-18.

50. Wei, X.; Wang, Z.; Chen, J.; Wang, J.; Wang, S., A novel method of surface modification on thin-film composite reverse osmosis membrane by grafting hydantoin derivative. *J. Membr. Sci.*, **2010**, *346*, 152-162.

51. Anis, S.; Hashaikeh, R.; Hilal, N., Microfiltration membrane processes: A review of research trends over the past decade. *J. Water Process Engineering*, **2019**, *32*, 100941.

52. Al-Qadami, E. H. H.; Ahsan, A.; Mustaffa, Z.; Abdurrasheed, A. S.; Yusof, K. W.; Shan, S. M. H., Nanofiltration membrane technology and its applications in surface water treatment: A review. *J. Desal. And Water Purif.*, **2020***, 18*, 3-9.

53. Roy, Y.; Warsinger, D. M., Effect of temperature on ion transport in nanofiltration membranes: Diffusion, convection and electromigration. *Desalination*, **2017**, *420*, 241-457.

54. Yang, Z.; Zhou, Y.; Feng, Z.; Rui, X.; Zhang, T.; Zhang, Z., A review on Reverse Osmosis and Nanofiltration Membranes for Water Purification. *Polymers*, **2019**, *11*, 1252.

55. Fane, A. G.; Beatson, P.; Li, H., Membrane fouling and its control in environmental applications. *Water Sci. and Tecnol.*, **2000**, *41*, 303-308.

56. Alzahrani, S.; Mohammad, A. W., Challenges and trends in membrane technology implementation for produced water treatment: A review. *J. Water Process Engineering*, **2014**, *4*, 107-133.

57. Mondal, S.; Wickramasinghe, S. R., Produced water treatment by nanofiltration and reverse osmosis membranes. *J. Membr. Sci.*, **2008**, *322*, 162-170.

58. Ebrahimi, M.; Willershausen, D.; Ashaghi, K. S.; Engel, L.; Placido, L.; Mund, P.; Bolduan, P.; Czermak, P., Investigation on the use of different ceramic membranes for efficient oil-field produced water treatment. *Desalination*, **2010**, *250*, 991-996.

59. Li, L.; Dong, J.; Nenoff, T. M.; Lee, R., Desalination by reverse osmosis using MFI zeolite membranes. *J. Membr. Sci.*, **2004**, *243*, 401-404.

60. Duke, M. C.; O'Brien-Abraham, J.; Milne, N.; Zhu, B.; Lin, J. Y. S.; Diniz da Costa, J. C., Seawater desalination performance of MFI type membranes made by secondary growth. *Sep. Purif Technol.*, **2009**, *68*, 343-350.

61. Holme, J. P.; Biomimetic Water Membrane comprising Aquaporins used in production of Salinity Power. EP 1937395 B1, **2011**.

62. Zhao, Y.; Qiu, C.; Li, X.; Vararattanavech, A.; Shen, W.; Torres, J.; Hélix-Nielsen, C.; Wang, R.; Hu, X.; Fane, A. G.; Tang, C. Y., Synthesis of robust and high-performance aquaporin-based biomimetic membranes by interfacial polymerization-membrane preparation and RO performance characterization. *J. Membr. Sci.*, **2012**, *423-424*, 422-428.

63. García-Ivars, J.; Corbatón-Báguena, M. J.; Iborra-Clar, M. I., Chapter 6—Development of Mixed Matrix Membranes: Incorporation of Metal Nanoparticles in Polymeric

Membranes. In *Nanoscale Materials in Water Purification*; Thomas, S.; Pasquini, D.; Leu, S. Y.; Gopakumar, D. A.; Elsevier; **2019**, pp 153-178.

64. Luo, X. B.; Liu, L. L.; Deng, F.; Luo, S. L., Novel ion-imprinted polymer using crown ether as a functional monomer for selective removal of Pb(II) ions in real environmental water samples. *J. Mater. Chem. A*, **2013**, *1*, 8280-8286.

65. Luo, X. B.; Guo, B.; Liu, J.; Deng, F.; Zhang, S.; Luo, S.; Crittenden, J., Recovery of Lithium from Wastewater Using Development of Li Ion-Imprinted Polymers. *ACS Sustainable Chem. & Eng.*, **2015**, *3*, 460-467.

66. Rajabi, H. R.; Shamsipur, M.; Pourmortazavi, S. M., Preparation of a novel potassium ion imprinted polymeric nanoparticles based on dicyclohexyl 18C6 for selective determination of K^+ ion in different water samples. *Mater. Sci. Eng. C*, **2013**, *33*, 3374-3381.

67. Yuan, C.; Zhang, L.; Li, H.; Guo, R.; Zhao, M.; Yang, L., Highly Selective Lithium-Ion Adsorbents: Polymeric Porous Microsphere with Crown Ether Groups. *Transactions of Tianjin University*, **2019**, *25*, 101-109.

68. Bartsch, R. A.; Czech, B. P.; Kang, S. I.; Stewart, L. E.; Walkowiak, W.; Charewicz, W. A.; Heo, G. S.; Son, B., High lithium selectivity in competitive alkali metal solvent extraction by lipophilic crown carboxylic acids. *J. Am. Chem. Soc.*, **1985**, *107*, 4997-4998.

69. Habata, Y.; Ikeda, M.; Akabori, S., Lithium Ion-selective Alkylphosphoric Acid Armed Dibenzo- and Benzo-14-crown-4 Derivatives. *J. Chem. Soc. Perkin Trans.*, **1992**, *20*, 2651-2655.

70. Pedersen, C. J., Cyclic polyethers and their complexes with metal salts. *J. Am. Chem. Soc.*, **1967**, *89*, 017-7036.

71. Buschmann, H. J., Stability constants and thermodynamic data for complexes of 12-crown-4 with alkali metal and alkaline-earth cations in methanol solutions. *J. Solution Chem,* **1987**, *16*, 181-190.

72. Smetana, A. J.; Popov, A. I., Lithium-7 nuclear magnetic resonance and calorimetric study of lithium crown complexes in various solvents. *J. Solution Chem.*, **1980**, *9*, 183-196.

73. D'Aprano, A.; Salomon, M.; Mauro, V., Solvent effects on complexation of crown ethers with $LiClO_4$, $NaClO_4$, and $KClO_4$ in methanol and acetonitrile. *J. Solution Chem.*, **1995**, *24*, 685-702.

74. Lu, J.; Qin, Y.; Zhang, Q.; Wu, Y.; Cui, J.; Li, C.; Wang, L.; Yan, Y., Multilayered ion-imprinted membranes with high selectivity towards Li^+ based on the synergistic effect of 12-crown-4 and polyether sulfone. *Appl. Surface Sci.*, **2018**, *427*, 931-941.

75. Sun, D.; Meng, M.; Qiao, Y.; Zhao, Y.; Yan, Y.; Li, C., Synthesis of ion imprinted nanocomposite membranes for selective adsorption of lithium. *Sep. Purif. Technol.*, **2018**, *194*, 64-72.

76. Sakamoto, H.; Kimura, K.; Tanaka, M.; Shono, T., Selective lithium ion transport through hollow-fiber membrane containing easily-dissociable 14-crown-4 derivative. *Bull. Chem. Soc. Jpn.*, **1989**, *62*, 3394-3396.

77. Hamilton, C. J.; Murphy, S. M.; Tighe, B. J., Synthetic hydrogels (10): Anomalous transport behavior in crown ether-containing hydrogel membranes. *Polymer (Guildf.*), **2000**, *41*, 3651-3658.

78. Yoshino, K.; Kotaka, M.; Okamoto, M.; Kakihana, H., ^{11}B-NMR Study of the Complex Formulation of Borate with Catechol and L-Dopa. *Bull. Chem. Soc. Japn.*, **1979**, *52*, 3005-3009.

79. Pizer, R.; Babcock, L., Mechanism of the Complexation of Boron Acids with Catechol and Substituted Catechols. *Inorganic Chemistry*, **1977**, *16*, 1677-1681.

80. Xia, N. N.; Zhang, H. Y.; Hu, Z. H.; Kong, F.; He, F., A functionalized bio-based material with abundant mesopores and catechol groups for efficient removal of boron. *Chemosphere*, **2021**, *263*, 128202.

81. Kluczka, J.; Tórz, A.; Łacka, D.; Kazek-Kęsik, A.; Adamek, J., Boron removal by adsorption on cobalt (II) doped chitosan bio-composite. *J. Polym.Environ.*, **2017**, *26*, 2039.

82. Sun, L.; Huang, J.; Liu, H.; Zhang, Y.; Ye, X.; Zhang, H.; Wu, A.; Wu, Z., Adsorption of boron by CA@KH-550@EPH@NMDG (CKEN) with biomass carbonaceous aerogels as substrate. *J. Hazard Mater.*, **2018**, *358*, 10-19.

83. Chen, T.; Wang, Q.; Lyu, J.; Bai, P.; Guo, X., Boron removal and reclamation by magnetic magnetite (Fe_3O_4) nanoparticle: an adsorption and isotopic separation study. *Separ. Purif. Technol.*, **2020**, *231*, 115930.

84. Lyu, J.; Zeng, Z.; Zhang, N.; Liu, H.; Bai, P.; Guo, X., Pyrocatechol-modified resins for boron recovery from water: synthesis, adsorption and isotopic separation studies. *React. Funct. Polym.*, **2017**, *112*, 1-8.

85. Zhang, X.; Wnag, J.; Chen, S.; Bao, Z.; Xing, H.; Zhang, Z.; Su, B.; Yang, Q.; Yang, Y.; Ren, Q., A spherical N-methyl-d-glucamine-based hybrid adsorbent for highly efficient adsorption of boric acid from water. *Separ. Purif. Technol.*, **2017**, *172*, 43-50.

Chapter 5

Incorporation of Crown Ether into an Norbornene Membrane Network

5.1 Introduction

Due to its use in energy applications, demand for lithium is projected to increase in the coming years.[1,2] This will require that we find more lithium sources, in order to keep up with the increasing demand. Currently, lithium is sourced largely from salt lake brines.[3]

Salt lake brines, while providing a large source of lithium, require geographically specific locations and vast amounts of time to obtain the lithium. This is due to the solar evaporation process that is utilized by salt lake brines, which relies on the sun to evaporate the brines. The locations of these brines are therefore limited to places that receive a lot of sunlight throughout the year, and even so, will take a long time to evaporate enough solution. The evaporation will eventually have some salts crash out of solution, and other salts concentrated into an enriched solution.[3,4]

Because of the geographically limiting and time-consuming nature of salt lake brines, it is therefore useful to look for other potential sources of lithium. Salt lake brines will generally have a lithium concentration in the range of 100-1000 mg/L.[5,6] A feedstock that has comparable lithium concentration and availability is produced water. Produced water is a waste stream that is used to extract oil and gas from the ground. Being able to harness the lithium from produced water is utilizing waste and environmentally relevant.[6]

Membranes have been used abundantly for water purification processes, but many commercial membranes are not able to distinguish between similar cations. Both lithium

brines and produced water contain various cationic species including Li^+, Na^+, K^+, Mg^{2+}, and Ca^{2+}. There has been some success separating monovalent and divalent cations utilizing charged membranes or ion-exchange membranes,[7,8] but separation of ions with the same valency has not had the same success.[9] Synthesizing a membrane that is able to selectively separate Li^+ from Na^+ and other cations would allow for lithium extraction from produced water, as well as easier isolation from salt lake brines.

To achieve Li^+/Na^+ selectivity, the incorporation of ligands containing a selective moiety to complex ions was chosen as the strategy. It has been shown in the literature that crown ethers are able to reversibly bind cations, depending on the crown ether cavity size as well as the ion radius. 12-crown-4 has been shown to complex with both Li^+ and Na^+, with the relative affinity being dependent on the surrounding chemical environment.[10-13] Most studies that have focused on 12-crown-4 binding lithium have been done in organic solvent systems and show lithium selectivity.

With those results in mind, we designed a polynorbornene membrane system to complex the lithium and allow sodium to pass through. However, upon experimentation, it was shown that the reverse was occurring, in that the sodium was being bound by the 12-crown-4 and the lithium was permeating through the membrane. This indicated that both the addition of the membrane bound 12-crown-4 and the aqueous environment had significant effects on the transport properties of these cations. To understand the experimental results, molecular dynamic simulations were done to investigate the interaction between the crown ether moiety and the cations in an aqueous environment.

In this chapter, I report on the synthesis and characterization of various norbornene crown ether ligands, as well as results that show the reverse permeability selectivity from what was expected.

5.2 Norbornene Monomer and Membrane Synthesis

The monomer synthesis for the norbornene system relies mainly on an EDC coupling reaction between a norbornene carboxylic acid and a hydroxymethyl crown ether (Figure 5.1). A norbornene acid is reacted with a hydroxymethyl crown ether in the presence of 1-ethyl-3-(3-dimethylaminopropyl) carbodiimide hydrochloride (EDC) and 4-(dimethylamino)pyridine (DMAP). Briefly, EDC deprotonates the carboxylic acid, which then can attack the newly protonated EDC to form a carboxylic acid-EDC intermediate. DMAP, being a better nucleophile than the alcohol will attack the carbonyl of the intermediate, releasing a urea byproduct and forming a reactive amide. The amide
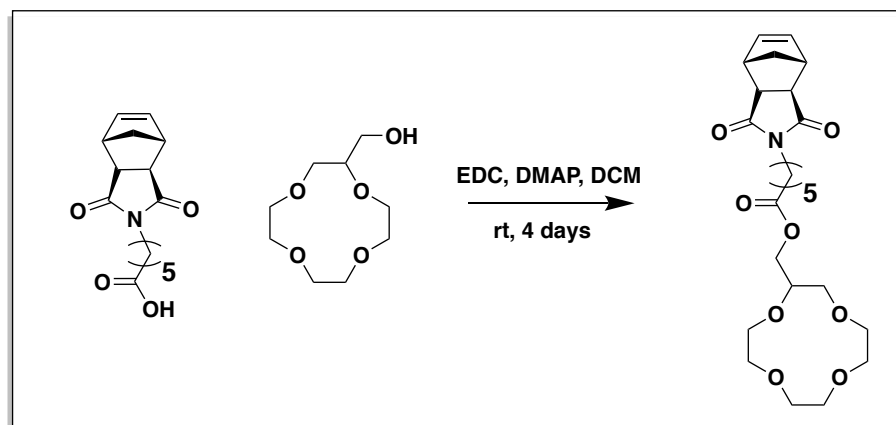
Figure 5.1. EDC coupling reaction of norbornene acid and hydroxymethyl crown ether.

intermediate will react rapidly with alcohols to give the desired product and release DMAP

molecule back into the solution (Figure 5.2).
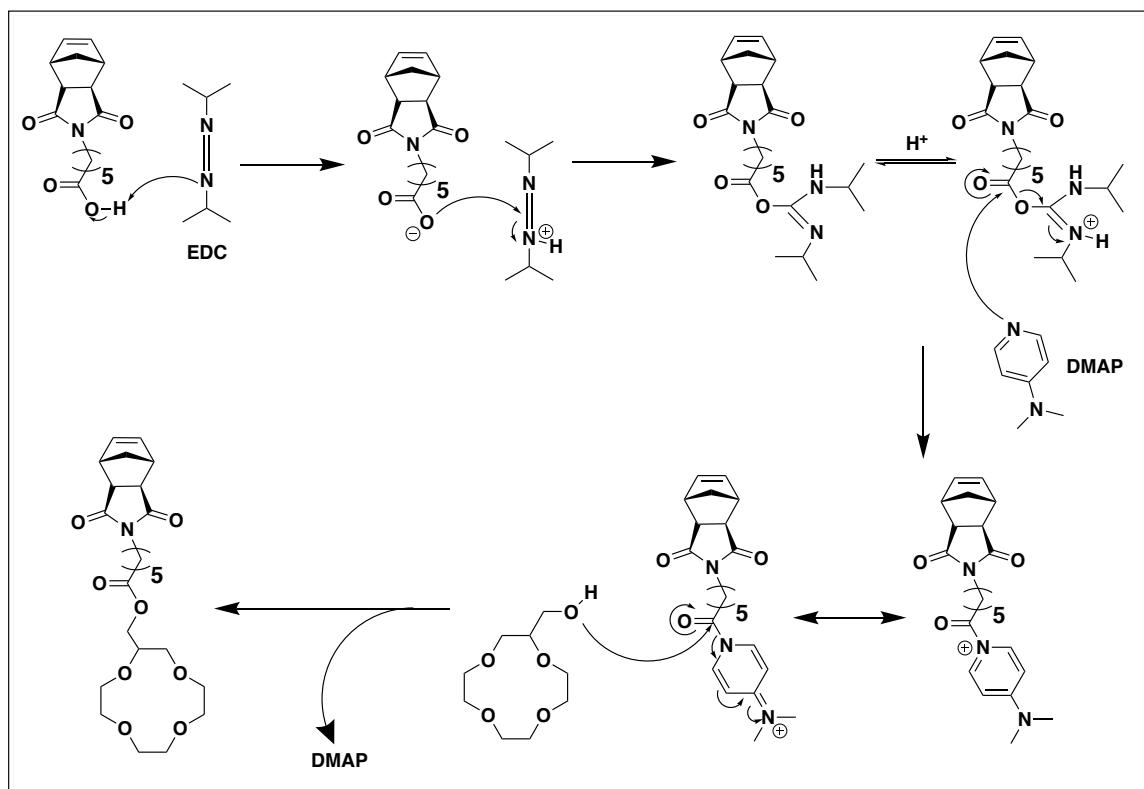
Figure 5.2. EDC coupling reaction mechanism.

5.2.1 Varying Crown Ether Size

To vary the crown ether size the same EDC coupling reaction was used with different

hydroxymethyl crown ethers. 15-crown-5 and 18-crown-6 were used for comparison to 12-

crown-4. The mechanism and the procedure are identical to that of the initial NB12C4

monomer. Incorporating a larger crown ether into the membrane system will allow different

size ions to interact with the crown ether moiety. This will have an effect on ion interactions

and transport properties of the membrane. It will also introduce more ether bonds into the

system, which will influence water uptake. Investigation into these effects will help elucidate

the fundamental interactions that occur in these membrane systems.

5.2.2 Varying Linker Length

Similarly, to vary the linker length the EDC coupling reaction was used again. To adjust the linker length, norbornene acids with different chain lengths were used. 2 carbon and 12 carbon linkers were synthesized in addition to the original 6 carbon linker to give a wide range of lengths. The linker length determines how far away from the polymer backbone the crown ether moiety is. Because the linkers are flexible aliphatic alkyl chains, a longer linker will give the crown ether more freedom of motion. This means that the crown ether will be able to interact with ions more freely in the membrane, acting more like a free solution state. Conversely, a short linker will anchor the crown ether close to the polymer backbone, and not allow much movement in solution. Varying the crown ether size and the linker length of these norbornene crown ether monomers gives range of monomers seen in Figure 5.3.
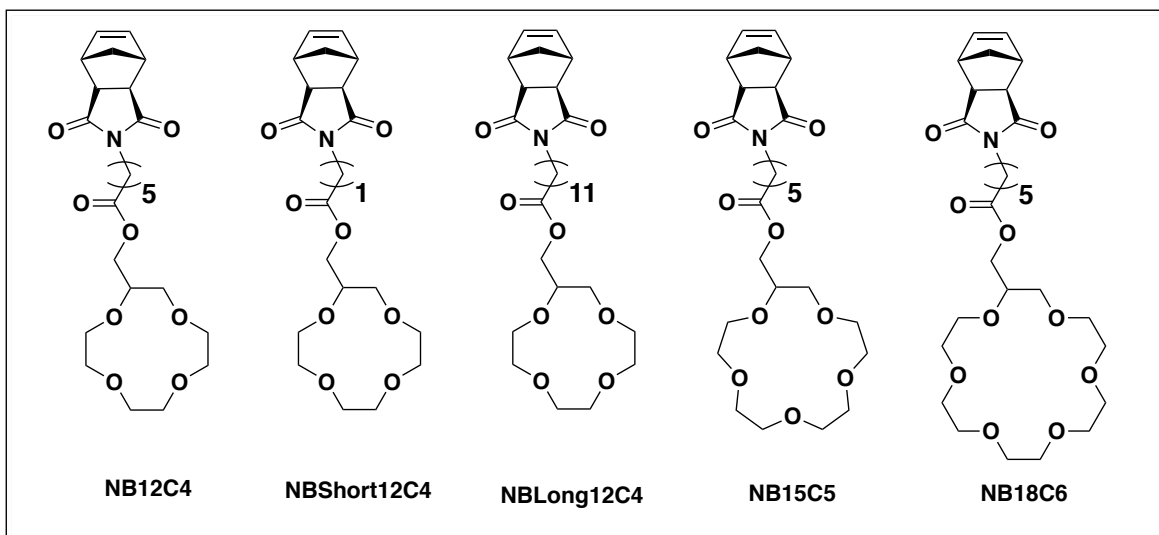
Figure 5.3. Norbornene crown ether monomers.

5.2.3 Synthetic Procedures

A carboxylic acid functionalized norbornene (13.45 g, 48.5 mmol), 2-hydroxymethyl 12-crown-4 (10.0g, 48.5 mmol), and DCM (200 mL) were mixed in a round bottom flask

equipped with a stir bar. The solution was brought to 0 °C and bubbled with argon for 30 minutes. 1-ethyl-3-(3-dimethylaminopropyl)carbodiimide hydrochloride (9.30 g, 48.5 mmol) and 4-(dimethylamino)pyridine (5.93 g, 48.5 mmol) were then added to the flask and stirred at 0 °C until dissolved. Once dissolved the reaction was sealed with a septum and bubbled with argon for an additional 30 minutes while being brought up to room temperature. The reaction was stirred at room temperature for 96 h under argon. The mixture was then washed with 2N HCl, brine, and dried with Na_2SO_4. The reaction mixture was concentrated in vacuo. The crude product was then purified through column chromatography, ethyl acetate:DCM 2:1. A light yellow viscous product was isolated (6.51 g, 85 %). **NB12C4** ^{1}H NMR (CDCl3, 600 MHz) δ: 6.24 (t, 2H, C=C-H), 4.10 and 4.06 (dq, 2H, O-CH2-), 3.64 (m, 15H, CR), 3.41 (t, 2H, N-CH2-), 3.22 (m, 2H, NB -CH-C=O), 2.63 (d, 2H, NB C=C-**C**H-CH), 2.27 (t, 2H, -CH2-C=O), 1.60 (m, 2H, -CH2-), 1.52 (m, 2H, -CH2-), 1.46 and 1.16 (ddm, 2H, NB bridging CH2), 1.28 (m, 2H, -CH2-). ^{13}C NMR (CDCl3, 600 MHz) δ: 178.0 (NB C=O), 173.21 (CH2-**C**=O), 137.85 (C=C), 71.4, 71.1, 70.9, 70.8, 70.7 (CR-CH2), 70.4 (CR-CH), 70.2 (O-CH2-CR), 63.9 (O-CH2-CR), 47.8 (NB (CH)2-**C**H-C=O), 45.3 (NB C=C-**C**H-CH), 42.8 (N-CH2-), 38.5 (NB bridging CH2), 33.9 (CH2-**C**H2-C=O), 27.5, 26.4, 24.4 (CH2 chain). **NB15C5** ^{1}H NMR (CDCl3, 600 MHz) δ: 6.26 (t, 2H, C=C-H), 4.19 and 4.06 (dq, 2H, O-CH2-), 3.64 (m, 19H, CR), 3.44 (t, 2H, N-CH2-), 3.25 (m, 2H, NB -CH-C=O), 2.65 (d, 2H, NB C=C-**C**H-CH), 2.30 (t, 2H, -CH2-C=O), 1.62 (m, 2H, -CH2-), 1.54 (m, 2H, -CH2-), 1.49 and 1.19 (dd, 2H, NB bridging CH2), 1.31 (m, 2H, -CH2-). **NB18C6** ^{1}H NMR (CDCl3, 600 MHz) δ: 6.26 (t, 2H, C=C-H), 4.19 and 4.08 (dq, 2H, O-CH2-), 3.65 (m, 23H, CR), 3.43 (t, 2H, N-CH2-), 3.25 (m, 2H, NB -CH-C=O), 2.65 (d, 2H, NB C=C-**C**H-CH), 2.29 (t, 2H, -CH2-C=O), 1.62 (m, 2H, -CH2-), 1.54 (m, 2H, -CH2-), 1.49 and 1.19 (dd, 2H, NB bridging CH2), 1.31 (m, 2H,

-CH$_2$-). **NBShort12C4** ^{1}H NMR (CDCl$_3$, 600 MHz) δ: 6.28 (t, 2H, C=C-H), 4.23 (t, 2H, N-CH$_2$-), 4.15 (dq, 2H, O-CH$_2$-), 3.66 (m, 15H, CR), 3.29 (m, 2H, NB -CH-C=O), 2.73 (d, 2H, NB C=C-**C**H-CH), 1.68 and 1.50 (dd, 2H, NB bridging CH$_2$). **NBLong12C4** ^{1}H NMR (CDCl$_3$, 600 MHz) δ: 6.27 (t, 2H, C=C-H), 4.07 (dq, 2H, O-CH$_2$-), 3.68 (m, 15H, CR), 3.43 (t, 2H, N-CH$_2$-), 3.26 (m, 2H, NB -CH-C=O), 2.65 (d, 2H, NB C=C-**C**H-CH), 2.30 (t, 2H, -CH$_2$-C=O), 1.59 (m, 2H, -CH$_2$-), 1.51 (m, 2H, -CH$_2$-), 1.49 and 1.21 (dd, 2H, NB bridging CH$_2$), 1.25 (m, 14H, -CH$_2$-) (Figure 5.4 and Figure 5.5).
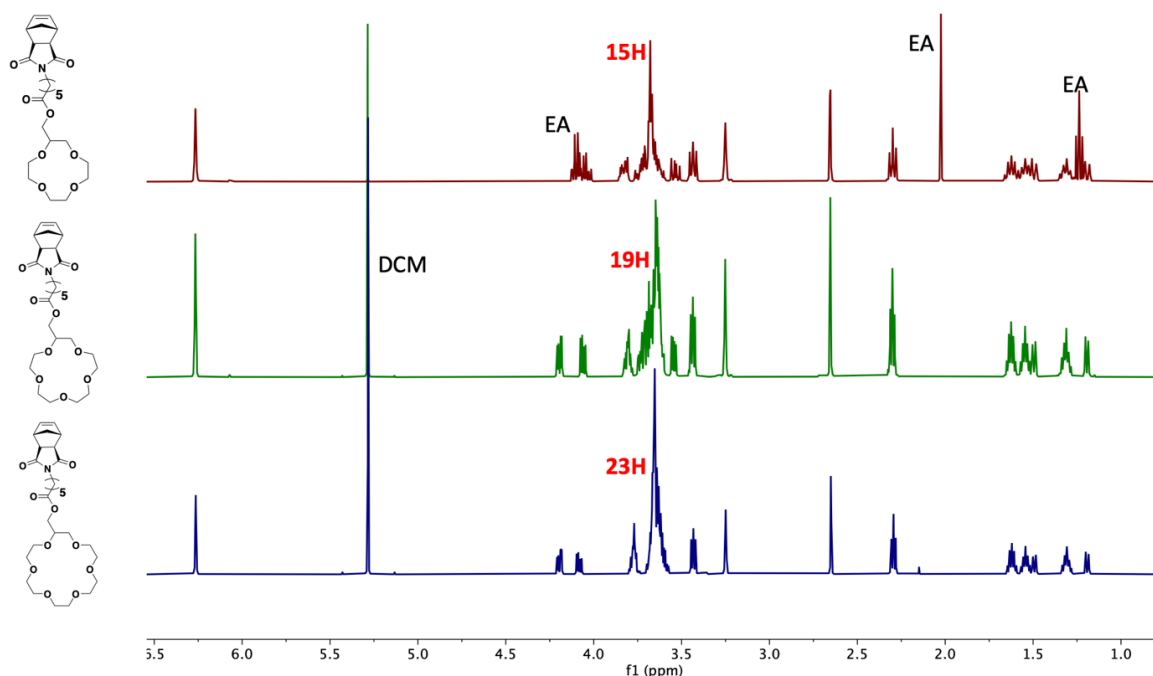
Figure 5.4. ^{1}H NMR spectra of NB12C4 (top), NB15C5 (middle), and NB18C6 (bottom) in CDCl$_3$. Spectra show nearly identical peaks, differentiated by the integration of the crown ether peaks around 3.6 ppm, which are labeled in red. Residual solvent peaks of ethyl acetate (EA) and dichloromethane (DCM) are labeled in black.

124
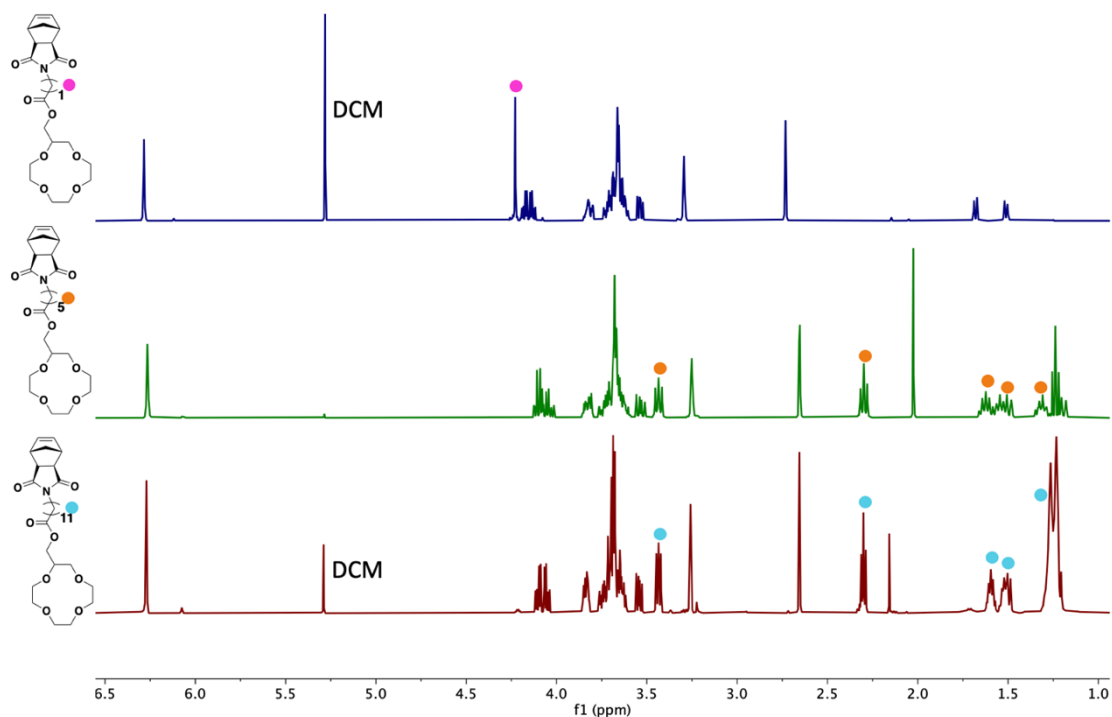
Figure 5.5. ^{1}H NMR spectra of NBShort12C4 (top), NB12C4 (middle), and NBLong12C4 (bottom) in CDCl[3]. The peaks indicating the change in linker length are highlighted.

5.2.4 Casting Procedure

All the monomers required for the desired membrane composition are weighed out and added to a 20 mL vial to prepare the pre-polymerization mixture. The vial is then taken into a nitrogen glove box and 8 mL of DCM is added and solution is swirled until all the components are dissolved. A solution of Grubbs' third generation catalyst (G3) is made by dissolving 1 mg of G3 in 5 mL of DCM. 1 mL of the G3 solution is added to the pre-polymerization vial to initiate ROMP. The reaction solution is stirred for approximately 10 seconds before being poured into a 9 cm diameter glass mold. The mold is left to sit in the glove box for 45 minutes before being moved to a hood to allow the DCM to evaporate at room temperature for 24 hours. The mold is then transferred into a vacuum oven to dry for an

additional 24 hours. DI water is then added to the mold to assist with the removal of the membrane from the mold. The membrane is removed from the mold with a metal spatula and tweezers and stored in a jar filled with DI water. A representative scheme of the cast procedure can be seen in Figure 5.6.
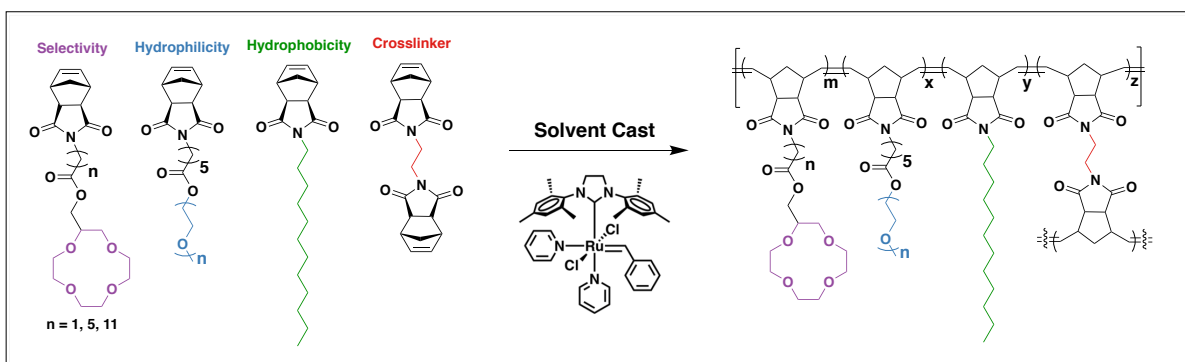
Figure 5.6. Scheme of norbornene membrane casting showing different monomers used, G3 catalyst structure, and resulting membrane structure.

5.3 Results and Discussion

5.3.1 Water Content

The water content of a membrane has a significant effect on the transport properties of solutes passing through, with higher water content corresponding with faster transport rates. The ability to adjust the water content of the polynorbornene membranes comes from the incorporation of a hydrophilic PEO monomer (NB-PEO) and a hydrophobic dodecyl monomer (NB-dodecyl). Incorporation of these monomers in varying amounts allows for the tuning of the water content of the membranes.

Initially, the 12-crown-4 monomer (NB12C4) was cast with NB-PEO and the bisnorbornene crosslinker. This system was optimized by varying the amount of NB-PEO (Figure 5.7). Figure 5.7 shows that there is a linear trend between the amount of NB-PEO and the water volume fraction of the membrane, and the polynorbornene membranes can be

tuned to be anywhere in the water content range of commercial membranes. The tunability of

the water content allows for the testing of membranes with various water contents to

elucidate the optimal composition for lithium selectivity.
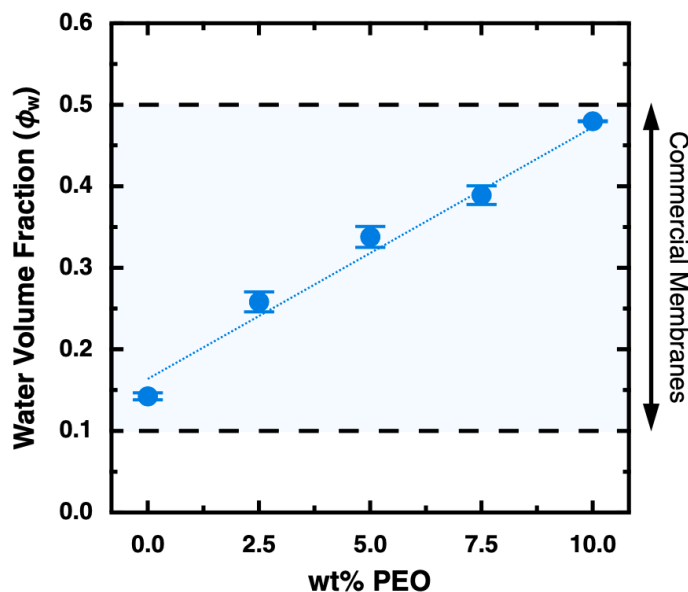
Figure 5.7. Linear relationship of water volume fraction and weight % of NB-PEO monomer. The water volume fraction range of common commercial membranes is indicated by the dashed lines.

5.3.2 Lithium/Sodium Selectivity

Three different selectivity parameters were measured, solubility selectivity,

diffusivity selectivity, and permeability selectivity. The experimental results are shown in

Figure 5.8. Notably, the solubility selectivity of <1 indicates that Na^+ is more soluble in the

membrane compared to Li^+. However, in terms of both diffusivity and permeability

selectivity, the value is >1, which indicates that the membrane is selective to Li^+ in those

respects. The greatest lithium selectivity was achieved at a water volume fraction of 0.34.

Likely, a higher water volume fraction increased the transport rate of sodium, making the

diffusivity of both sodium and lithium close in value, so the diffusivity and permeability

selectivity decreased.
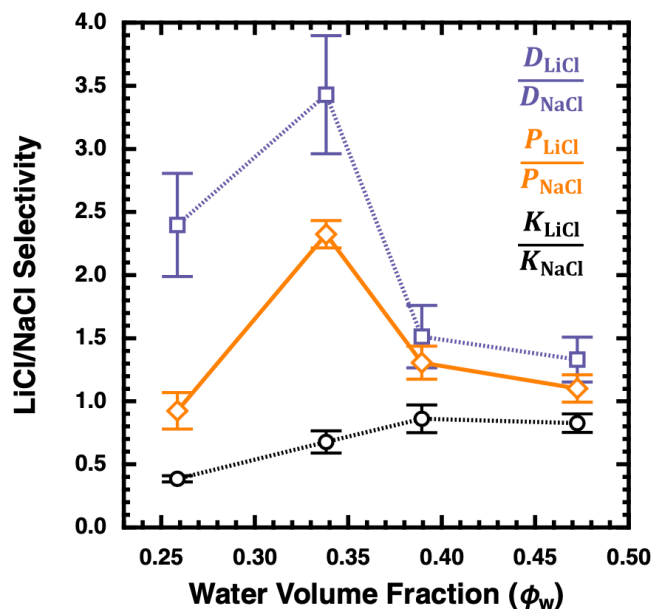
Figure 5.8. Experimental results of the relationship between water volume fraction and solubility selectivity (K_{LiCl}/K_{NaCl}), permeability selectivity (P_{LiCl}/P_{NaCl}), and diffusivity selectivity (D_{LiCl}/D_{NaCl}). The optimal lithium selectivity was seen to be at a water volume fraction of 0.34.

When considering a membrane without selective moieties in water, one would expect the permeability and diffusivity of sodium to be higher than lithium because of the hydrated radius, sodium is 3.6 Å compared to lithium at 3.8 Å. Since lithium has a larger hydrated radius, one would expect the lithium to move through the membrane at a slower rate. However, in the polynorbornene membrane system, the opposite was seen. The Na^+ is being slowed because it was binding to the 12-crown-4 moieties, leading to the increased lithium permeability selectivity. The high lithium permeability selectivity shown in this work is the reverse of many studies in the literature. This is largely because the literature works were commonly done in organic solvent, and this work was done in water.

The interaction between Li^+ and water compared to Li^+ and organic solvent molecules is stronger, and thus overcomes the affinity Li^+ has for 12-crown-4. The explanation for this reverse selectivity is due to the interactions of the crown ether with the cations as well as the

cation interactions with water. This is further explained by the molecular dynamic simulations.

5.3.3   Computational Results

To investigate the preferential binding of sodium, simulations were done (Figure 5.9). Figure 5.x compared the average coordination number of Na^+ and Li^+ with 12-crown-4 in a free solution scenario, and in the presence of the polynorbornene membrane. Simulations showed that with crown ether free in an aqueous solution, it binds in a 2:1 nature, with the two crown ether moieties surrounding one sodium ion. Lithium, on the other hand, is both being bound in a 1:1 ratio or not binding at all. When the crown ether was instead introduced to the salts in membrane form, sodium binding reverts to a 1:1 ratio and lithium is not being bound at all.
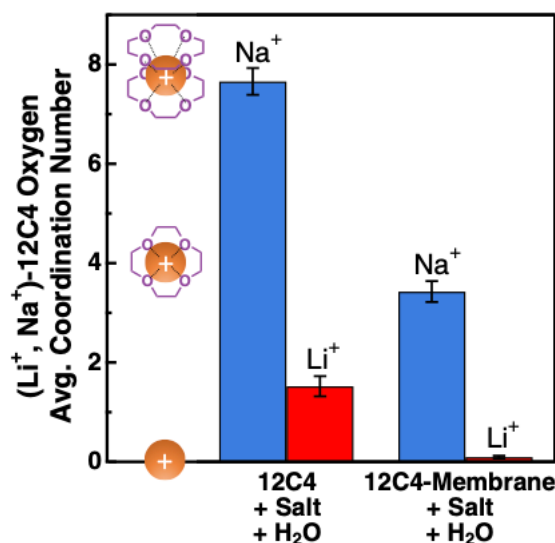
Figure 5.9. Simulation results of the average coordination number of crown ether oxygens to Na^+ and Li^+ in aqueous solution and a hydrated membrane environment. Sodium complexes with more crown ether than lithium in both scenarios.

The explanation of the aqueous binding of 12-crown-4 to Na^+ and Li^+ has to do with the hydration shell of the cation. Figure 5.10 shows the number of water molecules

coordinating to Na^+ and Li^+ in pure water compared to a hydrated 12-crown-4 membrane. The hydration shell of Li^+ does not change between the two environments. It retains its hydration shell and therefore its hydrated radius. Na^+, however loses part of the hydration shell, leading to binding with the 12-crown-4 moiety. Models of the binding states of Li^+ and Na^+ can be seen in Figure 5.11.
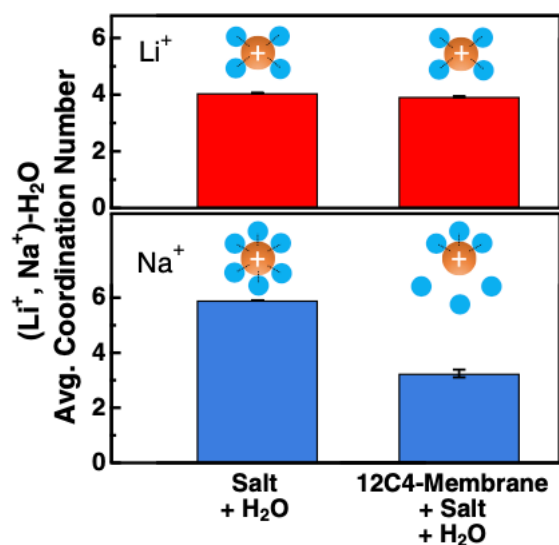
Figure 5.10. Simulation results of the average coordination number of water oxygens to Na^+ and Li^+ in aqueous solution and a hydrated membrane environment. Lithium retains its hydration shell and sodium is able to partially lose its hydration shell in a hydrated membrane environment.
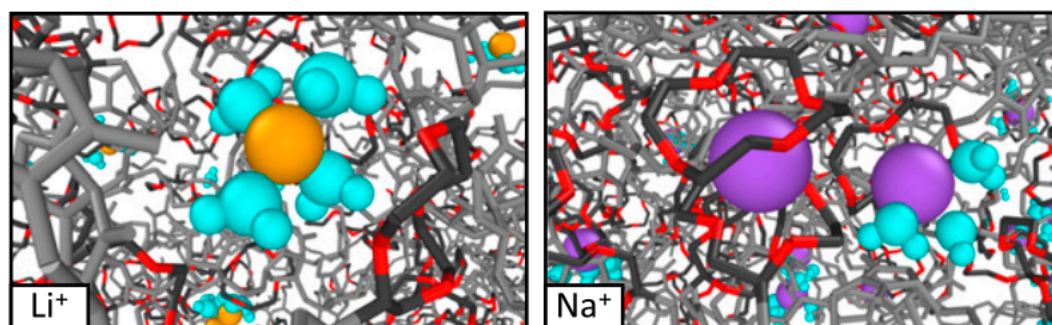
Figure 5.11. Renderings showing lithium retaining the hydration shell (left) and sodium complexing with crown ether (right)

5.3.4   Crown Ether Size Effect on Water Content

The optimized polynorbornene 12-crown-4 system had a water uptake of 74 % when testing on a small scale and 42 % when scaled up. When testing out different compositions for larger crown ethers, a water uptake of 74 % was the target with the assumption that when scaled up, the same decrease in water uptake would be seen. Initial membrane compositions incorporating both 15-crown-5 and 18-crown-6 into the network show large increases in water uptake. Using the same formulation as the optimized 12-crown-4 membrane, 15-crown-5 and 18-crown-6 gave water uptakes of 209 % and 400 % respectively (Table 5.1). The large increase in water uptake was due to the larger crown ethers, as all other factors remained the same. Larger crown ethers have more ether bonds, which are able to hydrogen bond with water molecules, thus increasing the water uptake of the membrane.

Table 5.1. Water Uptake percentages of Norbornene Monomers with Various Size Crown Ethers

Monomer	Mol % CE[a]	Water Uptake
NB12C4	92	74 %
NB15C5	91	200 %
NB18C6	91	409 %

[a]Mol% of NB-PEO and bisnorbornene were the same for all formulations

With such a large increase in water uptake, the pre-polymerization mixture of the membrane had to change in order to achieve the target of 74 %. The first step that was taken was replacing the hydrophilic NB-PEO monomer with a hydrophobic NB-dodecyl monomer. A test composition with an 18-crown-6 membrane showed that the replacement of PEO with dodecyl drove water uptake down from 400 % to 227 % (Table 5.2). While this was a good

result, it was still far from the targeted water uptake. This indicated that in order to obtain the optimal water uptake with larger crown ethers, the mol % of crown ether would need to decrease. Further test membranes incorporating 15-crown-5 and 18-crown-6 at varying mol % of crown ether are underway but have not yet been completed.

Table 5.2. Water Uptake Percentage of NB18C6 with NB-dodecyl monomer

Monomer	Mol % CE[a]	Water Uptake
NB18C6	91	227 %

[a]Mol% of NB-dodecyl was equal to the mol % of NB-PEO from Table 5.1

5.3.5   Linker Length Effect on Water Content

Similar to the crown ether variation, the linker length variation will have an impact on water uptake. A shorter linker corresponds to less hydrophobic CH_2 groups in the network, which will increase the water uptake. Conversely, a longer linker introduces more hydrophobicity into the network, decreasing the water uptake. This relationship was seen when making a test membrane with NBLong12C4 using the same composition as the optimized NB12C4 system. Where the NB12C4 system gives a water uptake of 74 %, the NBLong12C4 system of the same composition gave a water uptake of 17 %.

To optimize the NBLong12C4 system, a higher mol % of hydrophilic monomer (NB-PEO) needed to be added. Further test membranes incorporated more NB-PEO and less NMLong12C4 while keeping the bisnorbornene crosslinker constant. Results from those tests showed that decreasing the mol % of NBLong12C4 by only 3 % increased the water uptake of the system from 17 % to 112 % (Table 5.x). This showed that the water content can be

tuned to within that same commercial membrane range as the NB12C4 membrane, and with slight adjustment to the ratio of NBLong12C4 and NBPEO, the same optimal water content could be achieved.

Table 5.3. Water Uptake percentages of NBLong12C4 With Various Mol % of 12-Crown-4

Monomer	Mol % CE[a]	Water Uptake
NB12C4	92	74 %
NBLong12C4	91	17 %
NBLong12C4	89.5	46 %
NBLong12C4	88	112 %

[a] NB-PEO mol % increased as mol % of NBLong12C4 decreased; bisnorbornene mol % was held constant.

Test compositions for NBShort12C4 membranes have yet to be completed, but they will require NBdodecyl incorporation, because the shorter linker length will lead to a more hydrophilic membrane. The completion of the water uptake optimization will allow for studies on the effect of crown ether size and linker length on ion transport properties to be done.

5.4 Conclusion

A polynorbornene membrane system incorporating a crown ether moiety was designed and synthesized. At an optimized water volume fraction of 0.34, the 12-crown-4 moieties gave the membrane lithium permeability selectivity of approximately 2.3 over sodium. The high lithium permeability selectivity was due to the decrease in sodium diffusivity, which is because of the affinity sodium has to 12-crown-4 in a hydrated membrane. Molecular

dynamic simulations showed that this is because sodium partially dehydrates and therefore can bind to 12-crown-4, whereas lithium retains its hydration shell and does not interact with 12-crown-4. These results give some fundamental understanding of ion transport properties of polymeric ion-selective membranes in an aqueous environment. Further studies investigating the effect of crown ether size and the distance from the polymer backbone on ion transport are in progress.

5.5 References

1. Greim, P.; Solomon, A. A.; Breyer, C., Assessment of lithium critically in the global energy transition and addressing policy gaps in transportation. *Nature Communications*, **2020**, *11*, 4570.

2. Martin, G.; Rentsch, L.; Höck, M.; Bertau, M., Lithium market research—global supply, future demand and price development. *Energy Storage Materials*, **2017**, *6*, 171-179.

3. Zhang, Y.; Hu, Y.; Wang, L.; Sun, W., Systematic review of lithium extraction from salt-lake brines via precipitation approaches. *Minerals Engineering*, **2019**, *139*, 105868.

4. Tran, T.; Luong, V. T., Chapter 3—Lithium Production Processes. In Lithium Process Chemistry, Resources, Extraction, Batteries and Recycling. **2015**, pp 81-124.

5. Flexer, V.; Baspineiro, C. F.; Galli, C. I., Lithium recovery from brines: A vital raw material for green energies with a potential environmental impact in its mining and processing. *Sci. Total Environ.*, **2018**, *639*, 1188-1204.

6. Kumar, A.; Fukuda, H.; Hatton, T. A.; Lienhard, J. H., Lithium recovery from oil and gas produced water: A need for a growing energy industry. *ACS Energy Lett.*, **2019**, *4*, 1471-1474.

7. Yang, G.; Shi, H.; Liu, W.; Xing, W.; Xu, N., Investigation of Mg^{2+}/Li^+ separation by nanofiltration. *Chin. J. Chem. Eng.*, **2011**, *19*, 586-591.

8. Wu, H.; Lin, Y.; Feng, W.; Liu, T.; Wang, L.; Yao, H.; Wang, X., A novel nanofiltration membrane with [MimAP][Tf_2N] ionic liquid for utilization of lithium from brines with high Mg^{2+}/Li^+ ratio. *J. Membr. Sci.*, **2020**, *60*, 117997.

9. Sujanani, R.; Landsman, M. R.; Jiao, S.; Moon, J. D.; Shell, M. S.; Lawler, D. F.; Katz, L. E.; Freeman, B. D., Designing Solute-Tailored Selectivity in Membranes: Perspectives for Water Reuse and Resource Recovery. *ACS Macro Letters*, **2020**, *9*, 1709-1717.

10. Pedersen, C. J., Cyclic polyethers and their complexes with metal salts. *J. Am. Chem. Soc.*, **1967**, *89*, 7017-7036.

11. Buschmann, H. J., Stability constants and thermodynamic data for complexes of 12-crown-4 with alkali metal and alkaline-earth cations in methanol solutions. *J. Solution Chem,* **1987**, *16*, 181-190.

12. Smetana, A. J.; Popov, A. I., Lithium-7 numclear magnetic resonance and calorimetric study of lithium crown complexes in various solvents. *J. Solution Chem.*, **1980**, *9*, 183-196.

13. D'Aprano, A.; Salomon, M.; Mauro, V., Solvent effects on complexation of crown ethers with $LiClO_4$, $NaClO_4$, and $KClO_4$ in methanol and acetonitrile. *J. Solution Chem.*, **1995**, *24*, 685-702.

Chapter 6

Incorporation of Crown Ether into an Epoxidized Poly(allyl glycidyl ether) (EpPAGE) Membrane Network

6.1 Introduction

The Universal Membrane Chemistry Platform (UMCP) is a poly(styrene-*b*-[(ethylene oxide)-*co*-(allyl glycidyl ether)]-*b*-lactide$_n$) block polymer. The polylactide block can be decomposed[1] to yield an isoporous structure, the polystyrene block gives mechanical structure, and the poly(allyl glycidyl ether) block allows for easy functionalization of the pore walls. The general structure of the UMCP can be seen in Figure 6.1. Once the PLA block is decomposed, the isoporous structure allows water to flow through, much like a nanofiltration or ultrafiltration membrane. The pendant allyl groups can be functionalized with any moiety of interest and will be on the pore walls, free to interact with the water and components that pass through.

PS block — Hydrophobic
PAGE-co-PEO block — Functionalization
PLA block — Pores

PLA decomposition
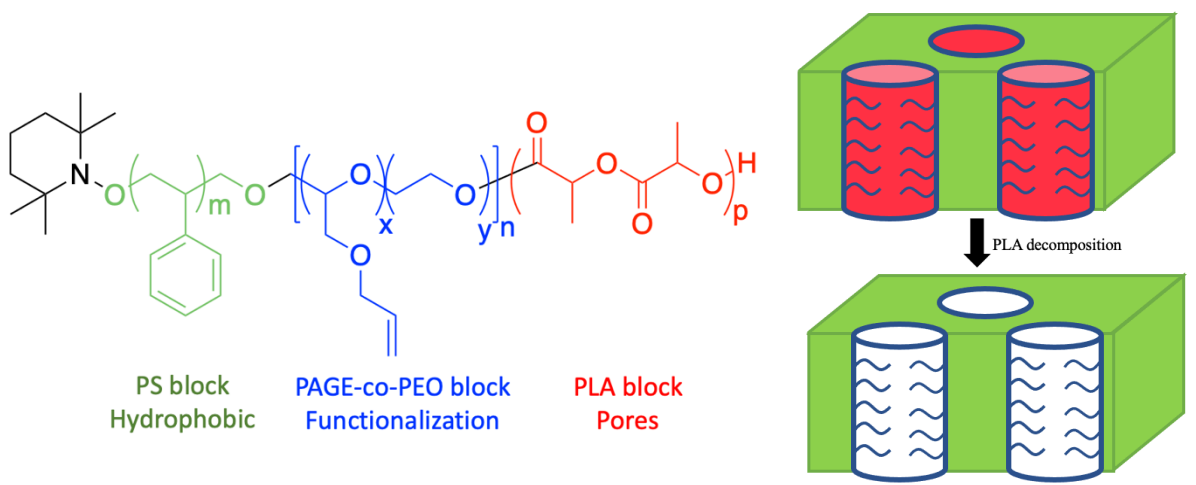
Figure 6.1. UMCP chemical structure (left) and illustrative depiction of pores (right). The components are color coordinated; polystyrene (green), PAGE-co-PEO (blue), and polylactide (red)

The particular interest of this chapter is the poly(allyl glycidyl ether) block, as that block would be the site for crown ether ligand attachment. Taking what we have learned from the polynorbornene system discussed in chapter 5, we can easily transfer a similar thought process to the UMCP. We can synthesize suitable crown ether ligands to attach to a poly(allyl glycidyl ether) backbone. Successful incorporation and study of 12-crown-4 on a poly(allyl glycidyl ether) backbone could also lead to an interesting backbone study comparing the effect of a more hydrophobic norbornene and a more hydrophilic poly(allyl glycidyl ether) backbone on ion transport and 12-crown-4 interactions.

6.2 Crown Ether Monomer Synthesis

To make use of the UMCP, crown ether ligands need to have a functional group that can easily react with an allyl group. Initial ligand design was focused on the incorporation of thiol groups to utilized thiol-ene "click" chemistry.[2] While some thiol functionalized ligands were synthesized, there were issues when attempting to click them onto the PAGE allyl groups. Some of these ligands and click attempts are discussed in Appendix B. Another strategy that was considered was utilizing double bonds and metathesis to incorporate ligands onto the PAGE backbone.[3,4] However, the strategy was problematic because there would be no way to stop the PAGE from reacting with itself.

With further thought, an epoxidation could be done to the PAGE system, converting the allyl groups into epoxide groups. Then, if an amine group was incorporated into the ligand epoxide-amine chemistry could be used. The reaction of an epoxide and an amine is commonly used for epoxy thermosets and is known to be highly reactive. A general scheme of this reaction can be seen in Figure 6.2. The amine ring opens the epoxide, which gives a

secondary or tertiary amine (depending on if the amine was primary or secondary initially) and a free hydroxyl group.
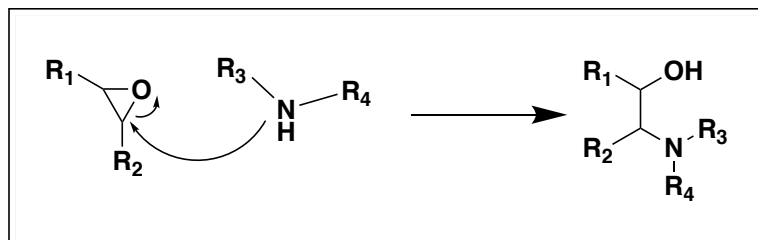
Figure 6.2. Reaction mechanism of an epoxide and an amine.

In order to utilize this chemistry, the PAGE backbone needs to be epoxidized and the ligands need to have a primary or secondary amine group. A scheme showing the epoxidation and casting reaction can be seen in Figure 6.3. The epoxidation of allyl groups is a well-known reaction, which uses mCPBA as the epoxidizing agent.[5] Once epoxidized, the EpPAGE can be cast into membranes with a multifunctional amine crosslinker and a combination of ligands. The crown ether amine will incorporate lithium selectivity into the membrane and the alkyl and hydroxyl amines will tune hydrophobicity and hydrophilicity respectively.
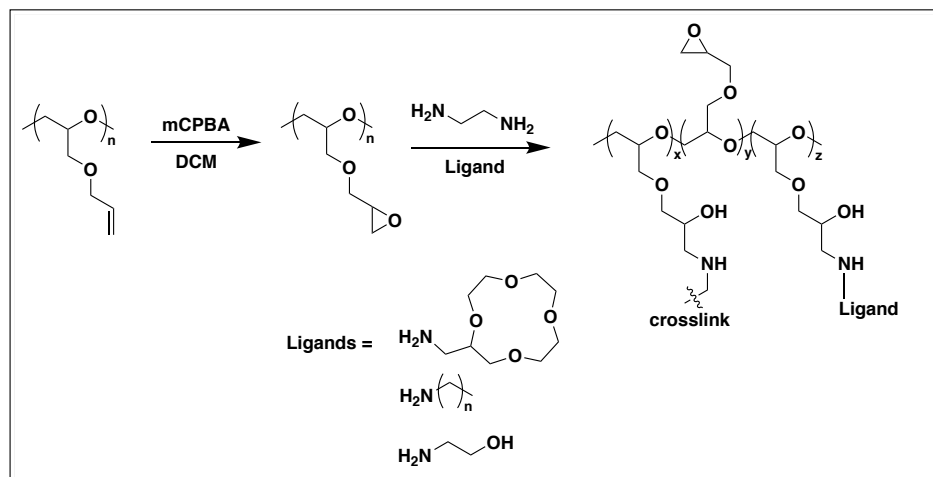
Figure 6.3. Reaction scheme showing the epoxidation of PAGE and the incorporation of a diamine crosslinker and amine functionalized ligands to impart selectivity and optimal water uptake into the membrane.

6.2.1 Amine Functionalized Crown Ether

To utilize the well understood and reactive amine-epoxide chemistry, the crown ether moiety needs to be modified to include amine functionality. Starting from 2-hydroxymehtyl 12-crown-4, the amine functionalized 12-crown-4 is synthesized via a 3-step route.[6] The synthetic route to obtain amine functionalized 12-crown-4 is shown in Figure 6.4. Briefly, thionyl chloride is used to replace the hydroxyl group with a chlorine to give a better leaving group. The chlorinated 12-crown-4 is then reacted with phthalimide potassium salt, which kicks off the chlorine and replaces it with the phthalimide group. The phthalimide intermediate product is then reduced with sodium borohydride and then acidified with acetic acid to give the amine functionalized 12-crown 4.
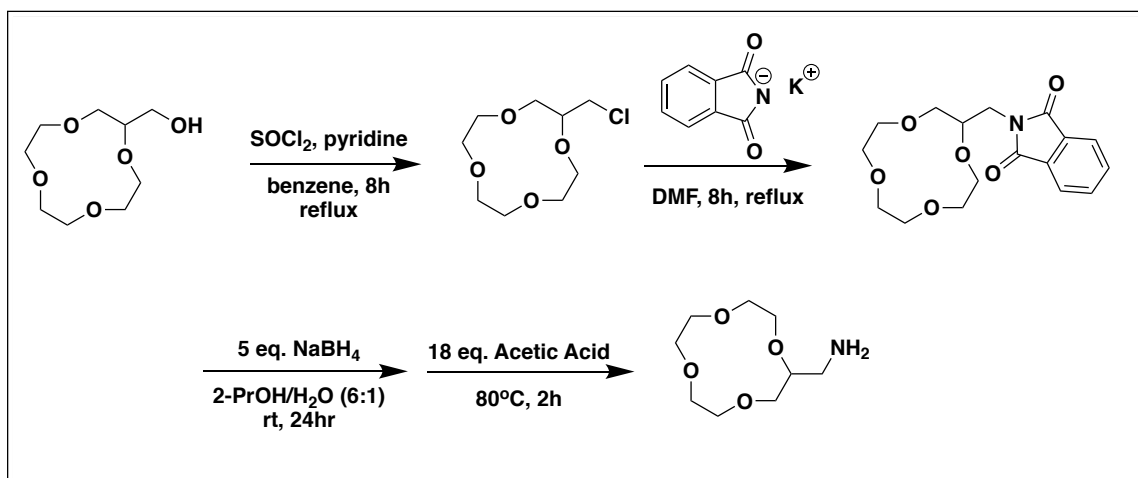
Figure 6.4. Synthetic route to amine functionalized 12-crown-4 ether.

The modification of 12-crown-4 to include an amine group allows it to react with the epoxide groups present in the EpPAGE system. Through that reaction the crown ether can be incorporated into the membrane framework.

6.2.2 Varying Crown Ether Size

In order to investigate the impact of crown ether size on the water uptake and transport properties of EpPAGE membranes, the same synthetic route seen in Figure 6.4 can be used. The only change is the starting material, where instead of 2-hydroxymethyl 12-crown-4, a hydroxymethyl 15-crown-5 or 18-crown-6 is used. The effect of crown ether size has been investigated using the norbornene system, yielding vast differences in water uptake depending on the crown ether incorporated as well as differences in ion selectivity preferences. It is expected that similar results will come from varying crown ether size in the EpPAGE system, though the more hydrophilic EpPAGE backbone, compared to the norbornene backbone, may mean that the hydrophilicity of the crown ether will have less impact on the water uptake of the membrane as a whole.

6.2.3 Varying Linker Length

Another study that could be done is to investigate the effect of linker length on the EpPAGE membrane properties. In order to synthesize amine functionalized crown ether with different linker length, the procedure seen in Figure 6.5 can be done. This procedure invloves using boc anhydride to protect the amine group of an amino acid,[7] then reacting the protected amino acid with 2-hydroxymethyl 12-crown-4 in an EDC coupling reaction. After the EDC coupling, the protected amine crown ether is obtained, and can be deprotected with trifluoroacetic acid to give the desired product.[8] The amino acid needs to be protected because if left as a primary amine it will react with the hydroxymethyl 12-crown-4 in the EDC coupling reaction. The length of linker between the crown ether moiety and the amine can be varied based on the starting amino acid used.
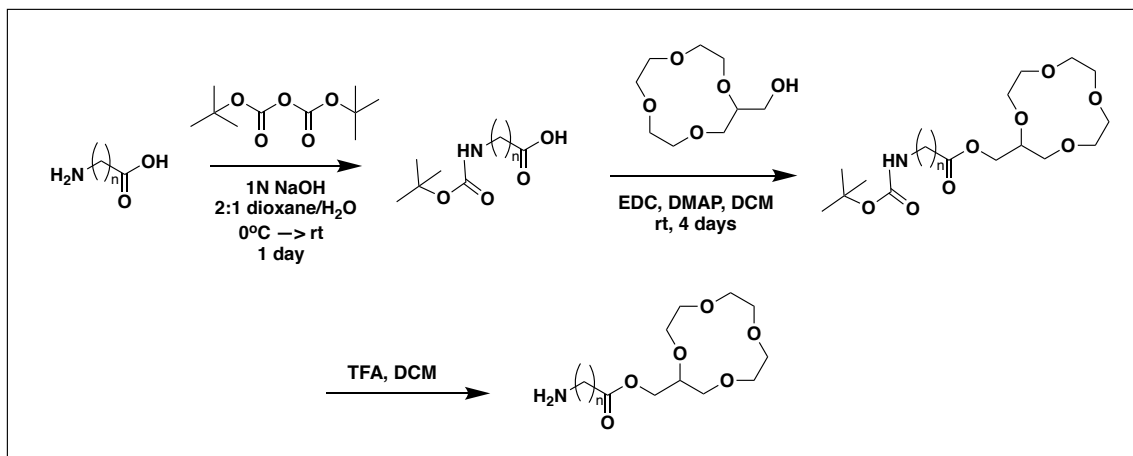
Figure 6.5. Synthetic route to amine functionalized 12-crown-4 ether with various linker lengths.

6.3 Synthetic Procedures for Crown Ether Monomers

Thionyl chloride was obtain from Spectrum Chemical. Boc anhydride, phthalimide potassium salt, dioxane, glycine, amino butyric acid, amino hexanoic acid, potassium hydrogen sulfate, 4-(dimethylamino)pyridine (DMAP), and ion exchange resin were obtained from Sigma. 2-hydroxymethyl 12-crown-4, 2-hydroxymethyl 15-crown-5, 2-hydroxymethyl 18-crown-6, and 1-ethyl-3-(3-dimethylaminopropyl) carbodiimide hydrochloride (EDC) were obtained from Fischer. All chemicals were used as received.

6.3.1 Chlorination of 2-hydroxymethyl Crown Ether[6]

To a round bottom flask was added 5.0 g (24.2 mmol) of 2-hydroxymethyl 12-crown-4, thionyl chloride (2.88 g, 24.2 mmol), pyridine (1.92 g, 24.2 mmol), and benzene (50 mL). The round bottom flask was fitted with a reflux condenser, stir bar added, and heated to 80 ºC. The reaction ran at reflux for 8 h. The resulting orange solution gives two layers. The benzene layer is isolated, the solvent evaporated, and the product used without further purification. This reaction can also be done with 2-hydroxymethyl 15-crown-5 or 18-crown-6 as the starting material. The 2-chloromethyl 12-crown-4 product was obtained as a

yellow/orange liquid (5.143 g, 94 %). Structure confirmed by NMR and Mass Spec. ^{1}H NMR

(600 MHz, CDCl$_3$) δ = 3.66 (m, 15H, crown ether), 3.50 (2H, -CH$_2$-Cl). All hydrogens

present in the crown ether peak, indicating that the starting hydroxyl group has been reacted.

M+ peak in the mass spec is m/z = 247.1, corresponding to the molecular weight of the

desired product plus a sodium ion. The ratio of the M+ (247) and M+2 (249) peaks is 3:1,

which is typical for the presence of chlorine (Figure 6.6 and Figure 6.7).
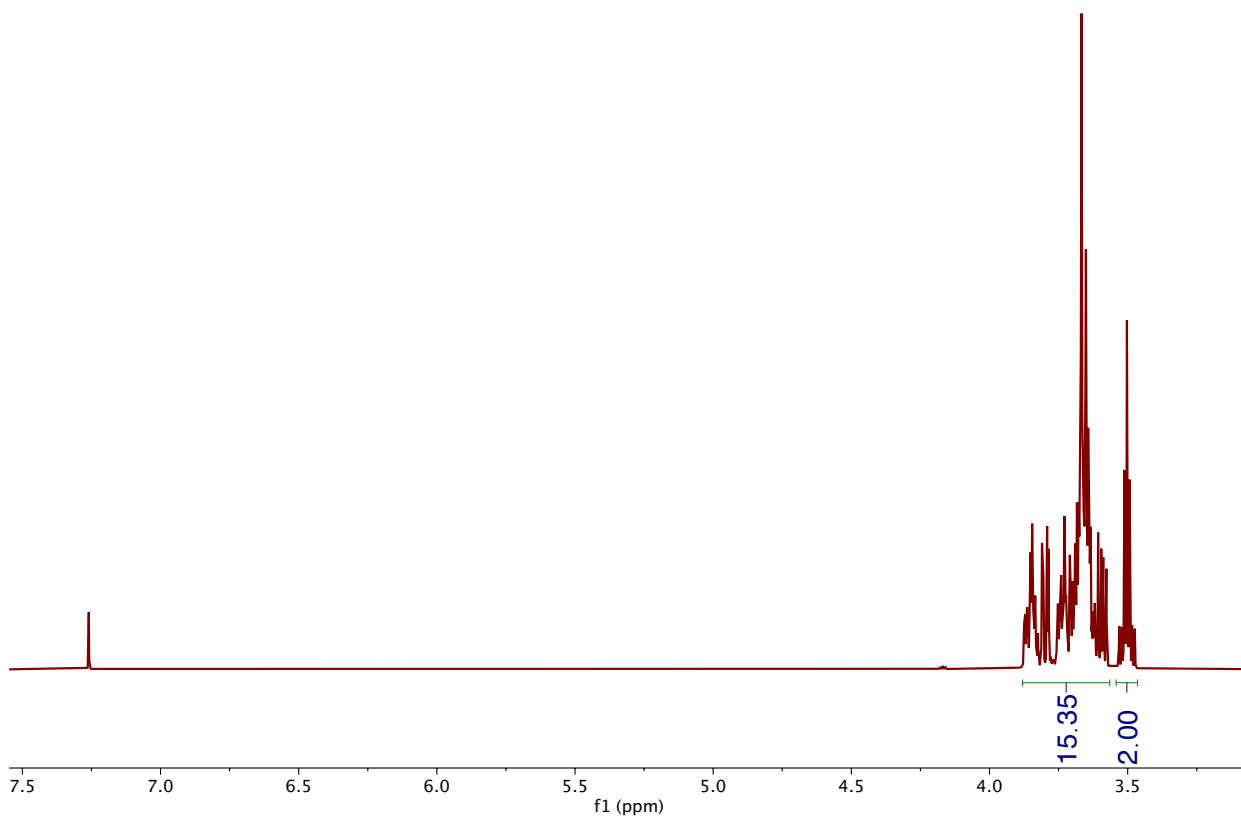
Figure 6.6. ^{1}H NMR in CDCl$_3$ of 2-chloromethyl 12-crown-4.
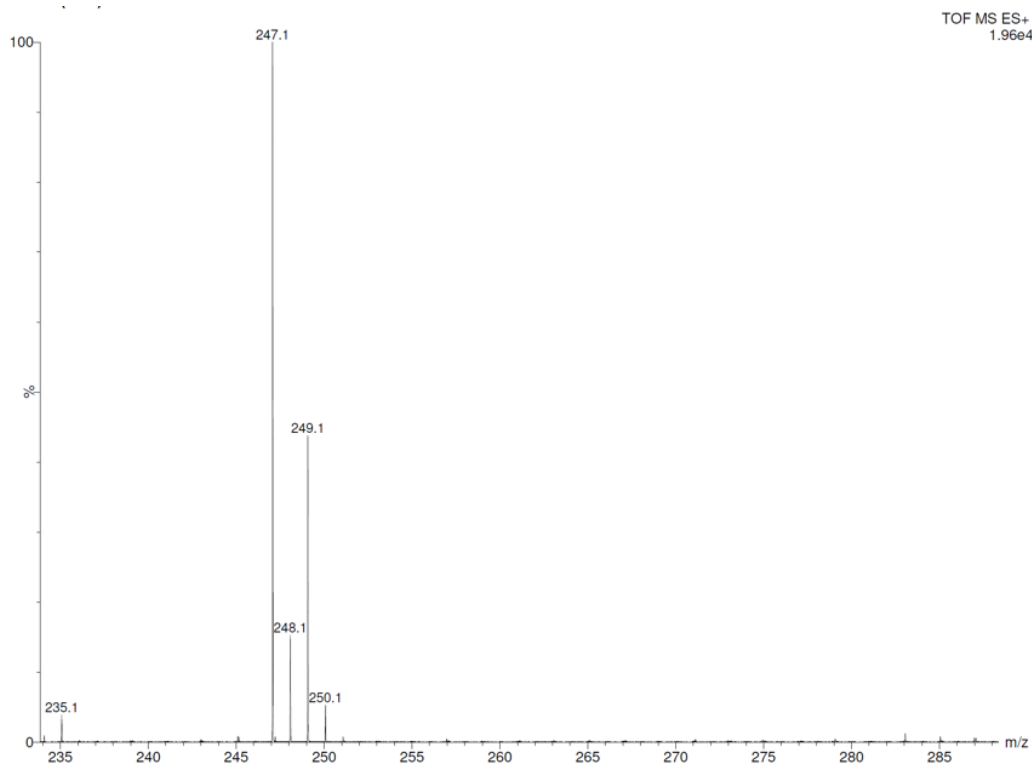
Figure 6.7. Mass Spec of 2-chloromethyl 12-crown-4. M+ = 247, M+2 = 249.

6.3.2 Phthalimide Protection of 2-chloromethyl Crown Ether[6]

2-chloromethyl 12-crown-4 (5.143 g, 22.9 mmol) was added to a round bottom flask

and dissolved in 25 mL of DMF. Phthalimide potassium salt (2.159 g, 22.9 mmol) was added

to the flask. The reaction mixture was fitted with a reflux condenser, heated to 153 °C, and

stirred at 153 °C for 7 h. After 7 h, the solution was cooled, and the solvent is evaporated off.

The crude product is dissolved in DI water and extracted with $CHCl_3$ (3 x 25 mL). The

combined organic layer is then washed with brine and dried with Na_2SO_4. The solvent was

then evaporated, and the product left on the high vac overnight. The phthalimide protected

12-crown-4 amine was obtained as a yellow/white solid (6.76 g, 88 %). Structure confirmed

by NMR. The two aromatic peaks indicate that the phthalimide group was successfully

incorporated, and the group of peaks around 3.6 ppm indicate that the crown ether is still

present (Figure 6.8). ^{1}H NMR (600 MHz, CDCl$_3$) δ = 7.84 (dd, 2H, ArH), 7.71 (dd, 2H, ArH), 3.67 (m, 17H, crown ether).
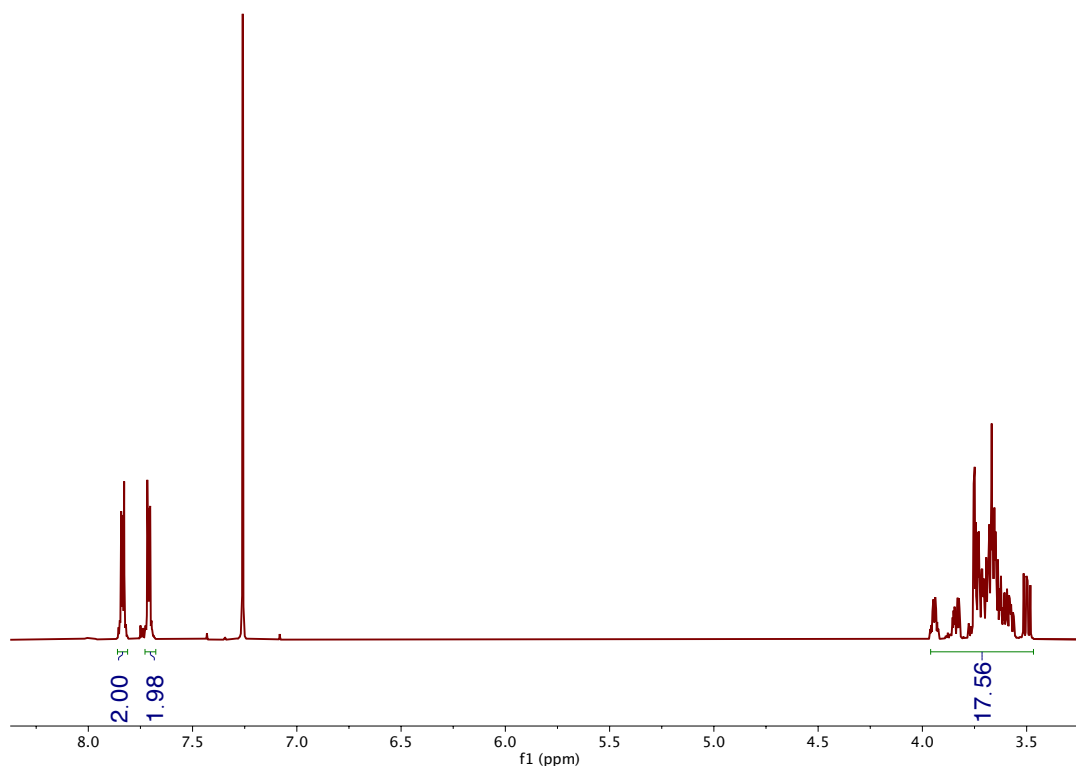
Figure 6.8. ^{1}H NMR of phthalimide protected 12-crown-4 amine in CDCl$_3$.

6.3.3 Phthalimide Deprotection of Crown Ether[6]

Phthalimide protected 12-crown-4 amine (5.0 g, 14.9 mmol) was dissolved in isopropanol (210 mL, 6 vol.) and water (35 mL, 1 vol.) in a round bottom flask. NaBH$_4$ (2.82 g, 74.5 mmol) is then added in portions to the flask. The solution is then stirred at room temperature for 24 h, after which glacial acetic acid (23.6 mL, 413 mmol) is added slowly to the reaction flask. Once settled, the flask was heated to 80 ºC for 2 h. After the 2 h, the reaction mixture is cooled and then loaded onto a Dowex H+ 50 column that had been packed with 0.25 N H$_2$SO$_4$. Once the reaction mixture was loaded onto the ion exchange column, 300 mL of DI water was then passed through, followed by 300 mL of 1 M NH$_4$OH.

The basic fraction was obtained and evaporated to give the deprotected product (1.34 g, 35 %). Structure confirmed by NMR. The peaks around 3.6 ppm correspond to the crown ether, and the peak around 2.7 ppm corresponds to the CH_2 adjacent to the amine (Figure 6.9). ^{1}H NMR (600 MHz, CDCl$_3$) δ = 3.68 (m, 15H, crown ether), 2.78 (2H, -**CH$_2$**-NH$_2$).
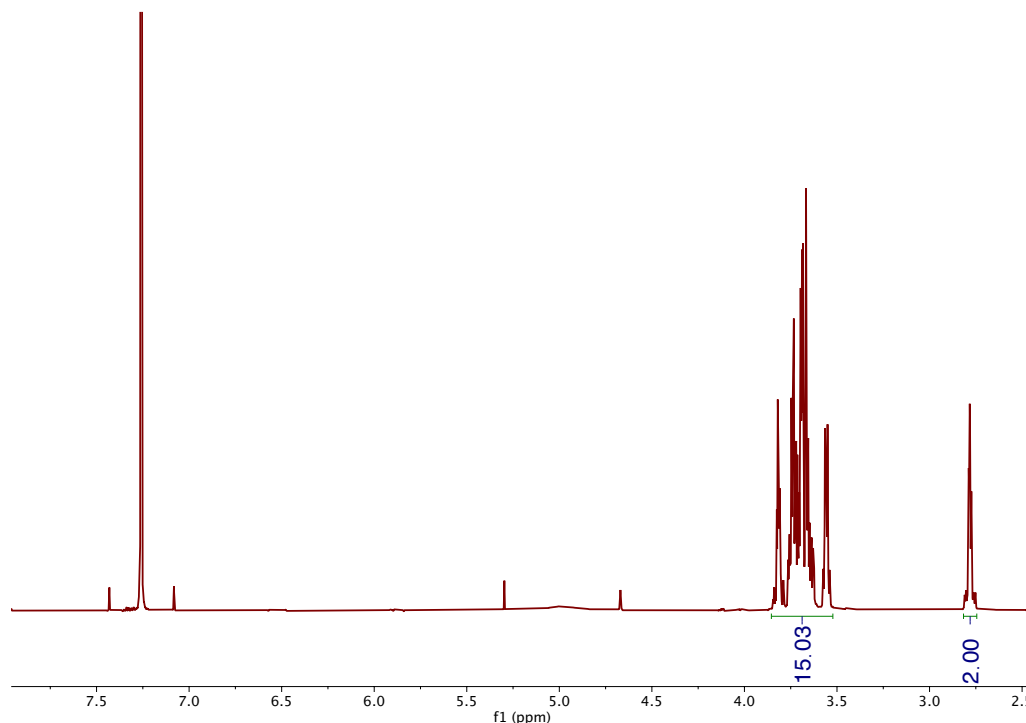
Figure 6.9. ^{1}H NMR of 12-crown-4 amine in CDCl$_3$.

6.3.4 Boc Protection of Amino Acids[7]

Amino hexanoic acid (5.24 g, 40.0 mmol) is dissolved in 60 mL of 1M NaOH in a round bottom flask. To the flask is then added 60 mL of dioxane followed by boc anhydride (8.72 g, 40.0 mmol). The reaction is stirred at room temperature for 12 h, after which the solution is concentrated. The crude product is dissolved in EtOAc, and then washed with 10 % KHSO$_4$ and brine. The organic layer was then dried with Na$_2$SO$_4$, concentrated, and put on the high vac overnight. A white solid was obtained (6.07 g, 67 %). This procedure was also carried out using glycine and amino butyric acid as the starting material (Figure 6.10).

Boc-Glycine ^{1}H NMR (600 MHz, CDCl$_3$) δ = 3.98 (d, 2H, -CH$_2$-), 1.46 (s, 9H, tBu). **Boc-Aminobutyric Acid** ^{1}H NMR (600 MHz, CDCl$_3$) δ = 3.20 (m, 2H, N-CH$_2$-), 2.41 (t, 2H, O=C-CH$_2$-), 1.83 (quintet, 2H, -CH$_2$-), 1.46 (s, 9H, tBu). **Boc-Aminohexanoic Acid** ^{1}H NMR (600 MHz, CDCl$_3$) δ = 3.11 (m, -N-CH$_2$-), 2.35 (t, 2H, -CH$_2$-), 1.65 (quintet, 2H, -CH$_2$-), 1.49 (m, 2H, -CH$_2$-), 1.44 (s, 9H, tBu), 1.37 (m, 2H, -CH$_2$-).
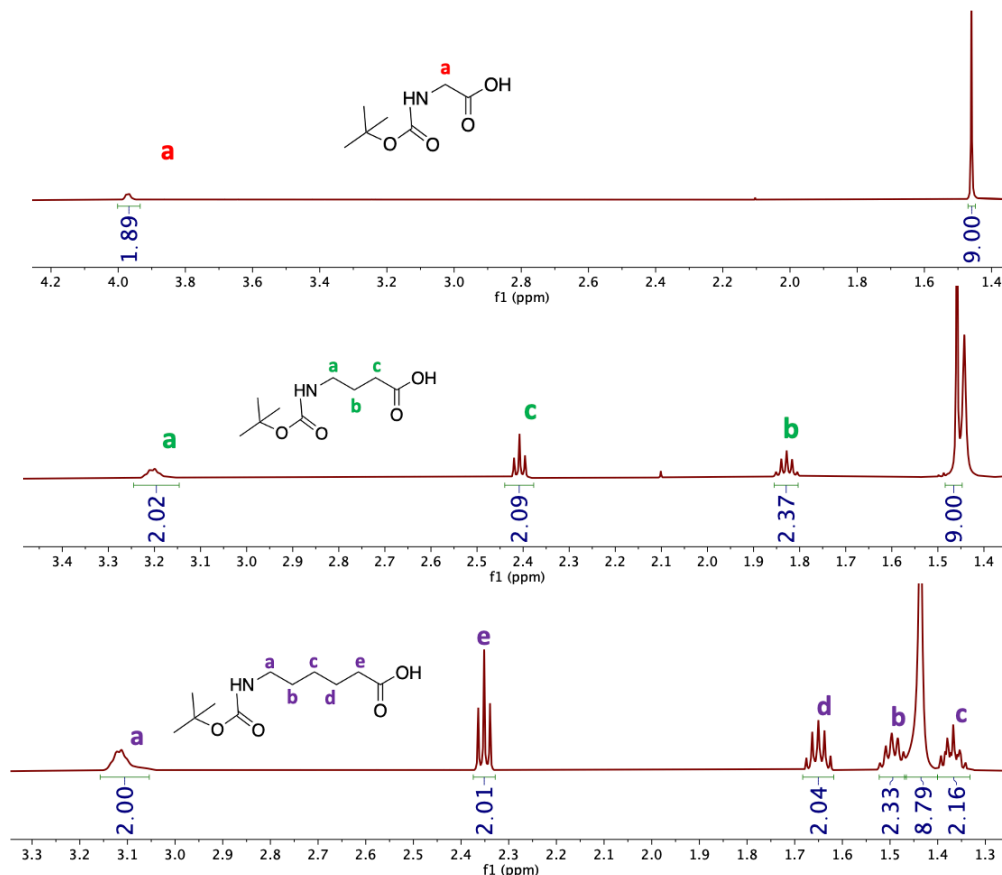
Figure 6.10. ^{1}H NMR of boc-protected amino acids including glycine (top), amino butyric acid (middle) and amino hexanoic acid (bottom) highlighting the difference in CH$_2$ groups present. The tBu group around 1.45 ppm confirms the presence of the boc protection group.

6.3.5 EDC Coupling of Boc-protected Amino Acid with 2-hydroxymethyl 12-crown-4

Boc-protected amino hexanoic acid (BocAHA) (4.20 g, 18.2 mmol), 2-hydroxymethyl 12-crown-4 (3.75 g, 18.2 mmol), and DCM (150 mL) were mixed in a round bottom flask equipped with a stir bar. The solution was brought to 0 °C and bubbled with

argon for 30 minutes. 1-ethyl-3-(3-dimethylaminopropyl)carbodiimide hydrochloride (3.49 g, 18.2 mmol) and 4-(dimethylamino)pyridine (2.22 g, 18.2 mmol) were then added to the flask and stirred at 0 °C until dissolved. Once dissolved the reaction was sealed with a septum and bubbled with argon for an additional 30 minutes while being brought up to room temperature. The reaction was stirred at room temperature for 96 h under argon. The mixture was then washed with 2N HCl, brine, and dried with Na_2SO_4. The reaction mixture was concentrated in vacuo. The crude product was then further purified through column chromatography, ethyl acetate:DCM 2:1. A light yellow viscous product was isolated (6.51 g, 85 %). The procedure was also carried out using boc-protected glycine (BocGly) and boc-protected amino butyric acid (BocABA) as the starting material (Figure 6.11). **12c4_BocGly** ^{1}H NMR (600 MHz, $CDCl_3$) δ = 4.21 (1H, dd, crown ether), 4.14 (1H, dd, crown ether), 3.93 (d, 2H, glycine CH_2), 3.68 (m, 15H, crown ether), 1.45 (s, 9H, tBu). **12c4_BocABA** ^{1}H NMR (600 MHz, $CDCl_3$) δ = 4.15 (dd, 1H, crown ether), 4.06 (dd, 1H, crown ether), 3.68 (m, 15H, crown ether), 3.15 (m, 2H, N-CH_2-), 2.37 (t, 2H, O=C-CH_2-), 1.81 (quintet, 2H, -CH_2-), 1.43 (s, 9H, tBu). **12c4_BocAHA** ^{1}H NMR (600 MHz, $CDCl_3$) δ = 4.1 (dd, 1H, crown ether), 4.05 (dd, 1H, crown ether), 3.68 (m, 15H, crown ether), 3.09 (m, 2H, N-CH_2-), 2.31 (t, 2H, O=C-CH_2-), 1.62 (quintet, 2H, -CH_2-), 1.47 (m, 2H, -CH_2-), 1.42 (s, 9H, tBu), 1.33 (m, 2H, -CH_2-).
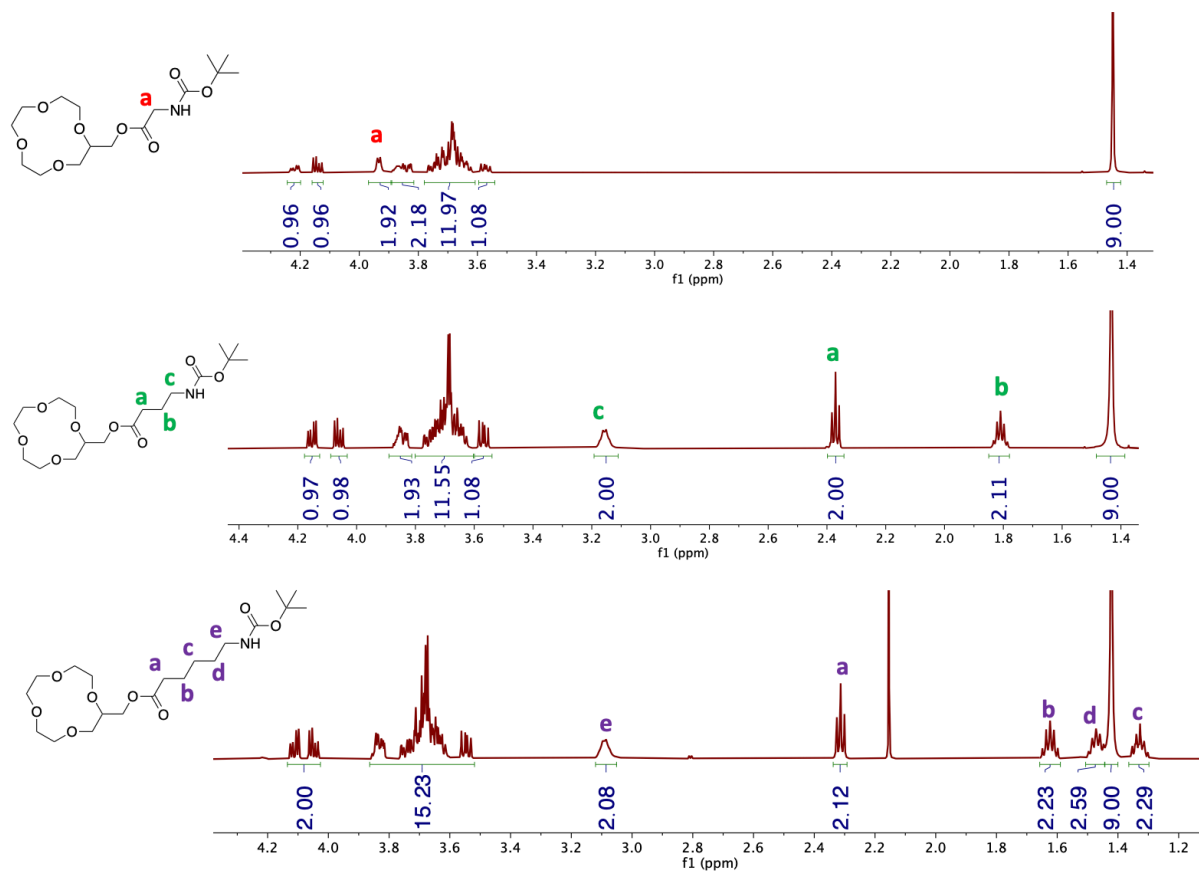
Figure 6.11. ^{1}H NMR in CDCl$_3$ of the EDC coupled products illustrating the two different amino acids used in the coupling reaction. Crown ether peaks are still present around 3.7 ppm, and the tBu peak around 1.4 ppm indicated the boc protection group is also still present.

6.3.6 Boc deprotection of Varied Linker Length 12-crown-4 Amine[8]

Boc-protected 12-crown-4 aminohexanoate (0.461 g, 1.1 mmol), trifluoroacetic acid (18 mL, 23.5 mmol), and DCM (18 mL) are added to a round bottom flask. The reaction mixture was stirred in an ice bath for 1 h. The solution is acidified to ph = 2, and then loaded onto a Dowex H+ 50 column that was packed with 0.25 N H$_2$SO$_4$. ~200 mL of DI water is then passed through the column, followed by ~200 mL of 1 M NH$_4$OH. The basic layer is collected and concentrated *in vacuo*. The crude product is a slightly yellow viscous liquid (0.142 g, 40 %).

6.4 Incorporation of Crown Ether into EpPAGE Membrane

6.4.1   Casting Procedure

Utilizing the EpPAGE backbone, the casting procedure involved a variety of amine functionalized monomers. For the water uptake, mechanical robustness, and crown ether content to be optimized various ligands must be incorporated into the membrane framework. This includes the amine functionalized 12-crown-4 for the crown ether moiety, a di- or tri-functional amine in order to crosslink the membrane, amine functionalized alkyl chains for hydrophobicity, and amine functionalized hydroxyls or ethers for hydrophilicity. The ratios of all the ligands can give membranes with a wide range of water uptakes, transport properties, and mechanical properties.

To cast the EpPAGE membranes, the EpPAGE and amine functionalized ligands are weighed out and added to a vial. The casting solvent (tetrahydrofuran (THF) or dichloromethane (DCM)) is then added, and the solution is stirred until all components are completely dissolved. Then the crosslinker, a di- or tri-functional amine, is added to the vial and the solution is stirred for about ten seconds before being cast into a glass mold. The mold is then heated at 45 °C overnight to evaporate off excess solvent and to ensure the crosslinking process had occurred. The membrane is then weighted, submerged in DI water, and carefully peeled off of the glass mold. Once free of the mold, the membrane is left submerged in DI water for two days so that any monomer trapped in the framework can be released, and water uptake can be calculated. After two days, the wet membrane is blotted off and weighed before being put into a vacuum oven for an additional two days in order for it to

dry completely. Initial attempts at membrane casting used THF as the casting solvent and ethylene diamine as the crosslinker.

6.4.2   Challenges

Though the amine-epoxide chemistry works well, there have been a few challenges obtaining usable crown ether incorporated EpPAGE membranes. Two of the main challenges are EpPAGE self-crosslinking and the mechanical robustness of the EpPAGE membranes.

Attempts of synthesizing EpPAGE have been successful at epoxidation, but the product will quickly self-crosslink leaving it unusable for membrane casting. Additionally, when EpPAGE membranes are successfully cast the outcome is not mechanically robust. Initial attempts have yielded very brittle membranes that curl up into a boat-like shape when dried and were not able to stand up to the transport measurements required of them. These challenges will need to be worked out before the EpPAGE framework can be utilized for future studies.

6.5 Plan for Future Work

6.5.1   Membrane Synthesis

In regard to membrane casting, there are a few aspects of the process that can be experimented with in order to obtain more robust membranes. Based on the solubility of the crown ether amine ligand being used, a different casting solvent can be employed. For example, initial tests with the original 12-crown-4 amine showed low solubility in THF so the casting solvent was changed to DCM. Any studies using other crown ether ligands should also include solubility testing to ensure an even distribution of ligand throughout the membrane.

There has also been preliminary testing, done by a collaborator at UT Austin, casting on a porous mesh support to impart more structure to the membrane This work would need to be expanded upon as well. This technique has also been used for previous studies incorporating N-methyl-D-glucamine (NMDG) into the EpPAGE system. (Landsman, 2021 submitted).

Another factor that needs to be better understood is the reactivity of the crown ether amine with the epoxide rings. Since the crown ether ligands are primary amines, it is likely that they will react with two different epoxide rings creating a more highly crosslinked network than was intended. To investigate this reaction, the epoxide ring openings could be tracked by NMR or FTIR to see if twice the number of epoxides are reacting. If the primary amine of the crown ether ligands become an issue because of the excessive crosslinking, an approach that could be taken is to react the amine group of the ligand to give a secondary amine. That would ensure that each ligand would react with only one epoxide. In the case of the varying linker length ligands, it could be possible to just use the boc-protected product and skip the deprotection step.

6.5.2 Membrane analysis and Backbone Study

Once the membrane synthesis gives consistent results, the membranes will need to be tested. One test that will need to be done is lithium sorption, both to help confirm the incorporation of crown ether, as well as to see how much the crown ether incorporation affects the membrane's affinity for lithium. This can be simply done by introducing the membrane into a lithium solution, having it reach equilibrium, and then putting the membrane into DI water and measuring the lithium released into the DI water.

Another important test is lithium selectivity, specifically in regard to lithium and sodium ions, but also in a mixed ion solution. Similar to the tests done on the norbornene, diffusivity selectivity, solubility selectivity, and permeability selectivity should all be investigated. It will be interesting to see if the 12-crown-4 incorporated in the EpPAGE system still gives high LiCl/NaCl permeability selectivity.

Additionally, molecular dynamic simulations could be done to compare to those for the norbornene system. It would be of interest to know if the EpPAGE backbone makes the crown ethers interact with ions more or less like in free solution compared to the norbornene backbone. The norbornene backbone can be looked at next to the EpPAGE backbone in a comparative study. This would give insight into the role of the polymer backbone to transport properties, Li^+/Na^+ selectivity, and 12-crown-4 binding.

6.5 Conclusion

A variety of amine functionalized crown ether ligands have been successfully synthesized and characterized. The synthetic routes chosen allow for the easy interchange of reagents to give a variety of ligands. The variety allows for studies on crown ether size as well as linker length. The incorporation of crown ether into the EpPAGE system is underway. Initial results indicate the incorporation of the ligand but give membranes that do not have the desired mechanical robustness. Work is being done to address these challenges and once overcome, further studies can be undertaken.

6.7 References

1. Zaaba, N. F.; Jaafar, M., Review on degradation mechanisms of polylactic acid: hydrolytic, photodegradative, microbial, and enzymatic degrdadation. *Polym. Eng. Sci.*, **2020**, *60*, 2061-2075.

2. Kolb, H. C.; Finn, M. G.; Sharpless, K. B., Click Chemistry: Diverse Chemical Function from a Few Good Reactions. *Angew. Chem. Int. Ed.*, **2001**, *40*, 2004-2021.

3. Love, J. A., The mechanics of metathesis. *Nature Chemistry*, **2010**, *2*, 524-525.

4. Astruc, D., The metathesis reaction: from a historical perspective to recent developments. *New Journal of Chemistry*, **2005**, *29*, 42-56.

5. Kim, C.; Taylor, T. G.; Perrin, C. L., MCPBA Epoxidation of Alkenes: Reinvestigation of Correlation between Rate and ionization Potential. *J. Am. Chem. Soc.*, **1998**, *120*, 9513-9516.

6. Bubmis, B. P.; Pacey, G. E., Alkali Metal Ion Extraction Using Lariat Ethers Possessing a Chromogenic Group. *Tetrahedron Letters*, **1984**, *25*, 1107-1110.

7. Pan, Z.; Lin, X., Kinase Inhibitor and Method for Treatment of Related Diseases. US2014256759 (A1), September 11, 2014.

8. Fattori, D.; Rossi, C.; Fincham, C. I.; Caciagli, V.; Catrambone, F.; D'Andrea, P.; Felicetti, P.; Gensini, M.; Marastoni, E.; Nannicini, R.; Paris, M.; Terracciano, R.; Bressan, A.; Giuliani, S.; Maggi, C. A.; Meini, S.; Valenti, C.; Quartara, L., Design and Synthesis of Novel Sulfonamide-Containing Bradykinin hB$_2$ Receptor Antagonists. 2. Syntesis and Structure-Activity Relationships of α,α-Clycloalkylglycine Sylfonamides. *J. Med. Chem.*, **2007**, *50*, 550-565.

Appendix A

Supplemental Figures and Spectra for Chapter 2 and Chapter 3

¹H NMR
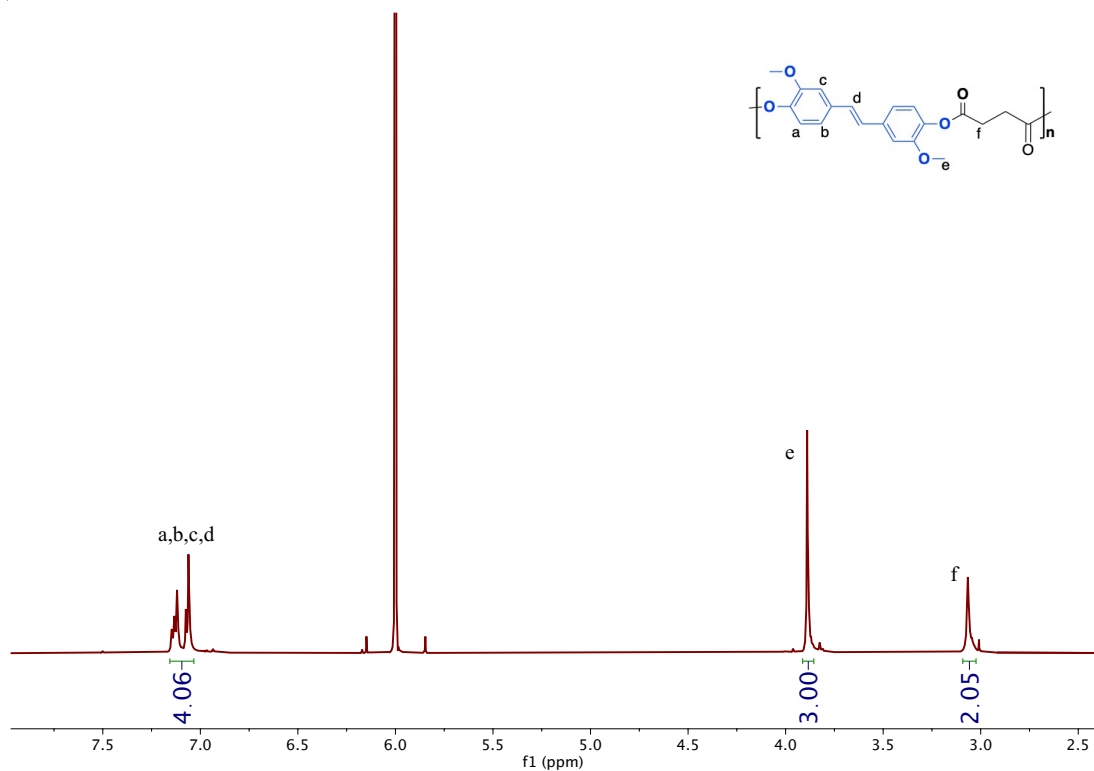
Figure A.1. ¹HNMR Spectrum of PBSU in TCE-d₂.
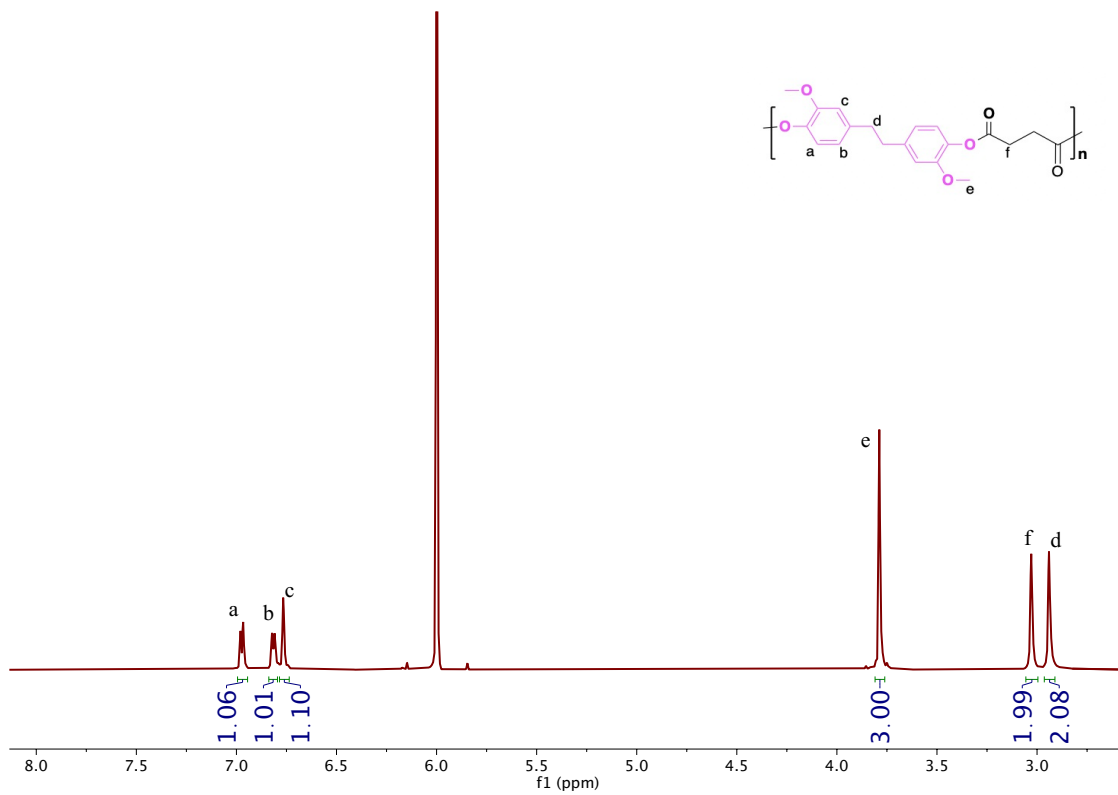
Figure A.2. ^{1}H NMR Spectrum of PHBSU in TCE-d_2.
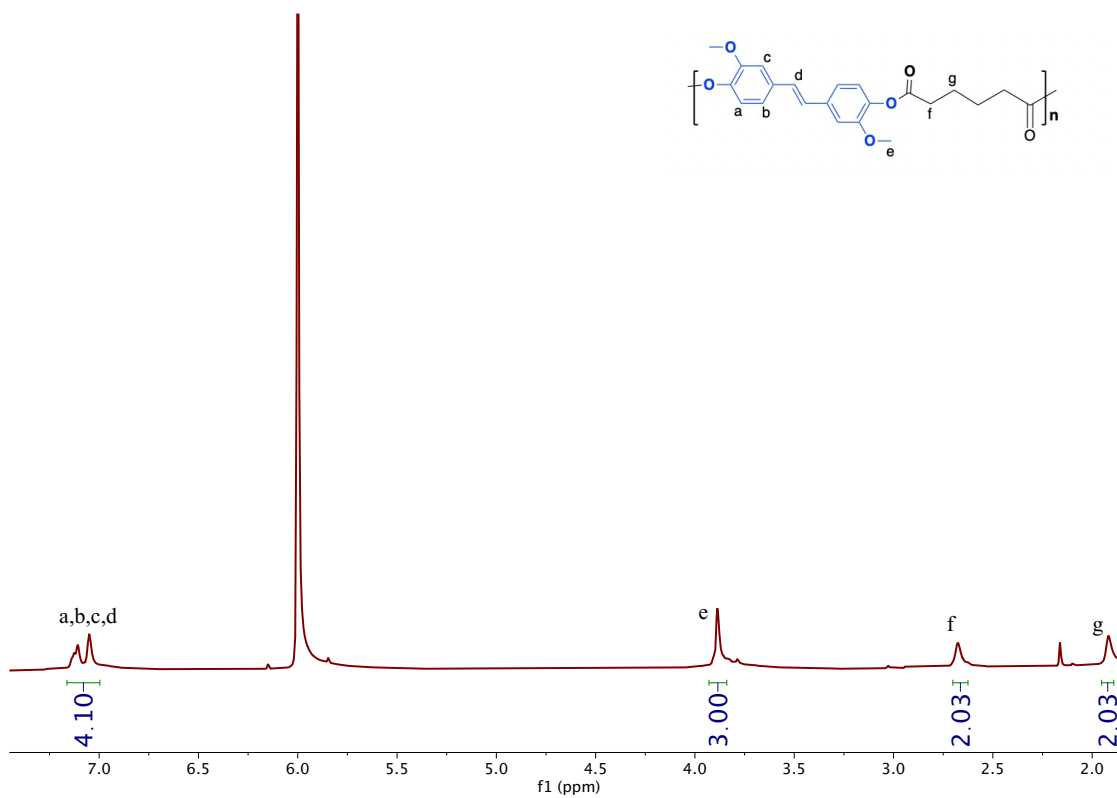
Figure A.3. ^{1}H NMR Spectrum of PBA in TCE-d_2.
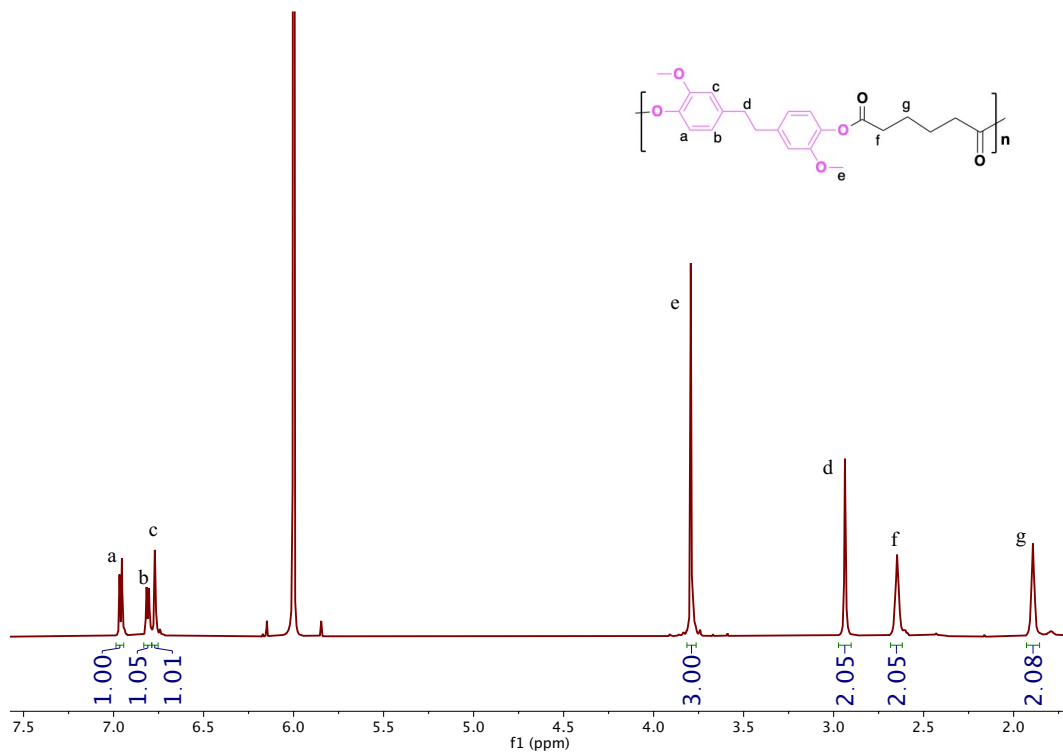
Figure A.4. ^{1}H NMR Spectrum of PHBA in TCE-d_2.
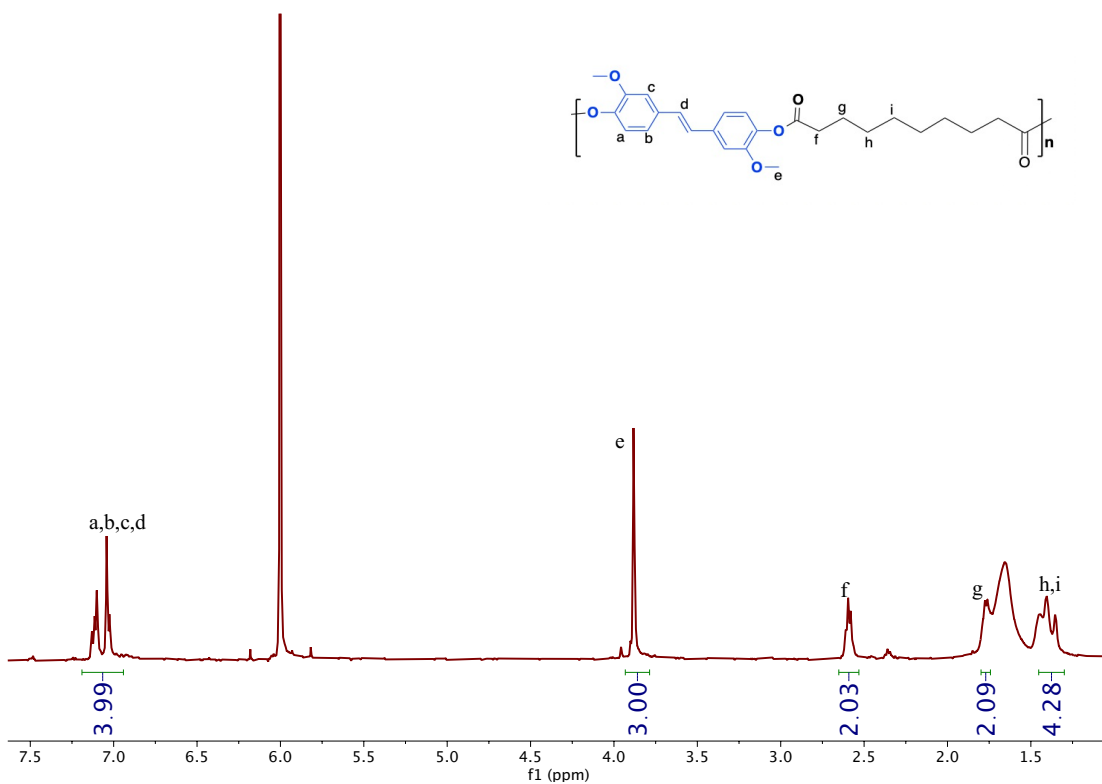
Figure A.5. ^{1}H NMR Spectrum of PBSE in TCE-d_2.
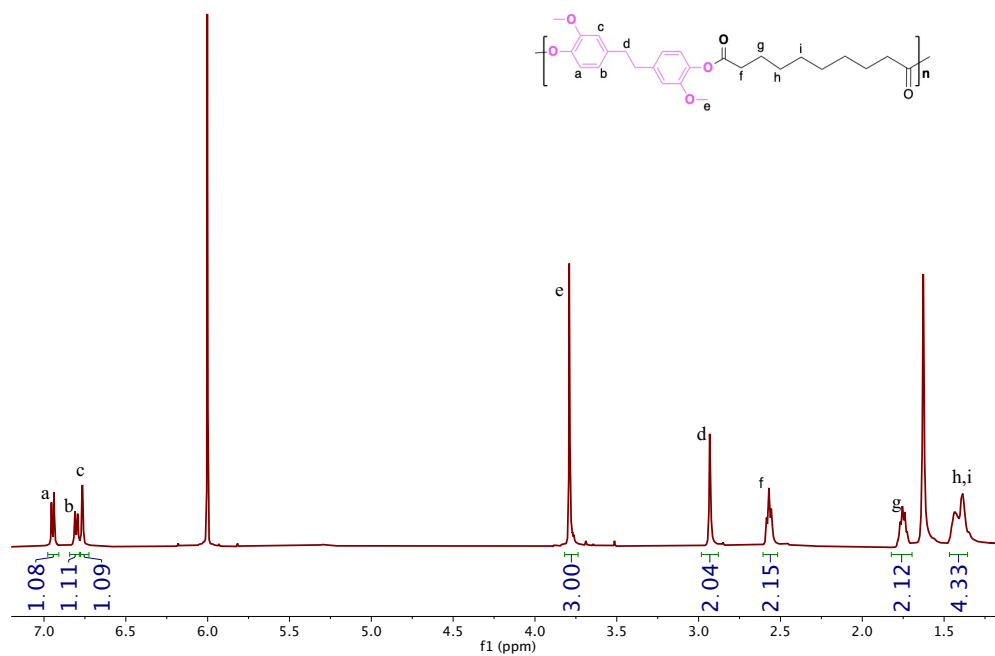
Figure A.6. ^{1}H NMR Spectrum of PHBSE in TCE-d_2.
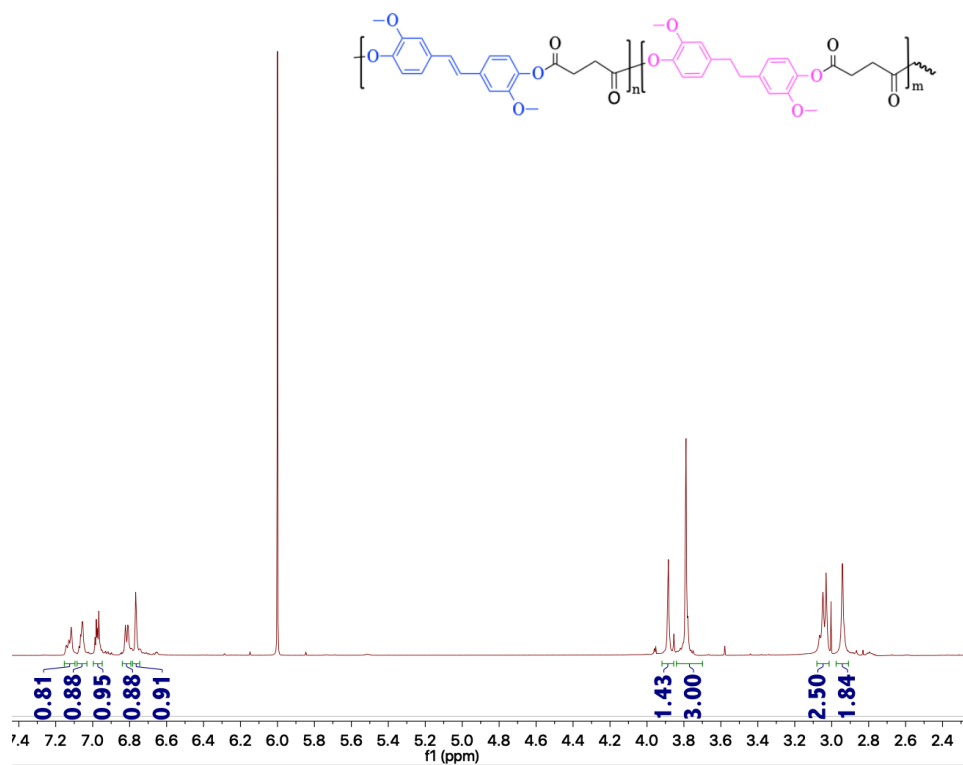
Figure A.7. ^{1}H NMR Spectrum of 2:1 HBIE:BIE + succinyl chloride polyester in TCE-d_2.

¹³C NMR
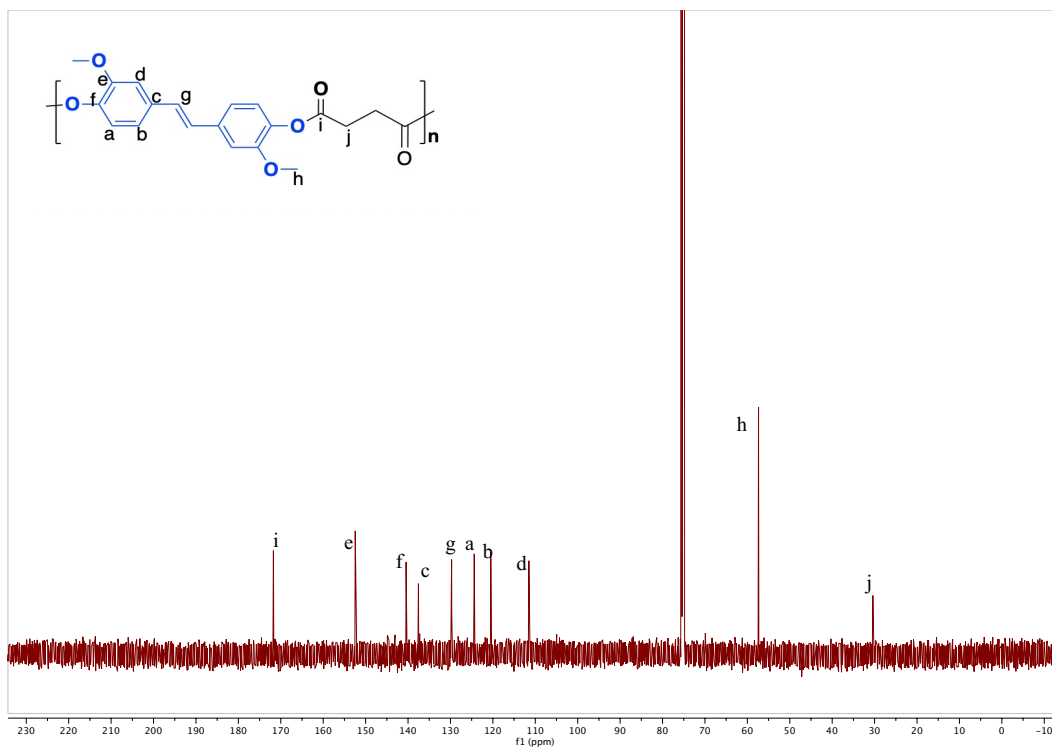
¹³C NMR

Figure A.8. ¹³C NMR Spectrum of PBSU in TCE-*d₂*.
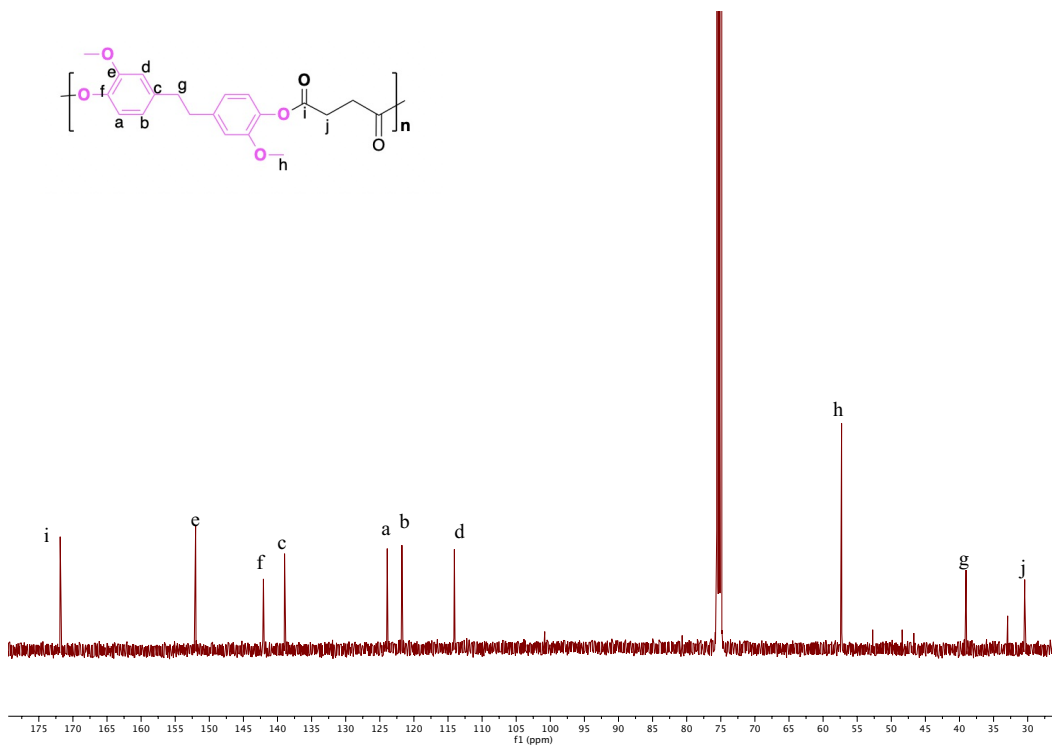
Figure A.9. ¹³C NMR Spectrum of PHBSU in TCE-*d₂*.
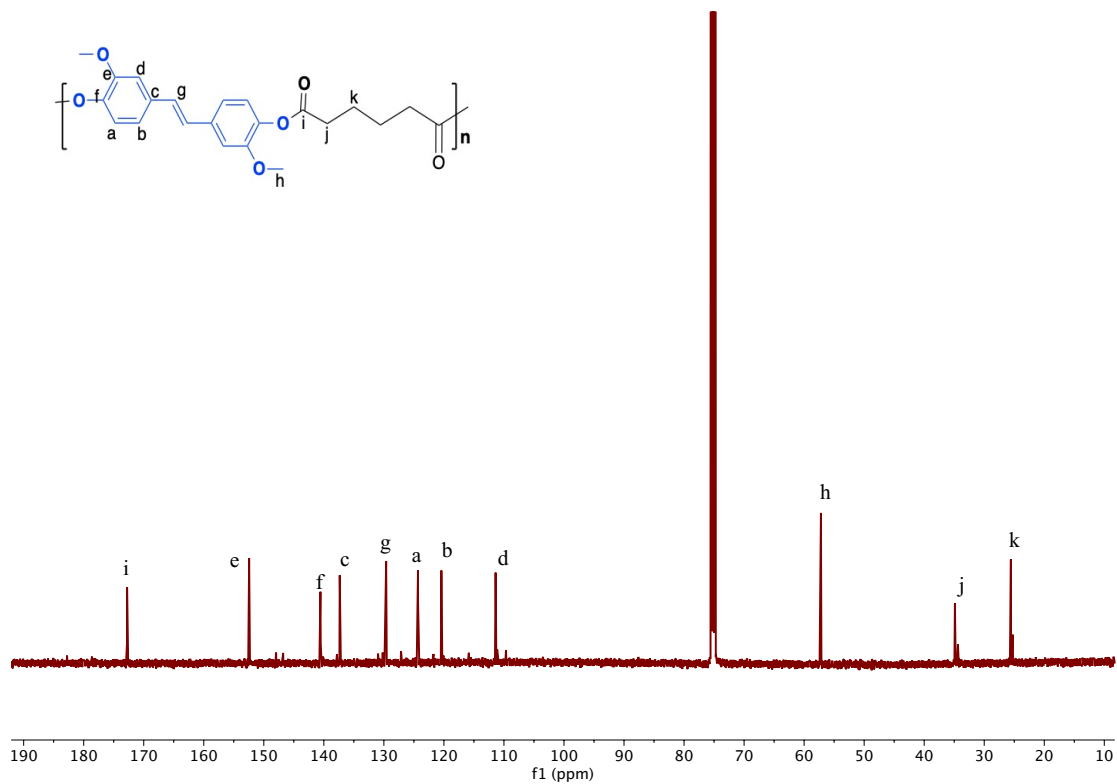
Figure A.10. ^{13}C NMR Spectrum of PBA in TCE-d_2.
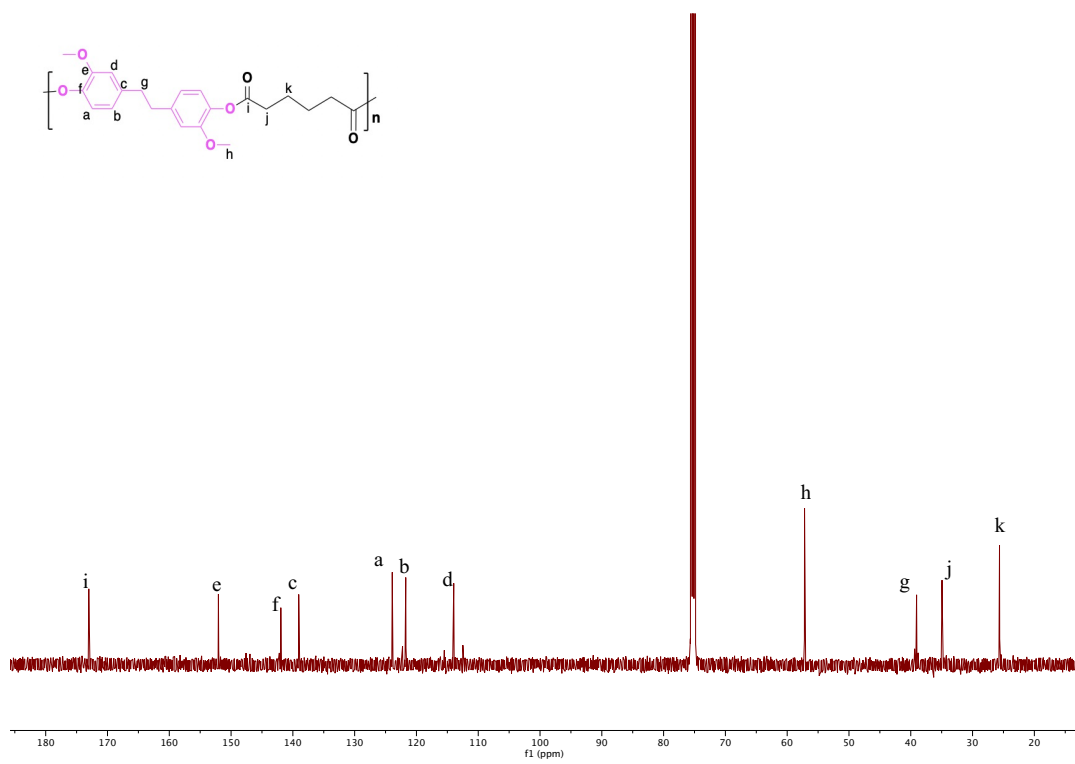
Figure A.11. ^{13}C NMR Spectrum of PHBA in TCE-d_2.
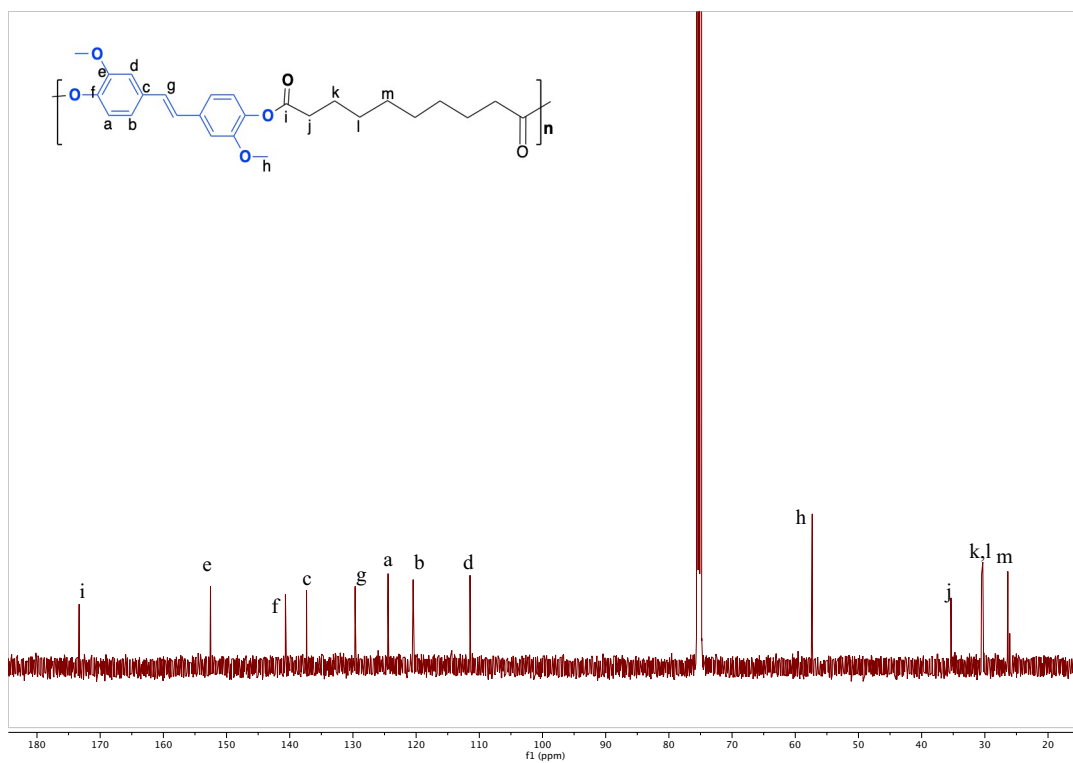
Figure A.12. ^{13}C NMR Spectrum of PBSE in TCE-d_2.
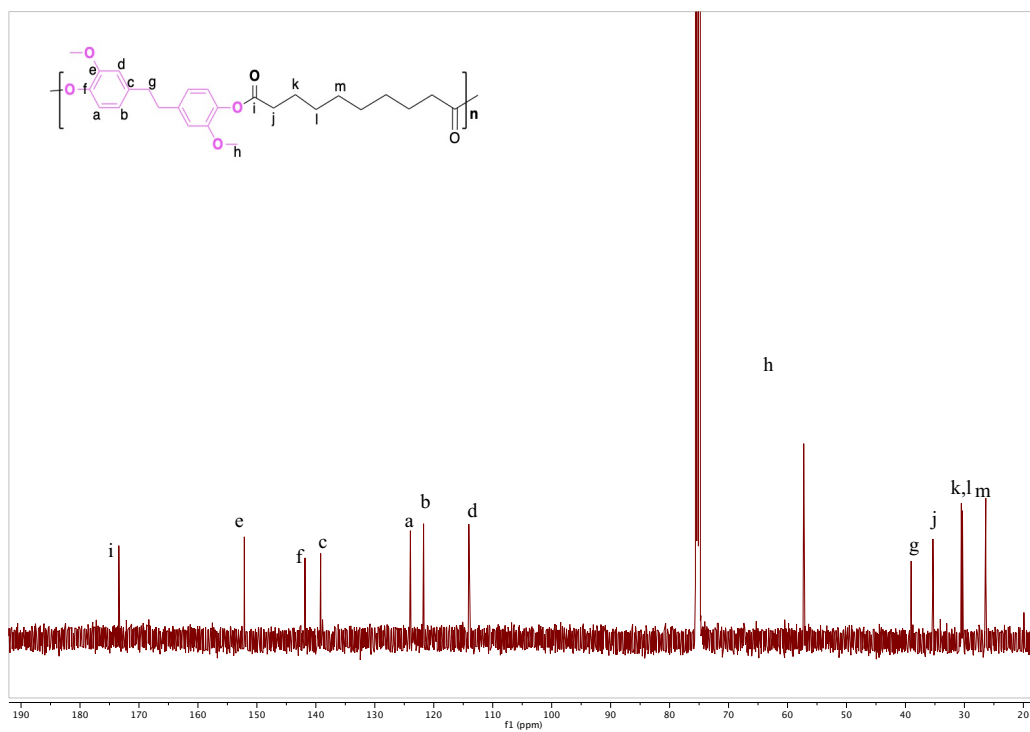
Figure A.13. ^{13}C NMR Spectrum of PBSE in TCE-d_2.
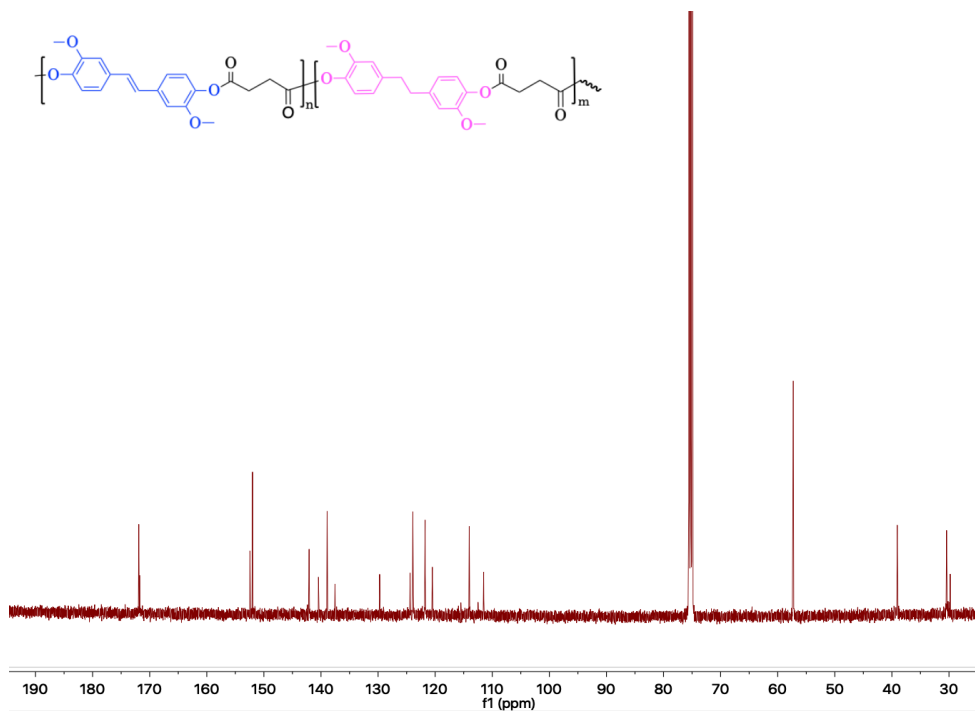
Figure A.14. ^{13}C NMR Spectrum of 2:1 HBIE:BIE + succinyl chloride polyester in TCE-*d₂*.
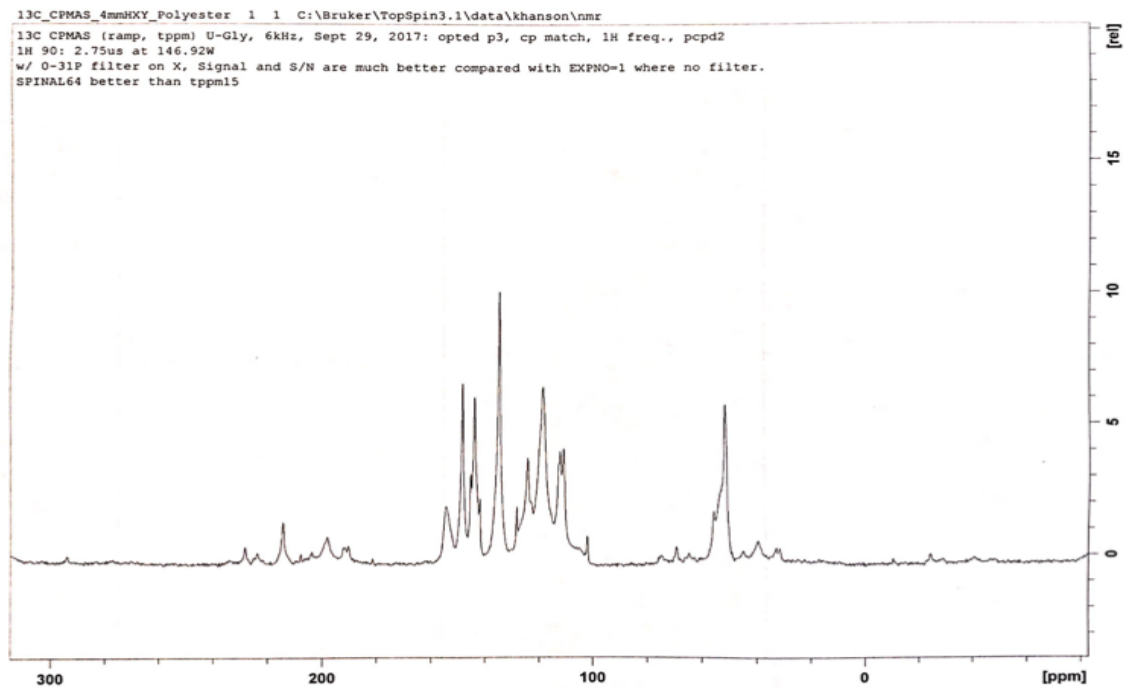
Figure A.15. ^{13}C Solid State NMR Spectrum of PHBF.

FTIR Spectra
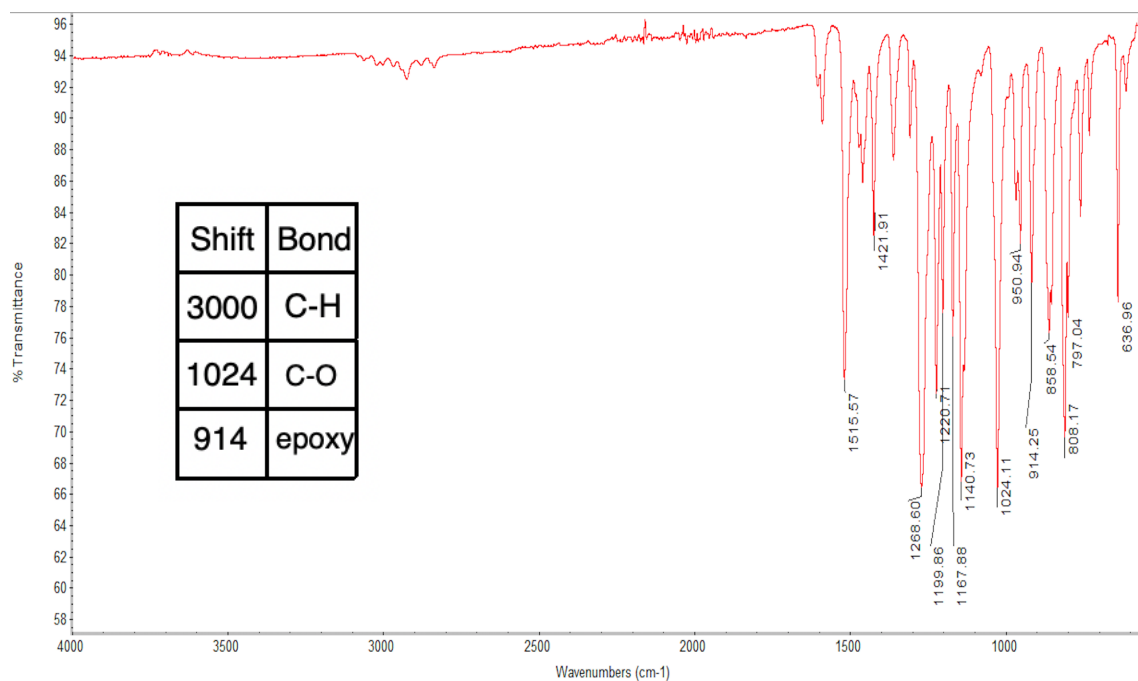
Figure A.16. FTIR spectrum of HBIEE showing epoxide peak at 914 cm^{-1} and absence of carbonyl peak (C=O).
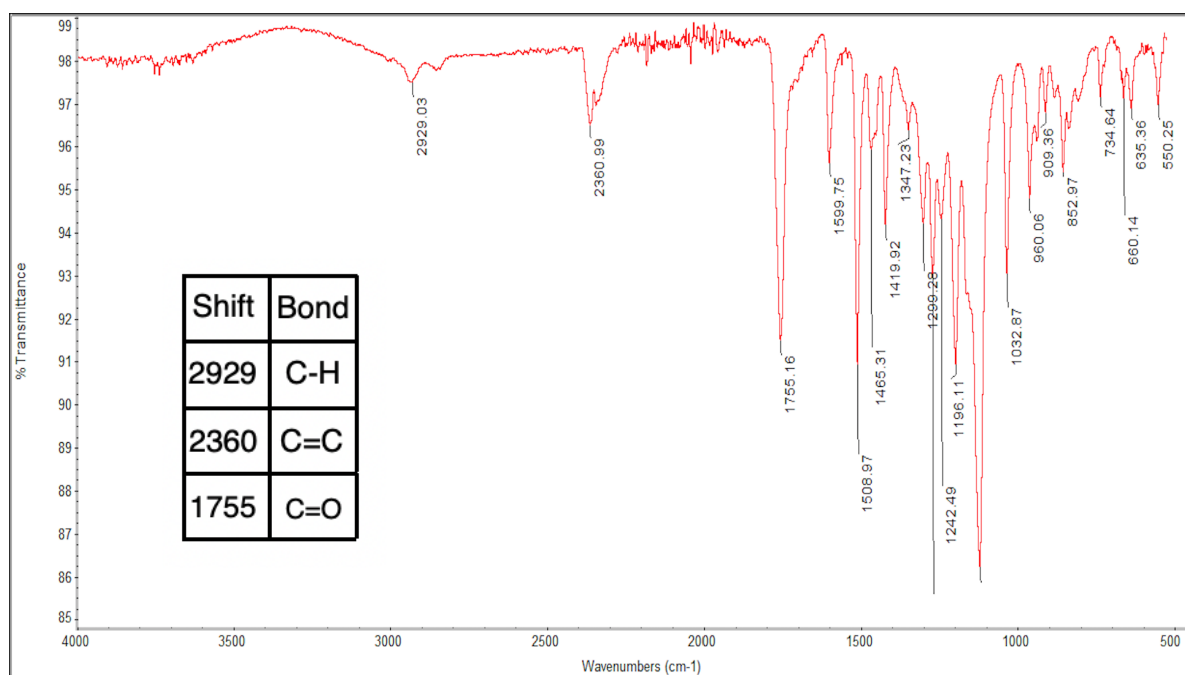
Figure A.17. FTIR spectrum of PBSU.
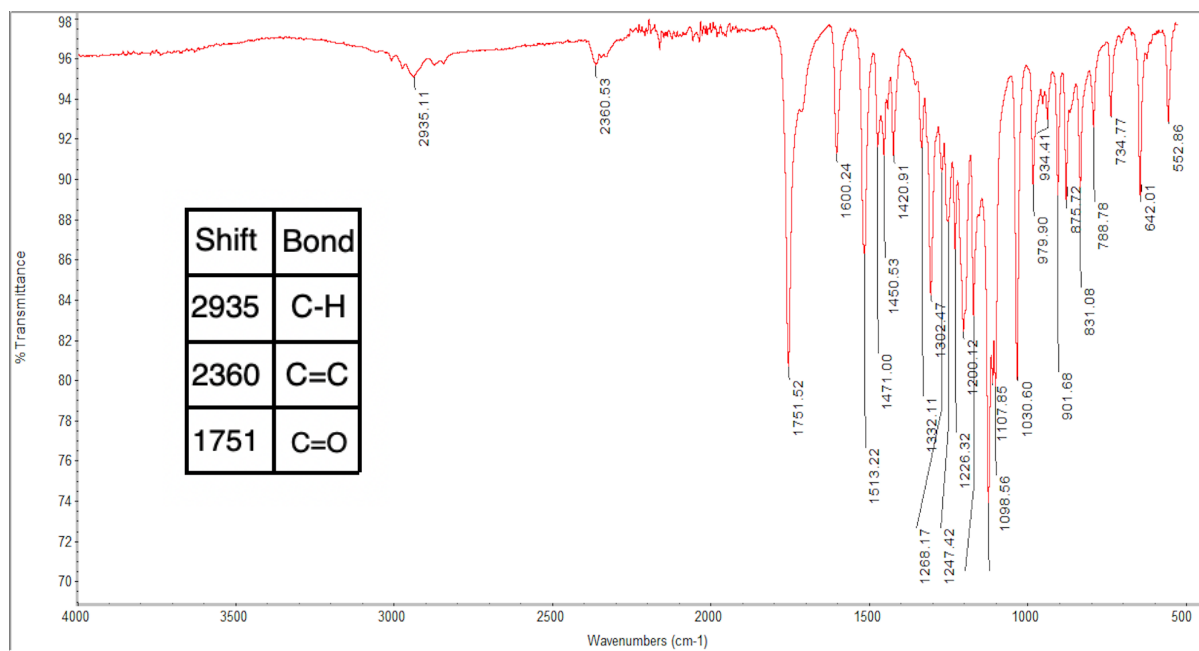
Figure A.18. FTIR spectrum of PHBSU.
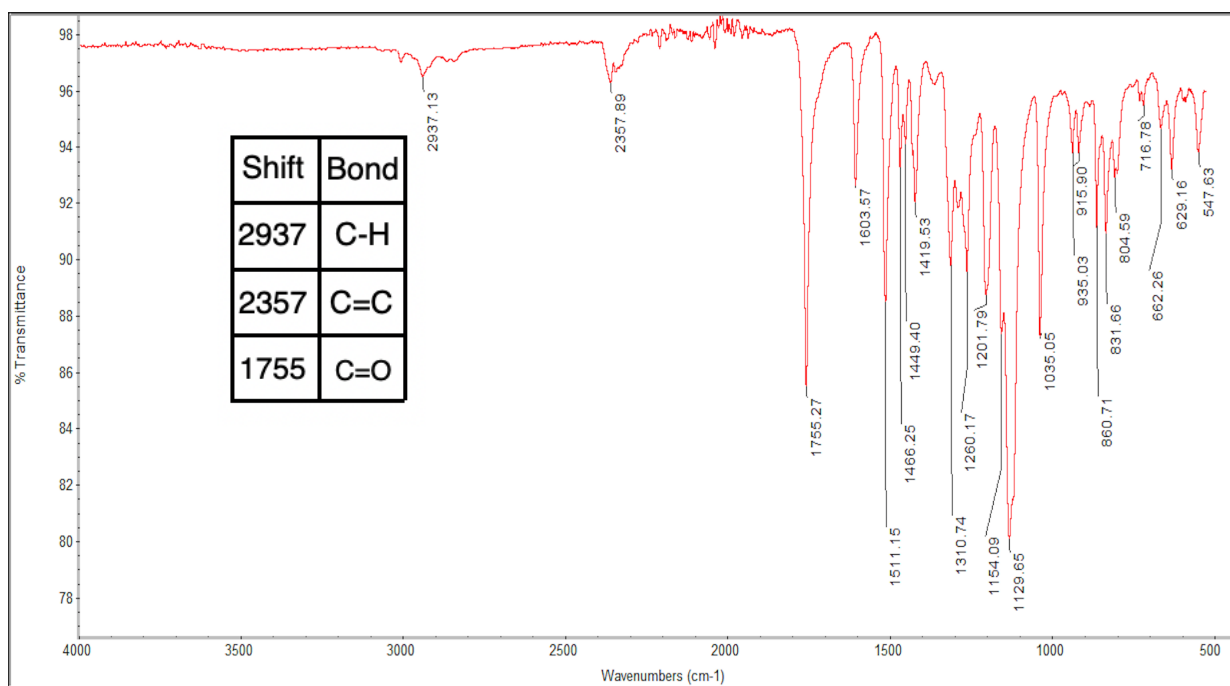
Figure A.19. FTIR spectrum of PBA.
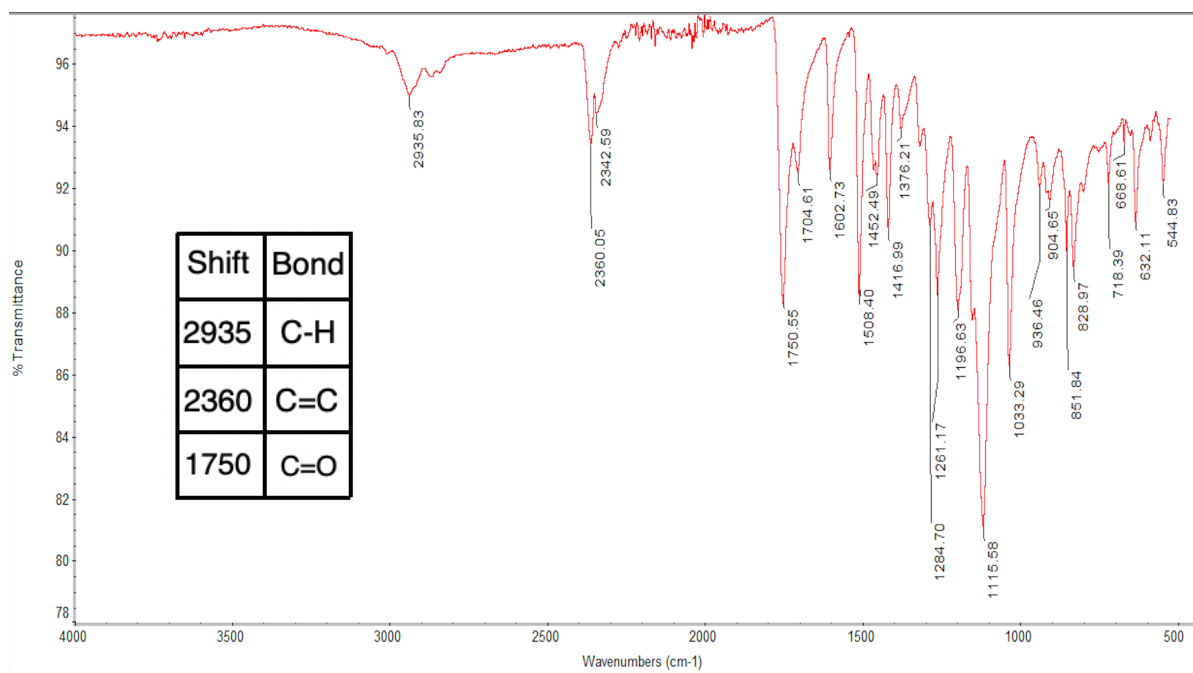
Figure A.20. FTIR spectrum of PHBA.
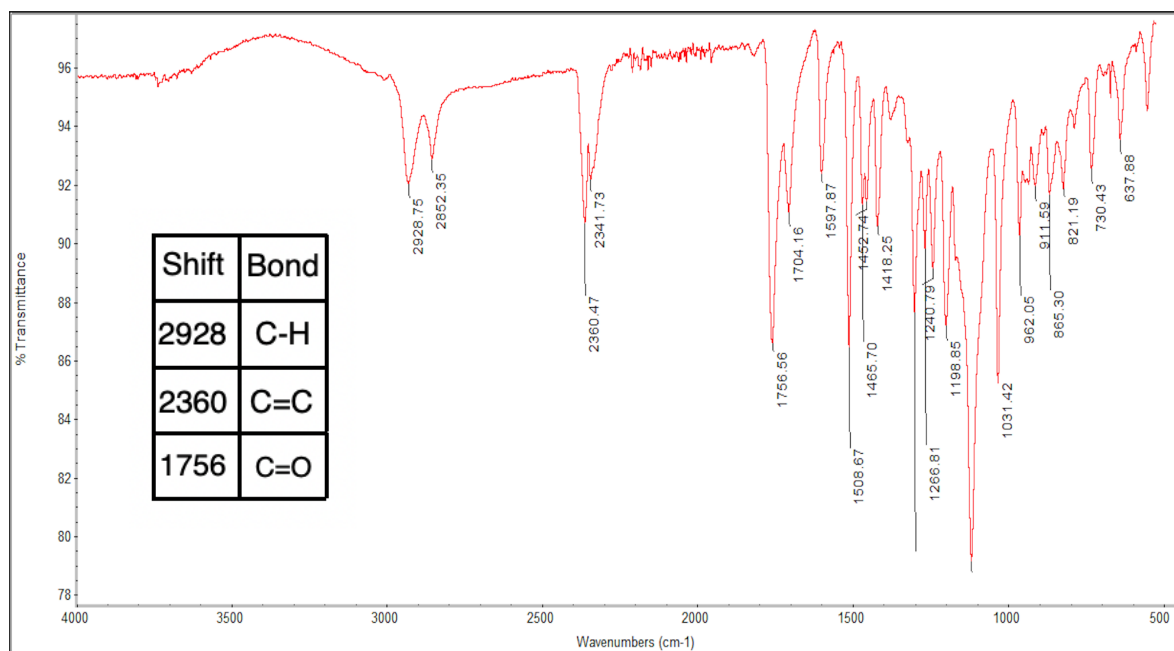
Figure A.21. FTIR spectrum of PBSE.
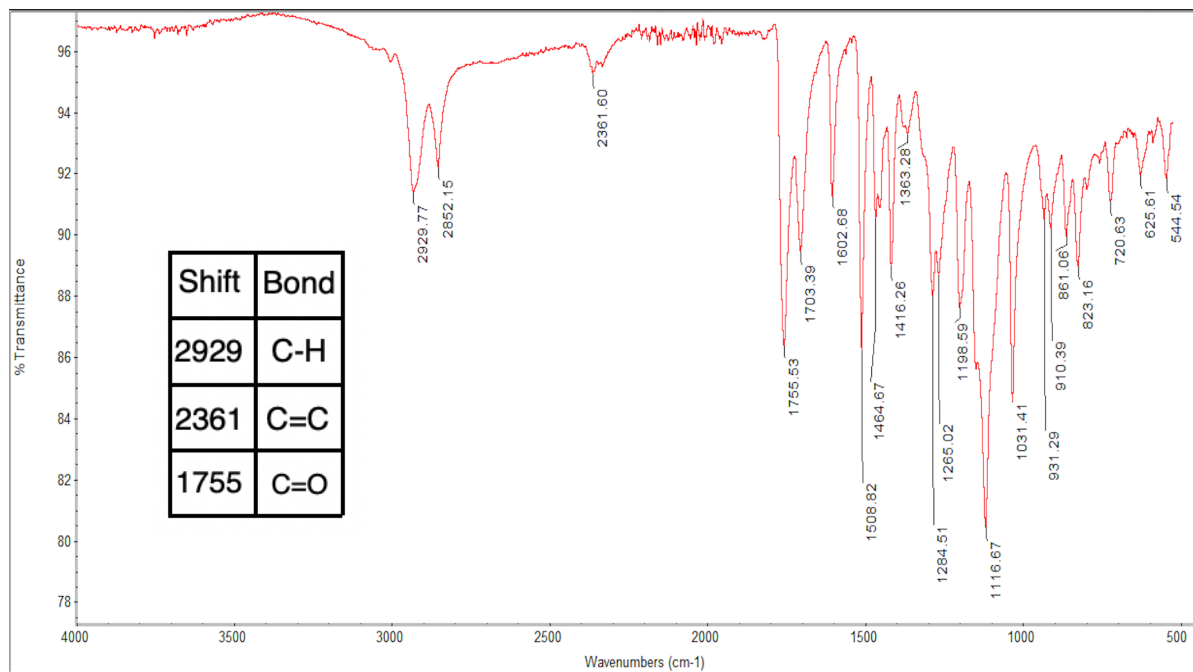
Figure A.22. FTIR spectrum of PHBSE.
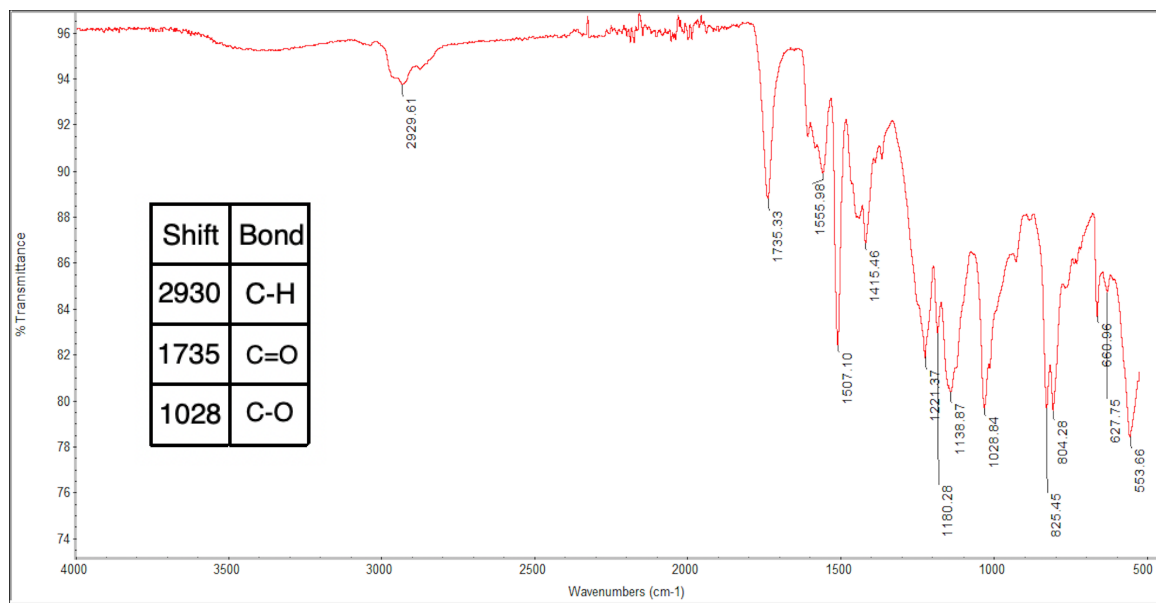
Figure A.23. FTIR spectrum of PHBSU_DGEBA.
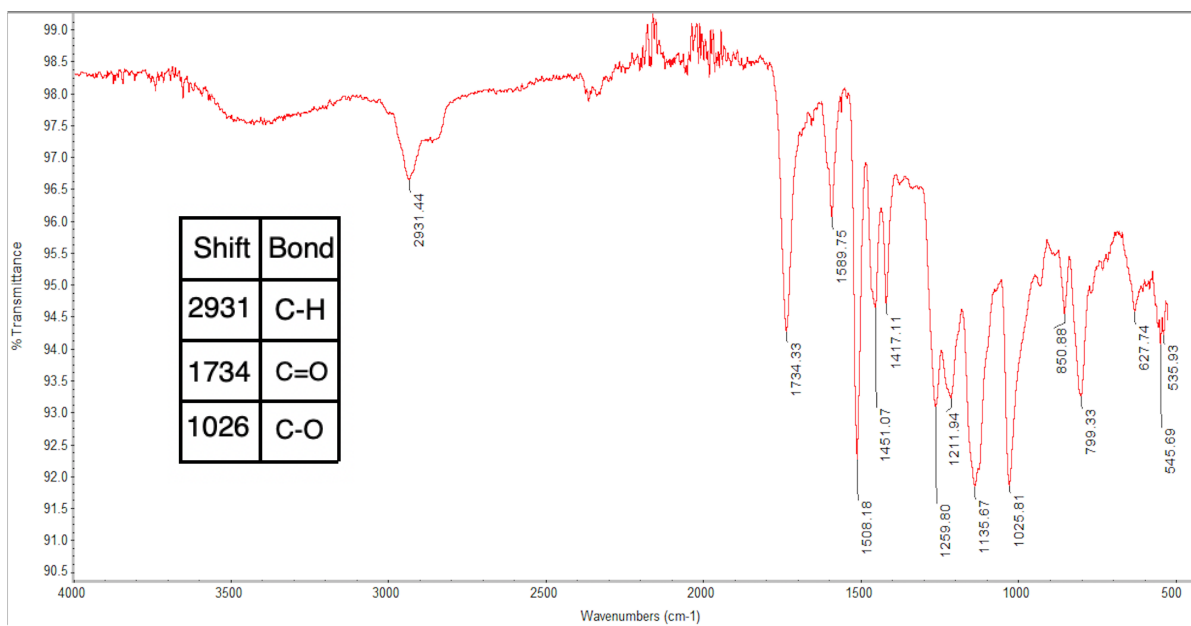
Figure A.24. FTIR spectrum of PHBSU_HBIEE.
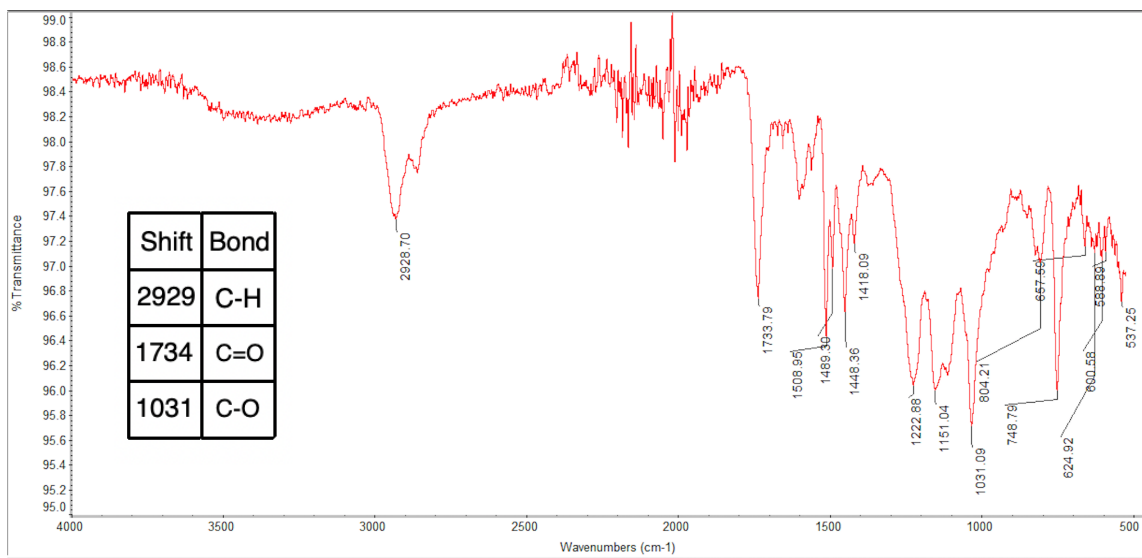
Figure A.25. FTIR spectrum of PHBSU_HP7200.
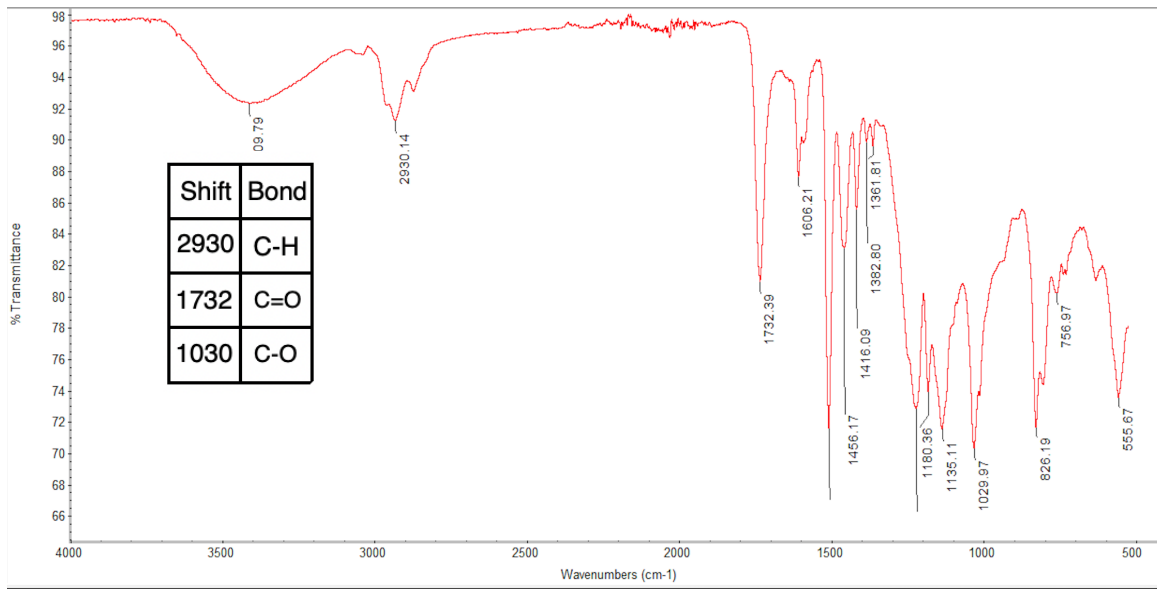
Figure A.26. FTIR spectrum of PHBA_DGEBA.
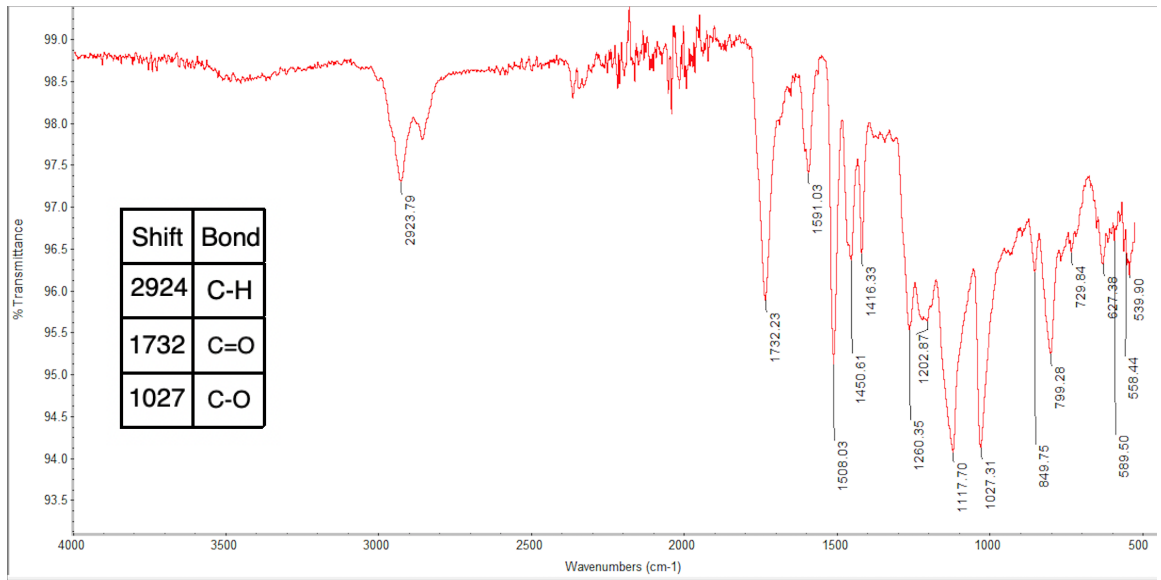
Figure A.27. FTIR spectrum of PHBA_HBIEE.

167
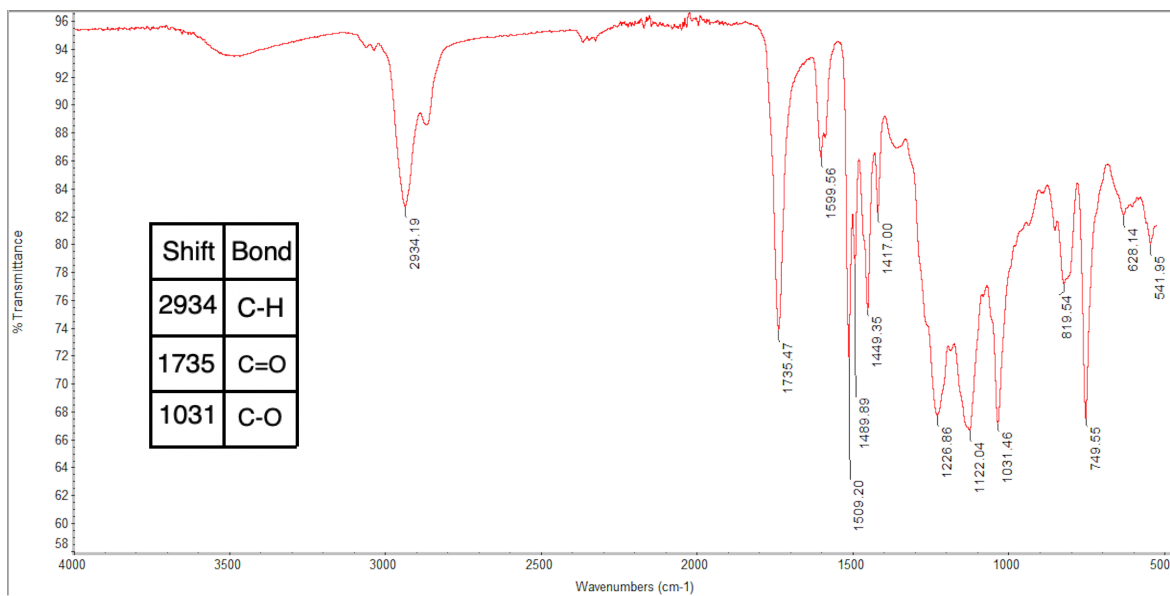
Figure A.28. FTIR spectrum of PHBA_HP7200.
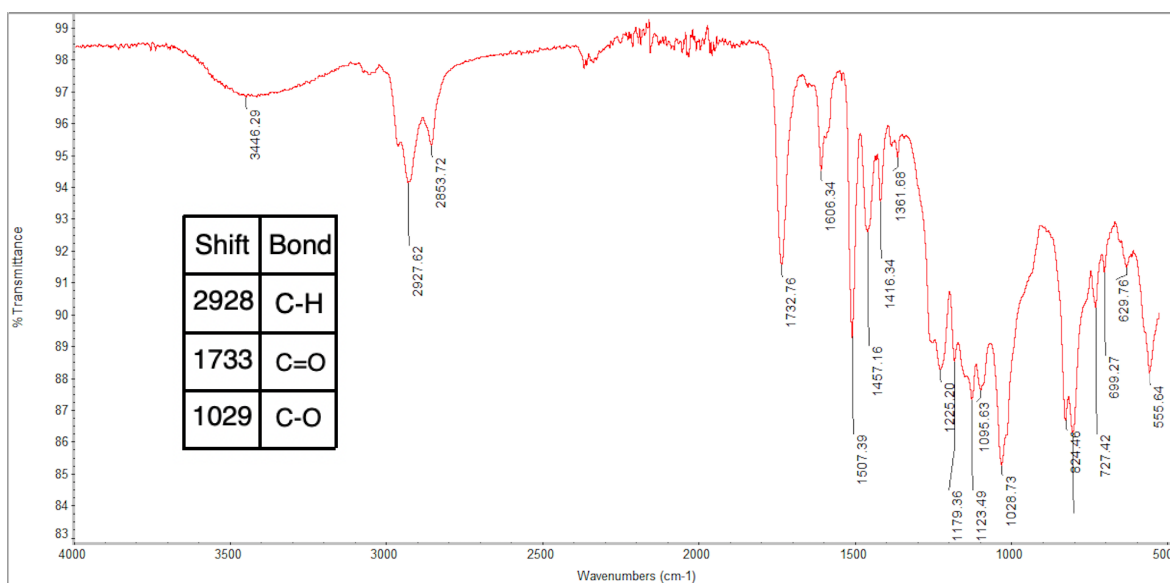
Figure A.29. FTIR spectrum of PHBSE_DGEBA.

168
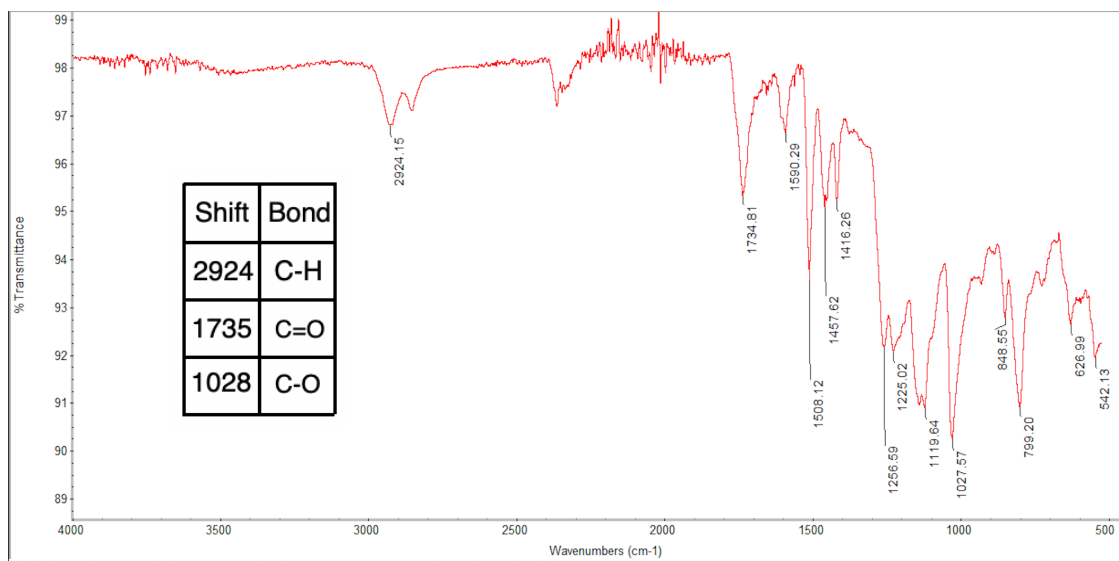
Figure A.30. FTIR spectrum of PHBSE_HBIEE.
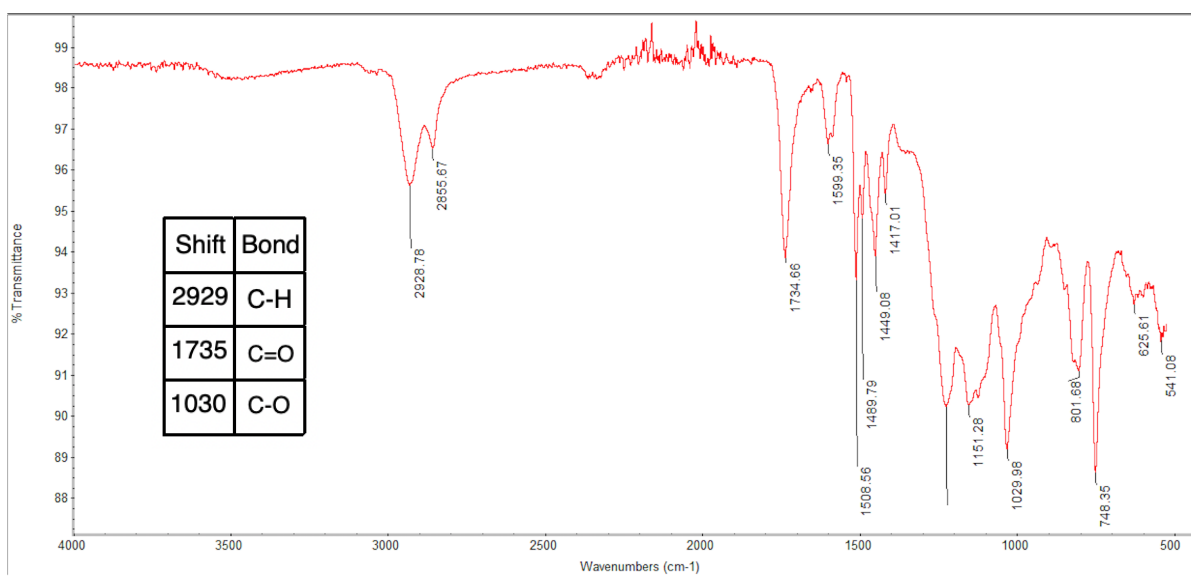
Figure A.31. FTIR spectrum of PHBSE_HP7200.

DSC Traces
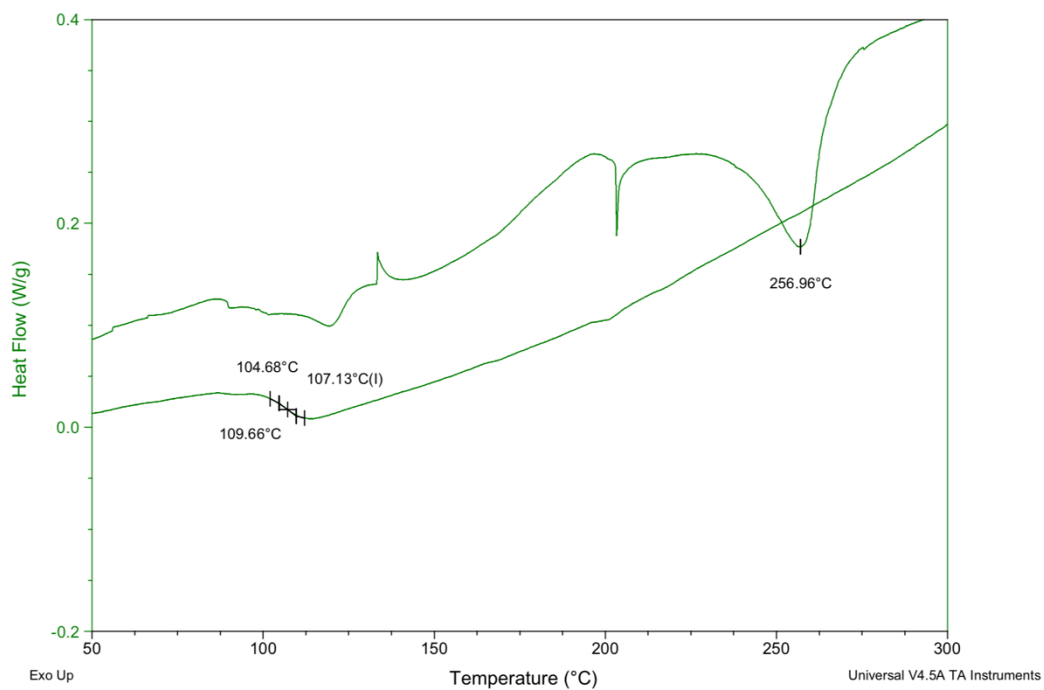
Figure A.32. DSC trace of PBSU showing T_g (107) and T_m (257).
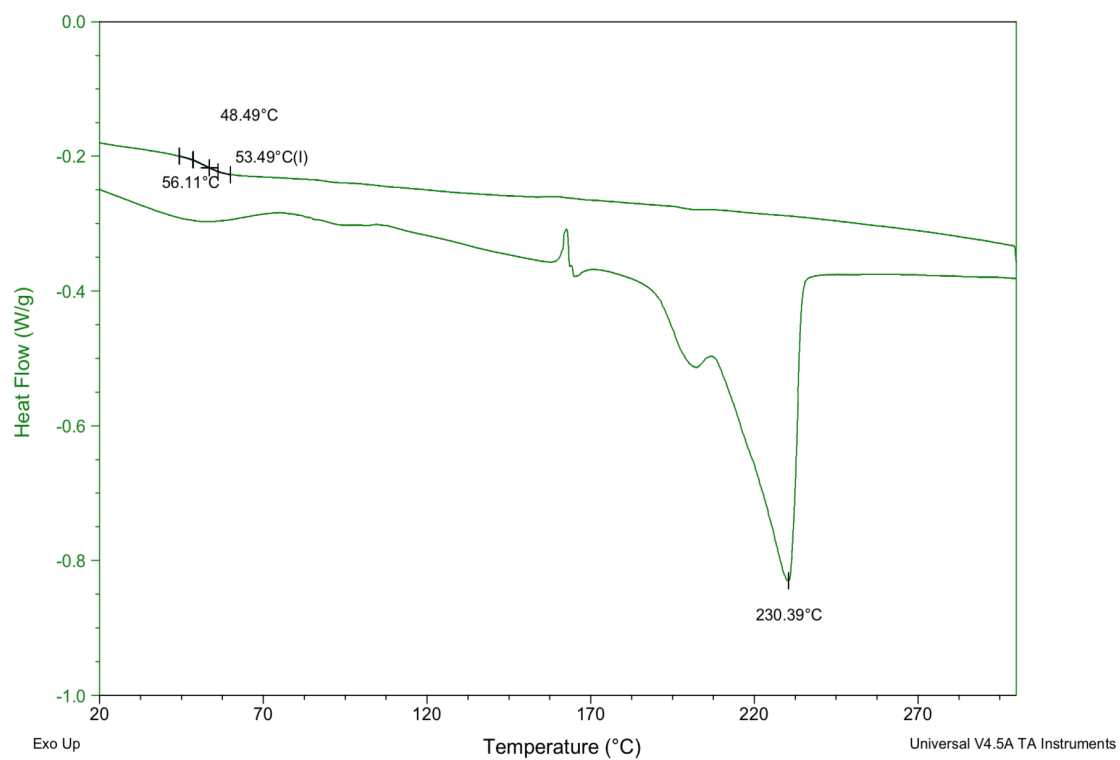
Figure A.33. DSC trace of PBA showing T_g (53) and T_m (230).
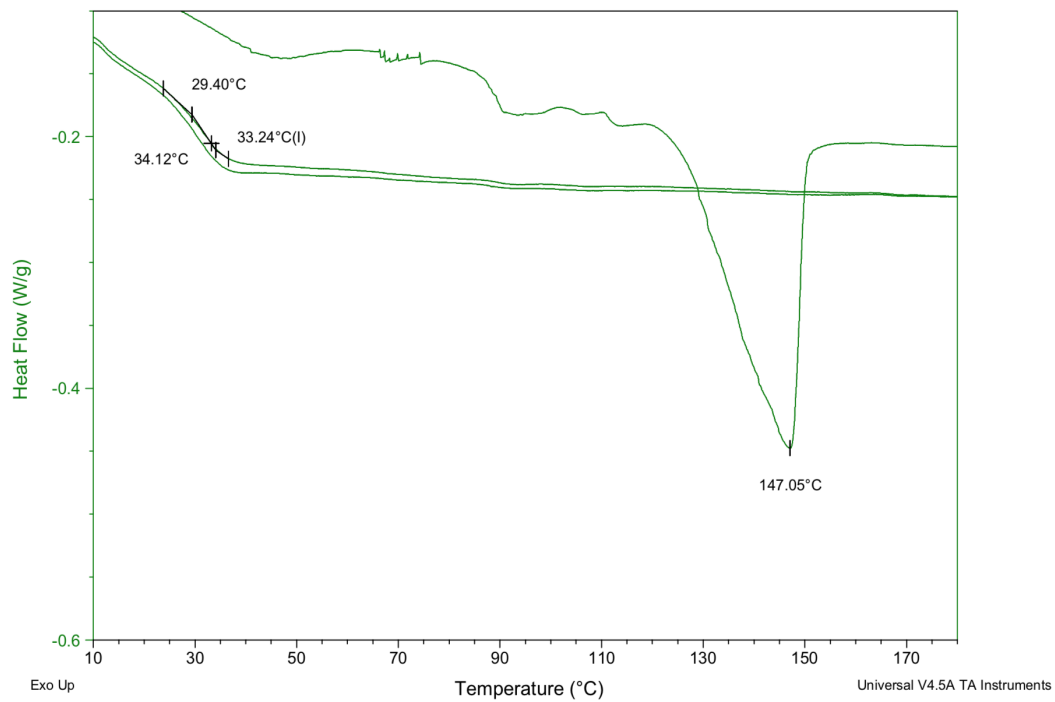
Figure A.34. DSC trace of PBSE showing T_g (33) and T_m (147).
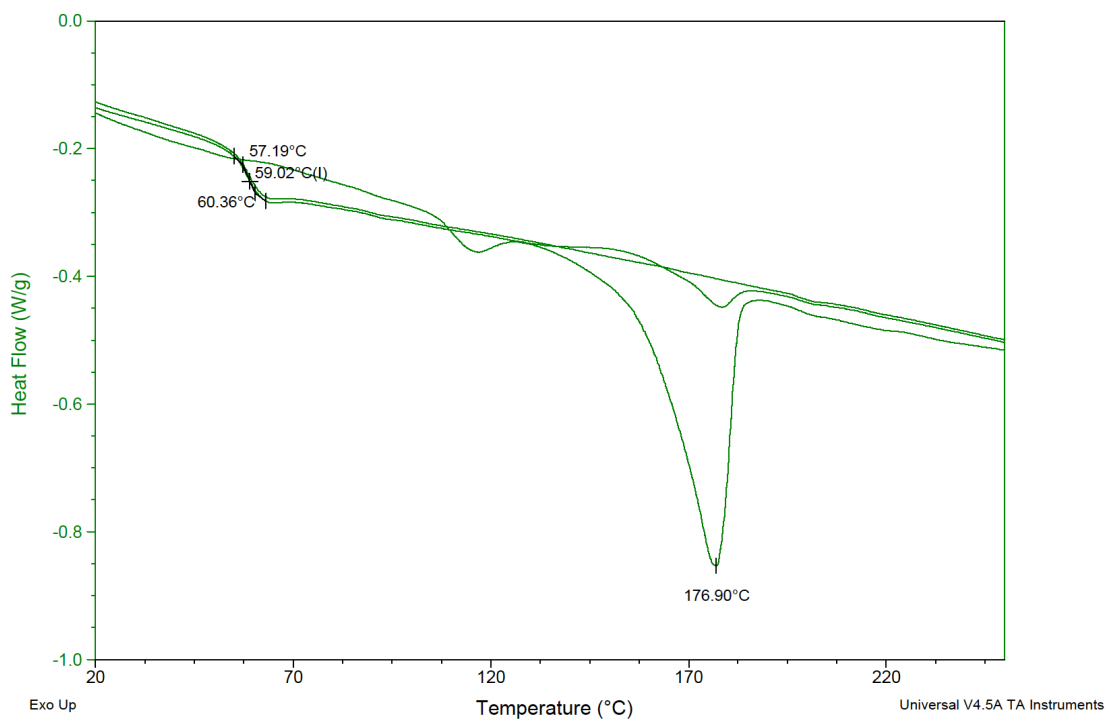
Figure A.35. DSC trace of PHBSU showing T_g (59) and T_m (177).
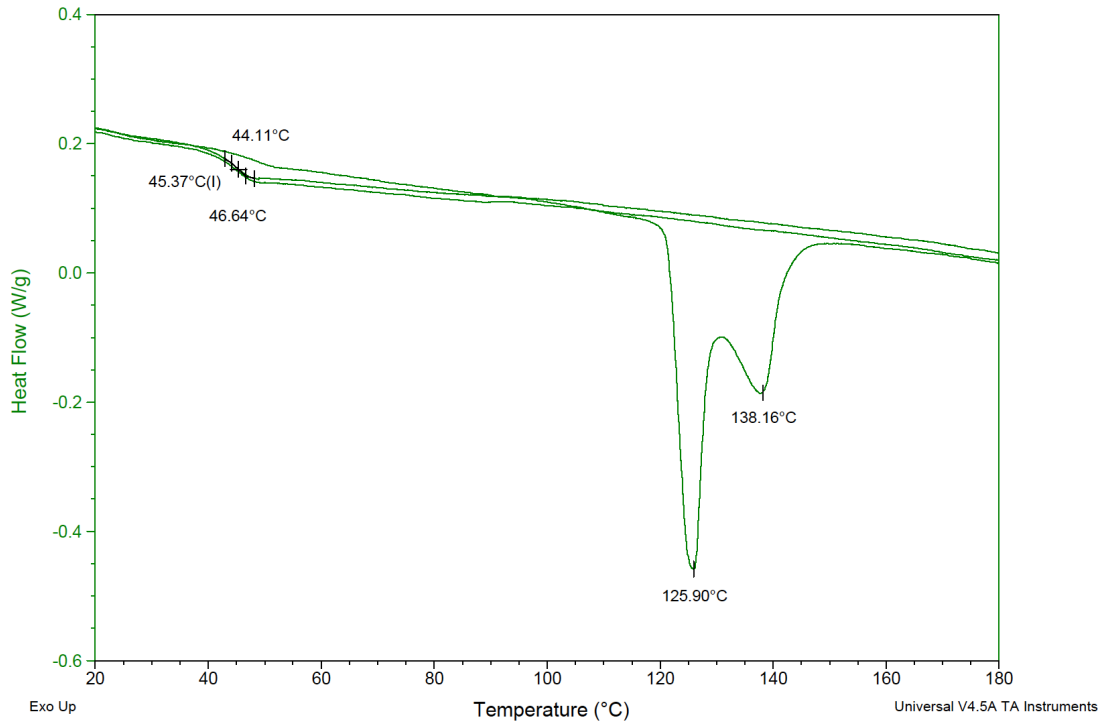
Figure A.36. DSC trace of PHBA showing T_g (45) and T_m (127).
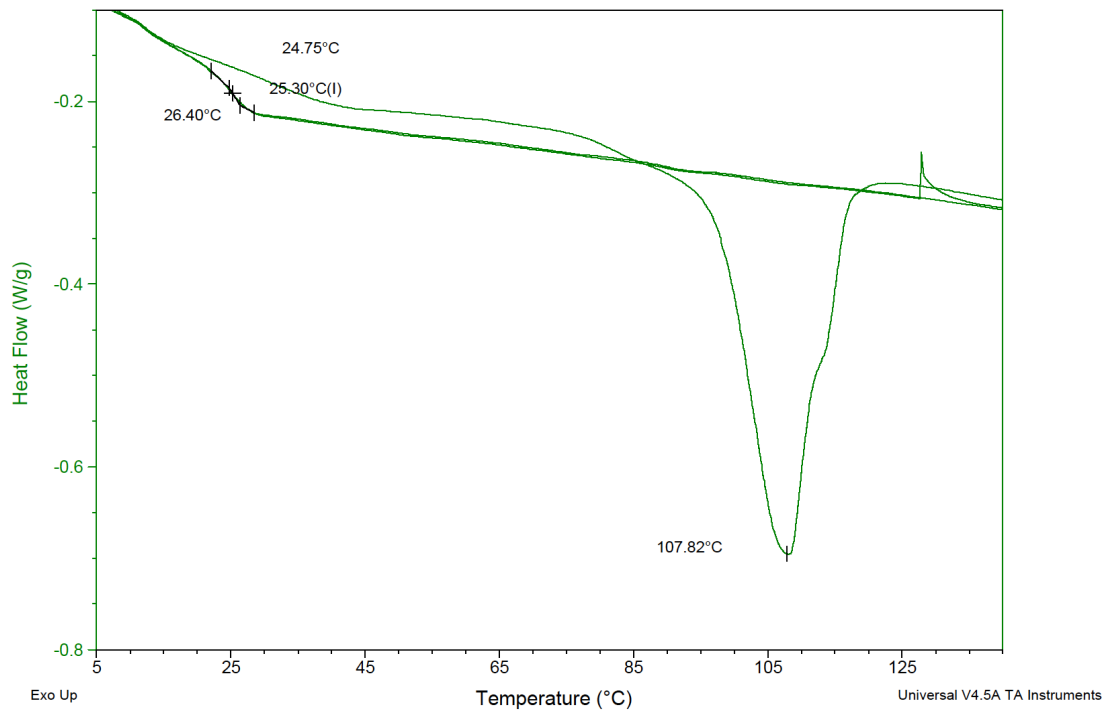
Figure A.37. DSC trace of PHBSE showing T_g (25) and T_m (108).
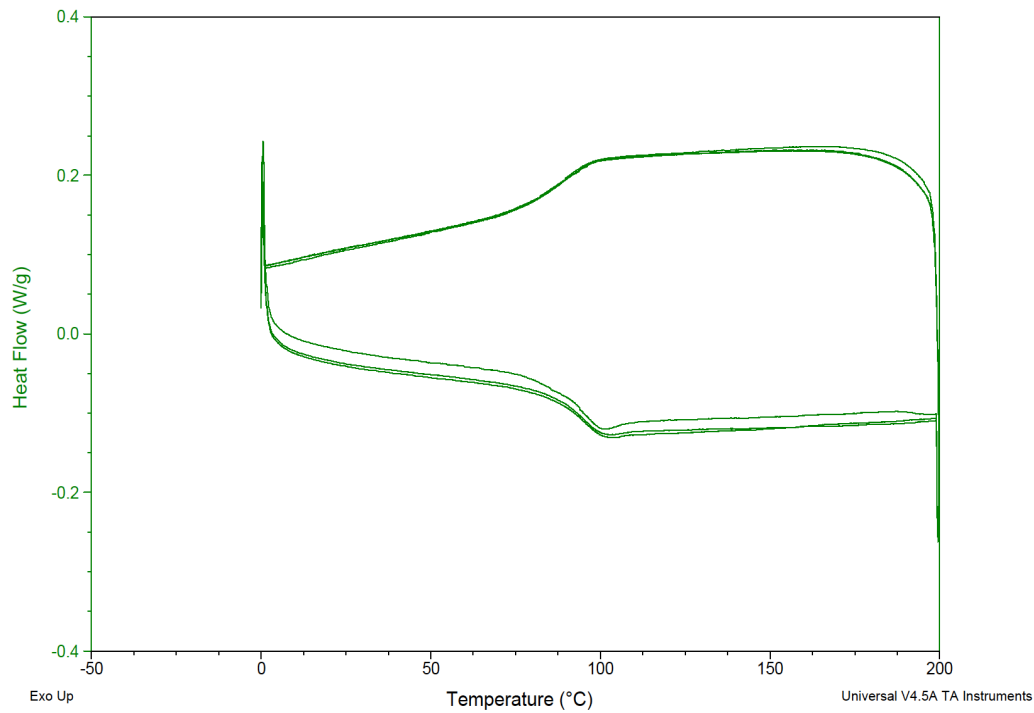
Figure A.38. DSC trace of PHBSU_DGEBA showing T_g (96).
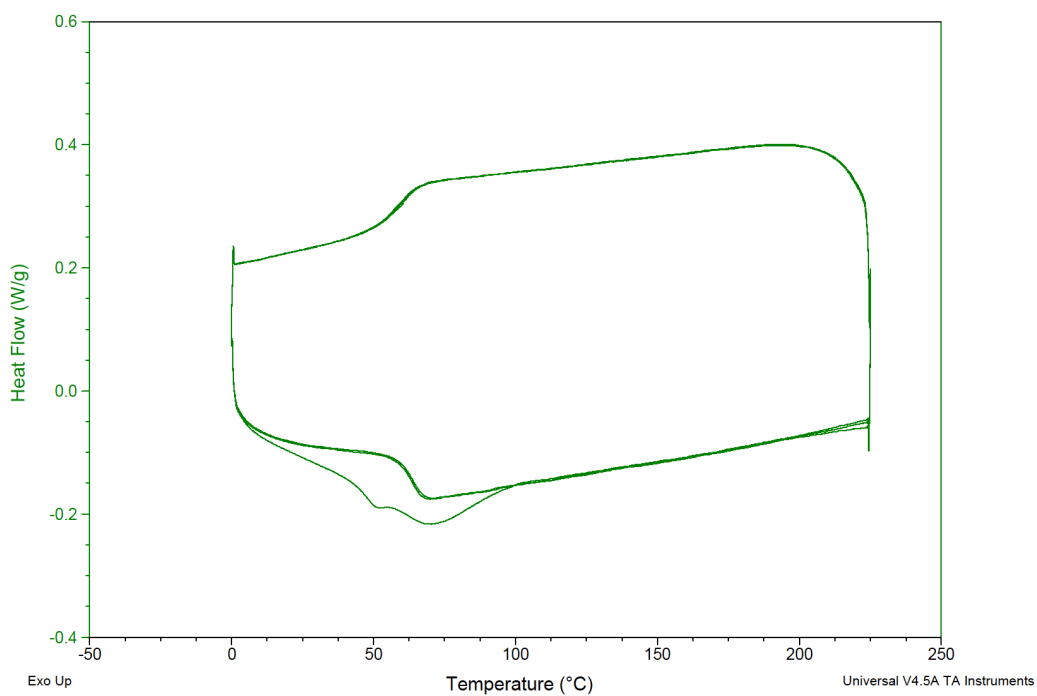
Figure A.39. DSC trace of PHBSU_HBIEE showing T_g (53).
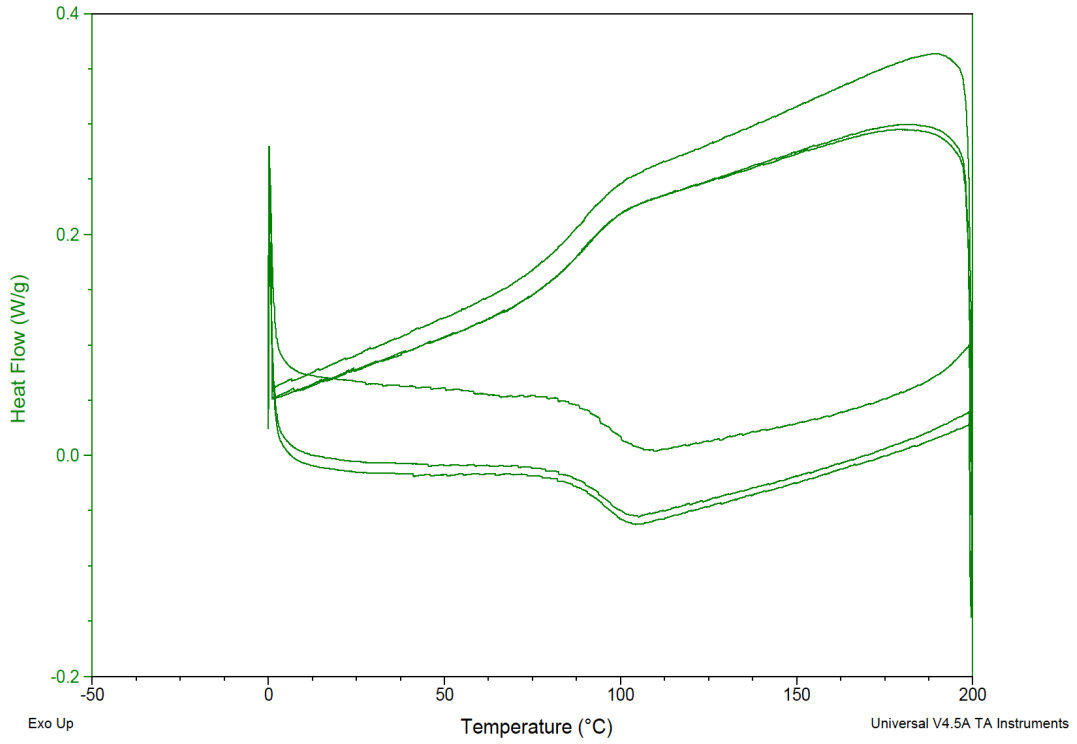
Figure A.40. DSC trace of PHBSU_HP7200 showing T_g (98).
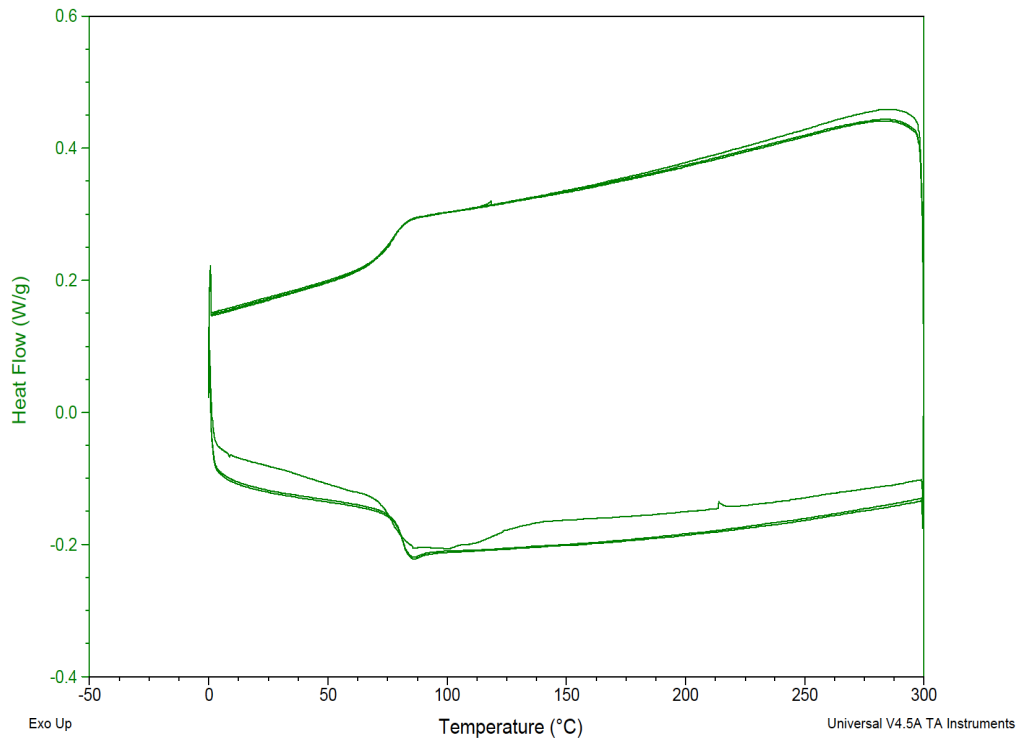
Figure A.41. DSC trace of PHBA_DGEBA showing T_g (80).
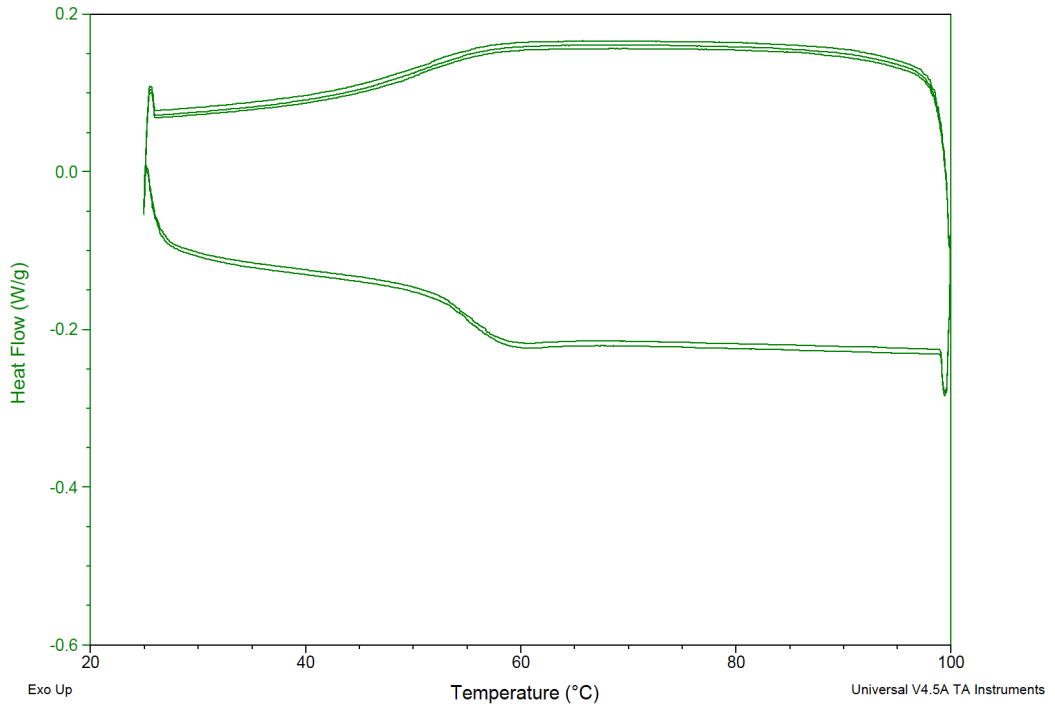
Figure A.42. DSC trace of PHBA_HBIEE showing T_g (54).
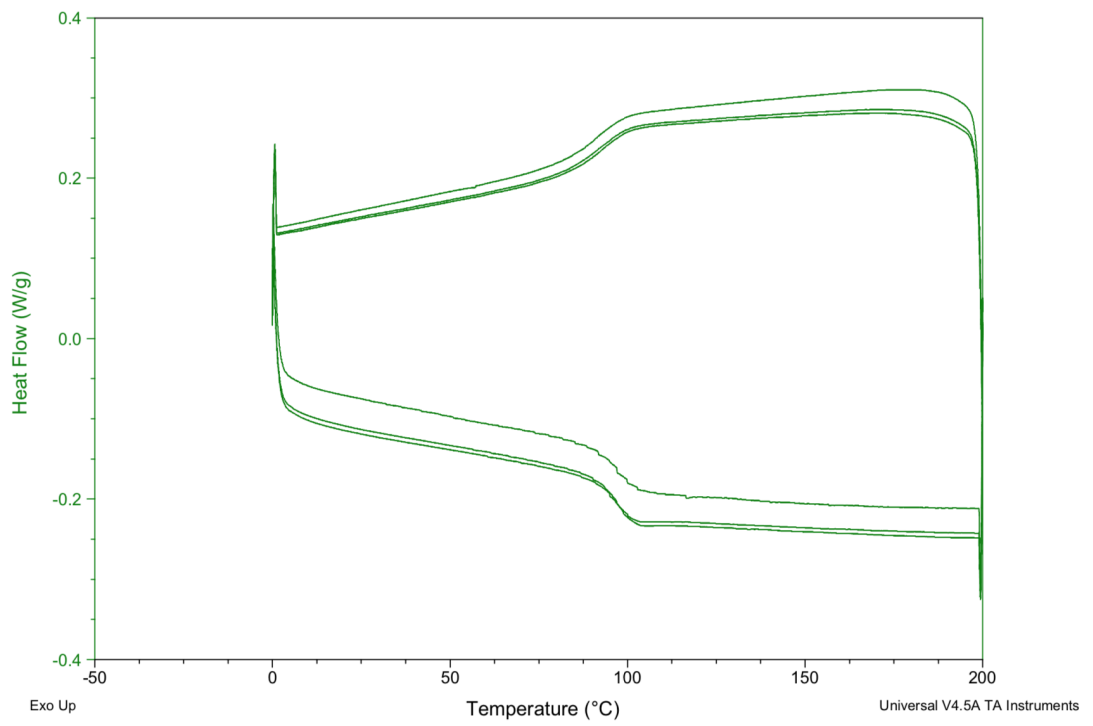
Figure A.43. DSC trace of PHBA_HP7200 showing T_g (102).
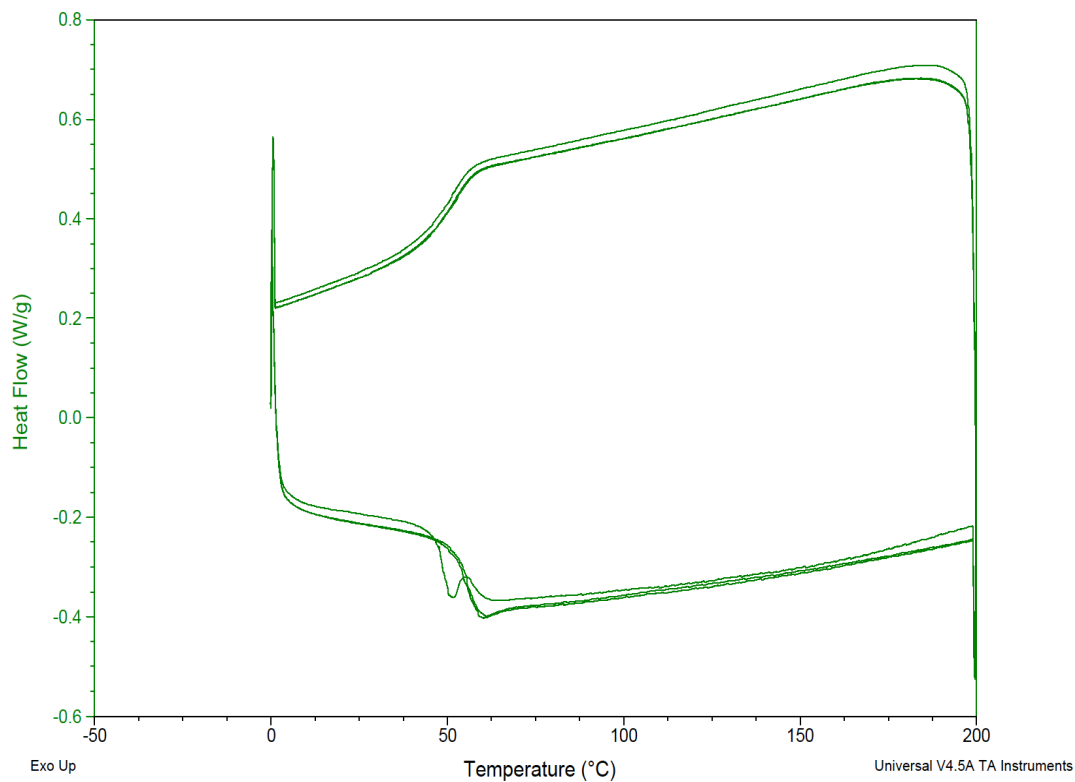
Figure A.44. DSC trace of PHBSE_DGEBA showing T_g (55).
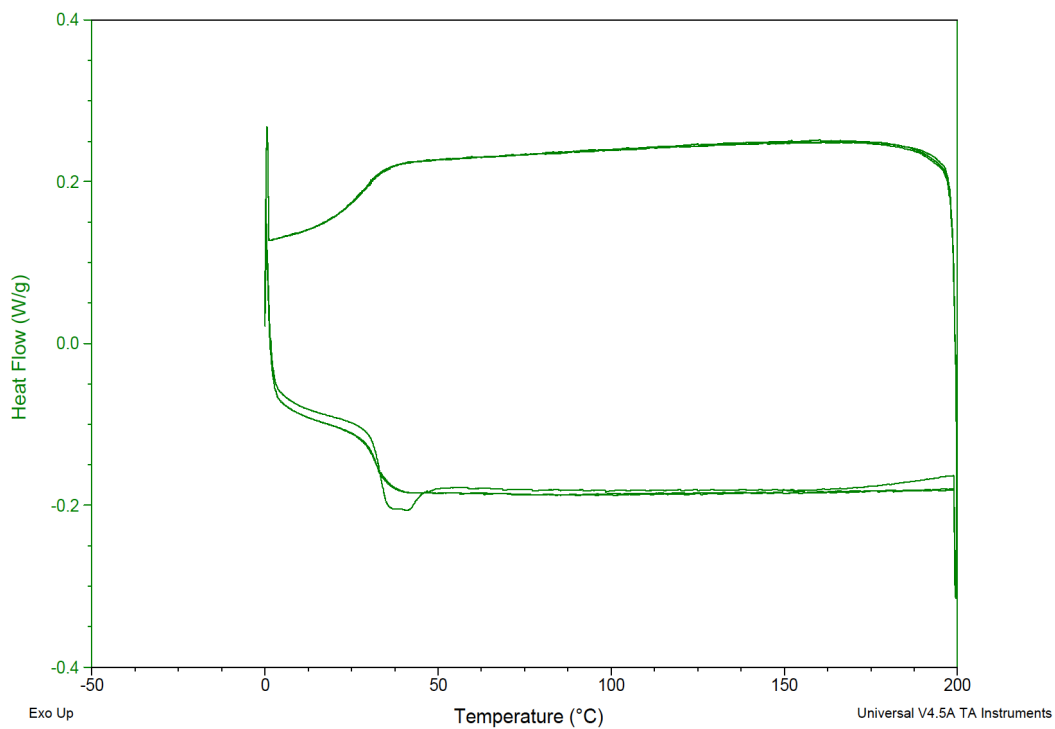
Figure A.45. DSC trace of PHBSE_HBIEE showing T_g (40).
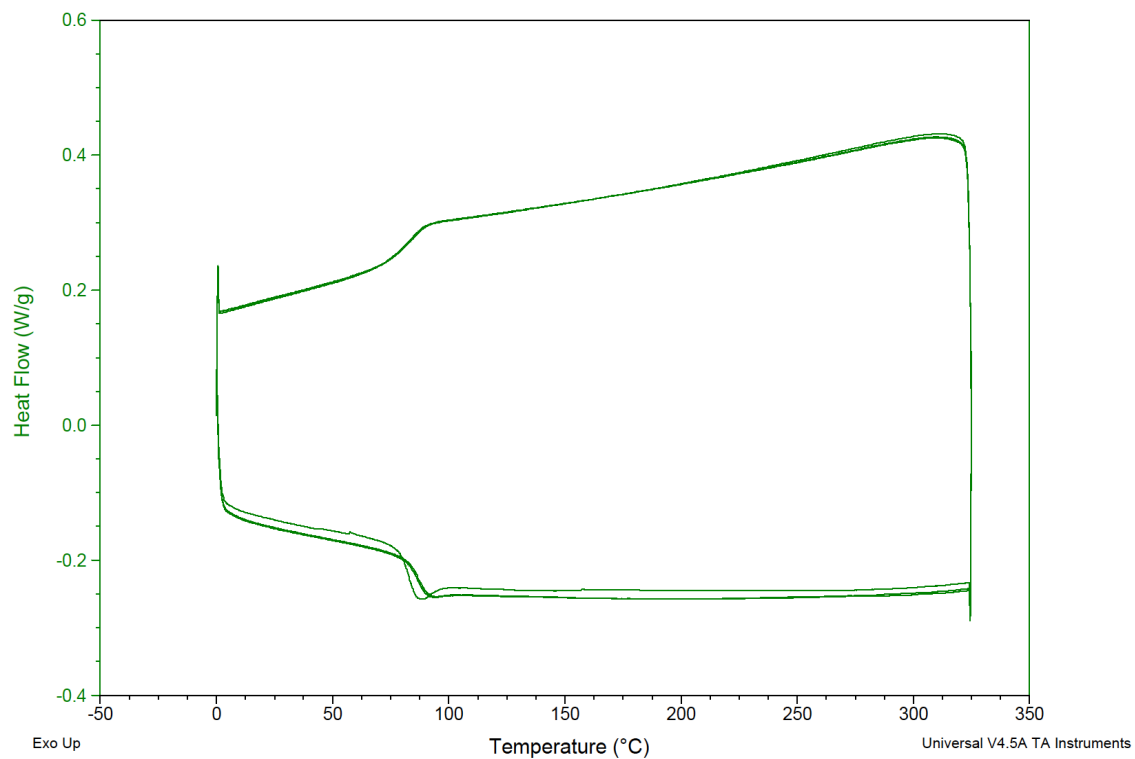
Figure A.46. DSC trace of PHBSE_HP7200 showing T$_g$ (90).

DOSY NMR Diffusion Constant Fitting Curves
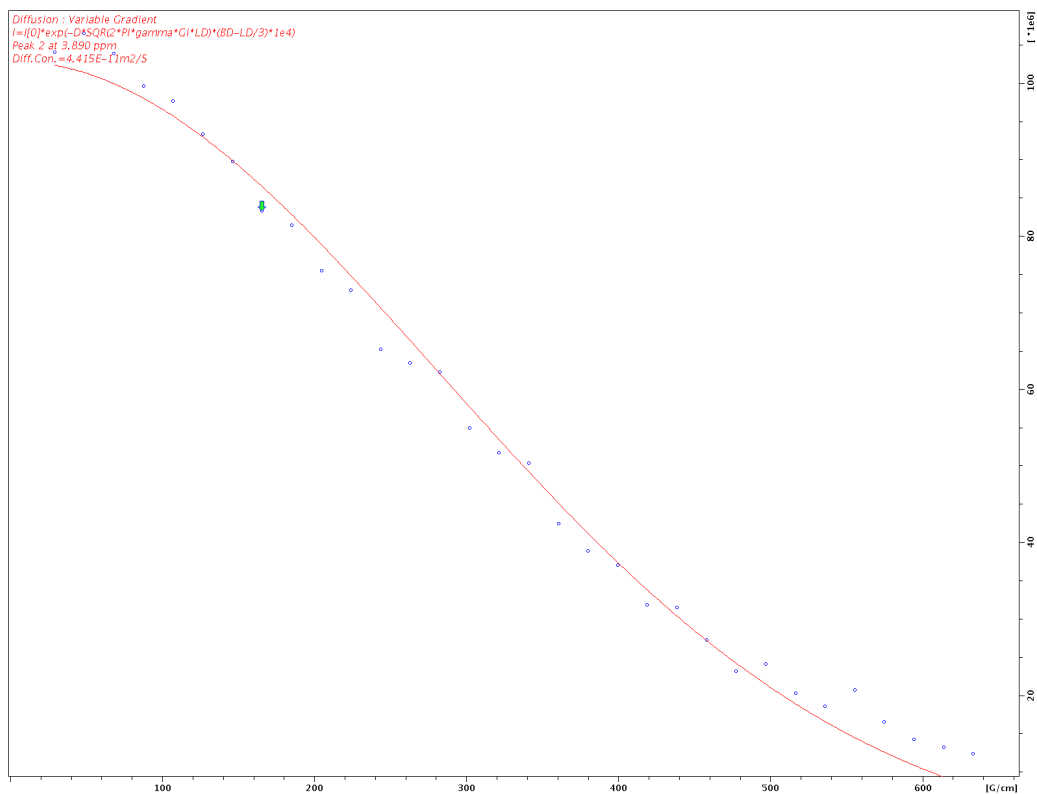
Figure A.47. Diffusion variable gradient fit of PBSU showing diffusion constant, D.
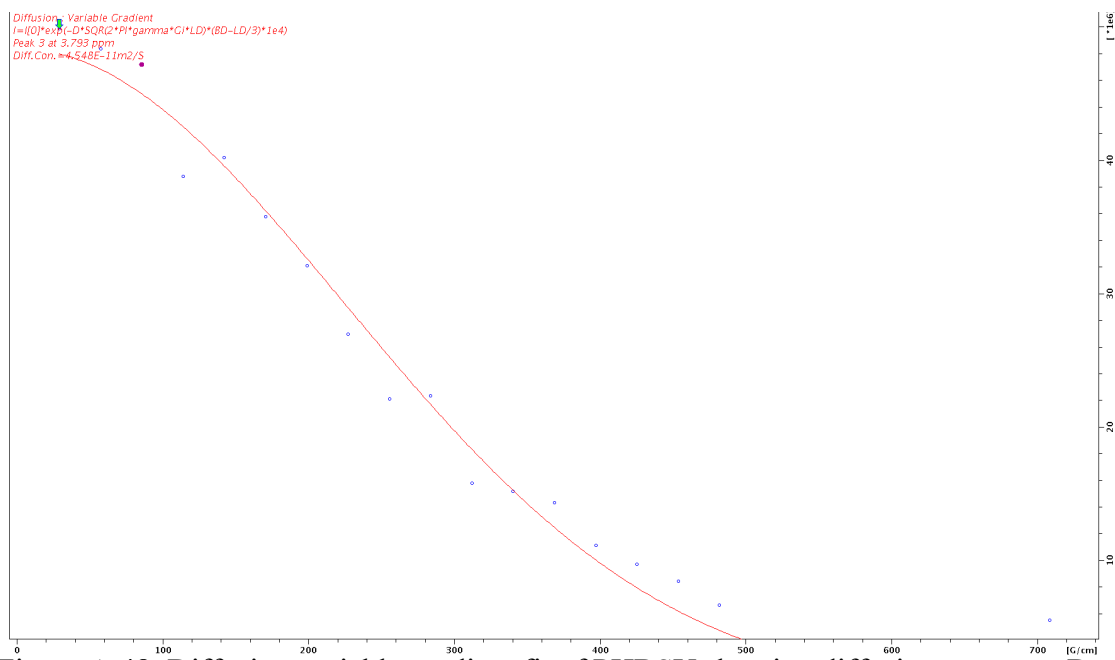
Figure A.48. Diffusion variable gradient fit of PHBSU showing diffusion constant, D.
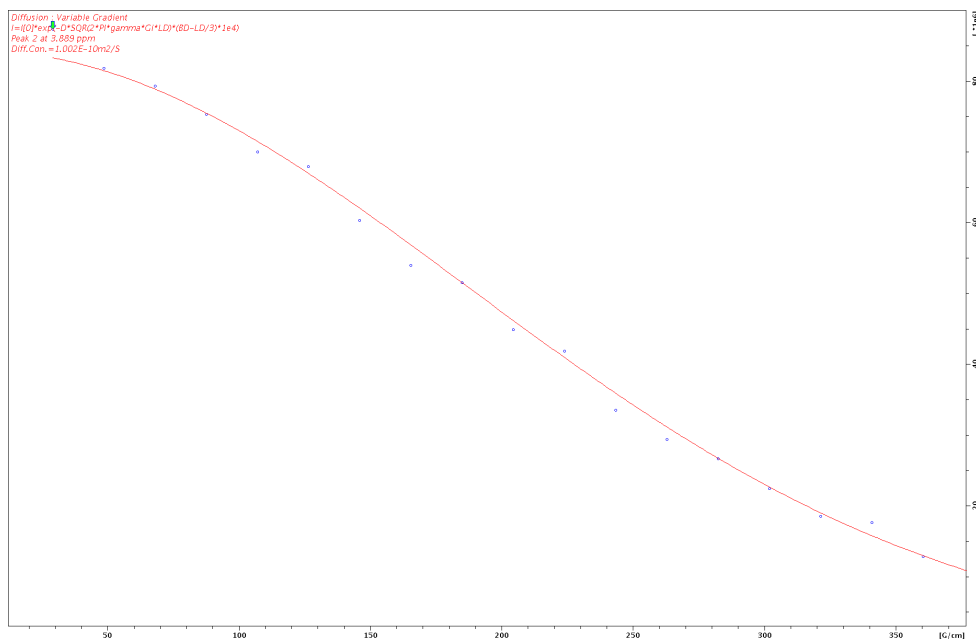
Figure A.49. Diffusion variable gradient fit of PBA showing diffusion constant, D.
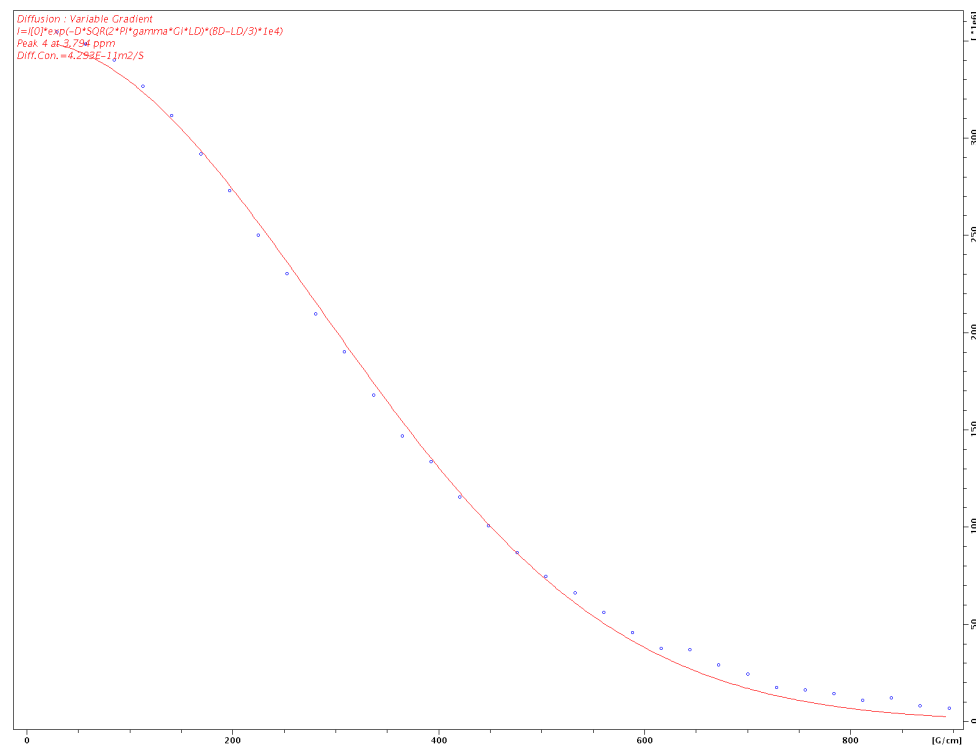
Figure A.50. Diffusion variable gradient fit of PHBA showing diffusion constant, D.
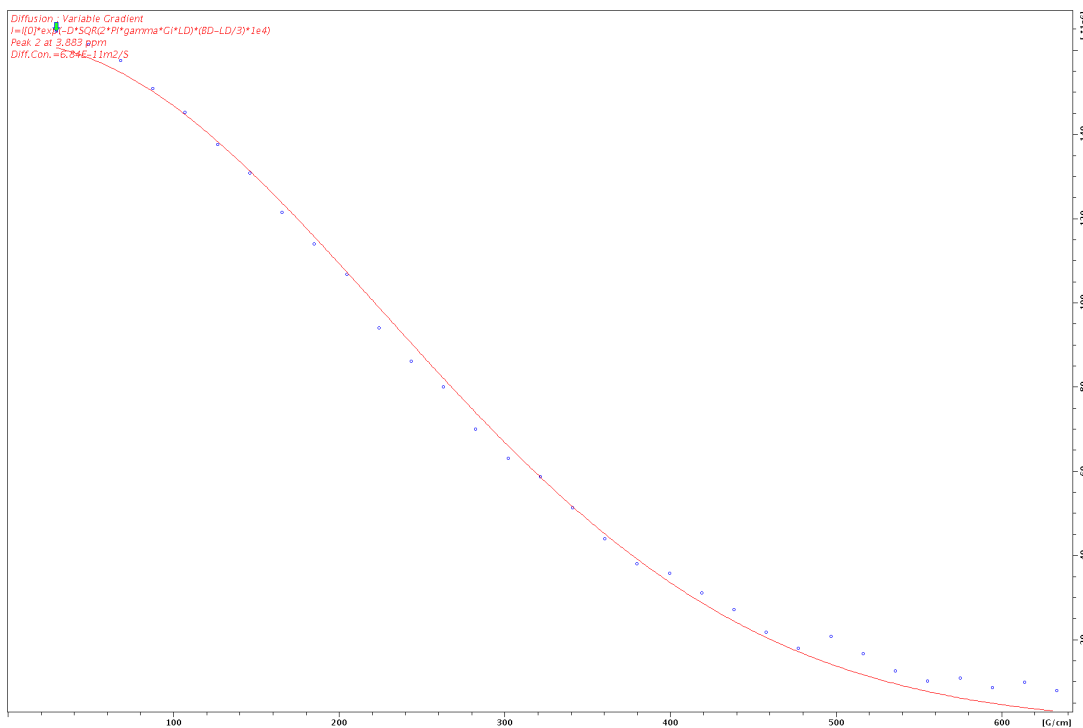
Figure A.51. Diffusion variable gradient fit of PBSE showing diffusion constant, D.
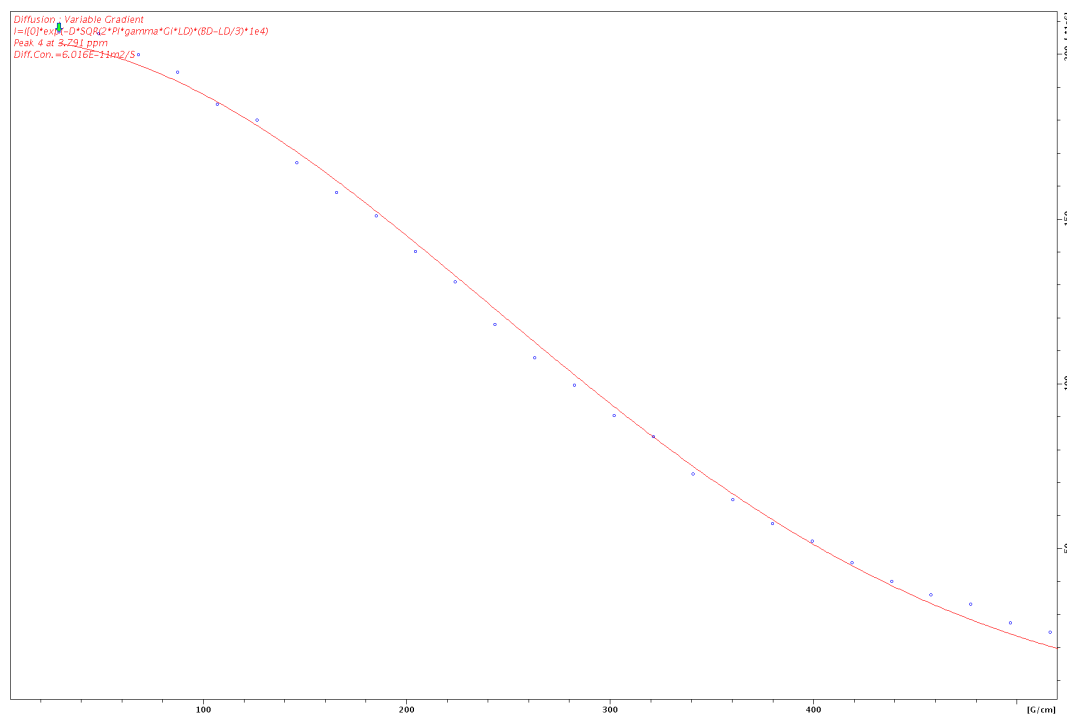
Figure A.52. Diffusion variable gradient fit of PHBSE showing diffusion constant, D.

Mass Spec of Polyesters
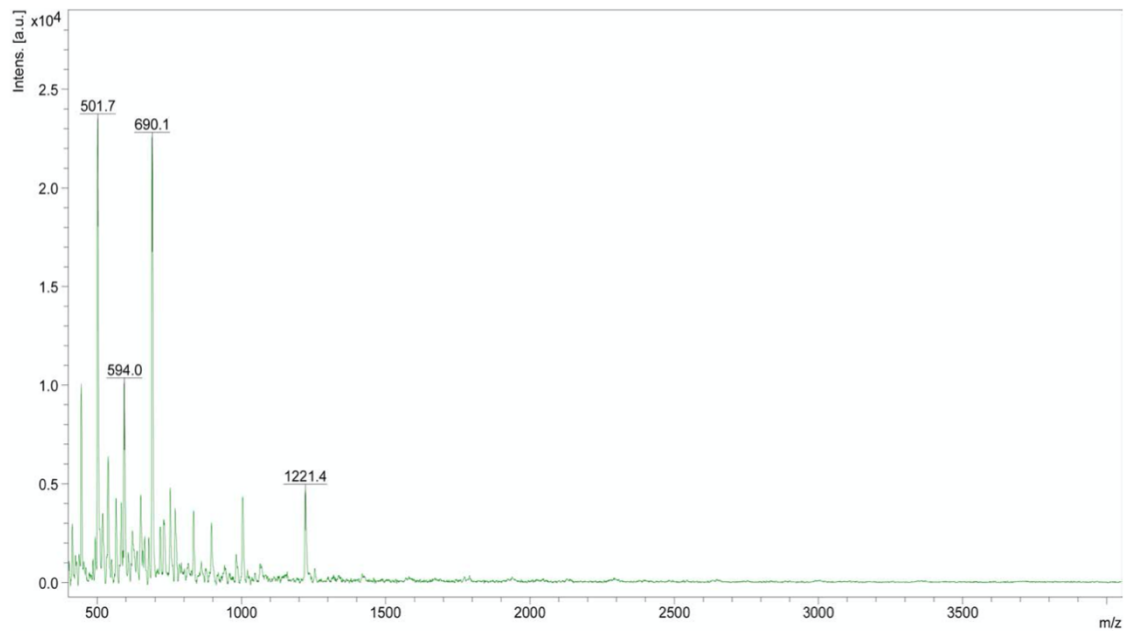
Figure A.53. MALDI Spectrum of PBSU.

Figure A.54. MALDI Spectrum of PHBSU.
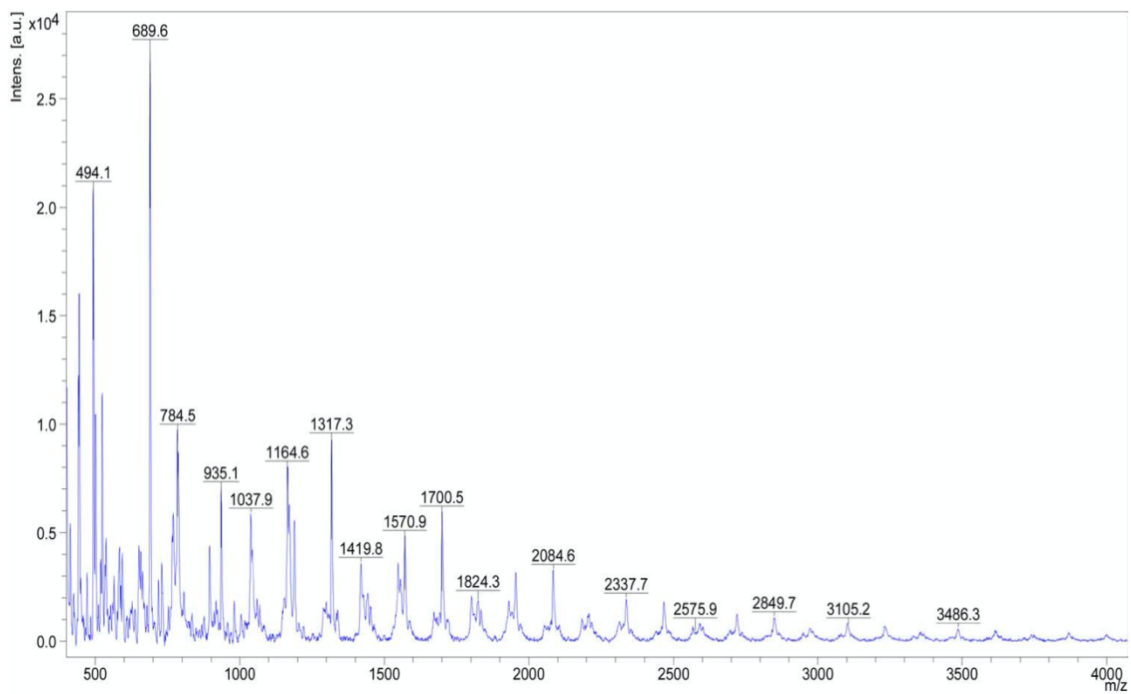
Figure A.55. MALDI Spectrum of PBA.
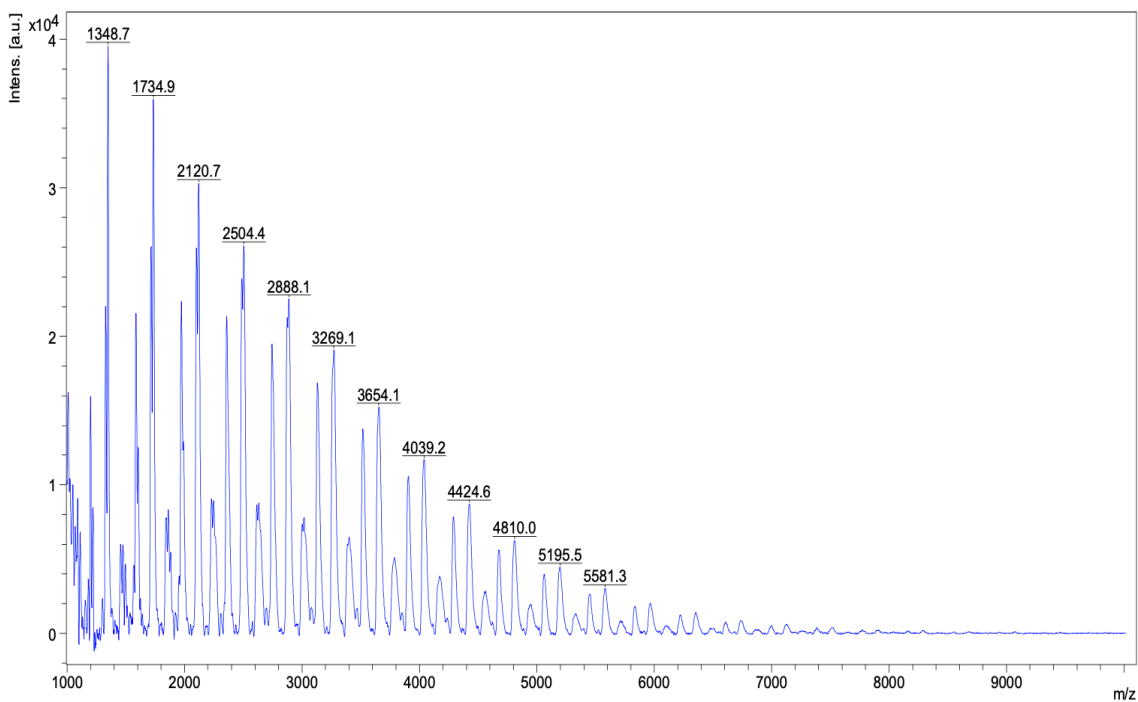
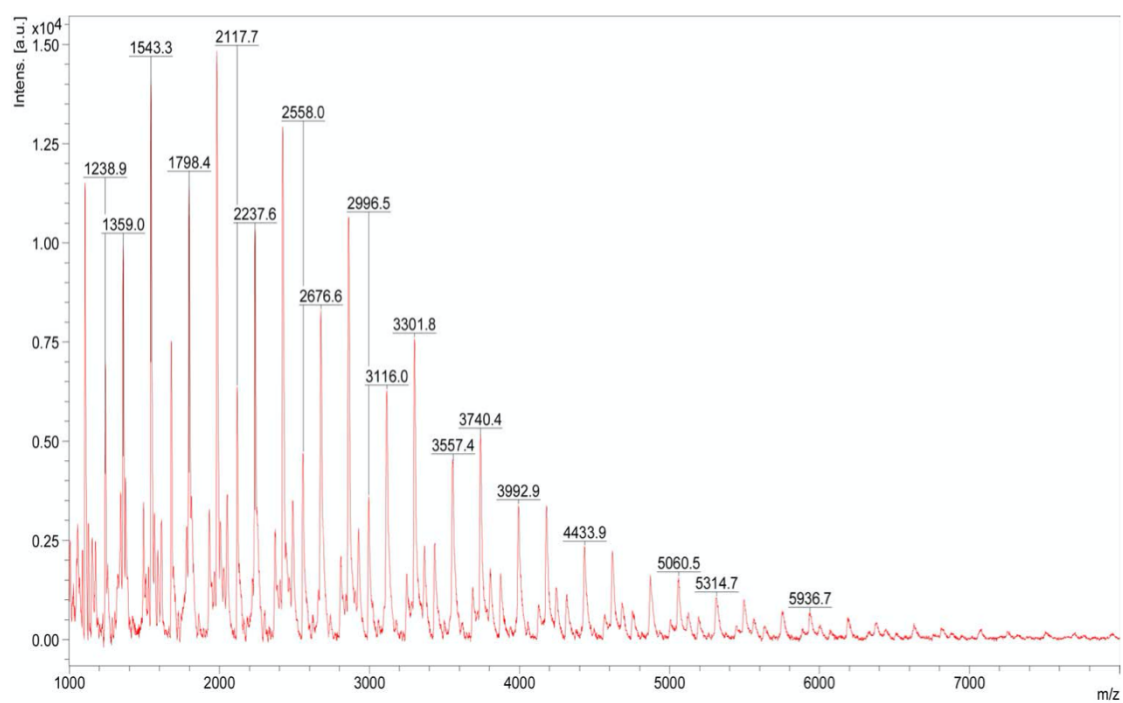Figure A.56. MALDI Spectrum of PHBA.
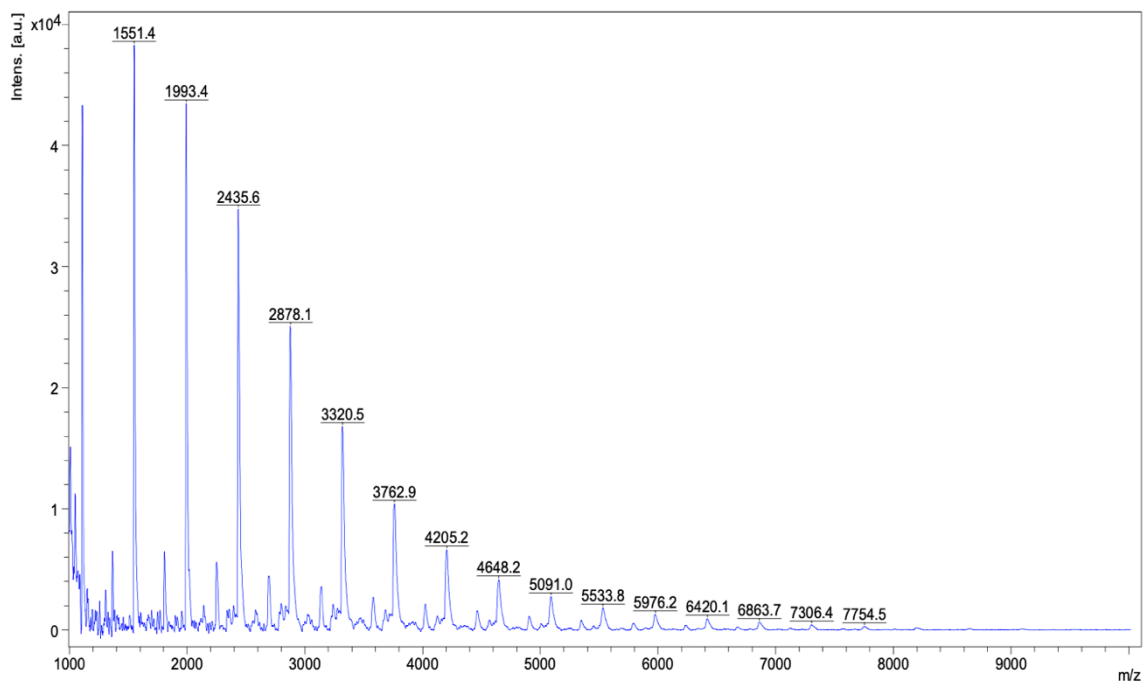
Figure A.57. MALDI Spectrum of PBSE.

Figure A.58. MALDI Spectrum of PHBSE.

Appendix B

Synthesis of Ligands with Catechol Functionality (work in progress)

B.1 Catechol Moieties for Boron and Metal Cations

Catechol moieties have shown affinity for binding boron (Figure B.1).[1] Certain metal cations, like iron, vanadium, and aluminum also commonly complex with catechol.[2] In aqueous solution, boron is commonly found in the form of boric acid ($B(OH_3)$) or tetraborate ($B(OH_4^-)$). Boron is considered a hazardous material, and can only be present in potable water at a concentration of 2.4 mg/L.[3] The concentration in wastewater can be upwards of 100 mg/L and the optimal concentration level for boron is a very narrow range. There can be too little or too much boron very easily. [3]
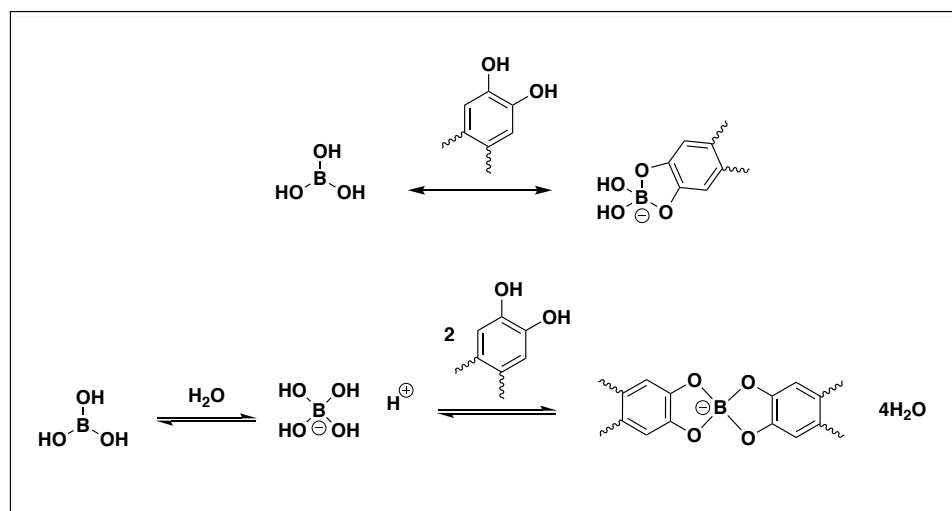
**Figure. B.1**. Catechol and boric acid complexation

Because of the balance that needs to be maintained in terms of boron concentration, the capture of boron would allow for the tuning of the boron concentration in the water product. Many studies have been done using catechol to bind boron,[3-8] though more work

needs to be done investigating the competitive binding of boron and metal cations to catechol

moieties before catechol containing membranes can be used on a produced water source.
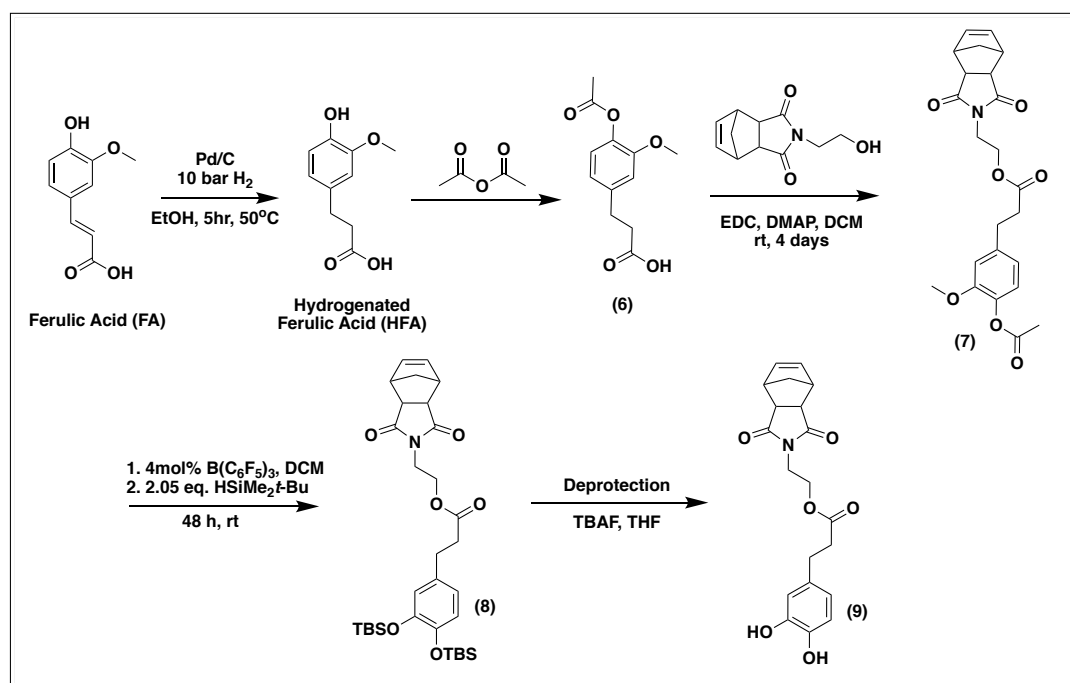
B.2 Norbornene Catechol Monomer

First attempt at a norbornene catechol monomer was planned to be thiol

functionalized in order to utilize thiol-ene click chemistry. Thiol-ene click could be used to

attach to an allyl functionalized norbornene, or poly(allylglycidylether) (PAGE) backbone.

The starting molecule, eugenol, can be sourced from lignin and easily silyl protected. The

allyl group on eugenol can also be easily functionalized to introduce the thiol group. The silyl

protected thiol can be, in theory, clicked with allyl functionalized norbornene (Figure B.2).

Experimentally, the click reaction did not work, and it is thought to be due to interference

from the bulky silyl groups and the impurities in the thiol. This led to other synthetic options

for a norbornene catechol monomer to be investigated.

Figure. B.2. First synthetic route to a norbornene catechol monomer from eugenol.
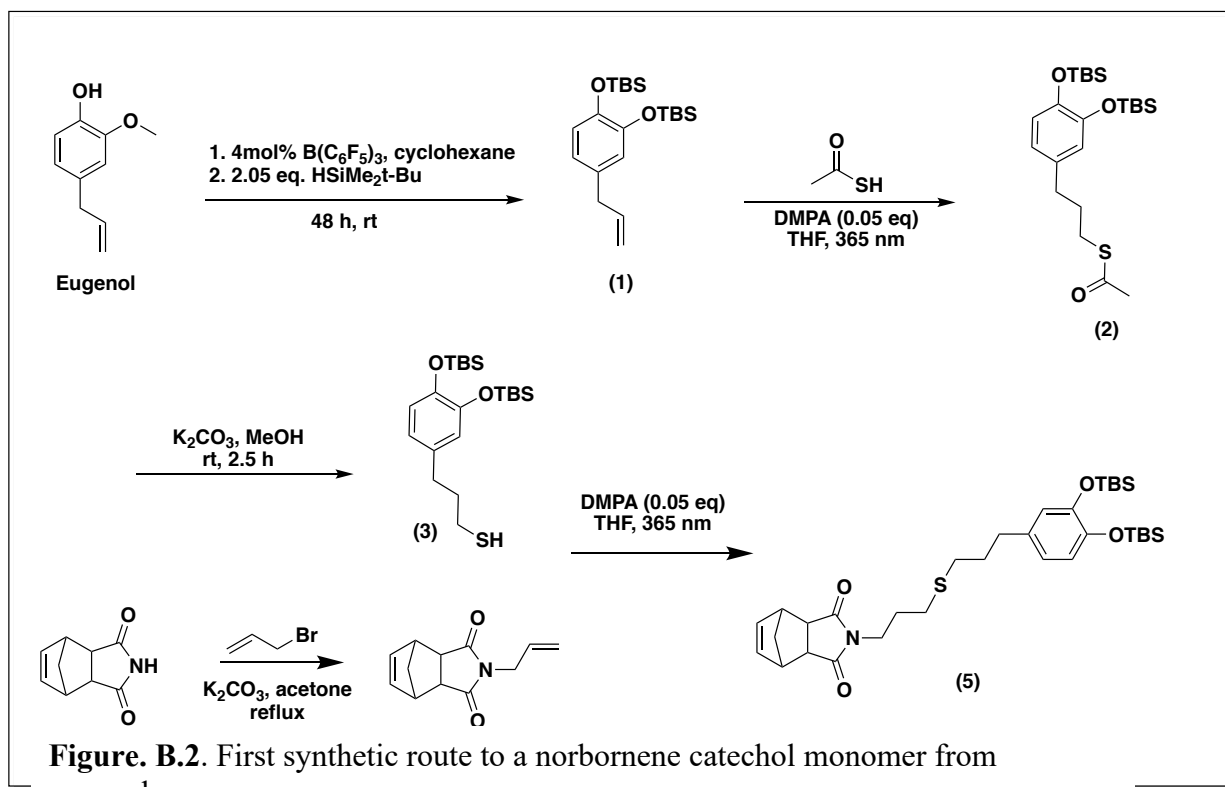
Ferulic acid, another lignin-derived monomer, contains a phenol as well as a carboxylic acid. These functional groups make it a monomer with great potential for ligand synthesis. The presence of an ortho methoxy group also means ortho-demethylation can be used to give catechol functionality. In order to incorporate catechol functionality into the norbornene membrane system, modified ferulic acid can be coupled with a norbornene monomer with a pendent alcohol group using an EDC coupling reaction.

For the synthesis of a norbornene catechol monomer (NBCat), ferulic acid was first hydrogenated, then the phenol group was protected so as to not react during the EDC coupling reaction. The coupling reaction connects the norbornene backbone with the modified ferulic acid. The phenol and methoxy group on the ferulic acid are then silyl protected, so deprotection can be done in one step (Figure B.3).


Figure. B.3. Second synthetic route to a norbornene catechol monomer from ferulic acid.

Experimental

Silyl Protection Reaction[9]

A Schlenk flask equipped with a stir bar was taken into an argon glove box. Tris(pentafluorophenyl) borane (0.5 g 0.98 mmol, 0.04 eq), was added to the flask with cyclohexane (20 mL), and then an addition funnel was attached. The flask with the addition funnel was then stoppered, taken out of the glove box, and put on the Schlenk line. Eugenol (4.0 g, 24.6 mmol, 1 eq) was then added to the flask, and the reaction stirred for approximately 10 minutes to ensure homogeneity. Tert-butyl dimethyl silane (5.87, 50.5 mmol, 2.05 eq) was then added to the addition funnel and added to the reaction dropwise. The reaction was then stirred at room temperature for 2 days under argon. The crude reaction mixture was then poured over a silica plug with DCM as the eluent to give (1) as a clear light-yellow liquid (8.80 g, 95 %) (Figure B.4). ^{1}H NMR (600 MHz, CDCl$_3$) δ= 6.77 (d, 1H, ArH), 6.68 (d, 1H, ArH), 6.63 (dd, 1H, ArH), 5.95 (m, 1H, -CH=C-), 5.05 (m, 2H, C=CH$_2$), 3.28 (d, 2H, Ar-CH$_2$-C-), 1.01 (d, 18H, tBu), 0.21 (d, 12H, methyl).
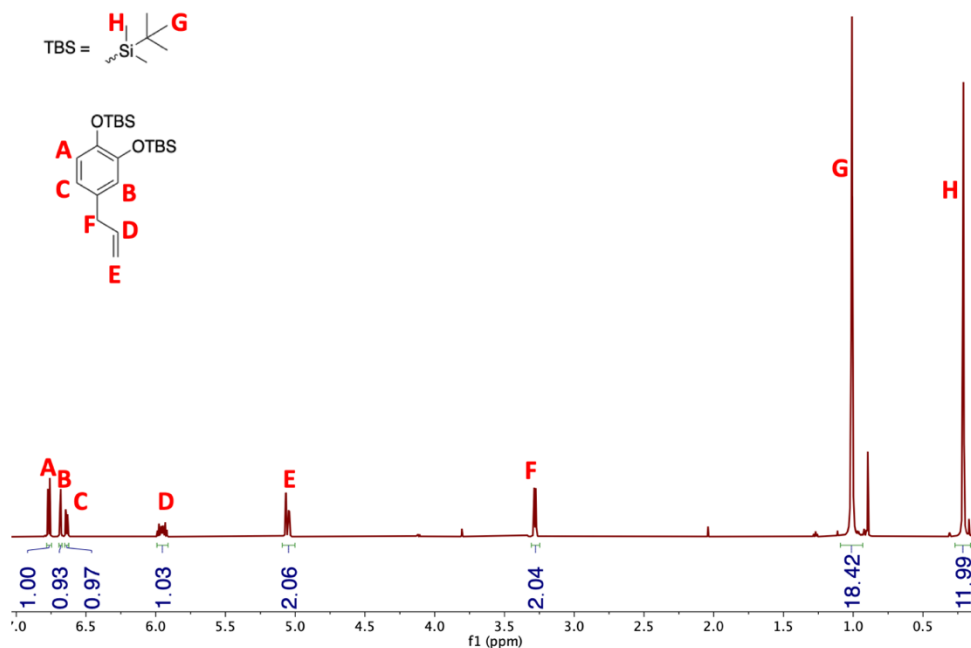
Figure. B.4. ^{1}H NMR of TBS protected eugenol (1) in CDCl$_3$.

Thioate Reaction[9]

(1) (7.80 g, 20.6 mmol) was added to a round bottom flask with thioacteic acid (1.73 g, 22.6 mmol) and 2,2-dimethoxy-2-phenylacetophenone (DMPA) (0.264 g, 1.03 mmol) and THF (3.1 mL). The reaction mixture was then degassed with three freeze-pump-thaw cycles, backfilled with argon, and then exposed to UV light (365 nm). The reaction was stirred for three hours, and then the solvent was evaporated to give the desired product (2) as a yellow liquid (9.11 g, 97 %). This was used in the next step without further purification (Figure B.5). ^{1}H NMR (600 MHz, CDCl$_3$) δ = 6.72 (d, 1H, ArH), 6.62 (d, 1H, ArH), 6.59 (dd, 1H, ArH), 2.85 (t, 2H, -CH$_2$-S-), 2.55 (t, 2H, Ar-CH$_2$-), 2.33 (s, 3H, O=C-CH$_3$), 1.83 (m, 2H, -CH$_2$-), 0.98 (d, 18H, tBu), 0.18 (d, 12H, methyl).
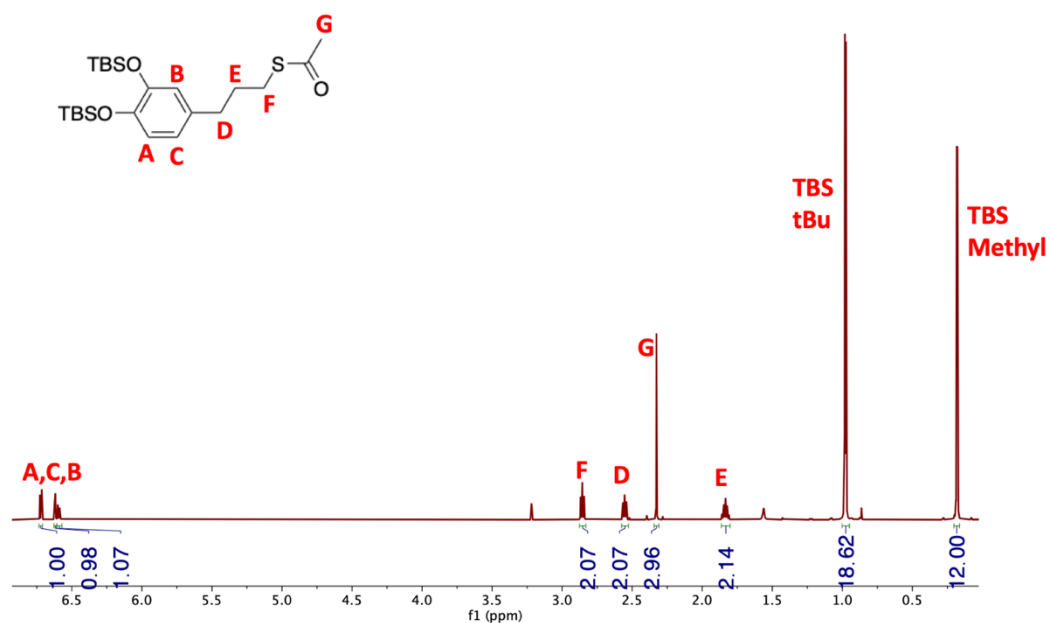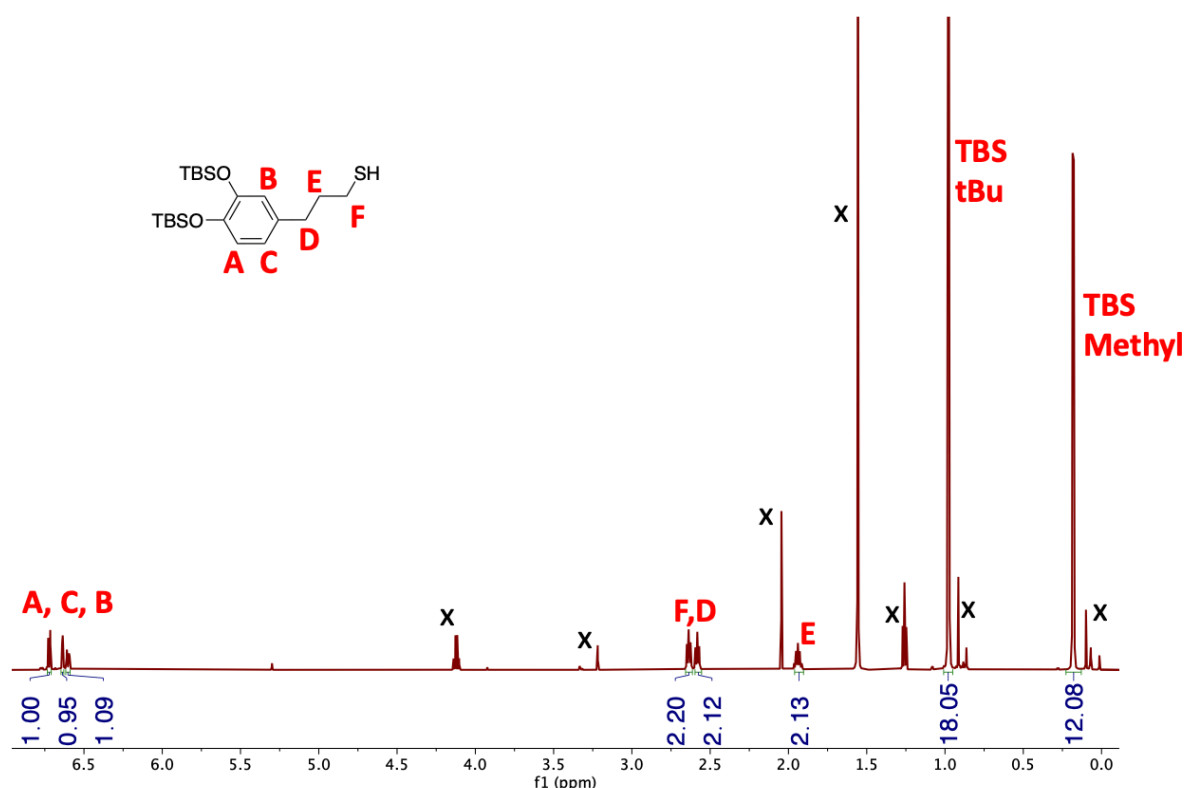

Figure. B.5. ^{1}H NMR of TBS protected eugenol thioate (2) in CDCl$_3$.

Thiol Deprotection[9]

(2) (8.0 g, 17.6 mmol) was added to a round bottom flask with methanol (1.3 mL). The flask was sparged with argon for one hour, after which a degassed solution of saturated K_2CO_3 in MeOH (2.6 mL) was added to the reaction flask via syringe. The reaction was then stirred at room temperature for an additional 2.5 h. The reaction was then quenched with saturated NH_4Cl and diluted with DI water. This aqueous solution was then extracted with ethyl acetate, the organic layer dried with $MgSO_4$, and concentrated *in vacuo*. The crude product was purified by column chromatography over a silica column with 9:1 hexanes:DCM as the eluent. (3) was obtained as a clear yellow liquid (5.03 g, 70 %). ^{1}H NMR (600 MHz, CDCl$_3$) δ = 6.72 (d, 1H, ArH), 6.62 (d, 1H, ArH), 6.59 (dd, 1H, ArH), 2.63 (t, 2H, -CH$_2$-S-),


Figure. B.6. ^{1}H NMR of TBS protected eugenol thiol (3) in CDCl$_3$. With x indicating an impurity peak.

2.58 (t, 2H, Ar-CH$_2$-), 1.94 (m, 2H, -CH$_2$-), 0.97 (d, 18H, tBu), 0.17 (d, 12H, methyl).

Norbornene Allylation[10]

5-norbornene-2,3dicarboximide (0.163 g, 1 mmol) was added to a round bottom flask equipped with a stir bar. To that flask was then added allyl bromide (0.121 g, 1 mmol), potassium carbonate (0.415 g, 3 mmol), and acetone (20 mL). The reaction was stirred at reflux for 8 h. The solvent was then evaporated *in vacuo*. The crude produce was dissolved in DI water, washed with ethyl acetate and dried with Na_2SO_4. The solvent was evaporated to give (4) as a white solid (0.169 g, 83 %) (Figure B.7).
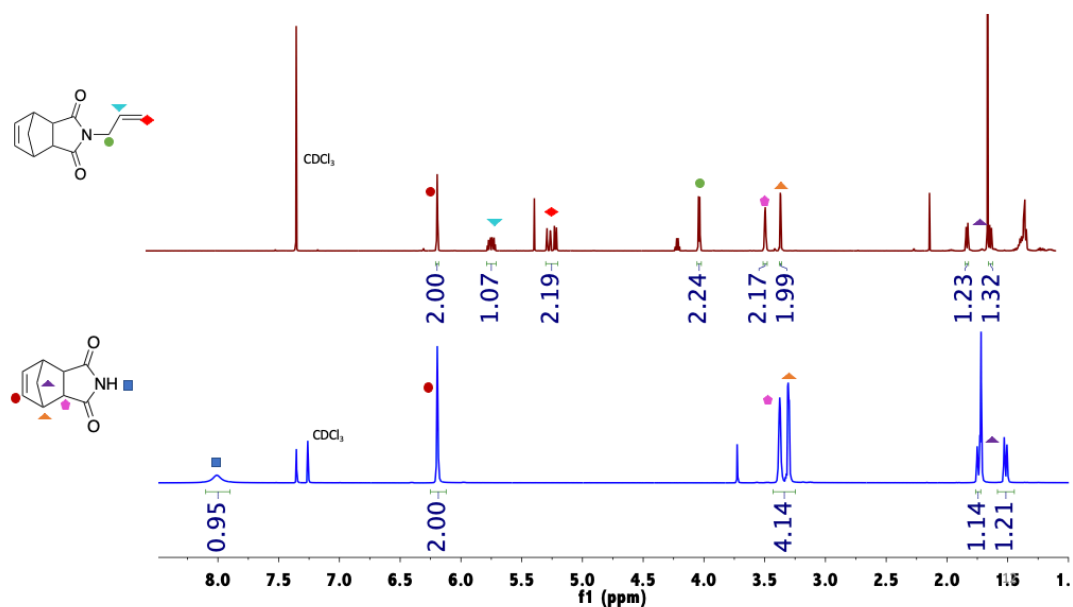

Figure. B.7. ^1H NMR of norbornene allyl (4) (top) and the starting material (bottom) in $CDCl_3$.

Thiol-ene Click Reaction[9]

(3) and (4) were added to a round bottom flask with anhydrous THF. 2,2-dimethoxy-2-phenylacetophenone (DMPA) was then added. The reaction mixture was then degassed with three freeze-pump-thaw cycles, backfilled with argon, and then exposed to UV light (365 nm). The reaction was stirred for 4 hours, and then the solvent was evaporated to give the desired product (5). This was not successful using (3) and (4).
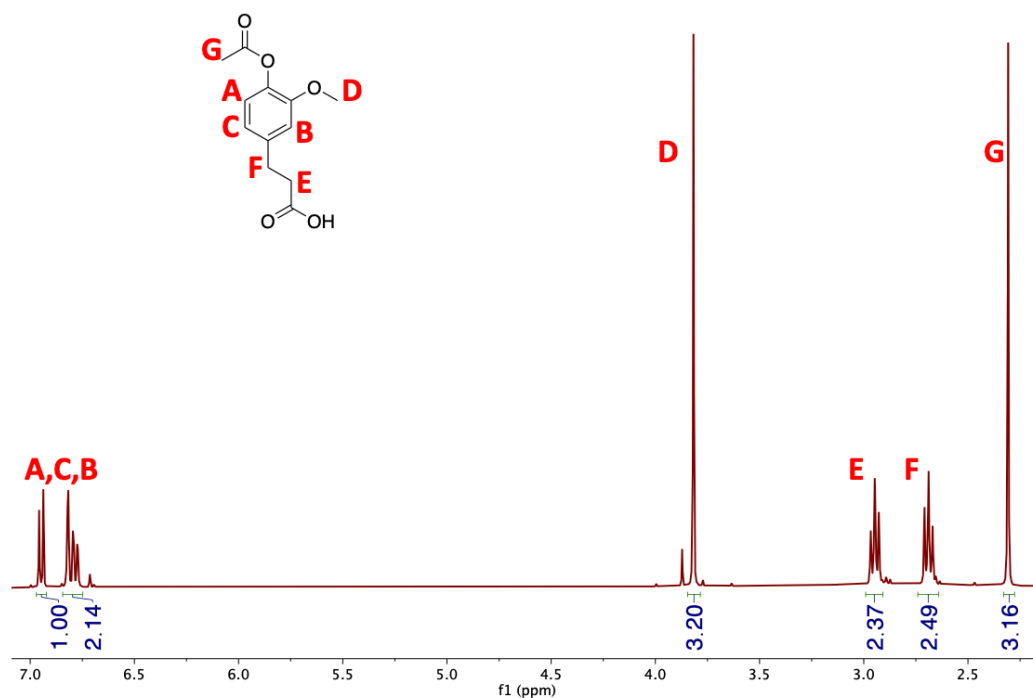
Hydrogenation of Ferulic Acid[11]

Ferulic acid (2.0 g, 10.3 mmol), Pd/C (0.313 g), and ethanol (40 mL) were added to a

Parr vessel. The vessel was then heated to 50 °C for 5 h under 10 bar of H_2. The resulting

reaction mixture was then hot filtered twice to remove the solid catalyst and then

concentrated in vacuo to give the hydrogenated product (HFA) as a white solid (1.72 g,

85 %). This product was used without further purification (Figure B.8). ^{1}H NMR (600 MHz,

$CDCl_3$) δ = 6.84 (d, 1H, ArH), 6.69 (m, 2H, ArH), 3.87 (s, 3H, -OCH_3), 2.89 (t, 2H, -CH_2-

C=O), 2.65 (t, 2H, Ar-CH_2-).
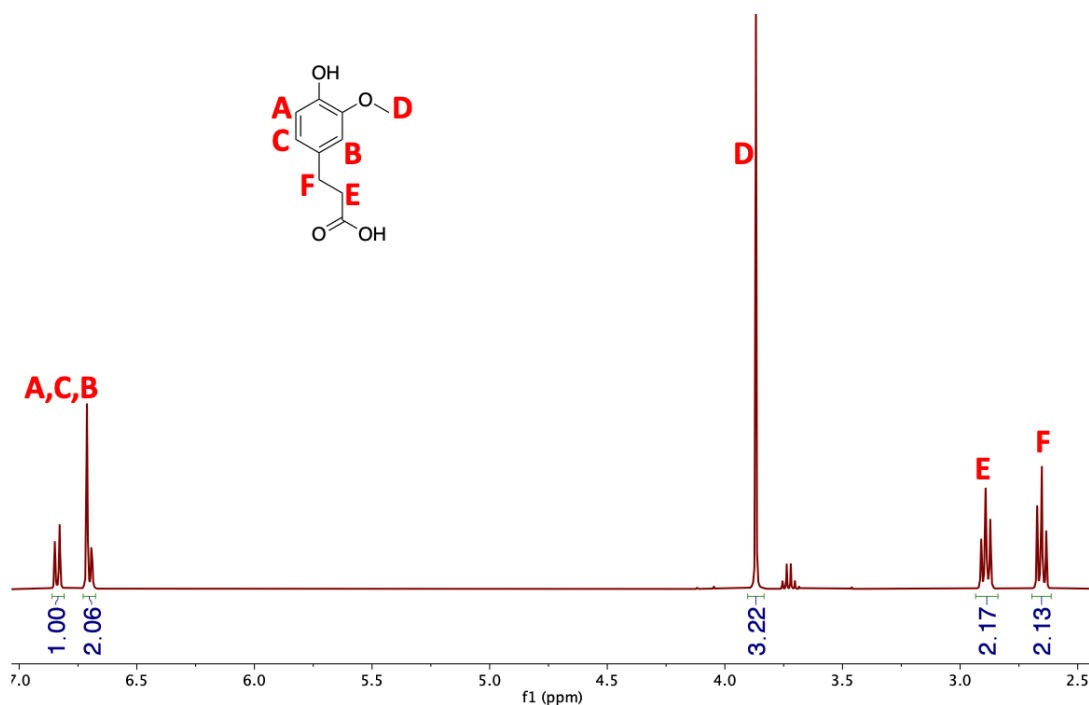
Figure. B.8. ^{1}H NMR of hydrogenated ferulic acid (HFA) in $CDCl_3$.

Acetyl Protection of Hydrogenated Ferulic Acid (HFA)[12]

HFA (0.5 g, 2.5 mmol) was added to a round bottom flask. 10 % NaOH (2.5 mmol) was added to the flask and stirred until all solid is dissolved. Acetic anhydride (0.306 g, 0.284 mL, 3 mmol) was then added to the flask and the reaction was stirred at room temperature overnight. (6) was afforded as a white solid (Figure B.9) (0.486, 80 %). ^{1}H NMR (600 MHz, CDCl$_3$) δ = 6.95 (d, 1H, ArH), 6.79 (m, 2H, ArH), 3.82 (s, 3H, -OCH$_3$), 2.94 (t, 2H, -CH$_2$-C=O), 2.69 (t, 2H, Ar-CH$_2$-), 2.30 (s, 3H, O=C-CH$_3$).


Figure. B.9. ^{1}H NMR of acetyl protected hydrogenated ferulic acid (6) in CDCl$_3$.

EDC Coupling Reaction

(6) (1.19 g, 5 mmol), norbornene alcohol (1.03 g, 5 mmol) and DCM (50 mL) were mixed in a round bottom flask equipped with a stir bar. The solution was brought to 0 °C and bubbled with argon for 30 minutes. 1-ethyl-3-(3-dimethylaminopropyl)carbodiimide

hydrochloride (0.959 g, 5 mmol) and 4-(dimethylamino)pyridine (0.611 g, 5 mmol) were then added to the flask and stirred at 0 °C until dissolved. Once dissolved the reaction was sealed with a septum and bubbled with argon for an additional 30 minutes while being brought up to room temperature. The reaction was stirred at room temperature for 96 h under argon. The mixture was then washed with 2N HCl, brine, and dried with Na_2SO_4. The reaction mixture was concentrated in vacuo. The crude product was then further purified through column chromatography, ethyl acetate:DCM 1:1 to give (7) as a viscous yellow liquid (1.54 g, 72 %) (Figure B.10). ^{1}H NMR (600 MHz, CDCl$_3$) δ = 6.91 (d, 1H, ArH), 6.78 (d, 1H, ArH), 6.73 (dd, 1H, ArH), 6.26 (t, NB C=C-H), 4.23 (t, 2H, -CH$_2$-O-), 3.79 (s, 3H, -OCH$_3$), 3.73 (t, 2H, -N-CH$_2$), 3.25 (s, 2H, NB C-H), 2.87 (t, O=C-CH$_2$-), 2.66 (s, 2H, NB C-H), 2.55 (t, 2H, Ar-CH$_2$-), 2.27 (s, 3H, Acetyl CH$_3$), 1.48 and 1.27 (dd, 2H, NB bridging
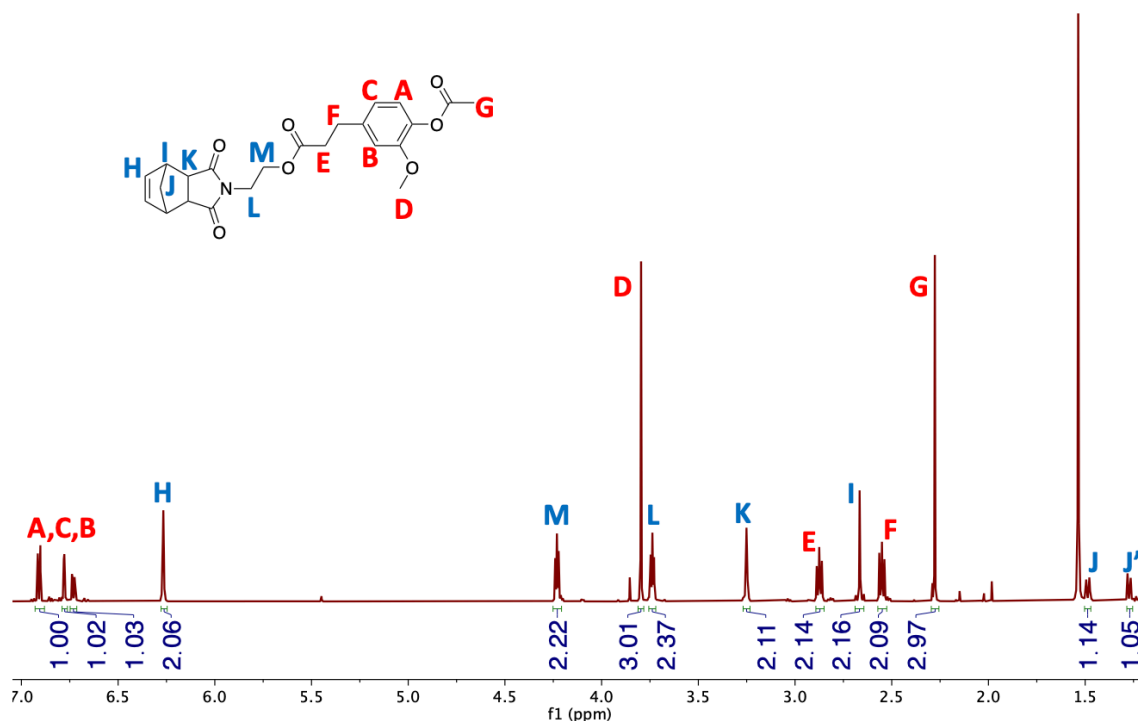
Figure. B.10. ^{1}H NMR of NorborneneHFA (7) in CDCl$_3$.

CH$_2$).

Future Synthesis

For future synthetic plans for a norbornene catechol monomer, (7) will need to be TBS protected to give (8) and then (8) deprotected to give (9). The literature procedure for the deprotection reaction is reported in the next section.

Catechol TBS Deprotection[14]

(8) is added to a round bottom flask and 12M HCl is then added dropwise. The flask was degassed with argon, sealed, and stirred at 60 °C overnight. The reaction mixture was then concentrated *in vacuo,* crude residue was dissolved in CHCl₃, and recrystallized with cold hexanes to give (9).

B.3 Amine Functionalized Catechol Monomer

For incorporation of catechol into the EpPAGE system, a ligand needs to be amine functionalized. To achieve this, creosol was reacted with glycine to give a biscreosol molecule with a carboxylic acid. The carboxylic acid can be coupled with a boc-protected ethanolamine to give the resulting ligand amine functionality (Figure B.11).
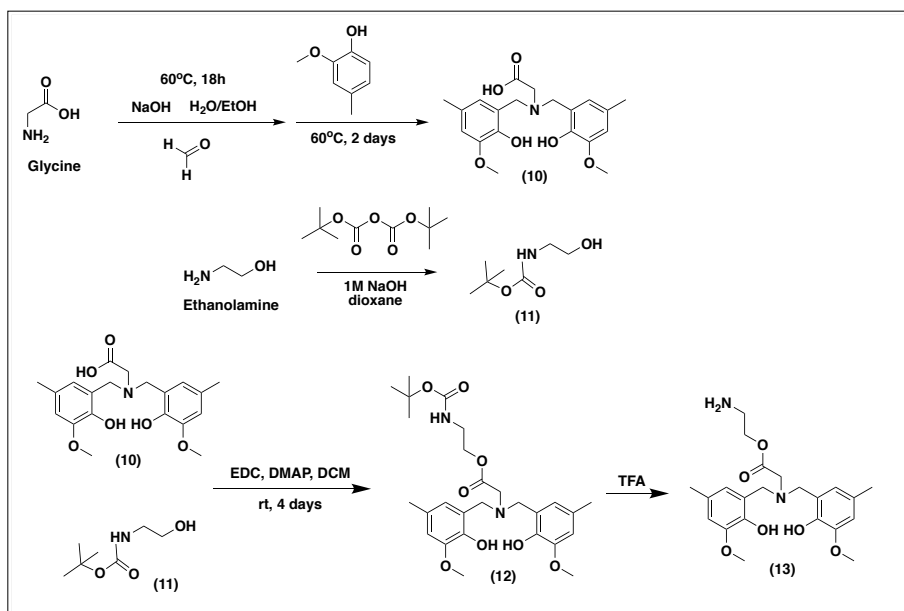
Figure. B.11. Synthetic route to an amine functionalized catechol ligand from glycine and biscreosol.

Initial attempts at the synthetic route presented in Figure B.4 were unsuccessful at the EDC coupling stage. This was most likely due to the unprotected phenol groups present in the bis creosol molecule which can also react in the EDC coupling reaction giving unwanted products. To remedy this, the phenol groups can be protected before the EDC coupling and then deprotected to give catechol. Depending on the protection group chosen, this could also lead to a monomer with two catechols (Figure B.12).
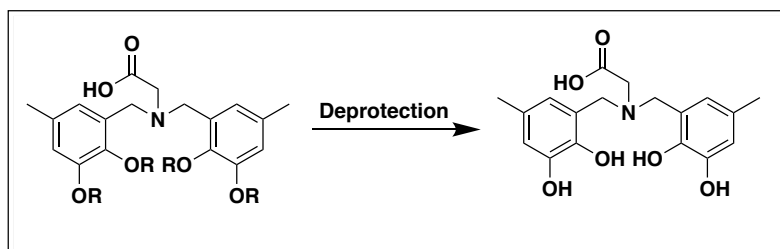

Figure. B.12. Potential route to a double catechol ligand utilizing phenol protection groups.

Experimental

Glycine and Creosol Coupling

Glycine (2.25 g, 30 mmol) and NaOH (2.98 g, 74.5 mmol) were added into a round-bottomed flask. To the flask was added a water/ethanol mixture (45/90 mL) and then 37% formaldehyde (13.8 g, 170 mmol). The mixture was stirred at 60 °C for 18 h. Creosol (8.28 g, 60 mmol) was then added dropwise and the mixture was stirred at 60 °C for another 2 days. The mixture was then concentrated with a rotavapor prior to the addition of 150 mL of water and several drops of hydrochloric acid to adjust the pH to 5. Dichloromethane was added to extract the mixture and the organic layer was dried by a rotavapor. The mixture was introduced with 50 mL of ethyl acetate and 200 mL of water. After sufficient mixing, the aqueous layer was kept. Leaving the aqueous solution at room overnight gradually afforded a slightly yellowish precipitate. Washing the precipitate with cold acetone several times

yielded the (10) as a slightly off-white powder (2.62 g, 24 %) (Figure B.13). ^{1}H NMR (600 MHz, CDCl$_3$) δ= 6.64 (s, 2H, ArH), 6.57 (s, 2HH, ArH), 3.95 (s, 4H, -N-CH$_2$-Ar), 3.83 (s, 6H, -O-CH$_3$), 3.40 (s, 2H, -N-CH$_2$-C=O), 2.25 (s, 6H, Ar-CH$_3$).
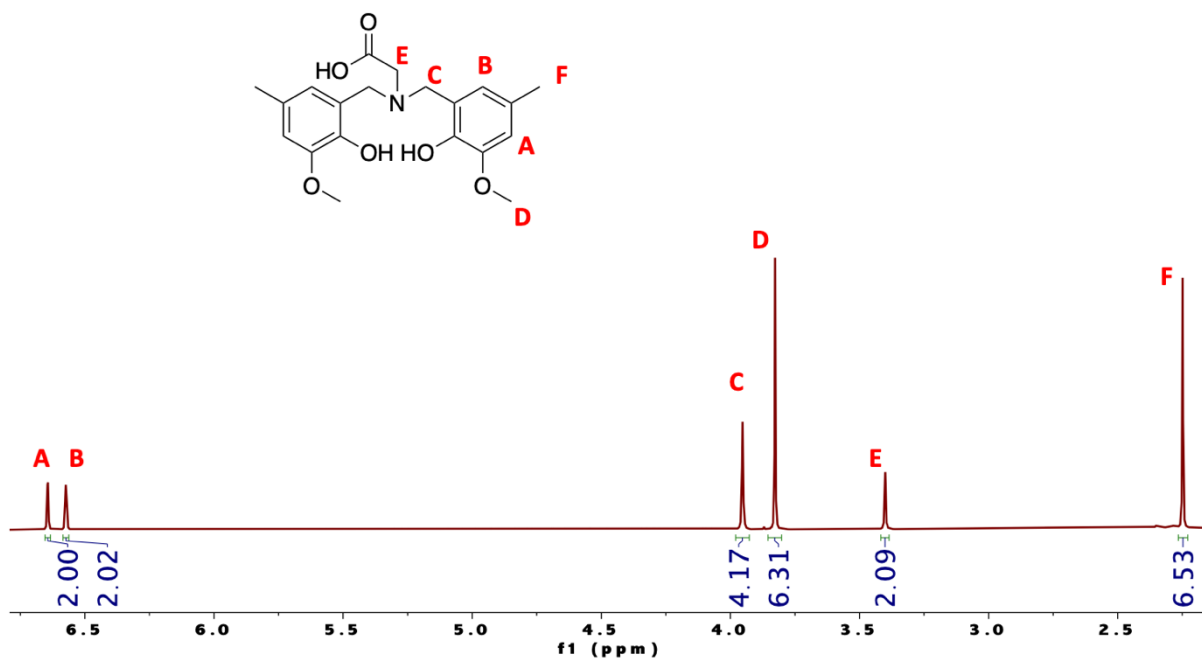
Figure. B.13. ^{1}H NMR spectrum of biscreosol product (10) in CDCl$_3$.

Boc Protection of Ethanolamine[13]

Ethanolamine (0.812 g, 0.803 mL, 13.3 mmol) was stirred in 20 mL of 1M NaOH in a round bottom flask. To the flask was then added 20 mL of dioxane followed by boc anhydride (3.52 g, 3.7 mL, 16.1 mmol). The reaction was stirred at room temperature for 12 h, after which the solution was concentrated. The crude product was dissolved in EtOAc, and then washed with 10 % KHSO$_4$ and brine. The organic layer was then dried with Na$_2$SO$_4$, concentrated, and put on the high vac overnight. A slightly yellow clear liquid was obtained (11) (1.397 g, 65 %) (Figure B.14). ^{1}H NMR (600 MHz, CDCl$_3$) δ= 3.70 (t, 2H, -N-CH$_2$-), 3.28 (t, 2H, -CH$_2$-OH), 1.44 (s, 9H, tBu).
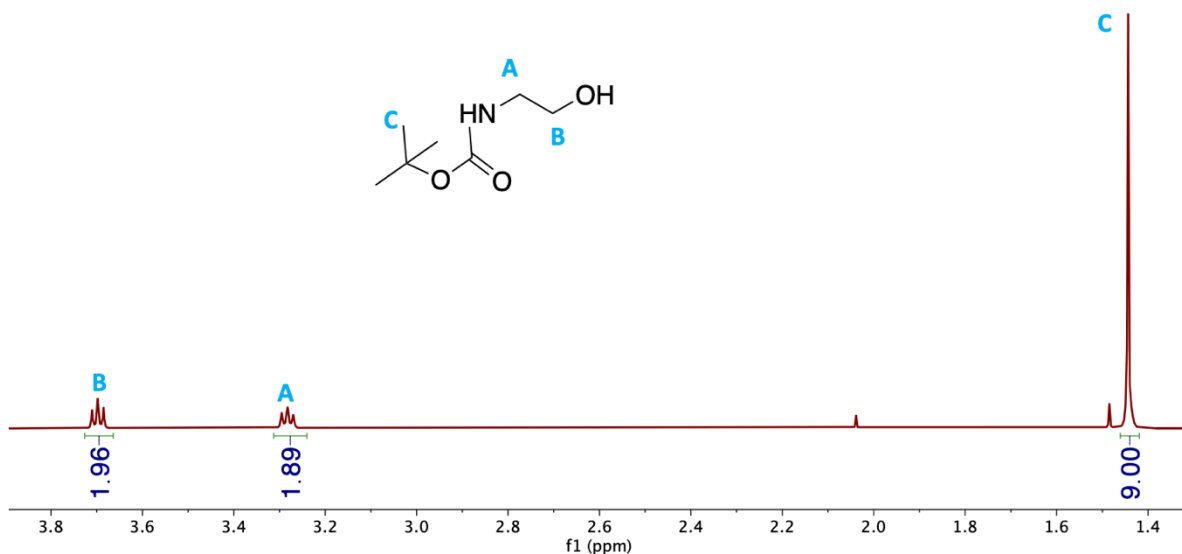
Figure. B.14. ^{1}H NMR spectrum of boc protected ethanolamine (11) in CDCl$_3$.

Future Synthesis

Future synthetic plans rely on investigation into the best phenol protection group so the EDC coupling reaction can proceed without unwanted products, the successful EDC coupling to give (12), and the eventual deprotection of the final desired biscreosol amine ligand (13). Literature procedure for the unfinished steps in the synthetic schemes presented are provided in the following section.

Boc Deprotection of BiscreosolAmine Ligand[15]

Boc-protected 12-crown-4 aminohexanoate (1 eq), trifluoroacetic acid (21 eq), and DCM are added to a round bottom flask. The reaction mixture is stirred in an ice bath for 1 h. The solution is acidified to ph = 2, and then loaded onto a Dowex H+ 50 column that is packed with 0.25 N H$_2$SO$_4$.. ~200 mL of DI water is then passed through the column, followed by ~200 mL of 1 M NH$_4$OH. The basic layer is collected and concentrated *in vacuo*.

B.4 References

1. Yoshino, K.; Kotaka, M.; Okamoto, M.; Kakihana, H., ^{11}B-NMR Study of the Complex Formulation of Borate with Catechol and L-Dopa. *Bull. Chem. Soc. Japn.*, **1979**, *52*, 3005-3009.

2. Holten-Andersen, N.; Jaishankar, A.; Harrington, M. J.; Fullenkamp, D. E.; DiMarco, G.; He, L.; McKinley, G. H.; Messersmith, P. B.; Lee, K. Y. C., Metal-coordination: using one of nature's tricks to control soft material mechanics. *J. Mater. Chem. B*, **2014**, *2*, 2467-2472.

3. Xia, N. N.; Zhang, H. Y.; Hu, Z. H.; Kong, F.; He, F., A functionalized bio-based material with abundant mesopores and catechol groups for efficient removal of boron. *Chemosphere*, **2021**, *263*, 128202.

4. Kluczka, J.; Tórz, A.; Łacka, D.; Kazek-Kęsik, A.; Adamek, J., Boron removal by adsorption on cobalt (II) doped chitosan bio-composite. *J. Polym.Environ.*, **2017**, *26*, 2039.

5. Sun, L.; Huang, J.; Liu, H.; Zhang, Y.; Ye, X.; Zhang, H.; Wu, A.; Wu, Z., Adsorption of boron by CA@KH-550@EPH@NMDG (CKEN) with biomass carbonaceous aerogels as substrate. *J. Hazard Mater.*, **2018**, *358*, 10-19.

6. Chen, T.; Wang, Q.; Lyu, J.; Bai, P.; Guo, X., Boron removal and reclamation by magnetic magnetite (Fe_3O_4) nanoparticle: an adsorption and isotopic separation study. *Separ. Purif. Technol.*, **2020**, *231*, 115930.

7. Lyu, J.; Zeng, Z.; Zhang, N.; Liu, H.; Bai, P.; Guo, X., Pyrocatechol-modified resins for boron recovery from water: synthesis, adsorption and isotopic separation studies. *React. Funct. Polym.*, **2017**, *112*, 1-8.

8. Zhang, X.; Wnag, J.; Chen, S.; Bao, Z.; Xing, H.; Zhang, Z.; Su, B.; Yang, Q.; Yang, Y.; Ren, Q., A spherical N-methyl-d-glucamine-based hybrid adsorbent for highly efficient adsorption of boric acid from water. *Separ. Purif. Technol.*, **2017**, *172*, 43-50.

9. Mattson, K. M.; Latimer, A. A.; McGrath, A. J.; Lynd, N. A.; Lundberg, P.; Hudson, Z. M.; Hawker, C. J., A Facile Synthesis of Catechol-Functionalized Poly(ethylene oxide) Block and Random Copolymers. *J. Polym. Sci.*, **2015**, *53*, 2685-2692.

10. Das, S. K.; Bhattacharya, S.; Kundu, A., Rationalized design, synthesis, and pharmacological screening of amino acid linked spiro pyrrolidino oxyindole analogs through environment friendly reaction. *J. Adv. Pharma. Technol. & Research*, **2013**, *4*, 198-205.

11. Trita, A. S.; Over, L. C.; Pollini, J.; Baader, S.; Riegsinger, S.; Meier, M. A. R.; Gooßen, L. J., Synthesis of potential bisphenol A substitute by isomerising metathesis of renewable raw materials. *Green Chem.,* **2017**, *19*, 3051-3060.

12. Huang, G. Y.; Cui, C.; Wang, Z. P.; Li, Y. Q.; Xiong, L. X.; Wang, L. Z.; Yu, S. J.; Li, Z. M.; Zhao, W. G., Synthesis and characteristics of (Hydrogenated) ferulic acid derivatives as potential antiviral agents with insecticidal activity. *Chemistry Central Journal*, **2013**, *7*, 33.

13. Pan, Z.; Lin, X., Kinase Inhibitor and Method for Treatment of Related Diseases. US2014256759 (A1), September 11, 2014.

14. White, J. D.; Wilker, J. J., Underwater Bonding with Charge Polymer Mimics of Marine Mussel Adhesive Proteins. *Macromolecules*, **2011**, *44*, 5085-5088.

15. Fattori, D.; Rossi, C.; Fincham, C. I.; Caciagli, V.; Catrambone, F.; D'Andrea, P.; Felicetti, P.; Gensini, M.; Marastoni, E.; Nannicini, R.; Paris, M.; Terracciano, R.;

Bressan, A.; Giuliani, S.; Maggi, C. A.; Meini, S.; Valenti, C.; Quartara, L., Design and Synthesis of Novel Sulfonamide-Containing Bradykinin hB$_2$ Receptor Antagonists. 2. Synthesis and Structure-Activity Relationships of α,α-Clycloalkylglycine Sylfonamides. *J. Med. Chem.*, **2007**, *50*, 550-565.